Title
Quantitative and high-throughput receptor affinity profiling system reveals distinct pathophysiological HIV-1 phenotypes

Author
Chikere, Kelechi C.

Publication Date
2012

Peer reviewed|Thesis/dissertation

UNIVERSITY OF CALIFORNIA

Los Angeles

Quantitative and high-throughput receptor affinity profiling system reveals distinct pathophysiological HIV-1 phenotypes

A dissertation submitted in partial satisfaction of the
requirements for the degree Doctor of Philosophy in Microbiology, Immunology and Molecular Genetics

by

Kelechi Clarence Chikere

2013

ABSTRACT OF THE DISSERTATION

Quantitative and high-throughput receptor affinity profiling system reveals distinct pathophysiological HIV-1 phenotypes

by

Kelechi Clarence Chikere

Doctor of Philosophy in Microbiology, Immunology, and Molecular Genetics

University of California, Los Angeles, 2013

Professor Benhur Lee, Chair

HIV-1 affinity for CD4 and CCR5 is associated with differential pathogenicity. Therefore, we pioneered a dually inducible cell line based system that could quantitatively and comprehensively characterize viral entry efficiency as a co-dependent function of CD4 and CCR5 expression levels. This receptor affinity profiling system (Affinofile) has revealed biologically relevant phenotypes in Envelopes (Envs) with differential CD4/CCR5 usage efficiencies, providing a more refined understanding of receptor and coreceptor affinities, which can have an impact on the development and use of HIV-1 therapeutics.

To facilitate a more rapid and refined analysis of CD4 and CCR5 usage efficiencies with even greater sensitivity, we engineered a reporter Affinofile system containing a tat-rev dependent e**G**FP-**G**aussia luciferase **R**eporter (GGR). Using this GGR Affinofile system, we (1) characterized the phenotypic and biological consequences for Envs with defined mutations that modulate CD4 or CCR5 binding, (2) determined Transmitter/Founder (T/F) Envs have differential CD4/CCR5 usage compared to Chronic Env, (3) revealed phenotypically distinct CD4/CCR5 usage patterns among the prevalent HIV-1 subtypes (A,B, C and D), and (4) uncovered that mutations that confer resistance to Broadly Neutralizing Antibodies (BNAbs) often compromised the efficiency of CD4/CCR5 usage and entry.

Analysis of mutations known to only modulate CCR5 (K421D, S142N) binding demonstrated that CD4 and CCR5 usage is an inter-related process as mutations that affect CD4 binding influenced the efficiency of CCR5 usage and vice versa. The relative entry efficiencies defined in GGR Affinofile system were also reflected in their entry efficiencies into primary CD4+ T cell subsets. In addition, we show that transmitter/founder and chronic envelopes have distinct entry efficiencies that yield characteristic vector metrics. Next, we analyzed over 28 pseudotyped HIV-1 viruses from four different subtypes, and noted that subtype C envelopes could be distinguished from the other subtypes based on their greater efficiency of CD4/CCR5 usage which was reflected in their vector metrics (increased vector angle and mean infectivity). Lastly, envelopes with engineered mutations known to confer resistance to BNAbs, VRC01 and PG6/PG19, invariably resulted in a decreased CD4/CCR5 usage efficiency.

Our results suggest that our GGR Affinofile system can quantify and reveal biologically relevant differences in CD4/CCR5 usage patterns in Envs that reflect their genetic-epidemiological differences, pathogenicity, cell tropism, and even fitness cost as a result of resistant-mutations to BNAbs.

The dissertation of Kelechi Clarence Chikere is approved.

_____

Otto O. Yang

_____

Paul A. Krogstad

_____

Jerome A. Zack

_____

Benhur Lee, Committee Chair

University of California, Los Angeles

2013

I would like to dedicate this work to the people of past and present that made it possible for me to pursue my goal of higher education.

TABLE OF CONTENTS

APPENDICES TO THE DISSERTATION

LIST OF FIGURES

Chapter 1

Chapter 3

Chapter 4

Chapter 5

LIST OF TABLES

Chapter 3

Chapter 4

ACKNOWLEDGMENTS

I would first like to thank my mentor, Dr. Benhur Lee, for giving me the opportunity to work in his laboratory. When I initially joined his lab, I had little experience with mammalian research. Despite this, Benhur welcomed me into his lab. I wholeheartedly thank Benhur for pushing me during those early years and for his continued support and guidance. I also thank him for supporting me, as well as the ideas I came up with over the years. It has definitely been fulfilling seeing myself grow as a scientist, and I believe that has much to do with Benhur's training and mentorship. I also thank my committee members, Dr. Jerome Zack, Dr. Paul Krogstad, and Dr. Otto Yang for their support, guidance, and advice over the years.

The work in this thesis would not have been possible without support provided by my colleagues over the years. From the beginning, Patrick Hong, has provided priceless guidance. Shirley Delair, I thank her for her companionship during the years of troubleshooting. I would also like to thank current and old lab members for all their advice and support.

I would like to thank all the friends that I have met during my years in graduate school. Specifically, I would like to thank Miguel Edwards and Aaron Chapman. You guys have been a source of laughter, relief and encouragement since we met that first day of the ACCESS 2007 class.

Finally, I would like to thank my family for all of their support. My parents, Maxwell and Gladys Chikere, have always encouraged me to follow my passions. Nkasi,

Erika, Nyema and my dearest Amara, you have been my personal source of strength throughout the hard times. I would especially like to thank Dr. Xylona Bibal for her encouragement and companionship.

This dissertation work was supported by a seed grant and fellowship from the UCLA AIDS Institute and the UCLA Center for AIDS Research (AI28697. B.L. , K.C.). Additionally, this work was supported by NIH grant AI092218 (B.L.),I would like to thank and acknowledge financial support from the Microbial Pathogenesis Training grant (NIH T32-AI07323, K.C.), the UCLA Graduate Division (Eugene V. Cota-Robles Fellowship, K.C.) and the Department of Microbiology, Immunology, and Molecular Genetics (Mitsuo Takasugi Award, K.C.).

Chapter Three in this thesis is a version of (Chikere *et al,* 2012): Chikere K, Chou T, Gorry P and Lee B. 2012. Affinofile Profiling: *How the Efficiency of CD4/CCR5 usage impacts the biological and pathogenic phenotype of HIV*. (Virology, Special Issue: Review 2012.09.043)

Chapter Four in this thesis is a version of (Chikere *et al,* 2012), which is currently under review : Chikere K, Webb N, Chou T, Gorry P, and Lee B. 2012. *Distinct pathophysiological HIV-1 phenotypes associated with transmission, neutralization resistance and subtype specificity identified by quantitative, high-throughput receptor affinity profiling.*

Appendix B was originally published in Journal of Leukocyte Biology: Salimi H, Roche M, Webb N, Gray L, Chikere K, Sterjovski J, Ellett A, Wesselingh S, Ramsland P,

Lee B, Churchill M and Gorry P. 2012. *Macrophage-tropic HIV-1 variants from brain demonstrate alterations in the way gp120 engages both CD4 and CCR5*. 10.1189/jlb.0612308 . It is reprinted here with permission from Society of Leukocyte Biology and John Wiley & Sons.

Appendix C contains work that is *in press* in Immunity: Liu S, Aliyari R, Chikere K, Marsden M, Li G, Wang Y, Su L, Zack J, Freiberg A, Lee B, and Cheng B. 2012.*The Interferon-Inducible Cholesterol-25-Hydroxylase Broadly Inhibits Viral Entry by Production of 25-Hydroxycholesterol*

Appednix D contains work that is *in press* in Journal of Virology*:* Palomares K, Pernet O, Vigant F, Chikere K, Hong P, Sherman S, Van Handel B, Patterson M, An DS, Lowry WE, Mikkola H, Morizono K, Pyle AD, and Lee B. 2012. *Nipah virus envelope pseudotyped lentiviruses efficiently target ephrinB2+ stem cell populations in vitro and bypass the liver sink when administered in vivo*

VITA

2006	B.S., Genetics; Minor in Economics, University of California, Davis Davis, California
2007	Eugene Cota-Robles Fellowship Recipient
2008 - 2010	Microbial Pathogenesis Training Grant Recipient
2011	UCLA Graduate Student Mentorship Fellowship Recipient
2012	National Institute of General Medical Science Ancillary Program Scholarship Recipient
2012	Mitsuo Takasugi Award Recipient

Publications

Chikere K, Webb N, Chou T, Gorry P, and Lee B. **2012**. *Distinct pathophysiological HIV-1 phenotypes associated with transmission, neutralization resistance and subtype specificity identified by quantitative, high-throughput receptor affinity profiling.* (Submitted)

Chikere K, Chou T, Gorry P and Lee B. **2012**. Affinofile Profiling: *How the Efficiency of CD4/CCR5 usage impacts the biological and pathogenic phenotype of HIV*. (Virology, Special Issue: Review 2012.09.043)

Liu S, Aliyari R, **Chikere K**, Marsden M, Li G, Wang Y, Su L, Zack J, Freiberg A, Lee B, and Cheng B. **2012.***The Interferon-Inducible Cholesterol-25-Hydroxylase Broadly Inhibits Viral Entry by Production of 25-Hydroxycholesterol.* (Immunity, *In Press*)

Palomares K, Pernet O, Vigant F, **Chikere K,** Hong P, Sherman S, Van Handel B, Patterson M, An DS, Lowry WE, Mikkola H, Morizono K, Pyle AD, and Lee B. **2012.** *Nipah virus envelope pseudotyped lentiviruses efficiently target ephrinB2+ stem cell populations in vitro and bypass the liver sink when administered in vivo.*
(Journal of Virology, *In Press*)

Salimi H, Roche M, Webb N, Gray L, **Chikere K,** Sterjovski J, Ellett A, Wesselingh S, Ramsland P, Lee B, Churchill M and Gorry P. **2012.** *Macrophage-tropic HIV-1 variants from brain demonstrate alterations in the way gp120 engages both CD4 and CCR5***.**

(Journal of Leukocyte Biology, 10.1189/jlb.0612308)

Parker Z, Iyer S, Wilen C, Parrish N, **Chikere K**, Lee FH, Didigu C, Berro R, Klasse, P Lee B, Moore J, Shaw G, Hahn B, and Doms R. **2012**.*Transmitted/Founder and Chronic HIV-1 Envelope Proteins are Distinguished by Differential Utilization of CCR5 (Journal of Virology, In Review)*

Duncan R, Roche M, Hamid S, Zappi S, Wilkin B, Jakobsen M.R., Sterjovski J, Flynn, Anne Ellett J, Moore M, **Chikere K,** Lee B, Jubb B, Westby M, Ramsland P.A., Payne R, Churchill M.J., and Gorry P.R. **2013**. *Increased HIV-1 dependence on the CCR5 N-terminus and altered recognition of the CCR5 extracellular loops defines a common mechanism of clinical resistance to the CCR5 antagonist maraviroc in vivo, and exposes a new drug target.* (Manuscript in preparation)

Patent

Chikere, K, et. al. 2012**.** A Novel Rapid And Highly Sensitive Cell Based System For The Detection And Characterization Of HIV. U.S. Provisional Application Serial No. 61/613,129, filed 03/2012.

Oral Presentation

Chikere K, et. al. 2012.Keystone Symposium on Frontiers in HIV Pathogenesis, Therapy and Eradication, Whistler, British Columbia, "High Throughput Receptor Affinity Profiling Reveals Distinct Entry Efficiency Patterns amongst HIV-1 isolates that Correlate with Pathogenic and Biological Phenotypes" *(Invited for plenary session)*

Selected Poster Presentations

Chikere K, et. al. 2011. Keystone Symposium on HIV Evolution, Genomics and Pathogenesis, Whistler, British Columbia. "Rapid and Highly Sensitive Profiling of HIV Receptor Usage Efficiencies using a *Gaussia* Luciferase Based Affinofile Reporter System" *(Updated)*

Chikere K, et. al. 2010. Palm Spring Symposium on HIV/AIDS, Palm Springs, CA. "Rapid and Highly Sensitive Profiling of HIV Receptor Usage Efficiencies using a *Gaussia* Luciferase Based Affinofile Reporter System"

Chapter 1

Introduction

Background and Significance

In the early 1980s, the first cases of a new disease appeared, characterized by a loss of CD4+ cells, development of cancer and opportunistic infections. The new disease was subsequently named Acquired Immune Deficiency Syndrome (AIDS). With a growing number of patients contracting AIDS, society and the medical profession placed great importance on determining the origins of the disease. The causative agent of AIDS was later determined to be Human Immunodeficiency Virus 1 (HIV-1).

Since HIV was discovered to be the causative agent of AIDS, an estimated 40 million or more people have become infected with the virus and more than 20 million have died of AIDS. Approximately 5 million new infections are estimated to occur annually. The overwhelming majority of these individuals live in third world countries with little or no access to antiretroviral therapies. As a consequence, HIV-1 is predicted to become the leading burden of disease in middle- and low-income countries by 2015 (1). Understanding the fundamental concepts of HIV-1 pathogenesis therefore remains an urgent priority.

The process of HIV-1 entry into cells of the immune system begins with the viral gp120 Envelope glycoproteins (Env) binding to cellular CD4 and then subsequently to a coreceptor, which is either of the chemokine receptors CCR5 or CXCR4 (2). Although HIV-1 has been shown to use other receptors *in vitro*, such as CCR3, their importance *in*

vivo is still debatable (166). This initial binding of gp120 to CD4 promotes the exposure of the coreceptor binding site, which facilitates CCR5 or CXCR4 binding. Upon coreceptor binding, the Env undergoes further conformational changes that reorient the gp41 glycoproteins to promote fusion between the viral and cellular membranes, facilitating the deposition of the viral contents into the cytoplasm of the cell, initiating infection of the cell. HIV primarily infects CD4 T cells, which leads to the overall depletion of T cells in the gut and its periphery (3-5). This T-cell depletion is thought to account for the characteristic pathogenesis of the disease, the increase incidents of opportunistic infections (3-5).

Several hosts and viral factors contribute to the clinical outcomes of HIV-1–infected individuals. Among the viral factors, it is unlikely that coreceptor tropism per se accounts for viral pathogenicity. For subjects who predominantly harbor CCR5-using (R5) viruses throughout their disease, a wealth of evidence demonstrates the relative efficiency with which HIV-1 uses CD4 and CCR5 and correlates with the pathogenic potential of the virus (6). Until recently, however, our ability to quantify the efficiency of CD4 and CCR5 usage has been limited by indirect and non-standardized measures for how efficiently a virus can interact with CD4 and/or CCR5. The development of new tools, such as the Affinofile and GGR systems, provides the ability to examine CD4- and CCR5-mediated viral entry efficiency in detail, potentially increasing our understanding of how entry efficiency influences HIV-1 pathogenesis and therapeutics management.

Structures and Steps Involved in HIV-1 Entry

HIV-1 Envelope (Env)

HIV Env proteins are derived from a 160 kDA protein (gp160), which is cleaved by the host protease, furin, into gp120 and gp41 subunits. gp120 is the external surface protein that is responsible for binding to CD4 and CCR5. gp41 is the viral transmembrane protein responsible for membrane fusion. After cleavage, gp120 and gp41 are non-covalently associated as a hetero-trimer on the viral surface. The cleavage of gp160 into its respective subunits is a required step for infectious viral particle formation. On the viral surface, studies have estimated there to be between 10 and 15 trimeric spikes(7). gp120 can be divided into five variable loops (V1–V5), found on the external surface of gp120, and five conserved regions (C1–C5), found on the internal region of gp120.

The sequential receptor binding scheme implemented by HIV has several added advantages when compared to other methods of viral entry. First, the sequential receptor binding scheme shields critical residues and motifs from neutralizing antibodies developed by the immune system. This is evident in the discovery of very few neutralizing antibodies that could bind to CD4- and CCR5-induced epitopes (2). Second, the sequential receptor binding scheme likely prevents the inadvertent triggering of the fusion process, thus reducing the fraction of noninfectious virions due to nonreversible

triggering.

Receptor and Coreceptors used By HIV-1

CD4 is a protein found on hematopoietic cells, including T cells, dendritic cells, and macrophages. CD4 is an immunoglobulin family member made up of four immunoglobulin-like domains, a transmembrane domain, and a short cytoplasmic domain. Closest to the extracellular matrix is the D1, while D4 is closest to the cellular membrane. CD4 is an important receptor in assisting the T-cell receptor (TCR) complex with the antigen-presenting cell.

CCR5 is a beta chemokine protein found on T cells, macrophages, dendritic cells, and microglia cells (8). CCR5 is a seven-transmembrane protein with an extracellular N terminus, three extracellular loops (ECL 2, 4, and 6), three intracellular cytoplasmic loops (ICL 1, 3, and 4), and a cytoplasmic tail. CCR5 is known to interact with beta chemokines, CCL3, CCL4, and CCL4 ligands. CCR5 plays a role in directing the migration of the immune cells in the presence of chemokines.

CXCR4 is an alpha chemokine protein found globally on a wide range of cells, including T cells, macrophages dendritic cells. CXCR4, similar to CCR5, is a seven-membrane spanning protein. CXCR4's natural ligand is SDF-1, which is important in mediating inflammation response. In addition, CXCR4 is important in hematopoietic

stem cell migration into the bone marrow.

HIV-1 Entry (Attachment, Fusion, and Entry)

The multifaceted entry process of HIV into susceptible cells likely begins with the loose interaction of HIV Env with an attachment factor. A myriad of attachment factors exist, such as DC-SIGN and, more recently, $\alpha_4\beta_7$ (9-13), which have been shown to increase infection efficiency through the promotion of virus-cell interaction. Although proven widely using *in vitro* assays, the importance of attachment proteins during *in vivo* HIV infections remains inconclusive.

The CD4 binding site of HIV Env binds to the D1 and D2 immunoglobulin-like domains of CD4. The CD4 binding region of Env is a noncontiguous motif consisting of the hydrophobic regions C2 and C4 and the hydrophilic C3 and C4 regions of HIV Env found on the apex of the Env. The binding of Env to CD4 initiates the rearrangement of the V1/V2 region of Env, exposing and creating the two primary sites for coreceptor binding: the V3 region and bridging sheet. It is also believed that gp120 binding causes conformational changes in CD4 that bring the HIV protein and membrane in closer proximity to the coreceptor, through the joint-like binding of CD4 between the D2 and D3 domains (7).

The interaction between Env and coreceptor begins with contact between the V3 tip and the second extracellular loop of the coreceptor. Evidence for this critical interaction is based on the observation that a single mutation in the V3 region can

abrogate or switch coreceptor preference for the virus (14, 15). The second most important interaction occurs between the base of the V3 loop and/or the bridging sheet and the N terminus of the CCR5(16). Modulation of the N terminus of CCR5 is known to abrogate entry into cells(17). A depiction of the HIV-1 entry process is shown in Figure 1.1.

Coreceptor binding is thought to displace gp120, exposing gp41. Once exposed, the N terminus of gp41 harpoons into the cellular membrane. Heptad repeats 1 (HR1) and heptad repeats 2 (HR2) of the destabilized gp41 are thought to collapse on themselves into a hairpin-like structure, forcing the viral and cellular membranes into a six-helix bundle. The six-helix bundle further forces membrane-mixing and fusion pore formation(18).

Post HIV-1 Entry

Once inside the cytoplasm, the HIV-1 core uncoats, permitting the formation of the reverse transcriptase complex. Reverse transcription is initiated, and the production of double-stranded DNA from the single-stranded RNA occurs. The double-stranded cDNA, integrase, Vpr, reverse transcriptase, and matrix proteins combined, form a pre-integration complex (PIC) that is transported into the nucleus, where the viral cDNA is integrated into the host chromosome. Production of the viral mRNA and genomic RNA is dependent on the expression of the HIV regulatory proteins, Tat and Rev. If Tat and Rev

concentrations are sufficient, production of viral proteins from full-length and spliced mRNA occurs. HIV-1 structural proteins are produced, processed, and shuttled to the cell membrane. The viral genomic RNA is shuttled to the cellular membrane, where it is incorporated into forming virion. The virion buds from the cellular membrane, incorporating the viral envelope and other proteins found on the cell surface. The maturation processes is completed with the final cleavage of the virion.

Stages of HIV-1 Infection and Cellular Tropism

HIV infection can be broadly divided into three main categories or stages: acute/ early, chronic/asymptomatic, and symptomatic/AIDS infection. Acute infection occurs from the initial transmission of the virus through the first 12 weeks of infection. During this period, most HIV-infected individuals suffer a 1–2 week period of flu-like symptoms. After the acute infection stage, the chronic/asymptomatic stage begins, a period that can last from months to years. During this time, the immune system is mounting a response to the virus; however, it is only able to control the amount of virus produced. The symptomatic/AIDS stage occurs due to loss of CD4 T cells and dysregulation of the immune system. As a result, ordinary microbial pathogens may become lethal.

Acute/Early Infection

In the case of sexual transmission, the first cells associated with the virus are resident T cells, Langerhans cells, and dendritic cells due to their location in the genital tract (3, 19, 20). SIV studies have shown that inoculation of SIV in non-human primates leads to the formation of a small founder population of infected T cells in the vaginal canal. This small and likely required population of cells locally expands and, within 48 hours, leads to the dissemination of the virus into the local draining lymph nodes, following soon after to other mucosal and lymph node locations (3). Alternatively, in the

case of intravenous transmission of virus, it is likely that T cells found in the blood and lymph nodes are the initial cells infected (21).

During acute infection, memory CD4 T cells are severely depleted(22). The decrease in CD4 T cells is most prominent in the gut mucosa, where more than 60% of T cells are lost. In addition to infecting CD4 T cells, HIV is known to infect cells of the myeloid-monocyte lineage (MC) and dendritic cells (DC), albeit at a lower rate. Unlike CD4 T cells, MCs and DCs continuously produce low levels of virus, which is thought to allow the cells to escape HIV-induced apoptosis and immune surveillance (4, 23, 24). The infection of these cells likely leads to a long-lasting population of cells that produce low levels of virus. The presence of the virus does elicit a strong CD8 T cell response, marked by expansion of the number of CD8 T cells. While the immune system is unable to clear the virus, it is able to control infection for a period of time.

Chronic/Asymptomatic Infection

During the chronic stage of HIV infection, CD8 T cells and neutralizing anti-HIV antibodies are able to control HIV replication; however, they are unable to clear it. During this period, the virus continually depletes the number of CD4 T cells and spreads to other anatomical locations, such as the distant lymph nodes and the brain(25). This stage is marked by the rapid diversification of HIV-1 sequence, which imparts broader cellular tropism (26, 27).

Symptomatic/Acquired Immune Deficiency Stage

At this point, due to the loss of CD4 T- cells, opportunistic infections occur. It can take up to several years to reach this stage, but once this stage is reached, treatment options are limited, although still effective.

HIV-1 Heterogeneity and the Influence on Cell Host Range

From the moment of productive infection, HIV-1 diversifies its sequence through changes in the nucleotide sequence during the reverse transcriptase process. Between individuals, the virus sequence can differ between 6–10% across the genome. The Env region of HIV has been shown to have the greatest number of non-synonymous sequence changes. These changes lead to the diversification of biological properties of the virus over time in an infected individual or in a continental region.

HIV-1 Heterogeneity in Infected Individuals

A growing number of studies have demonstrated that sexual transmission of HIV is the result of one transmitting virus, which is usually a CCR5-using virus. This gives rise to the phenomenon of HIV sequence diversity being relatively homogenous early in the infection, as infection progresses, heterogeneity of the viral sequences increases. As the sequence diversifies, resistance to neutralizing antibodies also increases, as do entry inhibitors and the cell host range(25, 28-30).

During late stage infection, selected subtypes (mainly B and D) have been shown to undergo coreceptor switch from being primarily CCR5-using to CXCR4-using. This switch in coreceptor usage usually coincides with advancement into AIDS(31, 32).

HIV-1 Subtypes Heterogeneity

HIV-1 is divided into nine different subtypes having from 20–30% amino acid inter-subtype diversity when the Env sequence is compared (33, 34). The distribution of HIV-1 subtypes is shown in Figure 1.2. Epidemiological data reveal that subtype C accounts for over 50% of all HIV infections worldwide (33-35). Additionally, in isolated populations, data reveal that certain subtypes have better transmission rates, while others have increased rates of disease progression (36, 37). These data suggest that there are inherent differences in the pathogenesis of various subtypes of HIV.

A number of limited reports suggest that subtypes C and A have a lower replicative capacity in PBMCs when compared to subtypes B and D in *in vitro* competition assays (38-40). In these reports, subtype specific envelopes and full length clones were compared for their ability to replicate However, this stands in direct contradiction to the epidemiological data that show high prevalence of subtype C. Moreover, reports suggest that these differences in "transmission and replicative fitness" are the result of differences in HIV entry (39-41). Consequently, it becomes important to determine whether or not any subtype-specific receptor- and coreceptor-usage patterns exist.

Methods for Studying HIV-1 Env Heterogeneity Influence on Entry

In early studies of HIV-1 entry, the ability of laboratory-adapted and primary viral isolates to grow on primary cell cultures and CD4+ cell lines (42-44) was used to categorize various isolates. These early studies led to the classification of HIV-1 laboratory and primary isolates according to their ability to grow on primary macrophages (M-tropic), T-cell lines (T-tropic), or both primary cell types (dual-tropic). Soon after CD4 was discovered as a critical receptor for HIV-1 entry, subsequent studies investigated the potential for soluble CD4 to inhibit HIV-1 infection (45-47). Although soluble CD4 was found to be a relatively weak inhibitor of primary HIV-1 isolates and, in some studies, an enhancer of infection, these initial studies unwittingly provided the first evidence for additional cofactors required for HIV-1 entry and showed that differences exist between primary isolates and laboratory-adapted isolates in their ability to utilize CD4. It was subsequently discovered that CD4 alone was not sufficient for HIV-1 entry into cells (48-50).

The discovery of the CCR5 and CXCR4 coreceptors offered an explanation for the observation that beta chemokines and SDF-1 could inhibit HIV-1 infection (51-53) Similarly, relatively early on, different soluble factors were observed to inhibit HIV-1 isolates to different degrees (26, 54). The discovery of the HIV-1 coreceptors ushered in the re-designation of HIV-1 isolates from M-,T-, or dual-tropic to CCR5, CXCR4, or R5X4 viruses based on their ability to enter cells expressing either or both coreceptors

(55). Initial studies that examined the efficiency of HIV-1 entry principally employed soluble factors, proteins, and antibodies as surrogate means to measure HIV-1 Env entry efficiency as a function of the ability of the viral Env to infect cells in the presence of each factor.

The study of CD4 and CCR5 mediated HIV-1 entry in a more physiologically relevant context was facilitated by the engineering of a series of cell lines by the Kabat laboratory (83-85). These clonal cells expressed fixed levels of CD4 and CCR5. The cell lines provided a much needed tool to determine whether a viral isolate required high levels of CD4 or CCR5 or could scavenge relatively low levels of CD4 or CCR5. These proved to be a significant improvement over studies that used transient transfection to generate differing CD4 and CCR5 levels. Although these clonal cells have been used for multiple studies, comparing viral isolates for differences in their relative ability to use CD4 and CCR5, most of the studies report relatively binary information regarding whether a particular isolate can use high or low levels of CD4 and/or CCR5. More importantly, the efficiency of HIV-1 entry into cells within the human host likely results from a complex interplay between the engagement of HIV-1 Env glycoproteins with the CD4 and CCR5 receptors found at varying levels on the surface of susceptible cells. The efficiency at which CCR5 is used for entry may depend on the level of CD4 present, and vice-versa, and this interdependence may vary between different viral isolates from different cohorts.

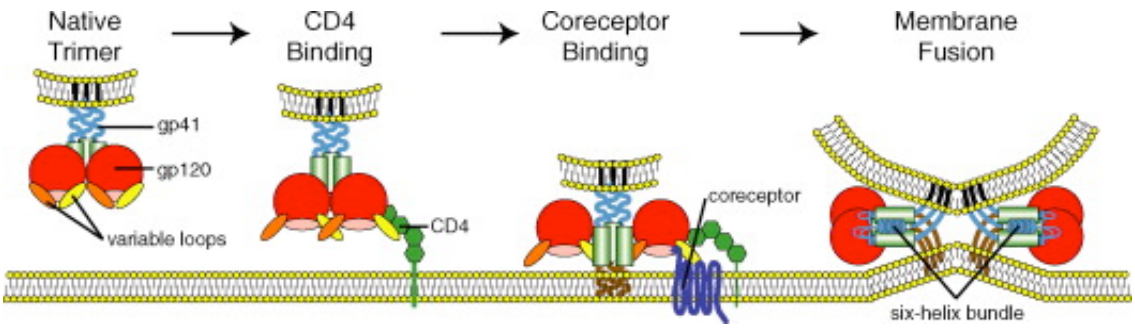

Figure 1-1: Illustration of HIV-1 entry (adapted from Tilton *et al* (56)) HIV entry is initiated with gp120 binding to CD4. Through conformational changes in gp120 and in CD4, gp120 is able to interact with a coreceptor, either CCR5 or CXCR4. Coreceptor binding induces further modifications in gp120, that exposes gp41, promoting viral /cell membrane fusion.

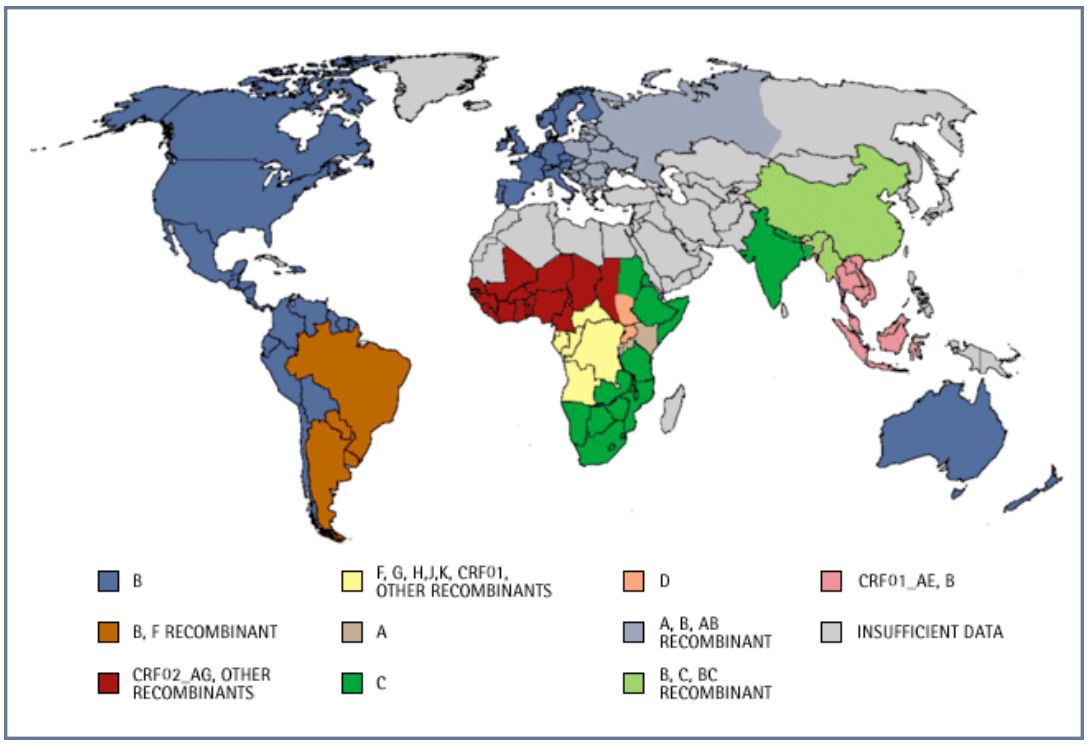

Figure 1-2: Distribution of various HIV-1 subtypes throughout the world (adapted from IAVI Report 2003).

Chapter 2

Material and Methods

GGR Affinofile Assay:

GGR Affinofile cells were seeded in a 96 well plate at 2 X 10^4 cells/well. Simultaneously, cell surface expression of CD4 and CCR5 was induced with 0 to 4.0 ng/mL of Doxycycline and/or 0 to 2 μM of Ponasterone A, respectively. 18hrs later the induction media was removed. Each well of cells was then inoculated with HIV-1 at an MOI of 0.25. The cells were then spinoculated (770 x *g*) for 2 hours at 37° C. Cells were then replaced with fresh D10 media (DMEM with 10% FBS and 1% Pen/Strep). At the indicated timepoints (hours post-infection) used in the various assays, 10ul of supernatant was combined with 10ul of substrate detection buffer (SDB: 50mM Tris-HCL (ph 7.5), 20% glycerol, 0.1 % TritonX-100, 10mM DTT). The supernatant and SDB mix was assayed for *Gaussia* luciferase (gLuc) activity using Coelenterazine substrate in 96-well black plates according to manufacturer's instructions (NEB, Ipswich, MA). gLuc-catalyzed bioluminescence was detected on the TECAN Infinite® M1000 microplate reader via luminescence scanning with an integration time of 8 seconds.

Data Analysis:

The Affinofile infectivity metrics were derived from raw or normalized data using the VERSA (Viral Entry Receptor Sensitivity Analysis) computational platform as previously described (57). The considerations for the use of raw versus normalized data, and the limitations of each have been extensively reviewed (58).

Virus Production:

Envelopes and backbone were obtained through the NIH AIDS and Research and Reference Reagent Program. Pseudovirons were generated by cotransfection of 293T cells with Env-deleted SG3Δenv vector and Env expressing vector at a 3:1 μg ratio with Bioline Bio T transfection reagent. 72 hours post transfection, viral supernatant was collected, clarified by low speed centrifugation and stored at -80°C. The number of infectious virus particles was determined by titration on Ghost HI-R5 cells, as described previously (59).

CD4 and CCR5 cell surface expression:

CD4 and CCR5 surface expression levels were determined by quantitative flow cytometry (qFACS) as described previously (60, 61).

GGR Vector Cloning:

pNL-GFP-RRE was obtained through the NIH AIDS Research and Reference Reagent Program (62, 63). pNL-GFP-RRE was digested with SacI and SalI. The *Gaussia* luciferase gene was PCR amplified from pCMV-Gluc (Promega). The PCR product was digested with SacI and SalI and subsequently ligated into the precut pNL-GFP-RRE vector.

GGR Virus Production:

GGR-expressing lentiviral transducing viruses were produced by cotransfection of 293T cells with pNL-GGR vector, pCMVΔR8.2, and pVSV-G at a ratio of 10:10:1,

respectively, using the calcium phosphate method. Two days post transfection the viral supernatant was collected, clarified by low speed centrifugation, and filtered through a .45μM filter. Viral supernatant was then concentrated by ultracentrifugation at 32,000 x g for 90 minutes and stored at -80C.

GGR Single Cell Cloning:

Affinofile cells were seeded into a 48 well plate at 5 X 10^4 per well. 24 hours later cells were infected with 1 μg of VSV-G pseudotyped GGR virus. Infected cells were then spinoculated for 2 hours at 37 degrees and 770 x g. Cells were washed once with PBS and replenished with fresh D10/B media. Cells were allowed to grow in a 10cm culture dish for three weeks, by splitting and replenishing media every 2-3 days. Single cell clones were then obtained by limiting dilution into 96-well plates. Single cell clones were passaged for three weeks, and clones with stable integration of the pNL-GGR vector were screened for optimal signal to noise ratio of *Gaussia* luciferase activity in the supernatant upon infection with JR-CSF virus, and that still maintained a robust CD4 and CCR5 inducible response to doxycycline and ponasterone A.

T Cell Infection:

Leukopacks from healthy uninfected donors were obtained from the virology core at the UCLA CFAR. For purification of CD4+ T-cells, buffy coats containing peripheral blood mononuclear cells (PBMC) were first Ficoll-purified, and CD8+ T cells were depleted using Invitrogen CD8 Dynabeads. CD8 depleted PBMCs were incubated in

RPMI supplemented with IL-2 , 20% FCS and stimulated with CD3/CD28 coupled Dynabeads for three days. Three days post-stimulation, cells were washed twice and infected with indicated virus. Infection was synchronized by spinoculation for 2 hours at 2,000 rpm at 4 °C. After spinoculation, infectious media was replaced with fresh media. Three days post infection cells were collected and stained for T-cell subset markers CD4 (RPT-4),CD3 (OKT3) , CCR7 (3D12) CD45RA (Hl100) (Ebiosciences), and intracellular p24 (KC57, BD Pharmingen).

Chapter 3

Affinofile profiling: How efficiency of CD4/CCR5 usage impacts the biological and pathogenic phenotype of HIV

Abstract

HIV-1 envelope (Env) uses CD4 and a coreceptor (CCR5 and/or CXCR4) for viral entry. The efficiency of receptor/coreceptor mediated entry has important implications for HIV pathogenesis and transmission. The advent of CCR5 inhibitors in clinical use also underscores the need for quantitative and predictive tools that can guide therapeutic management. Historically, measuring the efficiency of CD4/CCR5 mediated HIV entry has relied on surrogate and relatively slow throughput assays that cannot adequately capture the full spectrum of Env phenotypes. In this review, we discuss the details of the Affinofile receptor affinity profiling system that has provided a quantitative and higher throughput method to characterize viral entry efficiency as a function of CD4 and CCR5 expression levels. We will then review how the Affinofile system has been used to reveal the distinct pathophysiological properties associated with Env entry phenotypes and discuss potential shortcomings of the current system.

Introduction

Since human immunodeficiency virus type 1 (HIV-1) was discovered as the causative agent of acquired immune deficiency syndrome (AIDS), it has been estimated that >40 million people have become infected with the virus and >20 million have died of AIDS. Approximately 5 million new infections occur annually (64). The overwhelming majority of these individuals live in third world countries with little or no access to antiretroviral therapies. Moreover, HIV-1 is predicted to become the leading burden of disease in middle and low income countries by 2015 (65). Understanding the fundamental concepts of HIV-1 pathogenesis therefore remains an urgent priority.

The process of HIV-1 entry into cells of the immune system begins with the viral gp120 envelope glycoprotein (Env) binding to cellular CD4 and then subsequently to a coreceptor, which is either of the chemokine receptors CCR5 or CXCR4 (2). This initial binding of gp120 to CD4 promotes the exposure of the coreceptor binding site to facilitate CCR5 or CXCR4 binding. Upon coreceptor binding, the Env undergoes further conformational changes that reorient the gp41 glycoproteins to promote fusion between the viral and cellular membranes, facilitating the deposition of the viral contents into the cell cytoplasm. The principle steps of HIV-1 entry have been detailed in recent excellent review articles (18, 66, 67).

There are a multitude of host and viral factors that contribute to the varied clinical

outcomes of HIV-1-infected subjects. Amongst the viral factors, it is unlikely that coreceptor tropism *per se* accounts for viral pathogenicity. For subjects who harbor only CCR5-using (R5) viruses throughout their disease, a large body of evidence indicates the relative efficiency by which HIV-1 uses CD4 and CCR5 correlates with the pathogenic potential of the virus (6, 28). For patients with R5 viruses, HIV disease progression has been associated with enhanced macrophage (M)-tropism (68-70), the increased ability to use low levels of CCR5 (6, 70-72), and the increasing relative entry efficiency of the infecting virus (73, 74). Neurovirulence is also correlated with an isolate's ability to use low levels of CD4 and/or CCR5 present on microglial cells (72, 75). Furthermore, R5-viruses derived from late versus early disease not only show increased CCR5 usage but also greater sensitivity to inhibition by various ligands or antagonists of CCR5 (6, 15, 76-78). It is possible, then, that a viral isolate capable of using minute amounts of CCR5 to infect may allow for expanded tropism of target cells, and therefore, increased pathogenicity (79-81). Finally, in the SIVmac model, R5 SIV strains can clearly become virulent without coreceptor switching (82, 83). Thus it seems likely that the relative efficiency of CD4 and CCR5 usage during disease rather than a simple switch from R5 to X4 coreceptor tropism is a better predictor of viral pathogenicity.

Until recently our ability to quantify the efficiency of CD4 and CCR5 usage has been limited by indirect and non-standardized measures such as competition with soluble CD4, specific antibodies, or chemokine receptor ligands. The development of new tools, such as the Affinofile system, provides an unprecedented ability to examine the

mechanics and efficiency of CD4/CCR5 mediated viral entry in greater detail, using a more quantitative methodology, and with a higher throughput format, than was previously possible. The Affinofile system, published in late 2009, has been used in a number of studies that have increased our understanding of how entry efficiency influences HIV-1 pathogenesis and impacts on the clinical management of disease using an evolving class of entry inhibitors.

The Study of HIV-1 Entry

Initial studies of HIV-1 entry examined the ability of laboratory adapted and primary viral isolates to grow on primary cell cultures and CD4+ T cell lines(42-44). These early studies led to the classification of HIV-1 laboratory and primary isolates according to their ability to grow on primary macrophages (M-tropic), T cell lines (T-tropic) or both (Dual-tropic). Although CD4 was discovered as a critical receptor for HIV-1 entry soon after the discovery of HIV-1 as the causative agent of AIDS, it was soon realized that CD4 alone was not sufficient to support HIV-1 entry into non-permissive cells (48-50). A coreceptor was required. When CCR5 and CXCR4 were identified as bona fide coreceptors for HIV entry, they were initially thought to be the cognate coreceptors for all M- and T cell-tropic viruses, respectively, with the implication that dual-tropic isolates used both CCR5 and CXCR4. A new nomenclature re-designated M-, T-, or Dual-tropic HIV-1 strains as R5, X4 or R5X4 viruses based on their ability to enter cells expressing either or both coreceptors (55). Initial studies that examined the efficiency of HIV-1 entry principally employed soluble factors, proteins

and antibodies as surrogate means to measure HIV-1 Env entry efficiency as a function of the ability of the viral Env to infect cells in the presence of each factor.

The study of HIV-1 entry efficiency in a more direct manner was facilitated by the engineering of a series of HeLa cell –based lines by the Kabat laboratory(84-86). A binary library of clonal cells was generated that expressed fixed amounts of CD4 and CCR5: all clones had either high (HI-J, $1x10^5$) or low (HI-R, $1x10^4$) amounts of CD4, but individual subclones within each CD4 library covered a spectrum of CCR5 expression levels. These cell lines provided a much needed tool to determine whether a viral isolate required high levels of CD4 or CCR5, or could scavenge relatively low levels of CD4 or CCR5 for entry, and were a significant improvement upon studies that used transient transfection to generate differing CD4 and CCR5 levels(6, 75). Although these clonal cells have been used for multiple studies comparing viral isolates for differences in their relative ability to use CD4 and CCR5, most of the studies report relatively binary information regarding whether a particular isolate can use high or low levels of CD4 and/or CCR5. More importantly, the efficiency of HIV-1 entry into cells within the human host likely results from a complex interplay between the engagement of HIV-1 Env glycoproteins with the CD4 and CCR5 receptors, found at varying levels on the surface of susceptible cells. The efficiency at which CCR5 is used for entry may depend on the level of CD4 present and vice-versa, and this interdependency may vary between different viral isolates from various cohorts.

Affinofile System

Our understanding of HIV-1 entry has undergone significant refinement in the past two decades. A growing body of evidence suggests that there are nuances of HIV-1 entry phenotypes that have gone unappreciated, largely due to the inherent limitations of tools available to quantify such differences. To better understand how CD4 and CCR5 expression levels influence HIV-1 infectivity, we created the Affinofile system (60). This system consists of a CD4 and CCR5 dual-inducible cell line, and a mathematical approach to quantify the receptor usage pattern and entry efficiency of Env, as a function of CD4 and CCR5 expression. Together this system has provided a quantitative tool to examine and compare HIV-1 entry efficiency in greater detail compared to previous methods. In this review, we will discuss the details of the Affinofile system, and better specify the biological meaning of the metrics used to quantify the entry phenotype of Env. We will then review how different groups have used the Affinofile system to reveal the distinct pathophysiological properties associated with particular Env entry phenotypes, discuss potential shortcomings of the current system, and offer our opinion as to which future studies could benefit from the Affinofile system.

293 Affinofile Cell Line

At the crux of the 293 Affinofile system is a quadruple stable cell line that can be effectively induced to express combinatorial amounts of CD4 and CCR5 receptor levels. We generated this cell line sequentially using the selective reagents and strategy indicated

in **Fig. 3-1 (see legend).** The cell line was single-cell cloned at four different stages to select for a clone with low basal level of expression and inducible expression that covers the physiologic range of CD4 and CCR5 levels. Through this process, we eventually generated a dual inducible cell line where CD4 and CCR5 expression could be regulated independently and simultaneously by varying the concentration of tetracycline and Ponasterone A, respectively. In practice, we have found that the lipophilic tetracycline deriviatives offer a better degree of control over tetracycline itself. For ease of reference, we will simply refer to tetracycline induction unless otherwise stated. Ponasterone A is a potent inducer of the synthetic ecdysone-inducible mammalian expression system that is used in our Affinofile cells (87). Quantitative flow cytometry (qFACS) is used to determine the number of CD4 and CCR5 antibody binding sites (ABS)/cell. In the absence of any inducing reagent, the basal levels of CD4 expression can range from 1,800 to 5,000 ABS/cell (60, 88-90) whereas basal CCR5 levels range between 1,000 to 8,000 ABS/cell (60, 88-91). The published values for the maximally induced levels of CD4 and CCR5 from four to five independent labs are given in the inset tables in **Fig. 3-1**.

While there appears to be some variability in the range of CD4 and CCR5 levels that can be induced, we (and others) have found that the induced CD4 and CCR5 expression levels are generally reproducible within a lab. Nevertheless, the induction range can drift over time even in the same lab ((88)compare to (90)). The variability can be due to procedural differences, cell passage number, and importantly, the nature or

quality of the fetal calf serum (FCS) used. We have recommended the use of dialyzed FCS as the wide spread use of antibiotics (such as tetracyclines) in the agricultural industry might lead to trace amounts in the animal source used for FCS production. In addition, we cannot exclude the presence of cross-reactive small molecules in undialyzed fetal calf serum that might activate the synthetic VgRXR receptor used in the ecdysone-inducible system. Finally, we cannot exclude a systematic error inherent in the manufacturer's standards provided by the different kits used for qFACs (see (92) for a technical discussion of parameters that might affect the accuracy of qFACs measurements). Therefore, it is important that each operator conducts qFACs on the Affinofile cells prior to infection to insure consistent induction. However, Affinofile cells can be passaged for about 3 months before the CD4/CCR5 inducibility becomes unreliable. Regardless of the actual ABS/cell number that is obtained, the functional control for reproducible inducibility is whether a "standard" strain of R5 virus in each lab responds with the same infectivity profile as CD4 and CCR5 is induced. As will be discussed below, the infectivity profile of a given virus across a range of CD4 and CCR5 levels can be quantified by the **V**iral **E**ntry **R**eceptor **S**ensitivity **A**nalysis (VERSA) computational platform. We will show that our analytic method somewhat mitigates the variability inherent in our inducible biological system.

This dual inducible cell line was dubbed the 293 *Affinofile* cells to reflect its potential ability to profile the relative CD4 and CCR5 usage efficiencies of HIV-1 Envs (60), which is a surrogate measure of the relative binding affinities for CD4 and CCR5.

Viral Entry Receptor Sensitivity Analysis (VERSA)

Using 293 Affinofile cells, the infectivity of a given Env, in the context of a pseudotyped reporter virus, can be profiled across 24 to 48 distinct combinations of CD4 and CCR5 expression levels. These various studies are listed in Table 3-1. The infectivity profile of a typical R5 virus infection across 25 distinct levels of CD4/CCR5 expression levels is shown in Fig. 3-2A. To assist in describing and comparing the infectivity data associated with numerous viral Envs from various cohorts and research groups, we created an automated computational web-based tool: **V**iral **E**ntry **R**eceptor **S**ensitivity **A**nalysis at versa.biomath.ucla.edu. For a given Env, the VERSA program permits the rapid distillation of the set of infectivity data points into three metrics that grossly describe the Env's CD4 and CCR5 usage pattern and entry efficiency. Below we will first describe the analytical method used to determine these metrics, and then define the biological meaning of these metrics with respect to how they reflect the entry phenotype of Env. We will then review the studies summarized in Table 3-1 to illustrate how the Affinofile system, and the associated VERSA metrics, can help reveal the distinct pathophysiological Env phenotypes associated with differential CD4/CCR5 usage efficiencies.

Rescaling of CD4 and CCR5 expression levels

Since infectivities were measured across numerous (typically 25-48)

combinations of CD4 and CCR5 concentrations, we sought to reduce the dimensionality of the data into a geometrically meaningful form. First, the experimentally relevant CD4 and CCR5 concentrations (ABS/cell) are rescaled according to $0 \leq x, y \leq 1$:

$$x = \frac{\ln[\mathrm{CD4}] - \ln[\mathrm{CD4}_{\min}]}{\ln[\mathrm{CD4}_{\max}] - [\ln[\mathrm{CD4}_{\min}]} \quad \text{and} \quad y = \frac{\ln[\mathrm{CCR5}] - \ln[\mathrm{CCR5}_{\min}]}{\ln[\mathrm{CCR5}_{\max}] - [\ln[\mathrm{CCR5}_{\min}]}$$

(1)

where "min" and "max" refer to the common minimum and maximum receptor/coreceptor used across all measurements in a given experiment. The variability represented by the differential range of inducible CD4/CCR5 expression levels (when represented in units of ABS/cell) is somewhat dampened by this rescaling, where the minimum and maximum on both the *x* (CD4) and *y* (CCR5) axes are defined as 0 and 1, respectively. The use of natural logarithms for this rescaling also effectively reduces the magnitude of the variable expression levels (see inset tables in Fig. 3-1).

Transformation of the raw infectivity data

The infectivity profile exhibited by a given viral Env across a spectrum of CD4 and CCR5 expression levels, as illustrated by the 3-D column graph in Fig. 3-2A, can be mathematically fitted to a corresponding 3-D surface plot (Fig. 3-2B). The infectivity response as a function of CD4 and CCR5 expression level is described by the continuous polynomial function:

$$F(x,y) = a + bx + cy + dx^2 + ey^2 + fxy$$

(2)

which represents the surface of the plot indicated in Fig. 3-2B. The transformation of the raw infection data into the surface function $F(x,y)$ using normalized infectivity data and rescaled CD4 and CCR5 expression levels, allows for extraction of at least three parameters that quantify additional geometric features of $F(x,y)$. These three biophysically meaningful parameters capture the salient features of the surface plot in Fig. 3-2B, which represents the phenotypic response of Env to varying levels of CD4 and CCR5. We will now describe how these three metrics are derived and computed in VERSA, define the biophysical correlates of these metrics, and specify how they are used to quantify the entry phenotype of Env.

VERSA Metrics

The mean infectivity, *M,* provides a rough estimate of the overall efficiency of entry; it is the mean of the normalized function *F(x, y)* across the entire range of CD4 (x) and CCR5 (y) surface expression levels represented by the x-y plane:

$$M = \int_0^1 \int_0^1 F(x,y)\,\mathrm{d}x\,\mathrm{d}y$$

(3)

M is graphically represented by the height of the square plane (red) indicated in Fig. 3-2B.

Additional geometric features of the surface function $F(x,y)$ can be easily quantified by defining a sensitivity vector

$$\vec{S} = \int_0^1 \int_0^1 \vec{\nabla} F(x,y) \mathrm{d}x\mathrm{d}y \equiv S_x \hat{x} + S_y \hat{y} \tag{4}$$

which represents the average, across the relevant CD4 and CCR5 levels, of the local gradient vector on the surface $F(x,y)$. The vector $\left|\vec{S}\right|$ encodes the overall direction of the infectivity surface $F(x,y)$ and its overall steepness (Fig. 3-2C). This can be represented by two metrics: the vector angle, theta (θ) and the vector amplitude, delta (Δ). Specifically, the overall direction of the sensitivity vector $\vec{S}$ can be defined through the angle θ makes with the $\hat{x}-$axis:

$$\theta = \tan^{-1}\left(\frac{S_x}{S_y}\right) \tag{5}$$

The angle θ measures the overall *relative* sensitivity of the infectivity response between changes in CD4 and CCR5 expression levels; that is, θ is a measure of whether infectivity is more sensitive to changes in CD4 versus CCR5 levels. A virus that is predominantly sensitive to changes in CCR5 levels and not CD4 will have θ near 90º, while the converse (θ near 0º) is true for a virus that is only sensitive to changes in CD4 levels but not CCR5. A virus equally sensitive to changes in both CD4 and CCR5 levels exhibits θ of 45º.

The amplitude of the sensitivity vector, $\left|\vec{S}\right|$ = D, delta, measures the overall "steepness" of the normalized infectivity function *F(x,y)*, averaged across the entire matrix of CD4 and CCR5 expression levels; *it measures the combined rate of increase of infectivity as a function of CD4 and coreceptor concentrations.* It is graphically represented by the length of the sensitivity vector $\vec{S}$ in Fig. 3-2C. This metric was previously termed as the vector "magnitude" (60), which has the unfortunate coincidence of starting with the letter "m", and may lead to confusion with the mean infectivity metric, *M*, which is clearly distinct. Here, we formally designate the three metrics described in Fig. 3-2B-C as mean infectivity (*M*), vector angle (θ), and vector amplitude (D). These designations will be changed accordingly in the updated version of VERSA.

Inputting Normalized or Raw infection Data

VERSA supports the input of normalized or raw infection data (e.g. RLU if using luciferase reporter viruses). The mean infectivity and vector amplitude are dimensionless values, while the θ values are necessarily given in trigonometric units (degrees). Thus, the actual type of infection data used (RLU, or percent positive GFP cells, or percent positive p24 cells etc.) to obtain the VERSA metrics is immaterial as long as the same type of data is consistently used between experiments for comparisons. Given this flexibility, it is important understand the impacts or constraints that various kinds of input data may have on each vector metric. While the vector angle θ is insensitive to the use of

raw or normalized infectivity data, this is not true for mean infectivity (*M*) and vector amplitude (D). For example, since raw RLU data can have a large dynamic range (~3-5 logs), mean infectivity and vector amplitude differences between viral Envs can be magnified. In these cases, Affinofile assays can be sensitive and relative comparisons of Env phenotypes in the same lab are possible and probably meaningful. However, the numbers obtained have no independent meaning outside of a particular comparison cohort in a particular lab. This is because RLUs can be affected by arbitrary factors such as instrumentation sensitivity, integrated time of detection, concentration and quality of the substrate used, variations in room temperature, and a host of other systematic errors that may be particular to the experiment.

On the other hand, if input data is normalized to the maximum infectivity (set at 100%) obtained in each profiling experiment, the comparisons between divergent cohorts and infectivity conditions may be possible. However, normalization assumes that infectivity plateaus at maximally induced CD4 and CCR5 levels for a given Env, which is not always the case. Thus, the VERSA metrics obtained using normalized data may be less sensitive for detecting more subtle phenotypic differences in entry efficiencies. We will discuss specific instances where successful data interpretation has been obtained with one but not the other kind of input data.

Current Publications Using Affinofile System

Next, we review how the Affinofile system has been used to study (1) compensatory phenotypes mediated by unusual mutations and truncations in HIV-1 Env, (2) relationship between differential entry efficiencies and HIV disease pathogenesis, (3) the influence of entry inhibitors on CD4 and CCR5 usage patterns, and (4) the relationship between tropism and CD4/CCR5 usage. These studies are summarized in **Table 3-1**. In any given study, many lines of evidence are usually provided to support the authors' main conclusions. For the purposes of this review, we will mainly focus on the evidence provided by the Affinofile system. We do so in order to illustrate the phenotypic nuances that this system can reveal, and to highlight how the use of Affinofile cells can complement existing methodologies to gain a better understanding on R5 virus tropism and pathogenesis. It is not our intention to suggest that the evidence provided by the Affinofile system is of paramount importance in any given situation. We do, however, hope to show that the Affinofile system is a relatively convenient and high throughput way of evaluating HIV R5 Env in a quantitative and reproducible fashion.

Compensatory phenotypes mediated by unusual mutations and truncations in HIV-1 Env

The gp120 protein of HIV-1 Env includes five conserved (C1-C5) and variable (V1-V5) regions. The conserved regions, found in inner domain of gp120, play a critical role in the function of gp120. The variable regions, found on the outer domain, act as an evolving shield for the virion against the immune response. Of all the variable regions, the V3 loop

of HIV-1 gp120 has long been recognized as being particularly important due to its dual role in protecting the Env from neutralizing antibodies, as well as in determining coreceptor choice (93). Mutations and truncations in V3 usually result in an Env that is unable to promote entry, despite seemingly proper protein folding (94). In (88), the authors discovered that a dual tropic virus, termed R3A, could tolerate a deletion of 15 amino acids that removed the central portion of the V3 loop. This virus with the truncated Env, termed V3(9,9), was severely compromised in its ability to infect SupT1CCR5 cells compared to the parental R3A Env. Subsequent passage of the V3(9,9) virus on SupT1CCR5 cells, which express high levels of CCR5, partially restored the entry efficiency of the virus. Interestingly, the adapted virus, named TA1, retained the V3 truncation while gaining several other mutations and deletions in other areas of the Env.

In a vivid and elegant demonstration, the Doms lab used the Affinofile cells to profile the infectivity of the parental R3A virus, the initial V3(9,9) truncation mutant with compromised function, and the final TA1 virus adapted to grow well on SupT1- CCR5 cells. The infectivity plots (reproduced in Fig. 3-2D) reveal that the initial V3 truncation severely compromised R3A's ability to efficiently use low levels of CCR5—V3(9,9) no longer enter cells at low levels CCR5 (0.016 to0.063 mM Pon A) no matter how much CD4 was provided. This defect was maintained in the adapted TA1 virus Env. Instead, the infectivity profile on Affinofile cells revealed that the partially restored function of the TA1 virus Env was due to an increased ability to use low levels CD4 (0.16 to 0.31 ng/ml minocycline), provided that a sufficient amount of CCR5 was present. The gestalt

of the infectivity profiles between these three mutants is captured by angle metric *q*. Thus, R3A, which responds more readily to changes in CD4 levels (at all levels of CCR5) has a *q* of 22°, while the adapted TA1, which is now more responsive to changes in CCR5 levels has a *q* of 69°. Note that an increase in the angular metric (towards 90°) simply means an increased infectivity response to changes in CCR5 levels (and vice versa for CD4). An increase or decrease in *q* by itself says nothing about whether the change is due to more or less efficient usage of CCR5 or CD4. The angular metric needs to be interpreted in the context of the infectivity profile in order to make statements about receptor usage efficiencies. In this case, the authors rightfully point out that the scale on the *z* axis, representing the efficiency of entry as reported by luciferase activity, clearly indicates that the adaptive mutations in TA1 increased its infection efficiency over V3(9,9) by about 10-fold, mainly by enhancing the its ability to use low levels of CD4. This Affinofile data is consistent with the cumulative results from the myriad other inhibition and time-of-addition experiments conducted in the article.

Relationship between differential entry efficiencies and HIV disease pathogenesis

Using the Affinofile cell line and system, several publications have discovered differences between HIV-1 pathogenic categories that can be ascribed to disparities in entry efficiencies that are not always revealed by conventional entry assays.

In (Lassen*, et al.* (95), the authors used the Affinofile cells to examine a total of 70 Envs derived from chronic progressor (CP) and elite suppressor (ES) HIV+ subjects. The results of these studies revealed that, on average, ES Envs are less efficient at using

both CD4 and CCR5, when compared to CP Envs. Thus, when CCR5 levels were fixed, and CD4 levels varied or vice versa, ES Env pseudotypes achieved a moderately lower level of infection relative to CP Envs. Notably, due to the large variations in IC_{50}s between individual Env clones, even amongst clones from the same patient, there was no significant difference between ES and CP Envs in their sensitivity to CCR5 antagonism (via CCL5 (RANTES) or TAK779) or fusion (Enfuvirtide) inhibition. However, when the infectivity data were reexamined using VERSA (60), the mean infectivity (*M*) and vector angle (*q*) metrics were significantly higher for CP Envs compared to ES Envs. The data also indicate that the increased *M* values of the CP Envs were associated with their increased responsiveness to changes in CCR5 levels (higher *q values*). Together, the Affinofile data suggests that the increased responsiveness of the CP Envs to changes in CCR5 levels was likely due to their increased efficiency of CCR5 usage. Inspection of the infectivity plots confirmed this interpretation. As mentioned earlier, this increased efficiency of CCR5 usage was not evident using conventional inhibitor assays, as ES and CP Envs did not show differential susceptibility to CCL5 (RANTES) or TAK779.

The ability of the Affinofile system to phenotypically segregate potential pathogenic categories is supported by the following two studies. In (96), the authors demonstrated that R5 HIV-1 isolated from cerebralspinal fluid (CSF) of patients with or without HIV-1 associated dementia (HAD) segregated into two phenotypic categories: the ability or lack thereof to infect Affinofile cells induced at $CD4^{low}/CCR5^{high}$ levels.

Viral isolates that can infect $CD4^{low}/CCR5^{high}$ Affinofile cells can also infect monocyte derived macrophages (MDM), and thus are R5 M-tropic. Alternatively, isolates that can only infect $CD4^{high}/CCR5^{high}$ but not $CD4^{low}/CCR5^{high}$ Affinofile cells, can also only infect activated CD4+ T-cells, but not MDM, and thus are R5 T-tropic. The authors observed that CSF-derived viruses isolated from patients with HAD could be either R5 T cell-tropic and/or R5 M-tropic whereas viruses isolated from patients without HAD are invariably R5 T cell-tropic. Although the study is small and involved only eight HAD patients, at least for the cohort examined, it appears that the ability of infect $CD4^{low}/CCR5^{high}$ Affinofile cells at >10% levels relative to $CD4^{high}/CCR5^{high}$ Affinofile cells can be as sensitive a marker for detecting R5 M-tropic viruses as using MDM infection itself. Interestingly, in longitudinal samples from one patient, the authors were able to show that CSF-derived R5 M-tropic Envs that could infect $CD4^{low}/CCR5^{high}$ Affinofile cells could be detected many months prior to subsequent HAD diagnosis.

More recently, Salimi, *et al.*(97) examined brain (BR) and lymph nodes (LN) Envs derived from patients that succumbed to HAD. Using the Affinofile system the authors reveal that R5 macrophage (M)-tropic BR Envs can use limiting levels of CD4 whereas R5 non-M-tropic LN Envs cannot. Furthermore, a combination of all three VERSA metrics clearly revealed inter-subject phenotypic segregation of BR- from LN-derived Envs, which occurred independent of genetic signature alterations. *Inter*-subject genetic signature alterations associated with HIV-1 compartmentalization have not been identified in previous studies, principally because the functional affects of amino acid alterations in gp120 are usually strain-specific. However, the mathematical formulations

and the normalization techniques that were used to derive the VERSA metrics serve to quantify some intrinsic functional properties of Env, which are more likely to be conserved among Envs derived from different tissue sources. These metrics can therefore be used to identify conserved phenotypic Env signatures based solely on the Env CD4 and CCR5 usage profiles.

However, the efficiency of CD4 and CCR5 usage, or the ability to use low levels (co)-receptors, does not always correlate with the *in vivo* pathogenic potential of a viral isolate. In a recent study by (98), the authors isolated and examined an unusual R5 subtype B transmitter/founder (T/F) viral Env with a rare motif in the V3 crown. *In vivo*, this virus replicated very efficiently as shown by a high viral load during the time of acute primary infection (>10^7 RNA copies/ml during Feinberg stage III). However, examination of the Env entry phenotype using the Affinofile system showed that this particular Env used CCR5 very inefficiently, requiring high levels of both CD4 and CCR5 for efficient entry (θ close to 45°). Additionally, mutating the rare GPEK V3 crown motif of the wt T/F Env to the consensus subtype B motif, GPGK, conferred greater ability to use CD4 and CCR5 on Affinofile cells, as well as other cell lines and primary cells. The reversion to the consensus V3 crown motif (GPEK→GPGK) was accompanied by a marked decrease in θ (45° to near 0°**)** and a 10-fold increase in D. Inspection of the infectivity profile (Fig. 10 of the paper) revealed that the GPGK reversion mutant is only sensitive to changes in CD4 levels (hence $\theta \sim 0°$). The increase

in D could be accounted for by the accumulated increase of the infectivity response at low levels of CCR5 (as CD4 levels are increased) where no infectivity response was previously present. The authors suggest the decrease in entry efficiency exhibited the isolated virus may be due to unusual coreceptor usage or abnormal coreceptor protein conformation usage by this virus, which is known to occur *in vitro* (99, 100). This illustrates the possible dichotomy between *in vivo* and *in vitro* results.

Together, these studies demonstrate that the Affinofile system can be effectively used to examine, characterize and/or segregate the entry phenotypes of viruses that are associated with distinct pathophysiological properties *in vivo*.

Influence of Entry Inhibitors on CD4 and CCR5 Usage

The clinical use of CCR5 antagonists was initially accompanied by concerns that resistance could easily occur by coreceptor switching of the virus to the more pathogenic CXCR4-using variants. These concerns were substantiated by the observation that *in vitro* coreceptor switching can occur due to mutations of as little as one amino acid (31). Indeed, phenotypic and/or genotypic testing for coreceptor tropism is required before the use of maraviroc, currently the only FDA approved CCR5 antagonist, in combination antiretroviral therapy (101). In earlier clinical trials, the development of resistance to CCR5 antagonist was confounded by the relative insensitivity of the phenotypic coreceptor tropism test (trofile), which inadvertently allowed the outgrowth of pre-existing X4 or dual-tropic/mixed (D/M) strains (101, 102). In the absence of pre-existing X4 or D/M strains, the preferred pathway to resistance for R5 strains appears to be

evolving the ability use the antagonist bound form of CCR5 rather than *bona fide* coreceptor switching (103). Several groups have used the Affinofile system to shed more light on how HIV-1 circumvents entry inhibition mediated by CCR5 antagonists.

In one of the first studies that used the Affinofile cell line (104), the authors examined how the expression levels of CCR5 can alter the Maximum Percent Inhibition (MPI) of viral isolates resistant to the CCR5 antagonist vicriviroc (VVC). MPI indicates a plateau level of inhibition in the presence of excess of inhibitor, and is a mechanistically distinct from resistance that is attributed to increases in IC_{50}. A MPI effect is indicative that the virus is using the inhibitor-bound form of CCR5. The results of this study demonstrated that the CCR5 expression levels were inversely proportional to the resulting MPI, indicating that increasing levels of CCR5 can compensate for the inefficient usage of the inhibitor-bound form of CCR5 by VVC-resistant viruses. Interestingly, two different VVC-resistant clones independently derived from the drug sensitive parental clone (CC1/85) can exhibit differential levels of VVC-resistance that is revealed by the gradient of the MPI effect observed under varying levels of CCR5 in the Affinofile cells. The authors suggest that the CCR5 levels expressed on different cell lines or primary cells can lead to distinct MPI plateaus, thus altering one's interpretation of the degree of resistance.

These results were recently corroborated by (91), which reported that the commonly used "maraviroc (MVC) sensitive" CC1/85 Env (the parental derivative of

many CCR5-inhibitor resistant clones) has an inherent, albeit low-level, ability to use the MVC-bound form of CCR5. The authors show that when using U87-CD4/CCR5, JC53, TZM-bl cells and PBMC, the MVC-sensitive CC1/85 virus is completely inhibited by saturating concentrations of MVC, hence the MPI is 100% in these cells. However, when the same experiment was done in NP2-CD4/CCR5 cells, which express comparatively higher levels of CCR5, or Affinofile cells induced to express high levels of CCR5, the MPI is 96.2% and 53%, respectively. Moreover, the authors show that systematically decreasing the levels of CCR5 on Affinofile cells gradually increases the MPI to the levels seen in the other cells, thus illustrating a inverse relationship between the MPI and CCR5 expression levels by this ostensibly "MVC-sensitive" CC1/85 Env. The authors suggest that this low level ability to use the MVC-bound from of CCR5, which is only revealed on cells capable of expressing high levels of CCR5, likely predisposes the CC1/85 Env to gaining (cross)-resistance to CCR5 antagonists. The robust inverse correlation of MPI with CCR5 induction levels suggest that the Affinofile cells may detect baseline resistance to CCR5 antagonists with greater sensitivity than the other commonly used cell lines. If validated, this would facilitate the clinical use of CCR5 inhibitors. The gradient of MPI observed as CCR5 is induced on the same cellular background is a particularly useful property. Conversely, U87-CD4/CCR5 cells that are commonly used for phenotypic testing of CCR5 inhibitor resistance may not be sensitive enough to detect the incipient development of CCR5 inhibitor resistance.

Using the Affinofile system, several groups have examined how resistance to CCR5 entry inhibitors influences viral usage of CD4 and CCR5. In (105) and (106) the authors detailed how *in vivo* and *in vitro* derived Envs resistant to the CCR5 antagonists aplaviroc (APL) and MVC, respectively, have modified entry efficiencies in the presence of the inhibitor. In both studies, the authors showed that inhibitor sensitive and resistant Envs had similar 3-D infection plots and vector metrics, highlighted by vector angles ranging from 10° -17°, which implies a below average dependency on CCR5 expression levels. In both studies, examination of the inhibitor resistant clones in the presence of inhibitor resulted in infectivity plots with an overall reduced infection, but more importantly the vector angles shifted to 22.6° -30°. Additionally, the presence of the CCR5 antagonist reduced the non-normalized vector magnitude, which in this case would represent a lower maximum infection compared to experiment done without inhibitor. The standardization procedure implemented in the Affinofile system allows cross study comparison of results through the use of the vector metrics. These results together indicate an overall inefficient usage of the inhibitor bound form of CCR5. In both cases the reduced entry efficiency calculated by the Affinofile cell system correlated with reduced and altered entry into primary cells; more specifically, the Pfaff study showed an altered tropism in CD4 + T cells, while the Roche study showed an altered tropism for macrophages, both due to reduced ability of the resistant virus to interact with the drug-modified form of CCR5.

Finally, in a separate study, (90), examined CCR5 antagonist sensitive and resistant clones isolated from a patient who experienced virological failure on MVC. In the absence of inhibitor, the sensitive and resistant clones had vector angles that were similar, 6.7° and 7.6°, respectively. As expected, in the presence of inhibitor, infection with the sensitive clone was completely abrogated. However, unlike the previous reports, infection with the resistance clone was largely unaffected in the presence of inhibitor, as revealed by a similar vector angle of 7.2°**,** indicating a highly efficient usage of the drug-bound form of CCR5 by this particular resistant HIV-1 variant. Inspection of the infectivity plots confirmed that the MVC-resistant clone remained sensitive only to changes in CD4 levels. This latter study illustrates that CCR5 antagonist resistance can occur with diametrically opposed consequences on entry efficiency.

Cellular tropism and efficiency of CD4/CCR5 usage

In (89) the authors showed that dual-tropic Envs have varying degrees of CCR5 usage in the absence of CXCR4 by infecting Affinofile cells expressing fixed levels of CD4, and varying levels of CCR5. Moreover, the authors show that the ability of dual-tropic Envs to mediate entry into $CD4^{high}/CCR5^{low}$ induced Affinofile cells correlates with the efficiency of CCR5 mediated entry into lymphocytes. These results, coupled with other assays convincingly demonstrate that the use of CCR5 on primary T-cells by dual-tropic Envs is positively correlated with their CCR5 usage efficiency in Affinofile cells. Similarly, in a separate study, (107), were able to show that the ability of R5 primary isolates to enter MDM correlates with the ability to enter Affinofile cells induced

to express low levels of CCR5 and moderate levels of CD4. These results, as well as the reports discussed earlier, show that the Affinofile cell line may be useful as a surrogate to examine entry into primary cells as well as several other cell lines.

Limitations of 293 Affinofile System

One important issue to communicate is that due to the manipulations in engineering the quadruple stable cell line, there are inherent limitations to what assays and additional operations can be done. For example, we have determined that this cell line is not appropriate for conducting beta-lactamase based virus-cell fusion assays because of the relatively high background levels (data not shown). We suspect that the ampicillin resistance genes, on each plasmid used to make the quadruple stable cell line, collectively express enough beta-lactamase to increase the background level of CCF2-AM cleavage. Issues such as this should be considered before the using Affinofile cells outside designated parameters.

As with many cell lines, Affinofile cells express a basal level of CXCR4 that comes from its HEK 293 parentage. Therefore it is critical that the viral Env being examined is fully CCR5 dependent. This can be confirmed by the use of suitable CCR5 inhibitors; infection on the Affinofile cells should be abrogated by a known CCR5-inhibitor, or at least not affected by a known CXCR4-inhibitor. Alternatively, as done by previous authors, saturating amounts of CXCR4 entry inhibitor can be added to each well, preventing the use of CXCR4 for entry. However, if the objective of the experiment is to examine the efficiency of CD4 usage for CXCR4 viruses, the basal level of CXCR4 present in the cell will permit this, as the X4 Env HxB effectively gives a infectivity plot with a vector angle close to zero degrees (unpublished data).

Conclusions

We have reviewed all published studies that have used the Affinofile cells to reveal some new facet of the HIV entry process. We invite the reader to inspect the original articles summarized in Table 3-1. While expression levels of CD4 and CCR5 clearly impacts on the efficiency of R5 HIV-1 entry, they are clearly not the only host cell determinants that impact on the entry process. However, of the various soluble host cell factors that have been described to modulate HIV entry such as galectin-1 (12, 13, 108), galectin-9 (109), and 25-hydroxycholesterol (110), it would be of great interest to see if they do so in a manner dependent on CD4 and CCR5 expression levels. The VERSA website at versa.biomath.ucla.edu continues to accept suggestions as to further improvements, and we are working on developing more robust methods to facilitate more widespread usage of the Affinofile system. The Affinofile system will be deposited in the NIH AIDS Reagent Repository by early 2013.

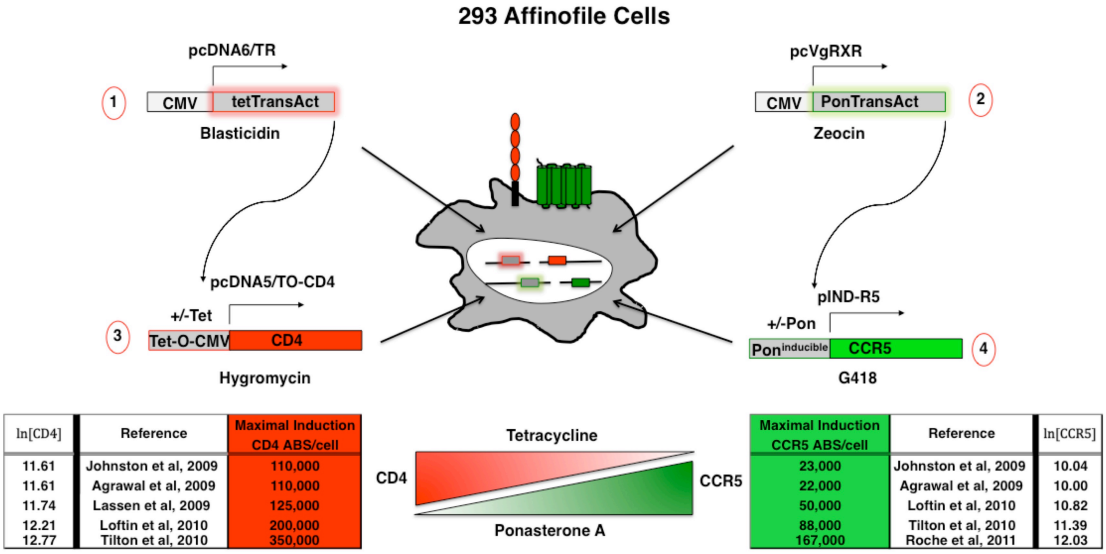

Figure 3-1. Generation of the 293 Affinofile cell line. CD4 expression is controlled by the Tet-On system in which constitutive expression of the tet transactivator from pcDNA/TR **(1)** represses expression from the Tet-O-CMV promoter **(3)** in the absence of tetracycline. In the presence of tetracycline, the tet transactivator is released from the Tet-O-CMV promoter on pcDNA5/TO-CD4 **(3)**, allowing CMV driven expression of CD4. CCR5 expression is controlled by the synthetic ecdysone-inducible system in which the pon A transactivator, VgRXR **(2)**, comprises of the modified heterodimeric subunits of the insect nuclear hormone receptors VgEcR and RXR. VgEcR and RXR are independently driven by constitutive promoters on the same plasmid (pcVgRXR) **(2),** but are shown simply as "ponTransAct" for clarity. In the presence of ponasterone A, the two subunits dimerize (VgRXR) and bind to the pon A inducible promoter on pIND-R5 **(4)** consisting of 5X Ecdysone/Glucocorticoid Response Element (5X E/GREs), driving expression of CCR5. Thus, the addition of varying amounts of tetracycline and/or

ponasterone A induces CD4 and/or CCR5 expression, respectively. The induced surface levels of CD4 and CCR5 is quantified by qFACS as described in the text. The inset tables represent the publications that specifically state the maximal number of CD4 (red) and/or CCR5 (green) Antibody Binding Sites (ABS)/cell induced. The natural logarithms of CD4 and CCR5 cell surface concentrations (ABS/cell) are indicated here for convenience. We will refer to these numbers when discussing the analytic methods used to quantify the efficiency of CD4/CCR5 usage.

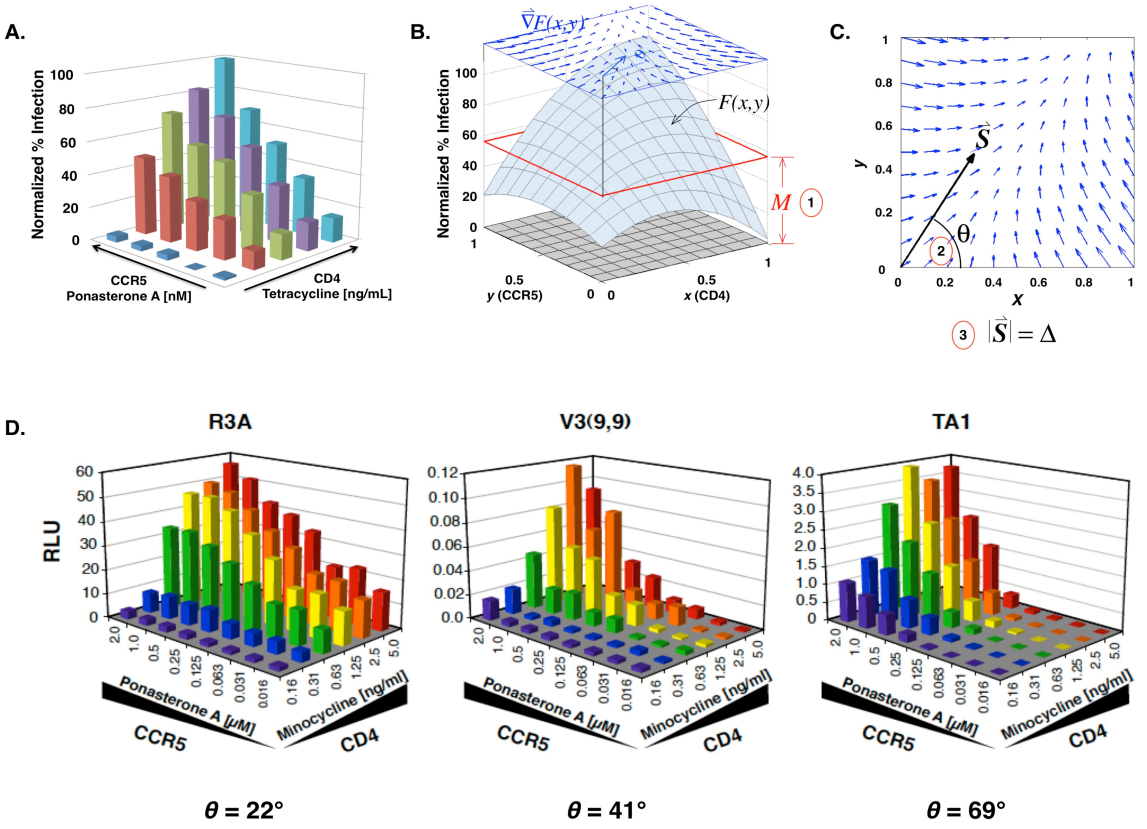

Figure 3-2. Derivation of VERSA metrics. (A) A prototypic R5 Env pseudotyped virus was used to infect Affinofile cells induced with varying concentration of tetracycline and ponasterone A. The infectivity profile generated in (A) can be mathematically fitted to the surface function $F(x,y)$ shown in **(B)**, where x and y are the mathematically rescaled values for the relevant CD4 and CCR5 concentrations (see text for details). Essentially, the surface plot in (B) represents the infectivity response of Env as a function of CD4 and CCR5 expression level, which is described by the continuous polynomial function $F(x,y)$.

As indicated in the text, three biophysically meaningful parameters can be extracted from this surface function that captures the essential phenotypic behavior of Env in response to varying levels of CD4 and CCR5. The three metrics (1) Mean infectivity (*M*), (2) Vector angle (θ), and (3) Vector amplitude (D), are graphically represented in **(B)** and **(C)**. The mathematical formulation of these metrics, their biophysical correlates, and how these metrics can be used to quantify the entry phenotype of Env are detailed in the text. **(D)** A reproduction of Fig. 5 from Agrawal-Gamse*, et al.* (88) illustrating how the nature of the infectivity plot is reflected in the angular metric. See text for details.

Table 1. Summary of Publications using the 293 Affinofile Cells

Category	Title	Env Phenotype Revealed by Use of 293 Affinofile Cells	Use of Full Induction Matrix	Use of VERSA Metrics	Reference
In-vitro Derived Mutations	Adaptive Mutations In A Human Immunodeficiency Virus Type 1 Envelope Protein With Truncate V3 Loop Restore Function By Improving Interaction With CD4	Lab adapted V3 truncation mutant compensates for inefficient CCR5 usage by efficient use of CD4; gains ability to enter cells at low levels of CD4	Yes	Yes	Agrawal et al., 2009
Cellular Tropism	An Altered And More Efficient Mechanism Of CCR5 Engagement Contributes To Macrophage Tropism Of Ccr5-using HIV-1 Envelopes	Ability of Envs to enter low CCR5/moderate CD4 induced cells are positively correlated with macrophage tropism	No	No	Steriovski et al., 2010
Cellular Tropism	Constrained Use Of CCR5 On CD4+ Lymphocytes By R5X4 HIV-1: Efficiency Of Env–ccr5 Interactions And Low CCR5 Expression Determine A Range Of Restricted Ccr5-mediated Entry	Ability to use low levels of CCR5 on Affinofile cells is strongly correlated with R5-mediated entry into primary lymphocytes for R5X4 viruses	No	No	Loftin et al., 2010
Cellular Tropism	Macrophage-tropic HIV-1 Variants From Brain Demonstrate Alterations In The Way Gp120 Engages Both CD4 And CCR5	Affinofile cellls reveal that brain R5 macrophage(M)-tropic Envs can use limiting levels of CD4 whereas non-M-tropic lymph node R5 Envs cannot; VERSA metrics reveal inter-subject phenotypic segregation of brain-from LN-derived Envs	Yes	Yes	Salimi et al. 2012
Pathogenesis	HIV-1 Replication In The Central Nervous System Occurs In Two Distinct Cell Types	R5 macrophage-tropic viruses derived from CSF have enhanced ability to enter $CD4^{low}/CCR5^{high}$ Affinofile cells compared to R5 T-cell tropic viruses dervied from the same compartment	No	No	Schnell et al., 2011
Pathogenesis	Primary Infection By A Human Immunodeficiency Virus With Atypical Coreceptor Tropism	Rare GPEK V3 crown motif found in T/F virus impairs efficiency of CCR5 usage in vitro, despite efficient replication in vivo; reversion to consensus GPGK motif restores ability to use low levels of CCR5 on Affinofile cells	Yes	Yes	Jiang et al., 2011
Pathogenesis	Elite Suppressor–derived HIV-1 Envelope Glycoproteins Exhibit Reduced Entry Efficiency And Kinetics	Envs derived from elite suppressors (ES) use CD4 and CCR5 less efficiently compared to Envs derived from chronic progressors (CP)	Yes	No*	Lassen et al., 2009 *Phenotypes confirmed by VERSA metrics in Johnston et al., 2009
Entry Inhibitor	HIV-1 Predisposed To Acquiring Resistance To Maraviroc (MVC) And Other CCR5 Antagonists In Vitro Has An Inherent, Low-level Ability To Utilize Mvc-bound CCR5 For Entry	Precursor MVC-sensitive Env that gave rise to many MVC-resistant Envs has low-level ability to use MVC bound form of CCR5, which is significantly revealed as levels of CCR5 is lowered on Affinofile cell line	No	No	Roche et al., 2011a
Entry Inhibitor	HIV-1 Escape From The CCR5 Antagonist Maraviroc Associated With An Altered And Less Efficient Mechanism Of Gp120 - CCR5 Engagement That Attenuates Macrophage Tropism	In presence of maraviroc, MVC resistant clone requires higher levels of CCR5 for efficient entry	Yes	Yes	Roche et al., 2011b
Entry Inhibitor	A Maraviroc-resistant HIV-1 With Narrow Cross-resistance To Other CCR5 Antagonists Depends On Both N-terminal And Extracellular Loop Domains Of Drug-bound CCR5	Rare in-vivo MVC resistant isolate can use CCR5 very efficiently, even in presence of inhibitor, provided that an adequate amount of CD4 is present	Yes	Yes	Tilton et al., 2010
Entry Inhibitor	HIV-1 Resistance To CCR5 Antagonists Associated With Highly Efficient Use Of CCR5 And Altered Tropism On Primarycd4+ T Cells	Presence of inhibitor increases sensitivity of MVC-resistant Env to changes in CCR5 levels; this is reflected in altered vector metrics (increased θ and Δ) which corresponded with altered T cell tropism ($T_{EM} > T_{CM}$) in presence of inhibitor	Yes	Yes	Pfaff et al., 2010
Entry Inhibitor	Inefficient Entry Of Vicriviroc-resistant HIV-1 Via The Inhibitor-ccr5 Complex At Low Cell Surface CCR5 Densities	Expression levels of CCR5 influences entry efficiency of VVC-resistant Env in the presence of VVC; resistance is more apparent at high CCR5 levels	No	No	Pugach et al., 2009
Pathogenesis/ Entry Inhibitor	A Quantitative Affinity-profiling System That Reveals Distinct CD4/CCR5 Usage Patterns Among Human Immunodeficiency Virus Type 1 And Simian Immunodeficiency Virus Strains	Original paper describing the Affinofile Cell System and use of the VERSA metrics for profiling CD4/CCR5 usage efficiencies; VERSA metrics confirm and quantify the phenotypic differences between ES and CP Envs described in Lassen et al., 2009	Yes	Yes	Johnston et al., 2009 →The definitions of the VERSA metrics in this review supercedes those given in the original paper
Gene Therapy	Targeted Transduction Via CD4 By A Lentiviral Uses Clathrin Mediated Entry Pathway	Novel Sindbis/Ab envelope transduction of cells is dependent on CD4 expression level	No	No	Liang et al., 2009
Review	R5X4 HIV-1 Coreceptor Use In Primary Target Cells: Implications For Coreceptor Entry Blocking Strategies	Review	No	No	Loftin et al., 2010

Chapter 4

Distinct HIV-1 entry phenotypes are associated with transmission, subtype specificity, and neutralization resistance.

ABSTRACT

The efficiency of CD4/CCR5 mediated HIV-1 entry has important implications for pathogenesis and transmission. The Affinofile HIV-1 receptor affinity profiling system analyzes the infectivity profiles of HIV-1 envelopes (Envs) across a spectrum of CD4/CCR5 expression levels, and Affinofile metrics quantify the infectivity of Env in response to varying CD4/CCR5 levels. The Affinofile system has revealed a divergent array of biologically-relevant Env phenotypes associated with differential CD4/CCR5 usage efficiencies. To facilitate a more rapid and sensitive analysis of HIV-1 entry phenotypes, we engineered a second-generation Affinofile system containing a tat-rev dependent **G**aussia luciferase-e**G**FP-**R**eporter (GGR) that has high-throughput capability for measuring CD4/CCR5 usage efficiency by HIV-1 Env. We validated this second-generation GGR Affinofile system on functionally well-characterized Env mutants, demonstrated that CD4/CCR5 usage was inter-dependent, and established that Affinofile metrics reflect differential entry phenotypes on primary CD4+ T-cell subsets. Next, we showed that subtype B transmitted/founder (T/F) Envs are more dependent on high levels of CD4 for efficient HIV-1 entry compared to chronic Envs, and that this phenotypic difference can be quantified by different sets of Affinofile metrics. Then, we examined 28 acute/early Envs derived from subtypes A-D, and discovered that the various subtypes have overlapping but distinct metrics. Finally, Affinofile profiling of subtype A-D Envs resistant to the broadly neutralizing Env antibodies PG9/PG16 and VRC01 revealed that resistance impairs entry efficiencies. In sum, GGR Affinofile profiling can discern subtle

but real differences in entry phenotypes and may facilitate and refine the study of pathophysiological phenotypes associated with varying HIV-1 entry efficiencies.

INTRODUCTION

Human immunodeficiency virus type 1 (HIV-1) enters target cells through the stepwise interaction of its envelope glycoproteins (Env) with CD4 and a coreceptor, either CCR5 or CXCR4. Receptor binding induces a series of conformational changes that results in fusion pore formation and virus/cell membrane fusion (66). Regardless of HIV-1 subtypes, acutely transmitted viruses invariably use CCR5 (R5). Furthermore, although CXCR4-using (X4, R5X4) viruses can emerge in approximately 40-50% of late stage HIV-1 subtype B infections (111, 112), most HIV-1 infected subjects, particularly those with subtype A and C viruses (34, 113), progress to late stages of infection whilst exclusively harboring R5 viruses.

While many viral and host factors contribute to HIV-1 progression, there is a strong body of evidence that supports some Env determinants of pathogenicity. For example, in patients with R5 viruses, isolates from late stages of infection have a greater capacity to infect macrophages (68-70), which correlates with more efficient usage of low levels of CD4 and CCR5 expressed on these cells (6, 70-72). These late stage R5 isolates can also cause increased levels of cell-cell fusion (114) and CD4+ T-cell apoptosis (115). Late stage brain isolates have also been shown to utilize low levels of CD4 and/or CCR5 for entry (8, 51, 116-122). Therefore, viruses capable of exploiting limiting levels of CD4 and/or CCR5 may have expanded target cell tropism, with possible consequences for pathogenicity (79, 80, 122). Furthermore, viruses that are resistant to the CCR5 antagonists vicriviroc (VVC) and maraviroc (MVC) exhibit

reduced ability to utilize lower levels CCR5 compared to their non-resistant counterparts (123, 124). Finally, the recent characterization of transmitter/founder (T/F) Envs has indicated that these R5 variants enter and replicate in activated primary T-cells but not macrophages (125), underscoring the increasingly evident notion that CCR5 usage is not equivalent to macrophage-tropism (113, 126). Together, these studies show that how efficiently a viral Env engages CD4 and/or CCR5 has a profound influence on pathogenicity, disease progression and resistance to CCR5 antagonists (28, 32, 113). Thus, a more refined understanding of how Env-CD4/CCR5 usage efficiencies develop and differ under alternate evolutionary histories will inform the development and use of HIV-1 vaccines and therapeutics that target HIV-1 entry.

The Affinofile system, based on a CD4 and CCR5 dual-inducible cell line, permits quantitative characterization of HIV-1 entry efficiency across 24-48 distinct combinations of CD4/CCR5 expression levels (57). Multiple groups have used this receptor affinity profiling system (Affinofile) to reveal differential CD4/CCR5 usage efficiencies associated with distinct pathophysiological phenotypes. These studies have shed light on the nature of CCR5-inhibitor resistance (91, 123, 124, 127, 128), the relationship between CD4/CCR5 usage efficiency and cellular tropism as well as disease pathogenesis (129), and the interdependence of CD4 and CCR5 usage (reviewed in (58)). In the Affinofile system, the infectivity of each Env can be examined under 24-48 distinct combinations of CD4 and CCR5 expression levels to determine the set of three parameters that describe its CD4 and CCR5 usage pattern and efficiency of entry. It is the

comparison of these Affinofile metrics between different Envs that are critical for revealing some of the biological insights gained in these studies. Affinofile metrics can be extracted from the infectivity data by an automated web-based computational platform (57), but comprehensive infectivity profiling still requires the examination of each Env under multiple distinct combinations of CD4/CCR5 expression levels.

To gain further insights into HIV-1 entry phenotypes associated with distinct pathophysiologies, we engineered a higher throughput, second generation Affinofile system that would: (1) improve the robustness of the infectivity data obtained, (2) ease the process of data sampling and analysis by permitting sequential time-point sampling of the infected cell supernatant without the need for end-point lysis, and (3) not require the presence of any virus-associated reporter gene, but is still compatible with the use of any live replication competent virus as well as any HIV-1 proviral backbones used for Env pseudotyping. To this end, we transduced Affinofile cells with a tat- and rev-dependent reporter engineered to express green fluorescent protein (GFP) and secrete *Gaussia* luciferase into the supernatant upon infection. This Gaussia luciferase-GFP Reporter (GGR) Affinofile cell line now permits the simple and rapid detection of HIV-1 infection by serial sampling a small volume of supernatant for Gaussia luciferase activity, while taking full advantage of the CD4 and CCR5 inducibility of the original Affinofile cells.

In this study, we comprehensively validated the new GGR Affinofile system and used it to better characterize the physiological meaning of the Affinofile metrics. Then,

we illustrate how the improved, high throughput GGR Affinofile system and associated metrics can be used to reveal distinct Env phenotypes associated with acute transmission, subtype specificity, and neutralization resistance.

Results

Generation and characterization of the reporter GGR Affinofile cell line. To generate our GGR vector, we modified a previously published tat/rev-dependent vector (63, 130) by cloning the *Gaussia* luciferase (gLuc) gene upstream of a GFP reporter gene, linked via an internal ribosomal entry site (IRES) (Fig. 4-1A). Judiciously placed splice donor and acceptor sites, in addition to the Rev-responsive element (RRE) placed downstream of the GFP reporter gene, ensures that only the full-length unspliced reporter mRNA will be translated in the presence of tat and rev, which is provided by commonly used HIV reporter vectors, and replication-competent HIV. Lentiviral VSV-G pseudotypes containing this gLuc-GFP Reporter (GGR) vector were used to transduce early passage Affinofile cells. Stable GGR Affinofile cell lines with optimal properties were single cell cloned as described in methods.

\

We first determined the dynamic range and sensitivity of an optimal GGR Affinofile cell line for detecting HIV infection. Fig. 4-1B shows that GGR Affinofile cells could detect R5-virus infection, as revealed by gLuc activity in the supernatant, as early as 17 hpi when using an MOI of 0.5. Increasing either the amount of viral inoculum used, or the amount of time post-infection before analysis of gLuc activity, increased the sensitivity of virus detection. Thus, while gLuc activity could be detected at 20-fold above background as early as 17 hpi using a relatively high MOI of 0.5, GGR Affinofile cells were also able to detect infection using ~10-fold less virus (MOI 0.0625), and with equal sensitivity, but only at 72 hpi (Fig. 4-1C). To determine if gLuc activity in the

infected culture supernatant reflected the level of virus infection monitored by more familiar assays, such as intracellular p24 staining, we infected GGR Affinofile cells with JR-CSF Env pseudotyped pNL-luc virus at an MOI of 0.25 over a range of CD4 and CCR5 expression levels. At 72 hpi, we simultaneously determined gLuc activity in the supernatant and intracellular p24 levels. Fig. 4-1D-1E, shows that gLuc activity in the infected culture supernatant mirrored the level of infection as reported by intracellular p24 staining.

Defining the parameters that impact on the infectivity metrics used for profiling the efficiency of HIV-1 entry. R5 virus infection of GGR Affinofile cells across a spectrum of CD4 and CCR5 expression levels generated an infectivity profile (Fig. 4-2A) that can be mathematically represented by a surface function $F(x, y)$ (Fig. 4-2B), which describes the infectivity response as a function of CD4 and CCR5 cell surface expression levels (57). The salient features of this surface plot can be captured by three biophysically meaningful parameters illustrated in Fig. 4-2B and C: the mean infectivity level M , and the angle θ and amplitude Δ of the sensitivity vector. The operational definitions of these parameters are indicated in the panels below Fig. 4-2A-C. Their mathematical definitions and formulations have been reviewed recently (58). Together, these three metrics quantitatively describe the phenotypic behavior of a given viral envelope in response to changes across a spectrum of CD4 and CCR5 expression levels.

To determine the precision and robustness of these three metrics across a range of infection and detection parameters, we infected GGR Affinofile cells—induced to express 25 distinct combinations of CD4 and CCR5—with a prototypic R5 virus (BaL), over a 16-fold range of viral inoculums, and monitored infectivity at 24, 48 and 72 hpi. Fig. 4-2D shows that the angle θ of the $\vec{S}$ is relatively insensitive to changes in the amount of viral inoculum used, remaining close to 45° except at the highest level of inoculum used (MOI=2). At high MOIs, the vector angles were more variable between repeats, likely due to multiple infections per cell and other inherent toxicities associated with a high viral inoculum. Notably, at MOIs less than 2, the angles did not change regardless of whether the infectivity data was obtained at 24, 48, or 72 hpi. The mean amplitude of the infection response (D), and the mean infectivity (*M*) were similarly stable across a wide range of MOIs (Fig. 4-2E-F). Similar to the angle metric, the amplitude (D) and mean infectivity (*M*) metrics obtained at a high MOI (of 2) were also more variable, and likely not reflective of the Env's true phenotype. In contrast to the stability of these VERSA metrics obtained using normalized infectivity data, the D and *M* metrics obtained using raw luciferase activity values varied markedly as a function of MOI and time of detection post-infection (Fig. 4-8).

GGR Affinofile cells can be used to characterize a range of distinct Env phenotypes (Fig. 4-9A-C) and the infectivity profile of each Env can be represented by the set of three metrics (Fig. 4-9D-F). Notably, all three metrics (θ, Δ, M) for a given Env can be represented on a polar plot, and the metrics for each Env appear to be highly

reproducible (Fig. 4-9G). These Affinofile derived metrics distill the phenotypic properties of a particular Env from a rich set of experimental data, and hence, may provide a quantitative tool to segregate Envs based on their functional phenotype. A better understanding regarding the physiological correlates of these Affinofile metrics might also help illuminate the biological behavior of HIV-1 Envs, and shed light on the complex determinants of HIV-1 tropism and entry.

Affinofile metrics illuminate the phenotype of functionally well-characterized point mutants. To further validate how Affinofile metrics may reflect changes in CD4/CCR5 usage efficiencies, we examined two point mutants in JR-CSF with well-described, but diametrically opposed effects on CCR5 binding. S142N, a V1 loop mutant (131), confers on JR-CSF the ability to enter a number of T-cell lines with vanishingly low levels of CCR5 (8, 79), while K421D is a "bridging sheet" mutant that reduces the affinity of gp120 for CCR5 (132, 133). Viruses pseudotyped with wild type (wt) JR-CSF, or with S142N or K421D Env mutants were produced and titrated on Ghost-R5 cells where CD4 and CCR5 levels were non-limiting. An equivalent MOI of each pseudotype was then used to infect GGR Affinofile cells expressing 25 distinct combinations of cell surface CD4 and CCR5 levels.

Compared to wt JR-CSF (Fig. 4-3A), the S142N mutant exhibited enhanced entry at every level of CCR5 at or above a specific threshold level of CD4 (0.4 ng/ml Dox) (Fig. 4-3B). This is apparent when comparing the rows of green, yellow, orange and red

bars along the CCR5 axis between Fig. 4-3A and 4-3B. Thus, S142N was more responsive to changes in CCR5 levels than wt JR-CSF. This phenotype is reflected as an increase in θ from 30.5° to 38° for JR-CSF and S142N, respectively. Recall that a relative increase in vector angle (towards 90° as θ approaches the y-axis) indicates that an Env's infectivity is more sensitive to changes in levels of CCR5. A summary of the vector metrics is given in Fig. 4-3D, and illustrated in Fig. 4-3E as a polar plot. For S142N, its ability to use CCR5 efficiently also enhances its infectivity at any given level of CD4; thus, the overall level of infection across the entire matrix of CD4/CCR5 expression levels is also higher. This overall increase in infectivity is reflected in the increase in M from 20 to 40.5 for wt JR-CSF and S142N, respectively (Fig. 4-3D, and also graphically represented by the size of the circle in Fig. 4-3E). The combination of an increase in θ and M supports the conclusion that S142N uses CCR5 more efficiently than wt JR-CSF.

In contrast, K421D showed inefficient entry at the lowest two levels of CCR5 (<20% of maximal infectivity at 0 and 0.25 mM PonA) regardless of how much CD4 was present (Fig. 4-3C), consistent with the known role of this K421 bridging sheet residue in mediating coreceptor interactions (132, 133). Interestingly, at high CCR5 levels (2 and 1 mM PonA), K421D responded more dramatically to increasing levels of CD4 than wt JR-CSF. These phenotypic properties are reflected by the decrease in θ for K421D (23°) compared to wt JR-CSF (30.5°), and a concomitant increase in Δ (50.5 to 69.5 for wt and K421D, respectively) (Fig. 4-3D and 3E). Just as an increase in θ for S142N indicates

that its infectivity is more sensitive to changes in levels of CCR5, a decrease in θ for K41D indicates that on average, the infectivity of K421D is more sensitive to changes in CD4 levels compared to wt JR-CSF. However, the mean infectivity (M) for K421D was only moderately decreased compared to wt JR-CSF (16.5 vs 20, Fig. 4-3D and 4-3E). This likely reflects K421D's compensatory increase in the magnitude of its infectivity response to high CD4/CCR5 levels. Collectively, these results reveal that high levels of CD4/CCR5 may compensate for the inefficient entry exhibited by the K421D mutation at low CCR5 levels.

Affinofile metrics reflect biologically relevant differences in T-cell tropism. To determine how these Affinofile metrics reflect the ability of a viral Env to infect primary CD4+ T-cells, we infected total PBMCs with pseudotyped luciferase reporter viruses bearing wt JR-CSF, S142N or the K421D Env mutants. 4-4A shows that the S142N virus infected PBMCs better than wt JR-CSF while the K421D virus exhibited the lowest level of infection. This pattern reflected the θ and M metrics of the respective viruses, as the limiting parameter on primary CD4+ T-cells are the levels of CCR5 (low), not CD4 (high).

Next, we infected CD3/CD28 stimulated CD4+ T-cells with wt JR-CSF, S142N or the K421D Env pseudotyped virus, and assessed the infection of the indicated CD4+ T-cell subsets via intracellular p24 staining and multiparametric FACS analysis three days post-infection. The overall levels of infection, as determined by the percentage of

p24+ cells, were consistent with the luciferase reporter results observed in Fig. 4-4A with S142N infecting the greatest proportion of cells and K421D the lowest (Fig. 4-4B). In most cases, the majority of p24+ cells were CD4+ T-central memory cells (T_{CM}, CCR7+CD45RO+), with the remainder comprising the effector memory subset (T_{EM}, CCR7-CD45RO+) or the naïve T-cell subset (T_{naive}, CCR7+CD45RO-) (Fig. 4-4C-D). Interestingly, the S142N mutant demonstrated not only an increase in overall infectivity, but also an altered pattern of cellular tropism. Compared to wt JR-CSF, the S142N mutant infected almost 4-fold more naïve T-cells (25.9% vs 6.8%) and 2-fold more T_{EM} cells (21.8% vs 12.4%). As a consequence, S142N infected fewer T_{CM} cells compared to wt JR-CSF (48.5% vs 79.9%) (Fig. 4-4C). Although K421D infected fewer CD4+ T-cells, the CD4+ T-cell subset distribution resembled that of wt JR-CSF infection. Thus, the differential ability to use CCR5 as quantified by the GGR Affinofile assay is reflected in the differential ability of the wt and mutant JR-CSF Envs (S142N) to infect CD4+ T-cell subsets where CD4 expression is relatively high and uniform, where CCR5 expression is low and variable (8, 134). Our results indicate that the differential entry efficiencies quantified by our GGR Affinofile system can reveal biologically relevant properties with regards to primary CD4+ T-cell subset tropism.

Affinofile metrics reveal differences in CD4/CCR5 usage efficiencies between chronic and Transmitter/Founder derived Envs. An accumulating body of evidence indicates that the majority of primary infections are established by a single viral clone (135-137). To discern whether relevant differences in entry efficiencies exist between T/F

and chronic Envs, we used the GGR Affinofile system to examine the infectivity of T/F Envs (isolated from acutely infected Feinberg stage II or III patients) (138), and compared their infectivity metrics (θ, Δ, M) with those from a standard panel of chronic Envs. The specific clones used are indicated in supplementary Table S3. The infectivity profile of each T/F and chronic Env was examined at 25 distinct CD4/CCR5 expression levels (Fig. 4-4), and their infectivity metrics (Fig. 4-5A-C) were obtained via VERSA as described in methods.

Fig. 4-5A shows that T/F Envs have a median θ that is significantly lower than that of chronic Envs (15° vs 25°, p=0.0003), and that this lower θ was also associated with a lower Δ (vector amplitude) (Fig. 4-5C). This correlation indicates that although the infectivity of T/F Envs is more dependent on changes in CD4 levels (lower θ), the gradient of the infectivity response to increasing CD4 levels is still less than that of chronic Envs (smaller Δ), especially at lower, more physiological levels of CCR5. This can be seen in Fig. 4-5D and E, which compares the infectivity response of T/F and chronic Envs as a function of CD4 levels at low (Fig. 4-5D) and high (Fig. 4-5E) levels of CCR5. The wedge plot in Fig. 4-5F also shows that the T/F Envs can be phenotypically segregated from the chronic Envs on the basis of their θ and Δ metrics, at least within the cohort of subtype B Envs examined. Finally, the 2-D contour plots of the averaged infectivity between T/F and chronic Envs across a spectrum of CD4/CCR5 expression levels help highlight the differences indicated by their infectivity metrics: that at low to moderate levels of CCR5 (0-0.5 μM Pon), only the highest level of CD4

allowed efficient entry for the T/F Envs (Fig. 4-5G, compare upper right quadrants). This phenotype is consistent with the observation that T/F Envs, despite being universally CCR5-using, are almost always primary T-cell tropic (high CD4/low CCR5) and not macrophage-tropic (low CD4/high CCR5) (125).

HIV-1 Envs exhibit subtype-specific differences in CD4/CCR5 usage efficiencies.

We next used the GGR Affinofile cells to characterize a panel of 28 subtype A, B, C and D Envs (Table 4-2). The infectivity data for each subtype Env examined are shown in Fig. 4-4. As might be expected from a random panel of subtype Envs, there was a high degree of intra- and inter- subtype variability in all three metrics (Fig. 4-6A). Despite this, significant differences in CD4/CCR5 usage patterns between HIV-1 subtypes can be appreciated. For example, subtype C Envs had the highest θ and M values (Fig. 4-6A), indicating that subtype C Envs, as a group, used CCR5 more efficiently than Envs from other HIV-1 subtypes. The infectivity data confirms that subtype C Envs do, indeed, achieve a higher level of infection in response to increasing CCR5 levels, especially when CD4 levels are limiting (Fig. 4-6B, compare the lower left quadrants). Interestingly, when CCR5 levels are low, subtype C Envs exhibited markedly reduced levels of infectivity compared to Envs from other HIV-1 subtypes, even at the highest CD4 levels (Fig. 4-6B, upper right quadrants). This particular nuance, although evident from the infectivity profile, is not captured by our current Affinofile metrics. Finally, Envs from both HIV-1 subtypes A and C have significantly higher M values than subtype B Envs (Fig. 4-6A). The polar plot in Fig. 4-6C shows that subtype C envelopes can be clearly

differentiated from other subtype envelopes based on their θ and M metrics even if the amplitudes (Δ) do not differ significantly between the subtypes.

Affinofile profiling reveals that resistance to broadly neutralizing antibodies also results in reduced entry efficiency. Recent technological advancements have resulted in the cloning and characterization of numerous broadly neutralizing antibodies (BNabs) with increased potency and breath of coverage compared to the "classical" BNAbs such as b12, 2G12 and 2F5. PG9/PG16 and VRC01 represent two of the major classes of these "next generation" BNabs with non-overlapping epitopes (139-141). Despite the breath and potency of these BNAbs, single point mutations, N160K and N279/280A, can confer resistance to PG9/PG16 and VRC01, respectively (139, 141). N160 and N279/280 are highly conserved residues across HIV-1 subtypes suggesting that these residues are under selective pressure.

To determine whether these BNAb resistance mutants have any consequence on the entry efficiency of the resulting Env, we generated resistant N160K and N279/280A mutants in 24 Envs representing subtypes A through D, and examined their CD4/CCR5 entry efficiencies in the GGR Affinofile system. Fig. 4-7A, B and C, shows the infectivity profiles for all 36 wt Envs, N160K, and N279/280A mutants, each Env examined across 25 distinct CD4/CCR5 expression levels. Compared to the wt counterparts, the PG9/PG16 (N160K) and VRC01 (N279/280A) resistance mutations reduce the efficiency of entry; both requiring higher levels of CD4 and CCR5 to achieve

similar levels of infection as their wt counterparts. This can be appreciated by comparing the CD4/CCR5 expression level combinations that give rise to low levels of infection (green areas), or conversely, those that give rise to the highest level of infection (red areas), between the wt and mutant Envs (Fig. 4-7A-C). This phenotype of reduced entry efficiency across all subtypes tested is quantitatively reflected in the M values, where the average M for PG9/PG16 and VRC01 resistant mutants is lower than that of their wt counterparts (Fig 4-7D and 4-7E). However, due to marked variability when comparing across all HIV-1 subtypes, only the difference between VRC01 resistance mutants and wt reached significance ($p=0.0065$). Our results suggest that resistance to BNAbs comes at the cost of reduced HIV-1 entry efficiency, and provides one functional explanation for the high conservation of these residues across HIV-1 subtypes. Both these reasons bode well for vaccine design that will elicit these kinds of BNAbs.

Discussion

The Affinofle system and associated VERSA metrics have provided investigators a more quantitative method to characterize viral entry efficiency as a function of CD4 and CCR5 expression levels. Quantitative comparisons of these three VERSA metrics—Mean infectivity (*M*), Vector Angle (θ) and Amplitude (D)—have facilitated our understanding of how CD4/CCR5 usage efficiencies correspond to distinct Env phenotypes associated with resistance to CCR5-inhibitors, and the myriad of *in vitro* or *in vivo* selective pressures that result in differential or altered cell tropism (57, 58, 90, 124, 127, 128, 142, 143) .

Although VERSA metrics should reflect an intrinsic phenotypic property of Env, it is not known how VERSA metrics can be affected by basic experimental parameters such as the amount of viral inoculum or whether raw or normalized infection data are used for input. Our high-throughput GGR Affinofile cells, where infection can be monitored by serial sampling of the infected cell supernatant, allowed for a rigorous analysis of such parameters. Our results demonstrate several salient points: (1) if normalized infectivity data are used, all three VERSA metrics are relatively stable at MOIs of ~0.1 to 1.0—this range likely falls between a viral input that gives enough signal to detect differences in CD4 and CCR5 usage, whilst not being too high as to promote entry of more than one infectious unit per cell (Fig. 4-2), and (2) if raw infectivity data are used, *M* and D varies positively with increasing MOI, but θ remains similar to the value determined using normalized data (Fig. S1). Thus, comparison of

VERSA metrics across divergent panels of Envs is best achieved using normalized infectivity data as input (Fig. 2 and S2). However, normalized data may limit the sensitivity of the VERSA metrics to differentiate Env phenotypes (reviewed in (58)). Nevertheless, intra-lab comparisons of VERSA metrics obtained using non-normalized data are likely to be meaningful if the parameters of infection and detection are held constant. The use of our clonal GGR Affinofile system will help further standardize the conditions used for obtaining VERSA metrics.

*Efficiency of CD4/CCR5 usage and T cell subset tropism***.** A salient feature of our GGR Affinofile system is the ability to distill the aggregate entry phenotype of Env into three metrics. Here, we demonstrate that these VERSA metrics reflect biologically relevant phenotypes for wt JR-CSF Env, and two point mutants (S142N and K421D) known to modulate its affinity for CCR5. Specifically, S142N, which had larger θ and M values relative to wt JR-CSF, also infected total PMBCs better, and exhibited an expanded CD4+ T-cell subset tropism marked by an increased infection of naïve T-cells (Fig. 4-4C**,** 25.9% vs 6.8%). Naïve T-cells have undetectable levels of CCR5 by FACS (134, 144, 145), much like the CCR5 "FACS-negative" T-cell lines (Molt 4 and SupT1) that the S142N Env virus is known to infect in a CCR5-dependent manner (79). Conversely, K421D, which had the smallest θ and M values, also infected PBMCs with the least efficiency, and lacked the expanded tropism seen with the S142N mutant.

What is the utility of being able to quantify the efficiency of CD4/CCR5 usage through a set of standardized metrics? For S142N, the ability to use lower levels of CD4 and CCR5 for entry correlates with its expanded tropism for naïve CD4+ T cells. HIV-1 preferentially infects memory, rather than naïve CD4+ T cells (146-148). However, loss of naïve T-cells is also clearly associated with immune system decline and disease progression, but is thought to be due to secondary factors such as lymph node fibrosis, which destroys the regenerative niche required for maintaining naïve T-cells (149, 150). To our knowledge, the infection of naïve T-cells in lymph nodes of late stage patients have not been directly examined. Since late stage R5 isolates are also more efficient in using low levels of CD4 and CCR5 for entry (6, 78), it is possible that infection of naïve T-cells by late stage R5 Envs might contribute to the diminishment seen. Currently, macrophage-tropism is widely used as a surrogate measure for R5 Envs that can use low levels of CD4 and/or CCR5 for entry (151), but it is not clear whether macrophage-tropic Envs also have an expanded tropism for naïve CD4+ T-cells. Use of our GGR Affinofile system and VERSA metrics to characterize extended panels of R5 macrophage-tropic and R5 non-macrophage tropic Envs will help shed light on this important issue related to R5 Env pathogenesis. Intriguingly, even a binary read-out, such as an increase ability to infect $CD4^{low}/CCR5^{high}$ relative to $CD4^{high}/CCR5^{high}$ Affinofile cells, has been observed in CSF-derived R5 Envs from a patient many months *before* the patient developed HIV associated dementia (152). Thus, it would also be of interest to determine the VERSA metrics of R5 Envs from a broader array of longitudinal cohorts, and evaluate whether a certain pattern of VERSA metrics is predictive of pathogenicity or disease progression.

T/F and chronic Envs. ~70-80% of heterosexual or IV drug use HIV-1 transmission cases are established by a single transmitted/founder (T/F) virus clone (138, 153-156). Concerted efforts have been made to discern genotypic and phenotypic differences between T/F and chronic Envs, since such differences may inform vaccine design, shed light on the biology of HIV-1 transmission and pathogenesis, or facilitate development of strategies to prevent HIV-1 transmission (135, 136). While T/F Envs are enriched in genotypic features such as an overall reduction in the number of potential N-linked glycosylation sites (PNGS) (157), no unique genetic signatures can be ascribed only to T/F Envs. Phenotypic differences between T/F and chronic Envs also appear subtle: no overt differences were found in multiple assays such as entry/fusion efficiency into cells expressing high or low levels of CD4/CCR5, infection of CD4+ T-cell subsets, dendritic cell mediated *trans*-infection, and sensitivity to entry inhibitors (158-162). However, moderate increases in sensitivity to neutralization by the CD4 binding site antibody b12, and more marked resistance to sCD4 inhibition, have been reported for some cohorts of subtype B T/F Envs relative to chronic Envs (160, 161).

Our Affinofile profiling of a small panel of subtype B T/F and chronic Envs reveals moderate but significant differences in the CD4/CCR5 usage efficiencies. The differences are subtle, but the combination of θ and D clearly distinguishes the T/F Envs from the chronic Envs (Figure 4-5F), and also indicates that T/F Envs are less efficient at using CD4 (lower θ *and* D). The implied decrease in CD4 binding affinity exhibited by

the T/F Envs in our study is consistent with the aforementioned cohort of T/F Envs with increased resistance to sCD4 neutralization (161). However, sensitivities to sCD4 or b12 neutralization are surrogate markers for CD4 utilization, and neither directly measures the true entry phenotype of a virus with regards to CD4/CCR5 usage efficiency. sCD4 sensitivity does not always correlate with gp120-CD4 binding affinity ((163) and references therein), and b12 neutralization can be affected by epitope changes that don't affect CD4 binding (164). For example, T/F Envs are enriched for the loss of a particular N-glycan site, mediated by *not* having a Thr at position 415 (T415X), that allows better access to key b12 binding residues at positions 417-419 (157). Thus, the increased sensitivity to b12 neutralization may be associated with a genetic signature (T415X) enriched in T/F Envs, rather than being a general property of T/F Envs *per se*. In our cohort, there is no obvious relationship with sensitivity to b12 or sCD4 neutralization even though all but one T/F Env have the T415X signature (Table S3). Yet, infectivity profiling across the full spectrum of CD4/CCR5 expression levels and VERSA metrics were able to reveal differences in entry phenotypes between T/F and chronic Envs. Clearly, our findings need to be extended by examination of larger groups. However, recent evidence suggest that T/F Envs and chronic Envs can differ in their ability to use the maraviroc bound form of CCR5, but this phenotype is more obviously revealed only on $CD4^{high}/CCR5^{high}$ Affinofile cells (165, 166). The ability to use MVC-bound form of CCR5 in this case is likely a surrogate marker for an expanded promiscuity in the use of CCR5 conformations. These results are not inconsistent with our current findings and

suggest that the full Affinofile profiling may have the requisite sensitivity to reveal subtle but real differences in Env phenotypes related to HIV-1 transmission.

*Subtype Env specific differences***.** Subtype C viruses, in pure or recombinant forms, comprise the majority of HIV-1 infections worldwide, and is associated with heterosexual transmission. Subtype Envs do exhibit phenotypic differences as evidenced by a significant correlation between CCR5 and FPRL1 usage for subtype A and C Envs, and between CCR5 and CCR3 usage only for subtype B Envs (167). These differences in alternate coreceptor usage in highly permissive NP2/CD4/CoR cells likely reflects the different evolutionary histories of the subtype Envs, and is more apt to be a surrogate marker for the efficiency of CCR5 usage or the use of a specific conformation of CCR5.

Subtype C Envs are indeed transmitted more efficiently *in utero* than subtype A or D Envs (168). Thus, it seems reasonable to intuit that subtype C Envs are more efficient in cell entry and/or transmission. However, *in vitro* and ex vivo assays indicate that viruses bearing subtype C Envs are invariably outcompeted by other subtype Envs in PBMC outgrowth assays (38, 73, 169). This decrease in replicative fitness presents an explanatory conundrum that may be illuminated by our Affinofile data. Our GGR Affinofile profiling results indicate that the average subtype C Env used CCR5 more efficiently than the other subtype Envs, but this was only true at low to moderate levels of CD4 (Fig. 4-6B, compare LL quadrants). At high levels of CD4 but lower (more physiologic) levels of CCR5 such as would be present on activated PBMCs (Fig. 4-6B,

compare UR quadrants), subtype C Envs are *less* efficient at entry. The difference in entry efficiencies between subtype C and the other subtype Envs, reflected in the UR and LL quadrants of their infectivity profile (Fig. 4-6B), might provide an explanatory framework that accounts for both the decreased replicative fitness observed *in vitro* (on activated PBMCs), and the notion that subtype C Envs must be more efficient at entry and/or transmission at some level. The VERSA metrics and infectivity profiles in Fig. 4-6 quantify a genuine phenotypic difference between subtype C and other subtype Envs, and can serve as a reference point for future studies into their physiological correlates. Despite the small number of Envs examined (n=28, 7 for each subtype), these are well-characterized reference subtype Envs, chosen carefully to represent acute/early infection isolates, so as to compare the "ancestral phenotypes" common to each subtype before disease stage-specific selective pressures come into play (Table 4-1).

*BNAb Resistance mutations***.** Our Affinofile profiling suggests that mutations in Env that confer resistance to at least two BNAbs come at a fitness cost. This is perhaps not surprising since the mutated residues N160 and N279/280 are themselves highly conserved amongst HIV-1 subtypes suggesting that selective pressures are at play. Nevertheless, we engineered mutations into 12 Envs from 4 different subtypes, and observed a general trend that both the N160K $(PG9/PG16)^R$ and N279/280A $(VRC01)^R$ mutations decrease the mean infectivity without a significant impact on the other two VERSA metrics. While the $(VRC01)^R$ mutation near the CD4bs (141) was likely to affect entry efficiency, it was not clear that the $(PG9/PG16)^R$ mutation would. Indeed, the

impact on entry efficiency is much greater for the VRC01)^{R} mutation compared to the (PG9/PG16)^{R}. It remains to be seen if resistant-mutations to the latest generation of BNAbs all come at a fitness cost or whether they are epitope dependent. For the first generation of BNAbs such as b12, 2F5, and 2G12, mutations that disrupt their epitope can result in Envs with subtle to no differences in entry efficiencies (170, 171). We recognize that our results regarding the impact of BNAb resistant-mutations on entry efficiency need to be confirmed and expanded with a larger set of mutants and antibodies. Our GGR Affinofile system provides an appropriately high throughput methodology to facilitate such future studies. The results from these further studies might inform the engineering of the most appropriate immunogen that will elicit the BNAbs that will best constraint the development of resistance.

In sum, Affinofile profiling not only interrogates the functional plasticity of HIV-1 Env in response to a spectrum of CD4 and CCR5 expression levels, it provides and distills the multi-dimensional data that captures this functional plasticity. Thus, Affinofile profiling may be a more sensitive method for discerning subtle but real differences in entry phenotypes that are not detected by other standard assays for evaluating CD4/CCR5 usage efficiency. A database of carefully curated VERSA metrics will help standardize the phenotypic characteristics of Envs from multiple cohorts and facilitate future studies into pathophysiology associated with Env phenotypes. We are currently creating a panel of GGR Affinofile cell lines that express alternate coreceptors as well as hybrid and mutant CCR5 that will help extend and refine such studies.

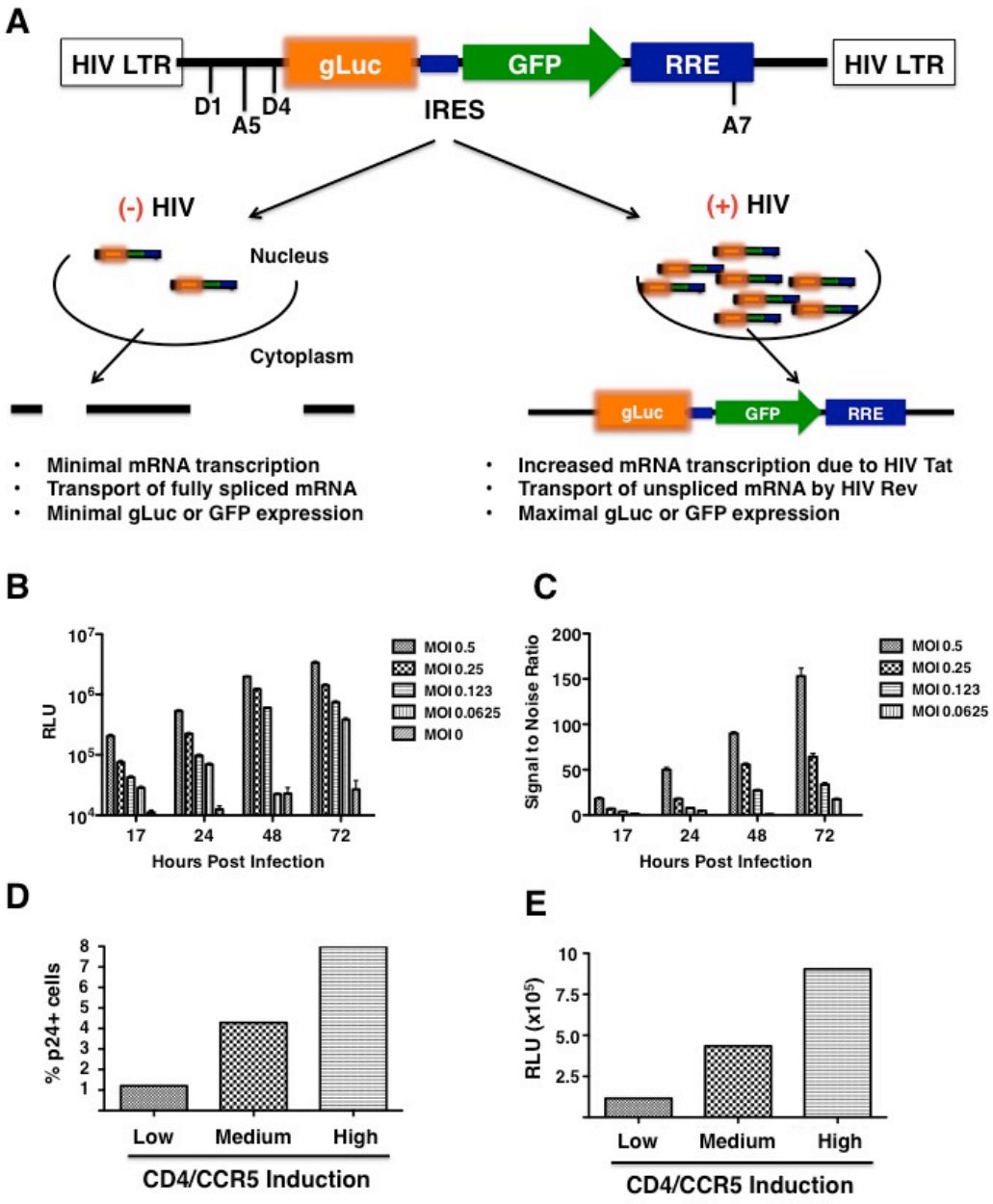

Figure 4-1. Generation and characterization of the GGR Affinofile Cell Line. (A) Schema of the tat-rev dependent *Gaussia* luciferase (gLuc)-GFP reporter (linked via an IRES sequence) vector as described in the text. The rationale for the tat-rev dependent

production of gluc and GFP is illustrated. **(B) and (C)** GGR cells were maximally induced with doxycline (Doxy, 4ng/ml) and ponasterone A (PonA, 4 mM) at the time of their seeding in 96-well plates. 16-21 hours post-seeding/induction, cells were infected with wt JR-CSF virus at varying multiplicities of infection (MOI). The titer of the virus was previously determined on stable CD4/CCR5-expressing GHOST cells. At 17, 24, 48, and 72 hpi, 10 ml (out of 150) of the infected cell supernatant was removed and analyzed for gLuc activity as per manufacturer's instructions. Luciferase activity (measured as relative light units, RLU), and the corresponding signal:noise ratios at each data point are shown in (**B)** and (**C),** respectively. Mock-infected cell supernatant served as the background signal. Mean +/- S.D. from duplicate samples are shown. (**D)** and **(E)** GGR cells were induced at high (3.2ng/mL Doxy, 2 mM PonA), medium (1.6ng/mL, 1um PonA), and low (0.4ng/mL Doxy, .25μM PonA) levels, and infected as above with pseudotyped virus at an MOI of 0.25. Three days post-infection, supernatant was collected and analyzed for gluc expression **(E)**, while cells from each well were individually processed for intracellular p24 staining **(D)** as described in methods. Data shown is representative of two independent experiments.

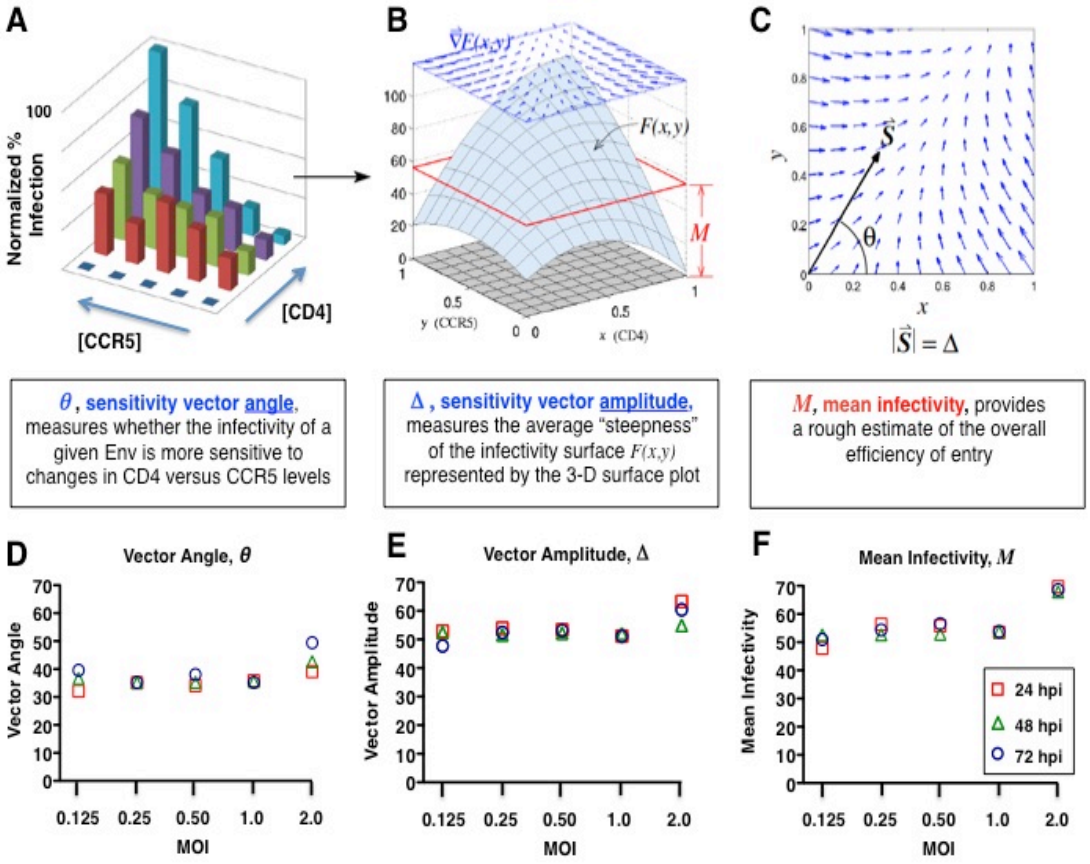

Figure 4-2. Defining the parameters that impact on the infectivity metrics used for profiling the efficiency of HIV entry. (A) Infectivity of an R5-virus (BaL) monitored across 25 distinct combinations of CD4 and CCR5 expression levels. The normalized infectivity profile is shown as a 3-D bar graph with the gLuc activity obtained at the highest CD4 and CCR5 induction level set at 100%. **(B)** This data can be transformed into a corresponding 3-D surface plot by fitting the infectivity profile to a continuous polynomial function *F(x,y)* as previously described (60). The surface function F(x,y) describes the infectivity response of Env as a function of CD4 and CCR5 expression

levels, and the resulting 3-D surface plot can be represented by three metrics that reflect distinct phenotypic properties of the infecting virus envelope: (i) the mean infectivity level (***M*),** (ii) the sensitivity vector angle (***θ***) and (ii) amplitude (**Δ**). The graphical representations of these three metrics with respect to the 3-D surface plot are indicated in **(B)** and **(C).** For clarity, the operational definitions of these metrics, and what they measure with respect to the infectious phenotype of Env, are also indicated. These definitions supersede those given in Johnston *et al* (60) as they more accurately described the phenotypic properties of Env that these metrics represent. **(D-F)** Bal was used to infect GGR Affinofile cells at 5 different MOIs, each MOI across 25 distinct combinations of CD4 and CCR5 expression levels. Every infection condition was monitored at 24, 48 and 72 hpi by sampling supernatant for gLuc activity. Each infection data point was performed in triplicates. Raw luciferase activity values were normalized to that obtained at the highest CD4/CCR5 induction levels (set as 100%). Normalized data were then used to determine the vector angle, θ **(D)**, vector amplitude, Δ **(E)**, and Mean infectivity level, ***M*** **(F)** via the VERSA computational platform as described in methods.

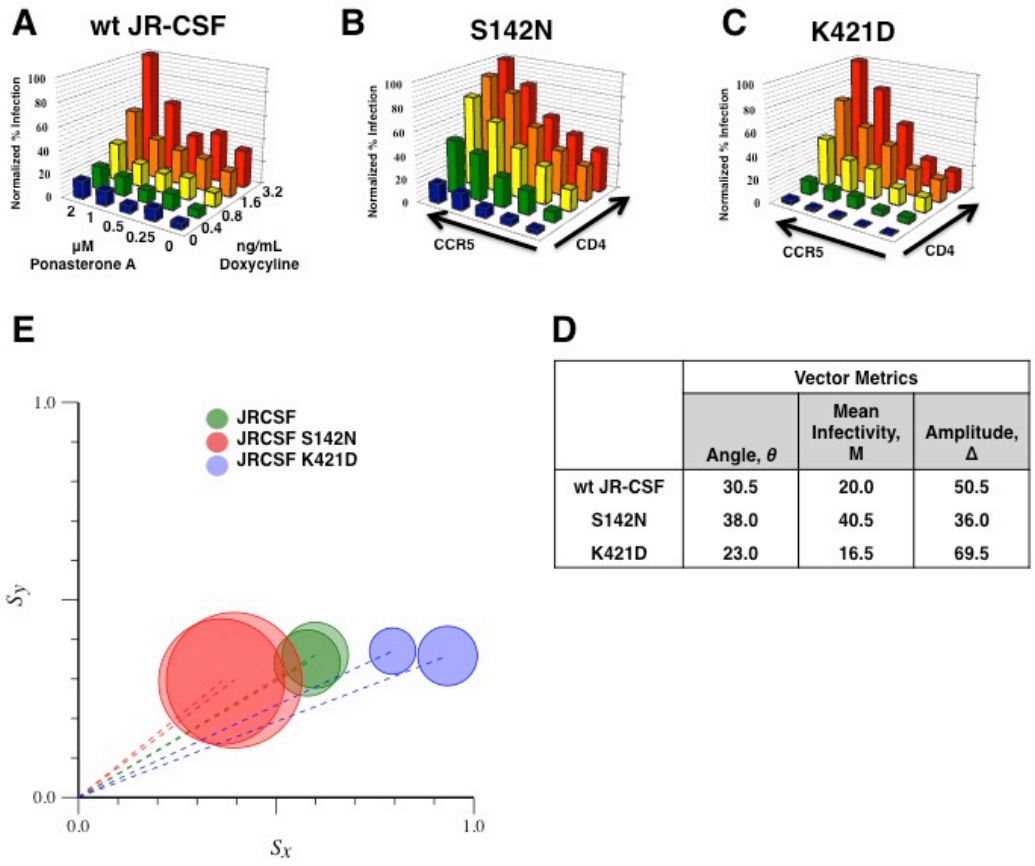

D

	Vector Metrics		
	Angle, θ	Mean Infectivity, M	Amplitude, Δ
wt JR-CSF	30.5	20.0	50.5
S142N	38.0	40.5	36.0
K421D	23.0	16.5	69.5

Figure 4-3. Affinofile metrics further illuminate the phenotype of well-characterized point mutants. (A) Infectivity profile of wt JR-CSF (R5) envelope, and two point mutants: **(B)** S142N and **(C)** K421D, previously shown to enhance or perturb CCR5 usage, respectively. Data shown is a representative of two experiments. **(D)** Table of the average metrics obtained from **(A-C)** and graphically shown in **(E)**. The infectivity profile of each Env was independently repeated twice. **(E)** Polar plot representing the metrics obtained from mathematical analysis of the infectivity profile in **(A-C),** using the VERSA program as described. The vector angle (θ) is the angle between the x-axis and

the dotted line. The vector amplitude (Δ) is represented by the length of the dotted line. The mean infectivity (M) is represented by the size of the circle.

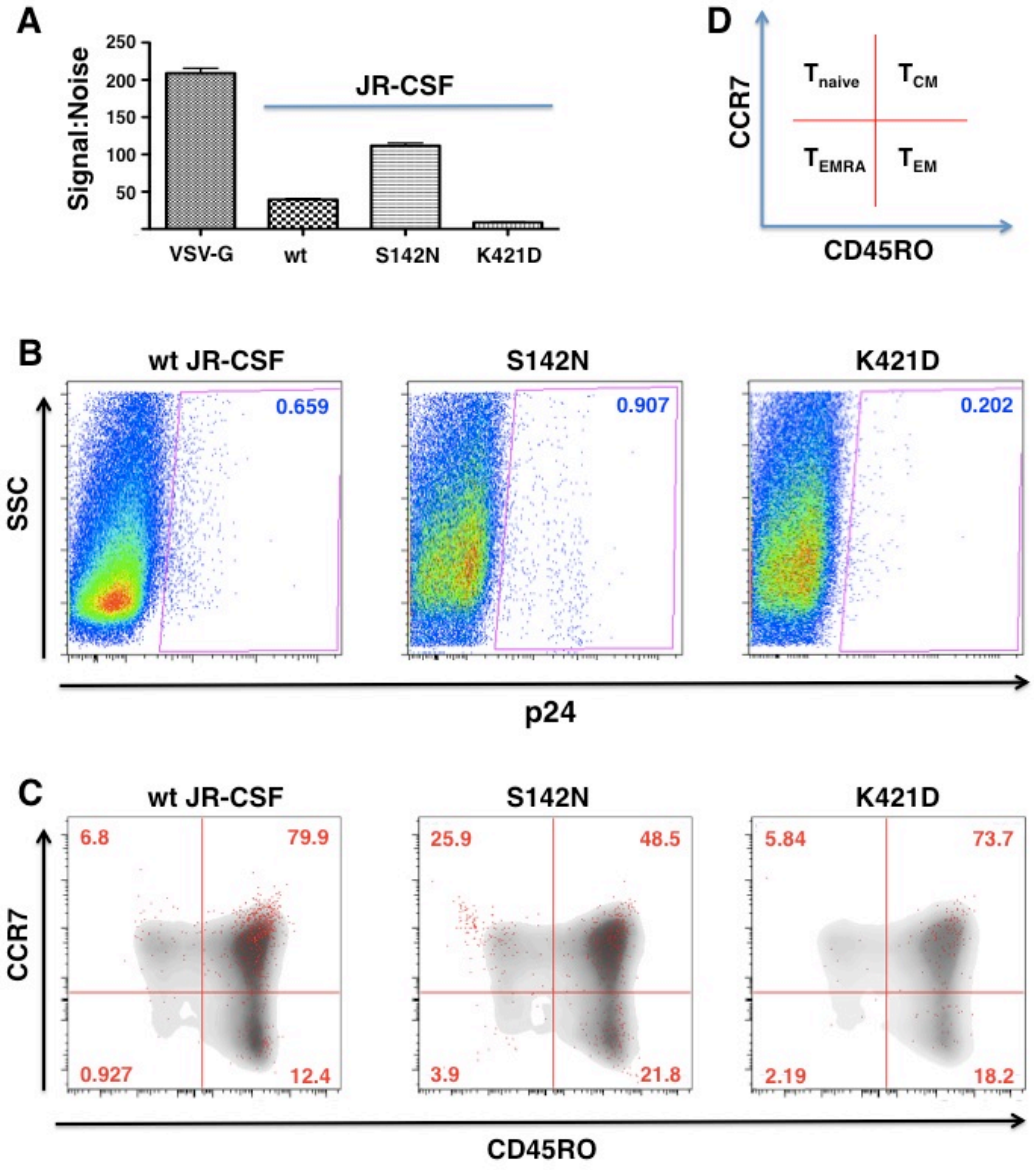

Figure 4-4. Affinofile metrics reflect biologically relevant differences in T cell subset tropism. **(A)** Total PBMCs were infected with luciferase reporter pseudotypes bearing wt, S142N, or K421D JR-CSF envelopes. VSV-G pseudotypes were used as positive controls. All infections (except for VSV-G) could be inhibited by maraviroc (>95%).

Error bars represent ranges between two experiments. **(B)** and **(C)** CD8-depleted PBMCs were infected with the indicated pseudotyped viruses at an MOI of 20 (as tittered on Ghost-R5 cells). Three days post-infection, cells were analyzed by multi-color flow cytometry. **(B)** Infected cells were identified by intracellular p24 staining using PE-conjugated KC57 Mab. **(C)** Uninfected T-cell subset distribution is shown in grey density plot, while infected p24+ cells are overlaid as the red dots. The percent of total p24+ cells are indicated in each quadrant. All infections could be inhibited by maraviroc (>90%). It is unclear whether the small number of p24+ cells found in CD4+ T-effector RA+ cells (T_{EMRA}, CCR7-CD45RO-) represents a reproducibly infectable population. **(D)** Scheme for using CCR7 (PE-Cy7) and CD45RO (FITC) to identify the following T-cell subsets: Naïve (CCR7+ CD45RO-), Central Memory (T_{CM}, CCR7+ CD45RO+), Effector Memory (T_{EM}, CCR7- CD45RO+), and Effector Memory RA (T_{EMRA}, CCR7- CD45RO-). Data shown here is a representative of two independent donors.

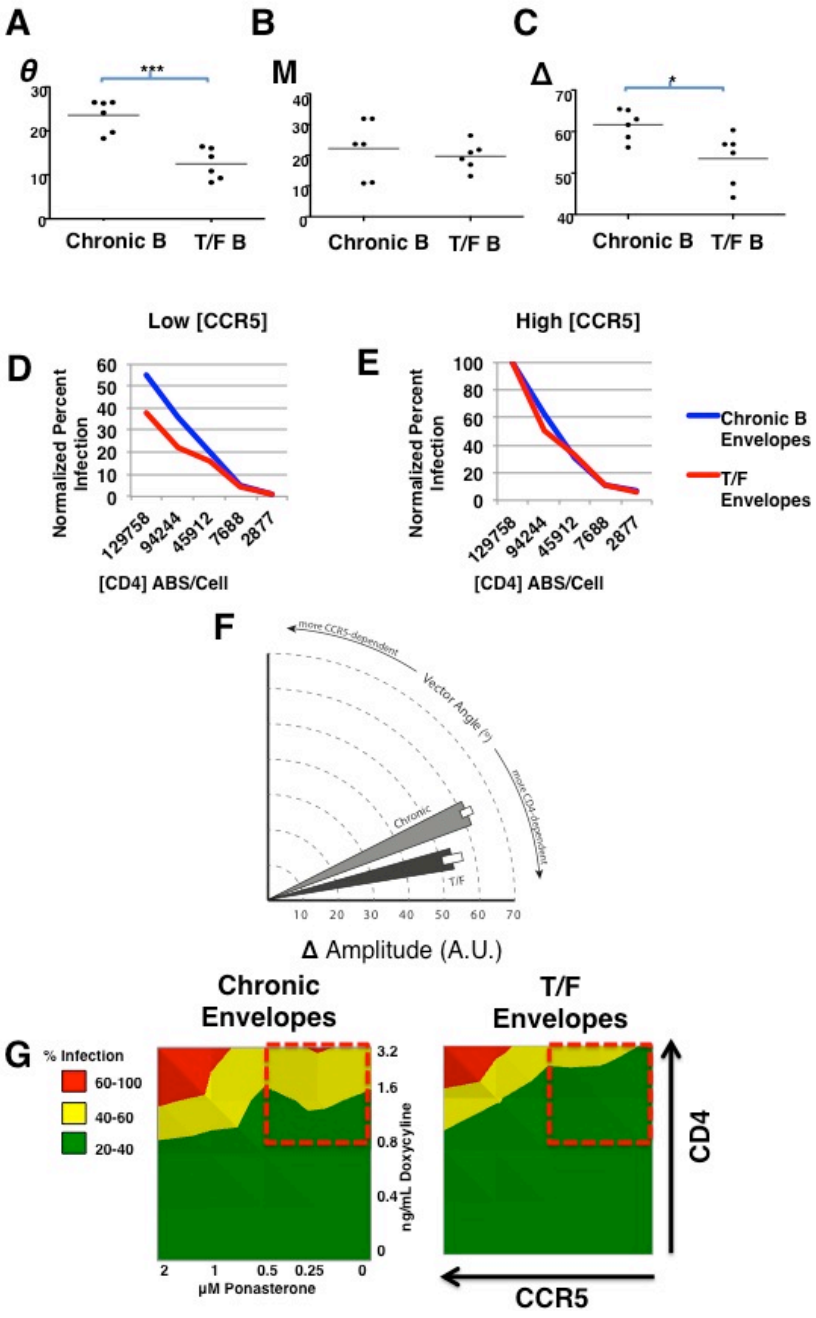

Figure 4-5. Affinofile metrics reveal differences in CD4/CCR5 usage efficiencies between Transmitter/Founder (T/F) and chronic envelopes. Normalized infection data using T/F and chronic Env clones were analyzed using VERSA. **(A)** Vector angle,

(θ), **(B)** mean infectivity (M), and **(C)** vector amplitude (Δ) values were obtained for each Env clone. The vector metrics were first averaged for each individual, and the averaged metrics from the 6 individuals in each group (T/F or chronic, N=12) were then compared. Each Env clone was independently profiled twice across 25 combinations of CD4/CCR5 levels (each data point was done in triplicates). Thus, the metrics were derived from a total of 1,800 infection data points (900 data points from 6 Envs in each group). The median value of each metric for the T/F and chronic Env cohorts is marked by a line. p values were generated by the non- parametric unpaired t test (***, p=0.0003; *, p=0.05). (**D and E)** The normalized infectivity for the chronic (blue line) and T/F envelopes (red line) are averaged, and compared as a group at **(D)** low and **(E)** high levels of CCR5 expression, across varying levels of CD4 as indicated. **(F)** Wedge plot of the average θ and Δ values (+/- S.D.) obtained for T/F (dark grey) versus chronic envelopes (light grey). **(G)** The infectivity profile of individual T/F and chronic Envs (from Fig. S3) were averaged to form their respective group profile. 2-D contour plots representing the averaged infectivity profiles of T/F and chronic envelopes are shown

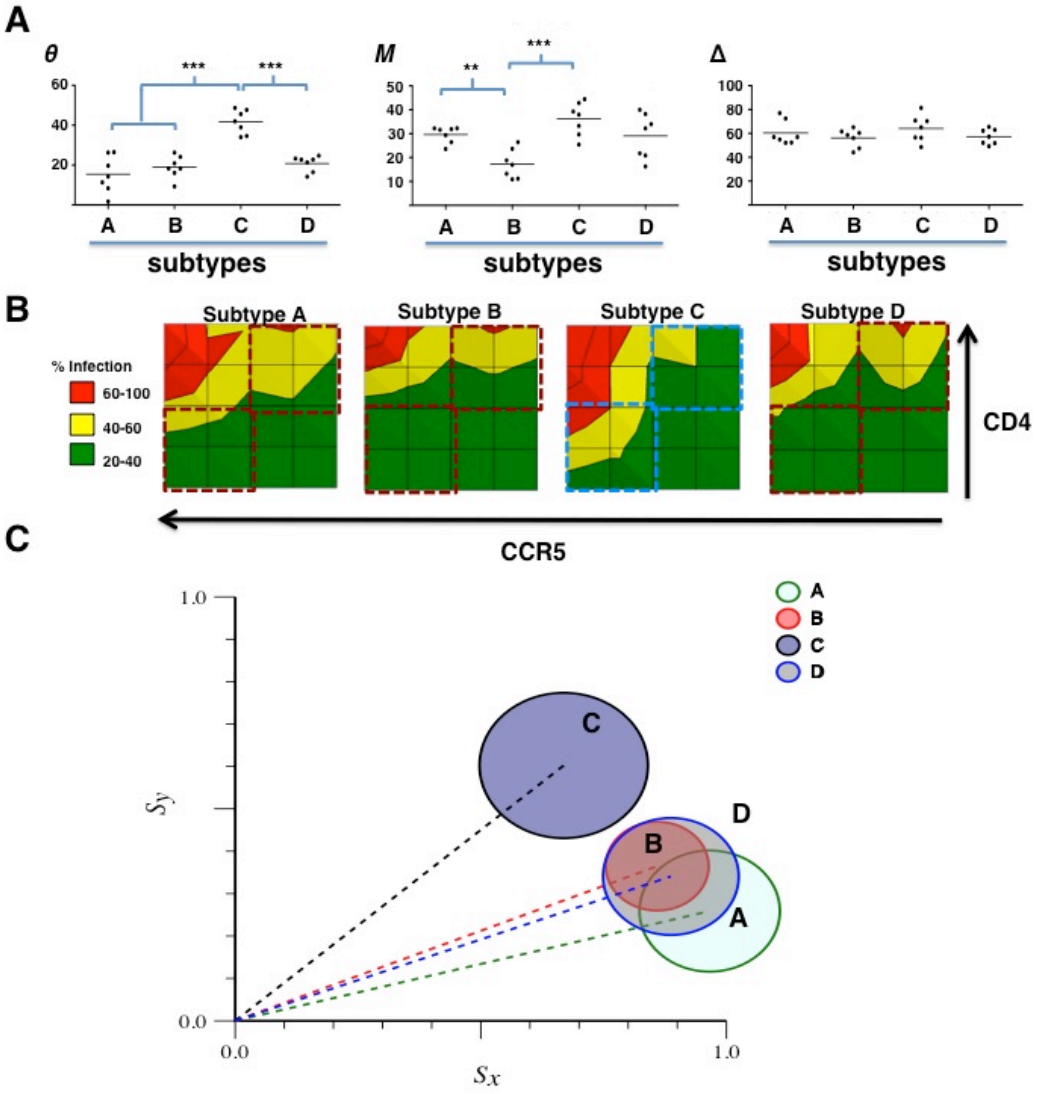

Figure 4-6. HIV envelopes exhibit subtype-specific differences in CD4/CCR5 usage efficiencies. (A) Normalized infection data from each Subtype A, B, C and D envelope clones (n=28) were analyzed by VERSA. The vector metrics were averaged for at least two independent infections (with a variance <5%) for each envelope in each subtype group. Vector angle (θ), mean infectivity (M), and vector amplitude (Δ) values for each envelope are shown as grouped by subtypes. P values were generated by the non-

parametric unpaired t test (p***<0.005, **p<0.05). **B)** 2-D contour plots of the average infectivity profile for each subtype, generated and color coded as in Fig. **4-5G**. The colored dashed square boxes compare the infectivity differences noted between subtype C (blue) Envs and others (red) in the lower left (LL) and upper right (UR) quadrants. Each Env clone was independently profiled twice. **(C)** Polar plot of the averaged sensitivity vectors obtained from each subtype, generated as in Fig**. 4-3E**.

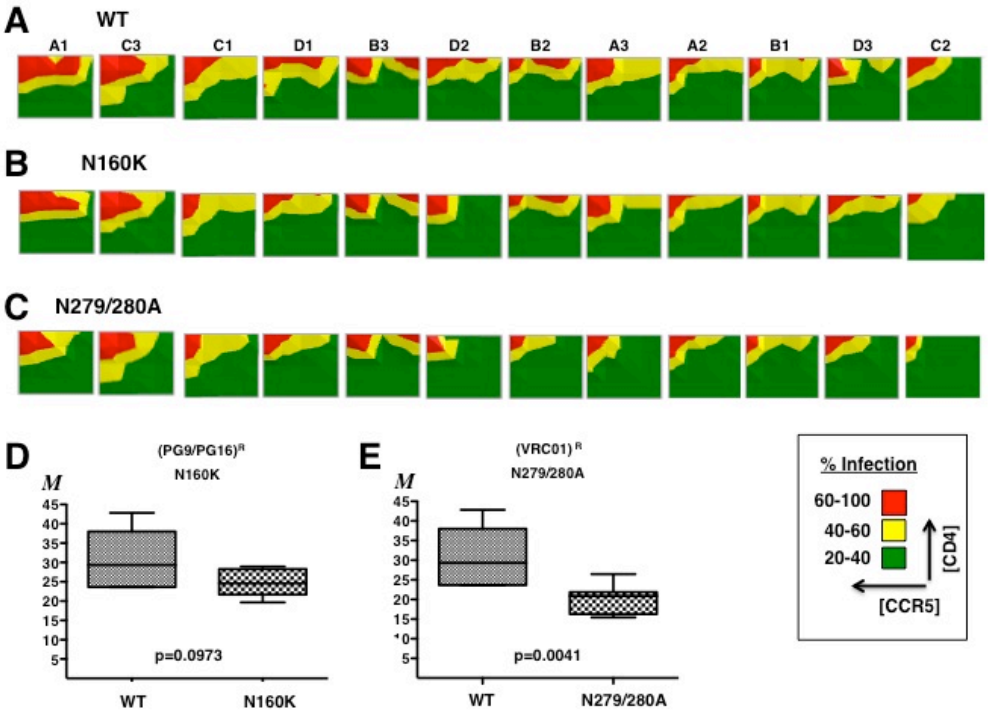

Figure 4-7. Affinofile profiling reveals that resistance to broadly neutralizing antibodies (BNAbs) also results in reduced entry efficiency. N160K and N279A mutations were engineered into a random sample of 12 subtype A-D Envs, The resultant $(PG9/16)^R$ and $(VRC01)^R$ resistant Envs were assayed for CD4 and CCR5 usage efficiency along with their parental BNAb sensitive Envs. GGR Affinofile profiling was performed as previously described. (**A-C**) 2-D contour plots of the infectivity profiles for WT, $(PG9/PG16)^R$, and $(VRC01)^R$ Envs are shown. Contour plots are ordered from highest mean infectivity to lowest, from left to right. **(D-E)** The mean values and interquartile ranges of the Mean infectivity (M) are shown for $(PG9/PG16)^R$ or

(VRC01)^{R} resistant Envs in all subtypes compared to their WT counterparts. P values calculated via a non-parametric paired t-test.

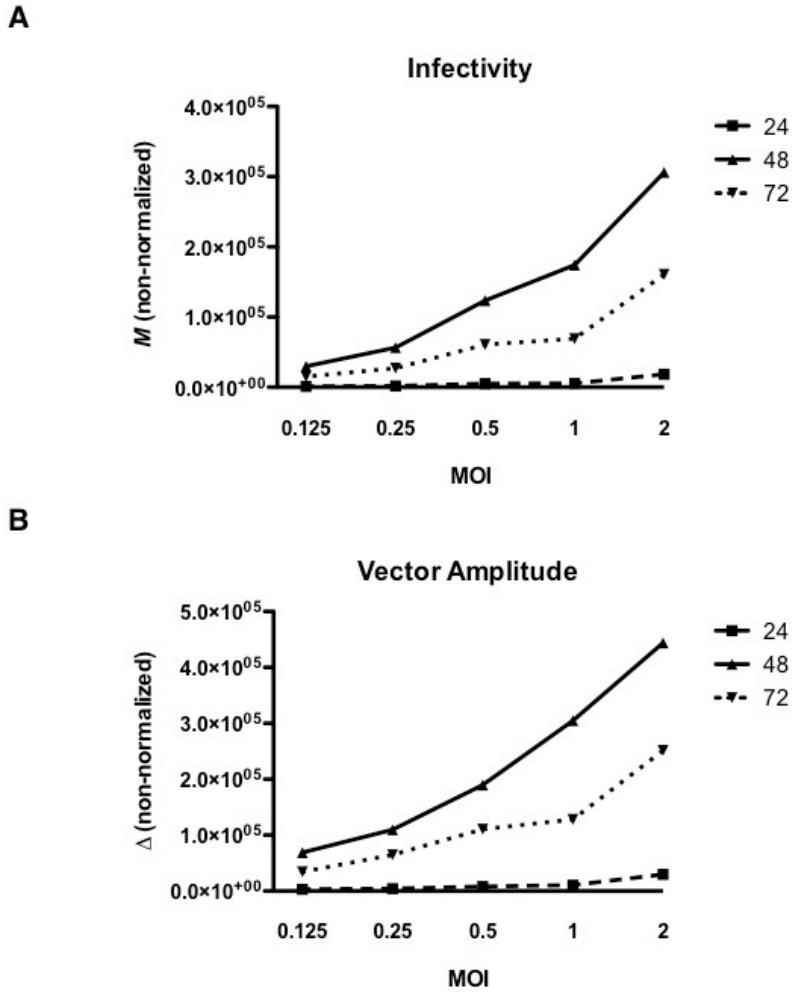

Figure 4-8. Use of Raw Luciferase Infection Data Results in Variable Vector Metrics. Mean infectivity and vector amplitude results. Raw luciferase infection data from the data set presented in Figure 2 was inputted into VERSA.

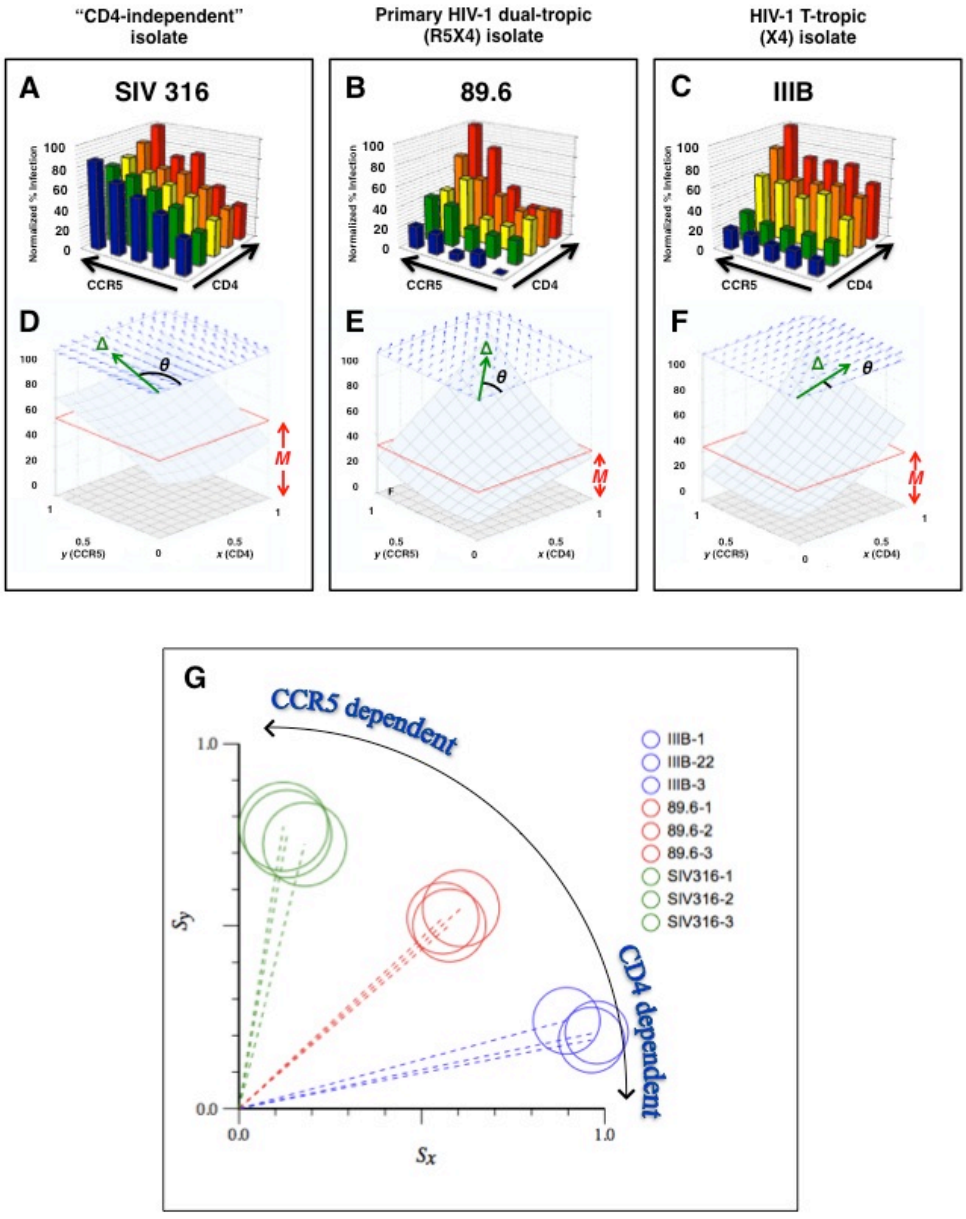

Figure 4-9. Isolates with different CD4 and CCR5 usage can be represented by distinct 3-D surface plots. GGR Affinofile cells induced to express 25 different combinations of CD4 and CC5 were infected with the **(A)** "CD4-independent" R5 SIV316, **(B)** R5X4 89.6, or **(C)** X4 IIIB pseudotyped viruses. The SIV 316 infection

profile indicated that SIV 316 is much more sensitive to changes in CCR5 levels, and is relatively insensitive to varying CD4 levels. Conversely, the HIV IIIB infectivity profile indicated a phenotype that was dependent on changes in CD4, but was relatively insensitive to changes in CCR5. This phenotype can be attributed to the use of low levels of CXCR4 present on the HEK293 cells, the parental derivative of GGR Affinofile cells. The 89.6 virus demonstrated an infectivity profile that was equally sensitive to changes in CD4 and CCR5 levels. The distinct infectivity profiles for each Env demonstrated in **A-C** can be mathematically transformed into the corresponding 3-D surface plots shown in **D-F**. These three envelopes represent the diverse range of infectivity profiles that can be demonstrated in GGR Affinofile cells. **(G)** A polar plot representing the three metrics describing the infectivity profiles of the three viruses is shown. SIV316 has a vector angle closest to 90 degrees which indicates that it is much more sensitive to changes in CCR5 levels and is relatively insensitive to varying CD4 levels. Conversely, HIV IIIB has a vector angle closest to zero degrees, which indicates the reverse phenotype from SIV316. 89.6 has a vector angle of ~45 degrees indicating that it is equally sensitive to changes in CD4 and CCR5 levels. Each circle represents one independent experiment profiling infectivity across 25 distinct CD4/CCR5 expression levels.

Env type	env clone	Gender	Age	Feinberg Stage	Viral Load (copies/ml)	Disease Status	Location	Risk factor	Accession Number	AIDS Repository Designation	D1Z IC_{50} (ug/ml)	sCD4 IC_{50} (nM)	T415 (Yes/No)
T/F	p6244_13.B5.4576	M		II	274,000	NA	USA	SPD	EU289191	p6244_13.B5.4576	>50	254	N
	p63358.p3.4013	NR		II	260,000	NA	USA	SPD	EU289192	p63358.p3.4013	>50	538	N
	p700010040.C9.4520	F		II	741,499	NA	USA	IVDU	EU289193	p700010040.C9.4520	0.7	97	N
	p1054.TC4.1499	M		II	320,000	NA	USA	SPD	EU289185	p1054.TC4.1499	4.2	113	Y
	pPRB926_04.A9.4237	NR		II	756,000	NA	USA	SPD	EU289197	pPRB926_04.A9.4237	0.5	93	N
	pSC45.4B5.2631	M		II	6,318,529	NA	Trinidad	Heterosexual	EU289201	pSC45.4B5.2631	0.7	268	N

Env type	env clone	Gender	Age	Time since sero-conversion	CD4 Count (cells/mm^3)	Disease Status	Location	Risk factor	Accession Number	AIDS Repository Designation
Chronic	92TH014.12	M	38	25.6	ND	AS	Bangkok, Thailand	IVDU	U08801	pSVIII-92TH014.12
	92US711.14	M	44	17	853	AS	Baltimore, USA	IVDU	U08448	pBA301711.14
	92US712.4	F	35	15	537	AS	Baltimore, USA	IVDU	U08449	pBA301712.4
	92US714.1	M	28	12	546	AS	Baltimore, USA	IVDU	U08450	pBA301714.1
	92US715.6	M	36	20	470	AS	Baltimore, USA	IVDU	U08451	pBA301715.6
	92US716.6	M	39	4	787	AS	Baltimore, USA	IVDU	U08452	pBA301716.6

NA, non-applicable
AS, asymptomatic
NR, not recorded
**Risk behavior where known. Subjects listed as "SPD" were source plasma donors who denied having sex for money, homosexual activity, IVDU, or receiving a blood transfusion or a tattoo in the preceding year.

Table 4-1: List of T/F and Chronic Envelopes

Env type	Env clone	Approximate length of time of infection	Viral Load (copies/ml)	CD4 Count (cells/mm^3)	Location	Mode of Transmission	Accession Number	Reference	Group PI	b12 IC_{50} (ug/ml)	sCD4 IC_{50} (mg/ml)
A1	Q259env.w6	81 dpi	2,000,000	NA	Kenya	NA	AF407151	1	Overbaugh	>20	NA
A2	QB726.70M.ENV.B3	70 dpi	61,940	NA	Kenya	NA	FJ866111	1	Overbaugh	>20	NA
A3	QH359.21M.ENV.C1	21 dpi	32,120	NA	Kenya	NA	FJ866121	2	Overbaugh	>20	NA
A4	QH209.14M.ENV.A2	14 dpi	28,600	NA	Kenya	NA	FJ866118	2	Overbaugh	>20	NA
A5	QF495.23M.ENV.A3	23 dpi	217,050	NA	Kenya	NA	FJ866114	2	Overbaugh	>20	NA
A6	Q769env.h5	61 dpi	9,000,000	NA	Kenya	NA	AF407159	2	Overbaugh	>20	NA
A7	QH343.21M.ENV.A10	21 dpi	40,750,000	NA	Kenya	NA	FJ866119	2	Overbaugh	>20	NA
B1	SC422661.8 (SVPB8)	4 wks	1,380,000	ND	Trinidad	F-M	A Y835441	3	Montefiori	4.7	0.2
B2	pCAAN5342 clone A2	NA	>1,000,000	278	USA	M-M	A Y835452	3	Montefiori	>50	16
B3	pREJO4541 clone 67	2 wks	722,349	848	USA	F-M	A Y835449	3	Montefiori	0.7	0.5
B4	pTRJO4551clone 58	1 wks	812,951	NA	USA	M-M	A Y835450	3	Montefiori	>50	20.2
B5	AC10.0, clone 29	4 wks	40,700	919	USA	M-M	A Y835446	3	Montefiori	1.8	8.5
B6	QH0692, clone 42	6 wks	9,611	NA	Trinidad	F-M	A Y835439	3	Montefiori	0.3	0.5
B7	pRHPA4259 clone 7	<8 wks	1,458,354	247	USA	M-F	A Y835447	3	Montefiori	0.1	1.8
C1	HIV-16055-2,	2 dpi	534,557	830	India	F-M	EF117268	4	Montefiori	>50	11.4
C2	HIV-16845-2,	20 dpi	199,655	579	India	M-F	EF117269	4	Montefiori	>50	1
C3	HIV-25710-2,	19 dpi	3523	350	India	F-M	EF117271	4	Montefiori	>50	2.6
C4	HIV-25711-2,	4 dpi	6,633,880	471	India	F-M	EF117272	4	Montefiori	25.9	29
C5	HIV-26191-2,	9 dpi	5,346,070	338	India	F-M	EF117274	4	Montefiori	4.9	17.1
C6	HIV-00836-2,	85 dpi	31,104	ND	India	M-F	EF117265	4	Montefiori	>50	>50
C7	HIV-001428-2, clone 42	11 dpi	217,812	454	India	M-F	EF117266	4	Montefiori	>50	5.2
D1	QA013.70I.ENV.H1	70 dpi	1,527,700	NA	Kenya	NA	FJ866134	2	Overbaugh	>20	NA
D2	QA013.70I.ENV.M12	70 dpi	1,527,700	NA	Kenya	NA	FJ866135	2	Overbaugh	>20	NA
D3	QA465.59M.ENV.D1	59 dpi	37,750	NA	Kenya	NA	FJ866137	2	Overbaugh	17.16	NA
D4	QD435.100M.ENV.B5	100 dpi	17,470	NA	Kenya	NA	FJ866140	2	Overbaugh	>20	NA
D5	QD435.100M.ENV.A4	100 dpi	17,470	NA	Kenya	NA	FJ866139	2	Overbaugh	>20	NA
D6	QD435.100M.ENV.E1	100 dpi	17,470	NA	Kenya	NA	FJ866141	2	Overbaugh	>20	NA
D7	QA465.59M.ENV.A1	59 dpi	37,750	NA	Kenya	NA	FJ866136	2	Overbaugh	9.09	NA

*may be defined differently in different studies; please specify time since last seronegative test, times since acue retroviral conversion syndrome, combination of clinical parameter

NA, Not available

Reference		Group PI
EM Long et al, ARHR 2002	1	Julie Overbaugh
CA Blish et al, JV 2009	2	Julie Overbaugh
M Li et al, JV 2005	3	David Montefiori
SS Kulkarni et al, Virology 2009	4	David Montefiori

Table 4-2: List of Subtype Envelopes

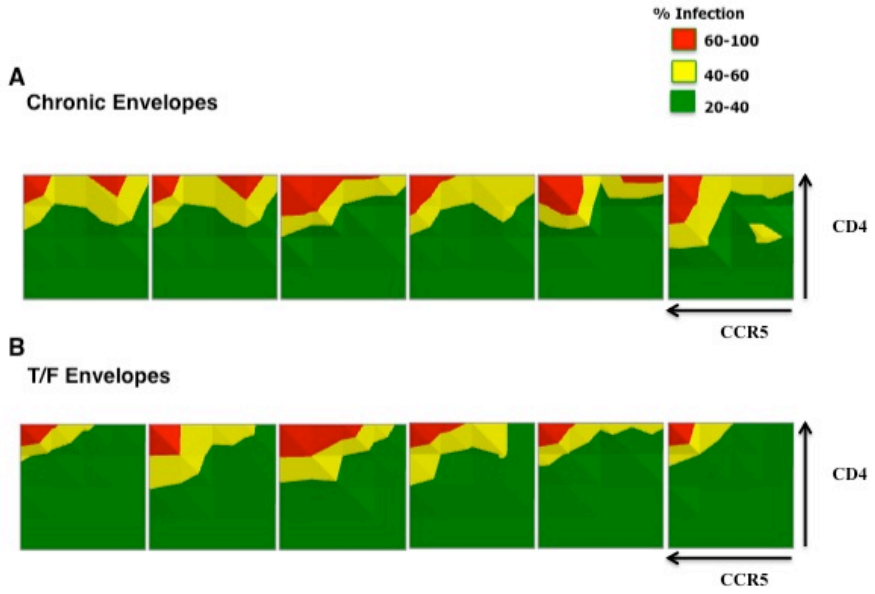

Figure 4-10. Individual GGR Plots for T/F and Chronic Envelopes. The GGR data for **(A)** Chronic and **(B)** T/F – derived envelopes, which are representative of at least 2 independent experiments, were generated and plotted as described in the Materials and Methods. The contour plots are arranged from highest to lowest mean infectivity, from left to right.

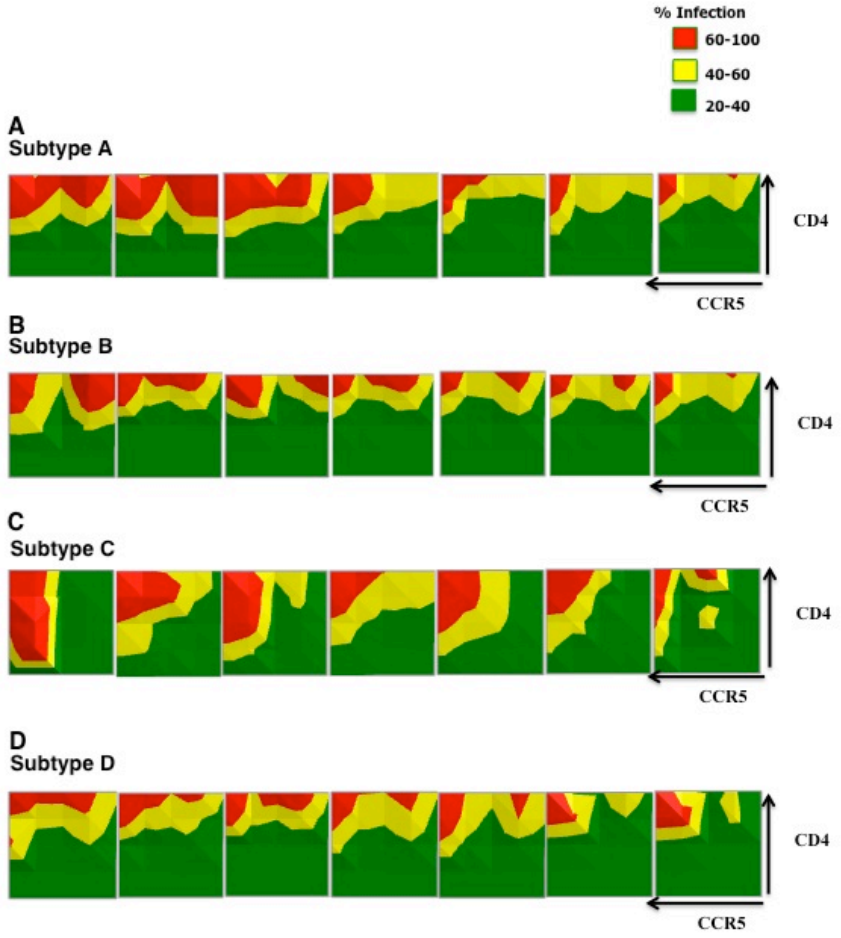

Figure 4-11. Individual GGR Plots for Subtype Envelopes. (A-D) The GGR data for Subtype A-, B-, C-, and D- derived Envs , which are representative of at least 2 independent experiments, were generated and plotted as described in the Materials and Methods. The contour plots are arranged from highest to lowest mean infectivity, from left to right.

Chapter Five

Conclusion

5.1 Abstract

This chapter is divided into two sections. The first section is a summary of the results and discussions of this dissertation. The second section describes future work, which focuses on the use of the GGR cell line and system in detecting HIV infection in patient samples.

5.2 Summary of Results and Discussion

The review in chapter 3 highlights the usefulness of the Affinofile cell line in examining entry efficiency of HIV-1 Envs derived from various cohorts. The results of studies, highlighted in Table 2.1, demonstrate that the Affinofile cell line can be used to examine entry efficiency influence on entry inhibitors, cellular tropism, and cellular pathogenesis. Moreover, these studies demonstrate that the Affinofile system can be used to reveal unappreciated nuance in entry efficiency. The usefulness of the Affinofile system, highlighted by the review, is the basis for creation of our high-throughput GGR Affinofile cell line.

Chapter 4 demonstrates our improved Affinofile cell line, which we dubbed the GGR cell line. The GGR system provides a rapid method to characterize the CD4 and CCR5 usage of replication-competent or pseudotyped HIV-1 viruses. We showed that our GGR Affinofile cell line has a rapid response to HIV-1 infection that is characterized by fast induction of *Gaussia* luciferase expression and secretion (Figure 4-1). We demonstrated the utility of this system by assessing receptor and coreceptor usage efficiency of HIV-1 Env cohorts important to the field of HIV-1 (Figures 4-4 to 4-7).

We showed that previously characterized mutants, described by previously using alternative assays, could be analyzed with our system to reveal unappreciated differences

in CD4 and CCR5 usage. Single point mutations in the Env of the laboratory strain JR-CSF, conferred differential CD4 and CCR5 usage that could be described in greater detail by our 3-D column plot and sensitivity vector metrics (Figure 4-3). The utility of our system is underscored by the clustering of the sensitivity metrics and visual demonstration (visible in the 3-D column plot) of the interdependent relationship between CD4 and CCR5 usage, such that an increased ability to use low levels of CCR5 is accompanied by increased ability to use CD4, and vice versa (Figure 4-3). These results offer quantitative and visual confirmation that the use of a system or cell line that only modifies one parameter (CD4, CCR5 expression, or amount of inhibitor used) may result in incomplete data. Admittedly, lower resolution and/or binary assays, at times, may be more than sufficient; however, when the differences are subtle or atypical, these assays may fail to capture the entry efficiency disparities that are present.

A growing body of evidence suggests that the ability to use low levels of CD4 and CCR5 corresponds with an increased and broader cellular tropism. Limited experimental methods exist, however, to directly quantify Envs ability to use CD4 and CCR5. A salient feature of our system is the ability to distill a viral Env's ability to use receptor and coreceptor into three metrics. As proof of principle, we demonstrated that the sensitivity metrics for the WT and single point JR-CSF mutants correlate with differential T-cell subset tropism infection efficiency. Specifically, infection of PBMCs with S142N mutation, which had an increased angle and mean infectivity, resulted in an increased and expanded T-cell subset that is marked by increased infection of naïve T-cells.

Alternatively, the K421D JR-CSF mutant had an increased angle and mean infectivity, which resulted in a decreased infection efficiency and tropism. The ability to use lower levels of CD4 and CCR5 revealed in our assay directly correlated with an expanded tropism. These explicit differences in the mutant's ability to enter different T-cell subsets validate our system and its ability to quantify a biologically relevant phenotype (Figure 4-4). It is important to note that it is believed that infection of central memory and/or naïve T-cells leads to more rapid pathogenesis of AIDS (134).

Recently, attempts have been made to find differences between transmitted/founder (T/F) and chronic Envs, since finding a difference may reveal a potential target for vaccine or inhibitor design to prevent HIV transmission (3, 135, 172). Studies have revealed several genetic differences between T/F and chronic Envs, including number of N-glycosylation sites and V1/V2 loop length (33). Studies that have examined entry/fusion efficiency, T-cell subset infection, dendritic cell-mediated trans-infection, and inhibition by entry inhibitors between T/F and chronic Envs, have shown no differences (160). However, our results indicate that T/F and chronic Env pseudotyped viruses have differential abilities to use CD4 and CCR5 (Figure 4-5). Despite the T/F and chronic Envs originating from different donors, we saw a significant difference in angle and amplitude. The differences in metrics indicate that T/F are less efficient at using CD4 when compared to chronic Envs (Figure 4-5). Limited evidence suggests that T/F virus Envs, unlike chronic Envs, are not macrophage-tropic (70), which would indicate decreased entry efficiency; our data complements this observation. Additionally, several

studies, including those that examined differences in entry efficiency, observed that T/F viruses were consistently more sensitive to the CD4 binding site MAb b12 (172-174). Shifts in sensitivity to the b12 antibody have been shown to modulate sensitivity to soluble CD4. Our observation of reduced entry efficiency of T/F Envs compared to chronic Envs on the surface seems counterintuitive. However, our results likely reveal the interplay between sometimes opposing Env properties essential in forming infection in a new individual. This is somewhat similar to the observation that CCR5 using viruses are the majority of transmitting/founding viruses, despite the observation that CXCR4 using viruses have a higher virulence *in vitro*. Moreover, these results support the rational of using CCR5 binding inhibitors in pre-exposure prophylactic microbicides, given are data indicates T/F viruses are inefficient in CCR5 usage. Interestingly, the use of entry inhibitors in microbicides may prove to more cost effective, and easier to reach pharmacological efficacy compared to oral pre-exposure prophylaxis.

In the case of our subtype studies, our GGR Affinofile system demonstrated that each subtype Env group had specific vector metrics, with subtype C Envs demonstrating a significant difference compared to the others (Figure 4-6). The specific vector metric clustering with subtype C Envs indicates that these Envs are less dependent on CCR5 levels when compared to other subtype Envs. This data adds a level of complexity to the epidemiological data because it suggests that subtype C Envs may compromise a greater number of infected people, because it is less dependent on CCR5 levels, contrary to previously published data that examined intersubtype replicative fitness in PBMCs(38,

40, 169). However, our results are consistent with *in vitro* and *in vivo* monoinfection, studies examining chimeric Env viruses (175). It is important to note that dissimilarities in this and other studies may be the result of experimental differences, and possible differences in the Envs tested.

Previous reports have explained decrease subtype C replicative fitness with the theory that decreased entry efficiency and replicative fitness permits a longer asymptomatic phase and, therefore, a greater period of transmission (40, 169). However, it is documented that transmission during the asymptomatic early and late phase is can be 8–10 times less likely compared to during the acute phase (176, 177), which calls into question whether a longer asymptomatic phase is the reason for which subtype C accounts for such a high percentage of infections. Additionally, it is interesting that a number of circulating intersubtype forms retain the Env region of subtype C while containing gag or pol genes from alternative subtypes.

Additionally, we have engineered single point mutations that confer resistance to PG9/PG16 and VRC01 into Envs of different subtypes and analyzed them using our GGR Affinofile system. Resistance to PG9/PG16 with the N160K mutant demonstrated a reproducible, albeit non-significant, decrease in entry efficiency. Additionally, the significant difference in entry efficiency seen with the VRC01 mutant is likely attributable to subtle changes in VRC01 binding motif, which is also the CD4 binding site **(**Figure 4-7) (141, 178). The results of these studies show that resistance to broadly

neutralizing antibodies comes at a cost to entry efficiency. We recognize that the engineering of resistances is an artificial system and that, under *in vivo* conditions, a decrease in entry efficiency due to resistance to BNAbs will likely be compensated for by substitutions in other locations in the Env that increases CD4 and CCR5 usage efficiency. This is fully expected, because PG9/PG16 and VRC01 were isolated from patients with active HIV replication, thus demonstrating that it is possible for the virus to become resistant while still retaining the ability to replicate. We do believe, however, that the results of this study indicate a window of opportunity during which proper vaccine design could be exploited. In summary, our results demonstrate that, with improved methods, demonstrated by our GGR Affinofile system, nuances in HIV entry that have gone unnoticed can be revealed.

5.3 Future Direction

Although there is no cure for HIV/AIDS, there are effective treatments that permit managed HIV positive individuals to live normal lives. Currently, there are limited methods to assay for a patient's viral response to antivirals. Moreover, these limited methods are very laborious, time consuming, and most importantly, only give a limited view of the viral strains fitness. In Figure 4-1 we show the robustness of HIV detection for the GGR cell line. We believe that with more optimization, the GGR cell line can be used to detect and examine HIV fitness in less time, and with higher sensitivity compared to what is commercially and publicly available.

With the lack of a vaccine for HIV, monitoring the growing population of individuals on anti-retrovirals is of importance. However due to the limitations of present detection systems, the use of the full repertoire of HIV antivirals is hindered. Currently all HIV indicator cell lines use the increase production of a fluorescent protein or a (firefly) luciferase protein as an indication of infection. The use of only a fluorescent protein requires the lengthy preparation of the cells and examining of cells on a fluorescent detection system. Alternatively, the use of non-secreted luciferase requires careful attention to non-trivial matters such as complete lysis of cells before assessment of luciferase activity. Moreover, GFP or firefly (or even renilla) luciferase detection are endpoint assays, since the cells have to be fixed or lysed to assess HIV infection.

Additionally, because of the lack of sensitivity, viral envelopes have to be PCR from serum and separately pseudotyped, a laborious and time-consuming process.

Furthermore, all indicator cell lines express the receptor (CD4) and coreceptor (CCR5) for HIV at fixed, often over-expressed supraphysiological levels. This hinders the utility of those cell lines because different HIV isolates have varying capacity to use the receptor and therefore, its response to entry inhibitors would vary as well. Available tests use cell lines with over-expressed CD4 and coreceptor levels that do not represent the physiological amounts (receptor density) present in relevant cell types *in vivo* (e.g. T-cells and macrophages) [1]. This may lead to inaccurate reporting of whether a virus is resistant to a particular CCR5 inhibitor, which poses a danger to the patient.

Preliminary data indicates that our GGR cell line can detect as low as 100 infectious units per ml in HIV spiked serum (Figure 5-1). The use of the *Gaussia* luciferase, which is 1000 fold brighter than the conventionally used firefly luciferase, provides a more sensitive method to detect HIV. Moreover, because *Gaussia* luciferase is secreted, multiple-day collection of infected supernatant may improve detection ability. Therefore, we will optimize the GGR system for HIV-1 virus from media and serum. *Gaussia* luciferase has the potential to not only provide greater sensitivity of detection, but also to provide kinetic information regarding the progression of infection, as only a small amount of supernatant (e.g. 10 ul) needs to be sampled at any given time point.

Additionally, preliminary data indicates that the GGR cell line can be used to culture HIV from media or serum at varying levels of receptor and coreceptor levels (Figure 5-2). This flexibility of applying selective pressure only at the level of CD4 and CCR5 usage will provide invaluable tools for the research and pharmaceutical industry as they try to understand the evolution of viral receptor usage and the resistance to entry inhibitors.

In summary, we believe that our GGR cell line can be used by itself or in combination with other systems to provide an improved (quicker and higher sensitivity) method of detecting and examining clinical samples containing HIV for laboratory research, clinical trial monitoring, and medical diagnostic purposes.

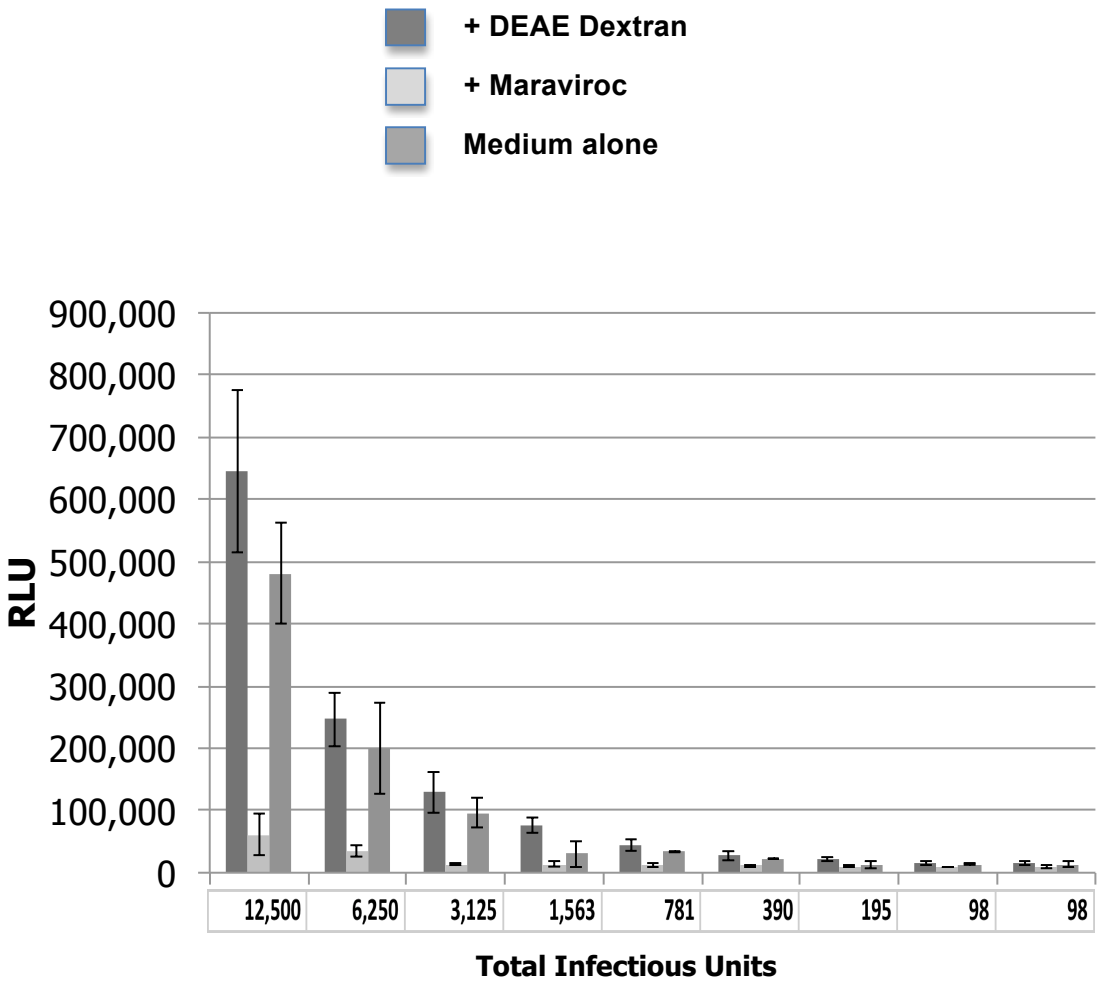

Figure 5-1. GGR cells can be used to detect HIV (functional viral load) in human serum. A prototypical CCR5-using HIV-1 isolate (live, replication-competent JR-CSF) was pre-titered on R5-GHOST cells (a standard procedure). The indicated amount of infectious units was spiked into an equal volume of HIV-negative human serum/plasma, which was then transferred onto GGR cells in 96-well plates that were maximally induced for CD4 and CCR5 expression. 48 hours post-infection, 10 ul of the supernatant was collected and analyzed for *Gaussia* luciferase activity using standard substrates and

luminometry. Viral infection was performed in the presence of (1) DEAE-dextran, a commonly used polycationic reagent to enhance viral infection (dark grey,1st bar), (2) Maraviroc, a FDA approved CCR5 inhibitor (light grey, 2nd bar), and (3) Culture Medium alone (medium grey, 3rd bar). Specific CCR5-mediated infection (i.e. signal could still be reproducibly reduced by maraviroc) could be measured at viral inoculum as low as 390-781 I.U. Data presented is a representation of two independent experiments

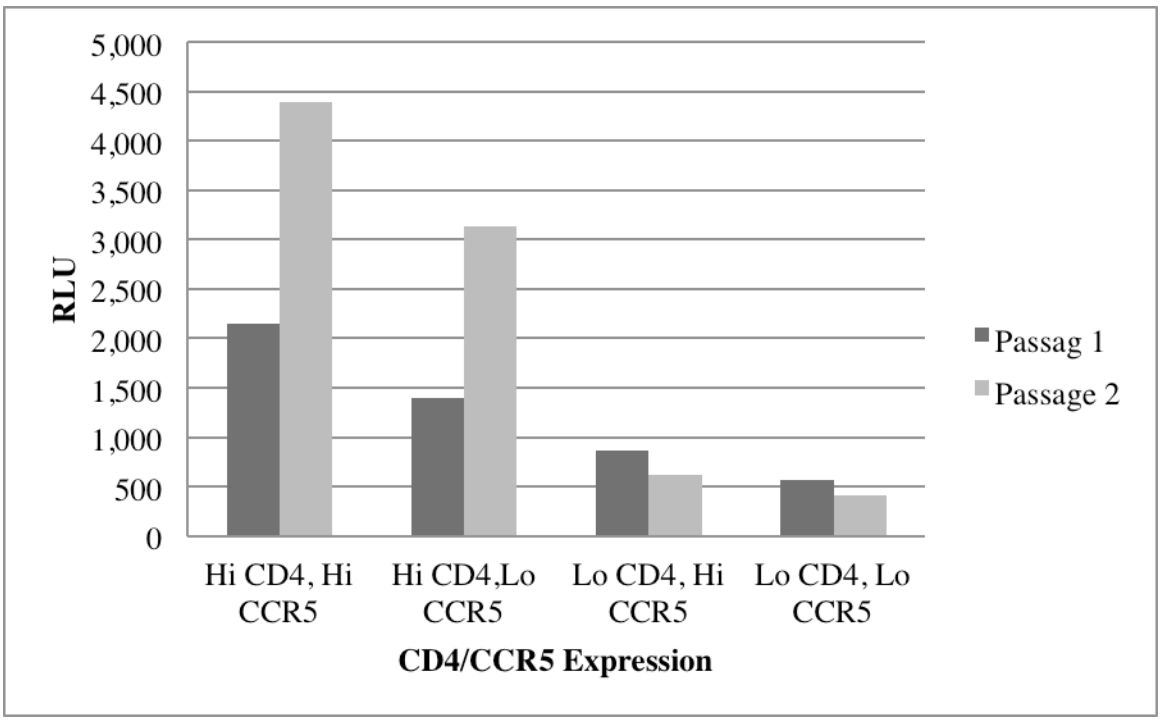

Figure 5-2. GGR Cells can be used to propagate virus from plasma cells. 1,000 RNA units of HIV infected plasma was transferred onto GGR cells in a 12 well plates that were induced at four different CD4 and CCR5 expression levels. After a four day growth period, gLuc expression was assessed (Passage 1) and 1/10 of cells and supernatant were passaged onto freshly induced GGR cells. Four days later, gLuc expression was assessed again (Passage 2). Data presented is a representation of one experiment.

References

1. Colin DM*, et al.* (2006) Projections of Global Mortality and Burden of Disease from 2002 to 2030. *PLoS Medicine* 3(11).
2. Wyatt R*, et al.* (1998) The antigenic structure of the HIV gp120 envelope glycoprotein. *Nature* 393(6686):705-711.
3. Haase A (2010) Targeting early infection to prevent HIV-1 mucosal transmission. *Nature* 464(7286):217-223.
4. Alexaki A, Liu Y, & Wigdahl B (2008) Cellular reservoirs of HIV-1 and their role in viral persistence. *Curr HIV Res* 6(5):388-400.
5. Virgin H & Walker B (2010) Immunology and the elusive AIDS vaccine. *Nature* 464(7286):224-231.
6. Gray L*, et al.* (2005) Uncoupling coreceptor usage of human immunodeficiency virus type 1 (HIV-1) from macrophage tropism reveals biological properties of CCR5-restricted HIV-1 isolates from patients with acquired immunodeficiency syndrome. *Virology* 337(2):384-398.
7. Liu J, Bartesaghi A, Borgnia MJ, Sapiro G, & Subramaniam S (2008) Molecular architecture of native HIV-1 gp120 trimers. *Nature* 455(7209):109-113.
8. Lee B, Sharron M, Montaner LJ, Weissman D, & Doms RW (1999) Quantification of CD4, CCR5, and CXCR4 levels on lymphocyte subsets, dendritic cells, and differentially conditioned monocyte-derived macrophages. *Proc Natl Acad Sci USA* 96(9):5215-5220.

9. Cicala C, Arthos J, & Fauci AS (2012) HIV-1 envelope, integrins and co-receptor use in mucosal transmission of HIV. *Journal of Translational Medicine* 9(Suppl 1).

10. Nawaz F*, et al.* (2012) The Genotype of Early-Transmitting HIV gp120s Promotes α4β7 –Reactivity, Revealing α4β7+/CD4+ T cells As Key Targets in Mucosal Transmission. *PLoS Pathogens* 7(2).

11. Jain P*, et al.* (2009) DC-SIGN mediates cell-free infection and transmission of human T-cell lymphotropic virus type 1 by dendritic cells. *J Virol* 83(21):10908-10921.

12. Sato S, Ouellet M, St-Pierre C, & Tremblay MJ (2012) Glycans, galectins, and HIV-1 infection. *Ann N Y Acad Sci* 1253:133-148.

13. St-Pierre C, Ouellet M, Tremblay MJ, & Sato S (2010) Galectin-1 and HIV-1 Infection. *Methods Enzymol* 480:267-294.

14. Gorry PR*, et al.* (2007) Changes in the V3 region of gp120 contribute to unusually broad coreceptor usage of an HIV-1 isolate from a CCR5 Delta32 heterozygote. *Virology* 362(1):163-178.

15. Lobritz MA, Marozsan AJ, Troyer RM, & Arts EJ (2007) Natural variation in the V3 crown of human immunodeficiency virus type 1 affects replicative fitness and entry inhibitor sensitivity. *J Virol* 81(15):8258-8269.

16. Laakso MM*, et al.* (2007) V3 loop truncations in HIV-1 envelope impart resistance to coreceptor inhibitors and enhanced sensitivity to neutralizing antibodies. *PLoS Pathog* 3(8):e117.

17. Hill CM, *et al.* (1998) The amino terminus of human CCR5 is required for its function as a receptor for diverse human and simian immunodeficiency virus envelope glycoproteins. *Virology* 248(2):357-371.

18. Melikyan GB (2008) Common principles and intermediates of viral protein-mediated fusion: the HIV-1 paradigm. *Retrovirology* 5(1):111.

19. Grivel J-C, Shattock RJ, & Margolis LB (2012) Selective transmission of R5 HIV-1 variants: where is the gatekeeper? *Journal of Translational Medicine* 9(Suppl 1).

20. Hu Q, Huang X, & Shattock RJ (2010) C-C chemokine receptor type 5 (CCR5) utilization of transmitted and early founder human immunodeficiency virus type 1 envelopes and sensitivity to small-molecule CCR5 inhibitors. *J Gen Virol* 91(Pt 12):2965-2973.

21. Denton P, *et al.* (2010) Systemic administration of antiretrovirals prior to exposure prevents rectal and intravenous HIV-1 transmission in humanized BLT mice. *PLoS One* 5(1):e8829.

22. Groot F, van Capel TM, Schuitemaker J, Berkhout B, & de Jong EC (2006) Differential susceptibility of naive, central memory and effector memory T cells to dendritic cell-mediated HIV-1 transmission. *Retrovirology* 3:52.

23. Bailey J, *et al.* (2006) Residual human immunodeficiency virus type 1 viremia in some patients on antiretroviral therapy is dominated by a small number of invariant clones rarely found in circulating CD4+ T cells. *J Virol* 80(13):6441-6457.

24. Coleman C & Wu L (2009) HIV interactions with monocytes and dendritic cells: viral latency and reservoirs. *Retrovirology* 6:51.

25. Gorry PR, Churchill M, Crowe SM, Cunningham AL, & Gabuzda D (2005) Pathogenesis of macrophage tropic HIV-1. *Curr HIV Res* 3(1):53-60.

26. Moore JP (1997) Coreceptors: implications for HIV pathogenesis and therapy. *Science* 276(5309):51-52.

27. Vignuzzi M, Stone JK, Arnold JJ, Cameron CE, & Andino R (2006) Quasispecies diversity determines pathogenesis through cooperative interactions in a viral population. *Nature* 439(7074):344-348.

28. Duenas-Decamp MJ*, et al.* (2010) Variation in the biological properties of HIV-1 R5 envelopes: implications of envelope structure, transmission and pathogenesis. *Future Virol* 5(4):435-451.

29. Goodenow M & Collman R (2006) HIV-1 coreceptor preference is distinct from target cell tropism: a dual-parameter nomenclature to define viral phenotypes. *J Leukoc Biol* 80(5):965-972.

30. Gorry PR & Ancuta P (2011) Coreceptors and HIV-1 pathogenesis. *Curr HIV/AIDS Rep* 8(1):45-53.

31. Pastore C, Ramos A, & Mosier DE (2004) Intrinsic obstacles to human immunodeficiency virus type 1 coreceptor switching. *J Virol* 78(14):7565-7574.

32. Mosier DE (2009) How HIV changes its tropism: evolution and adaptation? *Curr Opin HIV AIDS* 4(2):125-130.

33. Lynch R, Shen T, Gnanakaran S, & Derdeyn C (2009) Appreciating HIV type 1 diversity: subtype differences in Env. *AIDS Res Hum Retroviruses* 25(3):237-248.

34. Spira S, Wainberg M, Loemba H, Turner D, & Brenner B (2003) Impact of clade diversity on HIV-1 virulence, antiretroviral drug sensitivity and drug resistance. *J Antimicrob Chemoth* 51(2):229-240.

35. Liner KJ, 2nd, Hall CD, & Robertson KR (2007) Impact of human immunodeficiency virus (HIV) subtypes on HIV-associated neurological disease. *J Neurovirol* 13(4):291-304.

36. Kiwanuka N*, et al.* (2008) Effect of human immunodeficiency virus Type 1 (HIV-1) subtype on disease progression in persons from Rakai, Uganda, with incident HIV-1 infection. *J Infect Dis* 197(5):707-713.

37. Kiwanuka N*, et al.* (2009) HIV-1 subtypes and differences in heterosexual HIV transmission among HIV-discordant couples in Rakai, Uganda. *AIDS* 23(18):2479-2484.

38. Abraha A*, et al.* (2009) CCR5- and CXCR4-tropic subtype C human immunodeficiency virus type 1 isolates have a lower level of pathogenic fitness than other dominant group M subtypes: implications for the epidemic. *J Virol* 83(11):5592-5605.

39. Ball S*, et al.* (2003) Comparing the ex vivo fitness of CCR5-tropic human immunodeficiency virus type 1 isolates of subtypes B and C. *J Virol* 77(2):1021-1038.

40. Marozsan A, *et al.* (2005) Differences in the fitness of two diverse wild-type human immunodeficiency virus type 1 isolates are related to the efficiency of cell binding and entry. *J Virol* 79(11):7121-7134.

41. Rangel H, *et al.* (2003) Role of the human immunodeficiency virus type 1 envelope gene in viral fitness. *J Virol* 77(16):9069-9073.

42. Dalgleish AG, *et al.* (1984) The CD4 (T4) antigen is an essential component of the receptor for the AIDS retrovirus. *Nature* 312(5996):763-767.

43. Klatzmann D, *et al.* (1984) Selective tropism of lymphadenopathy associated virus (LAV) for helper-inducer T lymphocytes. *Science* 225(4657):59-63.

44. Klatzmann D, *et al.* (1984) T-lymphocyte T4 molecule behaves as the receptor for human retrovirus LAV. *Nature* 312(5996):767-768.

45. Ivey-Hoyle M, *et al.* (1991) Envelope glycoproteins from biologically diverse isolates of immunodeficiency viruses have widely different affinities for CD4. *Proc Natl Acad Sci U S A* 88(2):512-516.

46. Stamatatos L, Werner A, & Cheng-Mayer C (1994) Differential regulation of cellular tropism and sensitivity to soluble CD4 neutralization by the envelope gp120 of human immunodeficiency virus type 1. *J Virol* 68(8):4973-4979.

47. Levy JA (1996) Infection by human immunodeficiency virus--CD4 is not enough. *N Engl J Med* 335(20):1528-1530.

48. Chesebro B, Buller R, Portis J, & Wehrly K (1990) Failure of human immunodeficiency virus entry and infection in CD4-positive human brain and skin cells. *J Virol* 64(1):215-221.

49. Clapham PR, Blanc D, & Weiss RA (1991) Specific cell surface requirements for the infection of CD4-positive cells by human immunodeficiency virus types 1 and 2 and by Simian immunodeficiency virus. *Virology* 181(2):703-715.

50. Kikukawa R*, et al.* (1986) Differential susceptibility to the acquired immunodeficiency syndrome retrovirus in cloned cells of human leukemic T-cell line Molt-4. *J Virol* 57(3):1159-1162.

51. Choe H*, et al.* (1996) The beta-chemokine receptors CCR3 and CCR5 facilitate infection by primary HIV-1 isolates. *Cell* 85(7):1135-1148.

52. Cocchi F*, et al.* (1995) Identification of RANTES, MIP-1 alpha, and MIP-1 beta as the major HIV-suppressive factors produced by CD8+ T cells. *Science* 270(5243):1811-1815.

53. Oravecz T, Pall M, & Norcross MA (1996) Beta-chemokine inhibition of monocytotropic HIV-1 infection. Interference with a postbinding fusion step. *J Immunol* 157(4):1329-1332.

54. Berger EA, Murphy PM, & Farber JM (1999) Chemokine receptors as HIV-1 coreceptors: roles in viral entry, tropism, and disease. *Annu Rev Immunol* 17:657-700.

55. Berger EA*, et al.* (1998) A new classification for HIV-1. *Nature* 391(6664):240.

56. Tilton JC*, et al.* (2010) A maraviroc-resistant HIV-1 with narrow cross-resistance to other CCR5 antagonists depends on both N-terminal and extracellular loop domains of drug-bound CCR5. *J Virol* 84(20):10863-10876.

57. Johnston SH*, et al.* (2009) A Quantitative Affinity-Profiling System That Reveals Distinct CD4/CCR5 Usage Patterns among Human Immunodeficiency Virus Type 1 and Simian Immunodeficiency Virus Strains. *J Virol* 83(21):11016-11026.

58. Chikere K, Chou T, Gorry PR, & Lee B (2012) Affinofile Profiling: How the Efficiency of CD4/CCR5 usage impacts the biological and pathogenic phenotype of HIV. *Virology* 2012.09.043.

59. Morner A*, et al.* (1999) Primary human immunodeficiency virus type 2 (HIV-2) isolates, like HIV-1 isolates, frequently use CCR5 but show promiscuity in coreceptor usage. *J Virol* 73(3):2343-2349.

60. Johnston SH*, et al.* (2009) A quantitative affinity-profiling system that reveals distinct CD4/CCR5 usage patterns among human immunodeficiency virus type 1 and simian immunodeficiency virus strains. *J Virol* 83(21):11016-11026.

61. Lee B, Sharron M, Montaner LJ, Weissman D, & Doms RW (1999) Quantification of CD4, CCR5, and CXCR4 levels on lymphocyte subsets, dendritic cells, and differentially conditioned monocyte-derived macrophages. *Proc Natl Acad Sci U S A* 96(9):5215-5220.

62. Wu Y, Beddall M, & Marsh J (2007) Rev-dependent lentiviral expression vector. *Retrovirology* 4:12.

63. Wu Y, Beddall MH, & Marsh JW (2007) Rev-dependent indicator T cell line. *Curr HIV Res* 5(4):394-402.

64. UNAIDS (2008) *2008 Report on the Global AIDS Epidemic* (Geneva, Switzerland).

65. Colin DM*, et al.* (2006) Projections of Global Mortality and Burden of Disease from 2002 to 2030. *PLoS Medicine* 3(11):e442.

66. Wilen CB, Tilton JC, & Doms RW (2012) Molecular Mechanisms of HIV Entry. *Adv Exp Med Biol* 726:223-242.

67. Wilen CB, Tilton JC, & Doms RW (2012) HIV: Cell Binding and Entry. *Cold Spring Harb Perspect Med* 2(8).

68. Trkola A*, et al.* (1996) CD4-dependent, antibody-sensitive interactions between HIV-1 and its co-receptor CCR-5. *Nature* 384(6605):184-187.

69. Blaak H, Ran LJ, Rientsma R, & Schuitemaker H (2000) Susceptibility of in vitro stimulated PBMC to infection with NSI HIV-1 is associated with levels of CCR5 expression and beta-chemokine production. *Virology* 267(2):237-246.

70. Li S*, et al.* (1999) Persistent CCR5 utilization and enhanced macrophage tropism by primary blood human immunodeficiency virus type 1 isolates from advanced stages of disease and comparison to tissue-derived isolates. *J Virol* 73(12):9741-9755.

71. Tuttle DL*, et al.* (2002) Increased replication of non-syncytium-inducing HIV type 1 isolates in monocyte-derived macrophages is linked to advanced disease in infected children. *AIDS Res Hum Retrov* 18(5):353-362.

72. Smit TK*, et al.* (2001) Varied tropism of HIV-1 isolates derived from different regions of adult brain cortex discriminate between patients with and without AIDS dementia complex (ADC): evidence for neurotropic HIV variants. *Virology* 279(2):509-526.

73. Marozsan AJ, *et al.* (2005) Differences in the fitness of two diverse wild-type human immunodeficiency virus type 1 isolates are related to the efficiency of cell binding and entry. *J Virol* 79(11):7121-7134.

74. Rangel HR, *et al.* (2003) Role of the human immunodeficiency virus type 1 envelope gene in viral fitness. *J Virol* 77(16):9069-9073.

75. Gorry PR, *et al.* (2002) Increased CCR5 affinity and reduced CCR5/CD4 dependence of a neurovirulent primary human immunodeficiency virus type 1 isolate. *J Virol* 76(12):6277-6292.

76. Olivieri K, *et al.* (2007) The envelope gene is a cytopathic determinant of CCR5 tropic HIV-1. *Virology* 358(1):23-38.

77. Koning FA, *et al.* (2003) Decreasing sensitivity to RANTES (regulated on activation, normally T cell-expressed and -secreted) neutralization of CC chemokine receptor 5-using, non-syncytium-inducing virus variants in the course of human immunodeficiency virus type 1 infection. *J Infect Dis* 188(6):864-872.

78. Kwa D, Vingerhoed J, Boeser B, & Schuitemaker H (2003) Increased in vitro cytopathicity of CC chemokine receptor 5-restricted human immunodeficiency virus type 1 primary isolates correlates with a progressive clinical course of infection. *J Infect Dis* 187(9):1397-1403.

79. Dejucq N, Simmons G, & Clapham PR (1999) Expanded tropism of primary human immunodeficiency virus type 1 R5 strains to CD4(+) T-cell lines determined by the capacity to exploit low concentrations of CCR5. *J Virol* 73(9):7842-7847.

80. Pakarasang M, Wasi C, Suwanagool S, Chalermchockcharoenkit A, & Auewarakul P (2006) Increased HIV-DNA load in CCR5-negative lymphocytes without viral phenotypic change. *Virology* 347(2):372-378.

81. Peters P, Maria J. Dueñas-Decamp, W. Matthew Sullivan and Paul R. Clapham (2007) Variation of Macrophage Tropism among HIV-1 R5 Envelopes in Brain and Other Tissues. *Journal of NeuroImmune Pharmacology* 2(1):32-41.

82. Kimata JT*, et al.* (1999) Coreceptor specificity of temporal variants of simian immunodeficiency virus Mne. *J Virol* 73(2):1655-1660.

83. Kimata JT, Kuller L, Anderson DB, Dailey P, & Overbaugh J (1999) Emerging cytopathic and antigenic simian immunodeficiency virus variants influence AIDS progression. *Nat Med* 5(5):535-541.

84. Kozak SL*, et al.* (1997) CD4, CXCR-4, and CCR-5 dependencies for infections by primary patient and laboratory-adapted isolates of human immunodeficiency virus type 1. *J Virol* 71(2):873-882.

85. Platt E, Wehrly K, Kuhmann S, Chesebro B, & Kabat D (1998) Effects of CCR5 and CD4 cell surface concentrations on infections by macrophagetropic isolates of human immunodeficiency virus type 1. *J Virol* 72(4):2855-2864.

86. Platt EJ, Madani N, Kozak SL, & Kabat D (1997) Infectious properties of human immunodeficiency virus type 1 mutants with distinct affinities for the CD4 receptor. *J Virol* 71(2):883-890.

87. Saez E*, et al.* (2000) Identification of ligands and coligands for the ecdysone-regulated gene switch. *Proc Natl Acad Sci U S A* 97(26):14512-14517.

88. Agrawal-Gamse C, *et al.* (2009) Adaptive mutations in a human immunodeficiency virus type 1 envelope protein with a truncated V3 loop restore function by improving interactions with CD4. *J Virol* 83(21):11005-11015.

89. Loftin LM, *et al.* (2010) Constrained use of CCR5 on CD4+ lymphocytes by R5X4 HIV-1: efficiency of Env-CCR5 interactions and low CCR5 expression determine a range of restricted CCR5-mediated entry. *Virology* 402(1):135-148.

90. Tilton JC, *et al.* (2010) A Maraviroc-Resistant HIV-1 with Narrow Cross-Resistance to Other CCR5 Antagonists Depends on both N-Terminal and Extracellular Loop Domains of Drug-Bound CCR5. *J Virol* 84(20):10863-10876.

91. Roche M, *et al.* (2011) HIV-1 predisposed to acquiring resistance to maraviroc (MVC) and other CCR5 antagonists in vitro has an inherent, low-level ability to utilize MVC-bound CCR5 for entry. *Retrovirology* 8(1):89.

92. Lee B & Doms RW (2001) Quantification of HIV/SIV Coreceptor Expression. *Cellualr Aspects of HIV Infection*, eds Cossarizza A & Kaplan D (John Wiley & Sons, Inc., New York, USA).

93. Zolla-Pazner S & Cardozo T (2010) Structure-function relationships of HIV-1 envelope sequence-variable regions refocus vaccine design. *Nat Rev Immunol* 10(7):527-535.

94. Wyatt R, *et al.* (1993) Functional and immunologic characterization of human immunodeficiency virus type 1 envelope glycoproteins containing deletions of the major variable regions. *J Virol* 67(8):4557-4565.

95. Lassen KG*, et al.* (2009) Elite suppressor-derived HIV-1 envelope glycoproteins exhibit reduced entry efficiency and kinetics. *PLoS Pathog* 5(4):e1000377.

96. Schnell G, Joseph S, Spudich S, Price RW, & Swanstrom R (2011) HIV-1 replication in the central nervous system occurs in two distinct cell types. *PLoS Pathog* 7(10):e1002286.

97. Salimi H. RM, Webb N., Gray L., Chikere K., Sterjovski J., Ellett A., Wesselingh S., Ramsland P., Lee B., Churchill M., Gorry P., (2012) Macrophage‐tropic HIV-1 variants from brain demonstrate alterations in the way gp120 engages both CD4 and CCR5. *Journal of Leukocyte Biology*.

98. Jiang C*, et al.* (2011) Primary infection by a human immunodeficiency virus with atypical coreceptor tropism. *J Virol*, United States), Vol 85, pp 10669-10681.

99. Berro R*, et al.* (2011) Multiple CCR5 Conformations on the Cell Surface Are Used Differentially by Human Immunodeficiency Viruses Resistant or Sensitive to CCR5 Inhibitors. *J Virol* 85(16):8227-8240.

100. Nedellec R*, et al.* (2009) Virus entry via the alternative coreceptors CCR3 and FPRL1 differs by human immunodeficiency virus type 1 subtype. *J Virol* 83(17):8353-8363.

101. Lin NH & Kuritzkes DR (2009) Tropism testing in the clinical management of HIV-1 infection. *Curr Opin HIV AIDS* 4(6):481-487.

102. Wilkin TJ & Gulick RM (2012) CCR5 Antagonism in HIV Infection: Current Concepts and Future Opportunities. *Annu Rev Med* 63(1):81-93.

103. Westby M (2007) Resistance to CCR5 antagonists. *Curr Opin HIV AIDS* 2(2):137-144.

104. Pugach P*, et al.* (2009) Inefficient entry of vicriviroc-resistant HIV-1 via the inhibitor-CCR5 complex at low cell surface CCR5 densities. *Virology* 387(2):296-302.

105. Pfaff JM*, et al.* (2010) HIV-1 resistance to CCR5 antagonists associated with highly efficient use of CCR5 and altered tropism on primary CD4+ T cells. *J Virol* 84(13):6505-6514.

106. Roche M*, et al.* (2011) HIV-1 Escape from the CCR5 Antagonist Maraviroc Associated with an Altered and Less-Efficient Mechanism of gp120-CCR5 Engagement That Attenuates Macrophage Tropism. *Journal of Virology* 85(9):4330-4342.

107. Sterjovski J*, et al.* (2010) An altered and more efficient mechanism of CCR5 engagement contributes to macrophage tropism of CCR5-using HIV-1 envelopes. *Virology* 404(2):269-278.

108. St-Pierre C*, et al.* (2011) Host-soluble galectin-1 promotes HIV-1 replication through a direct interaction with glycans of viral gp120 and host CD4. *J Virol* 85(22):11742-11751.

109. Bi S, Hong PW, Lee B, & Baum LG (2011) Galectin-9 binding to cell surface protein disulfide isomerase regulates the redox environment to enhance T-cell migration and HIV entry. *Proceedings of the National Academy of Sciences* 108(26):10650-10655.

110. Liu S. AR, Chikere K., Marsden M., Li G., Wang Y., Su L., Zack J., Freiberg A., Lee B., Cheng G. (2012) The Interferon-Inducible Cholesterol-25-Hydroxylase Broadly Inhibits Viral Entry by Production of 25-Hydroxycholesterol. *Immunity*.

111. Connor RI, Sheridan KE, Ceradini D, Choe S, & Landau NR (1997) Change in coreceptor use correlates with disease progression in HIV-1--infected individuals. *J Exp Med* 185(4):621-628.

112. Bjorndal A*, et al.* (1997) Coreceptor usage of primary human immunodeficiency virus type 1 isolates varies according to biological phenotype. *J Virol* 71(10):7478-7487.

113. Gorry PR & Ancuta P (2010) Coreceptors and HIV-1 Pathogenesis. *Current HIV/AIDS Reports* 8(1):45-53.

114. Sterjovski J*, et al.* (2007) Asn 362 in gp120 contributes to enhanced fusogenicity by CCR5-restricted HIV-1 envelope glycoprotein variants from patients with AIDS. *Retrovirology* 4(1):89.

115. Wade J*, et al.* (2010) Enhanced CD4+ cellular apoptosis by CCR5-restricted HIV-1 envelope glycoprotein variants from patients with progressive HIV-1 infection. *Virology* 396(2):246-255.

116. Chang J*, et al.* (1998) Unique HIV type 1 V3 region sequences derived from six different regions of brain: region-specific evolution within host-determined quasispecies. *AIDS Res Hum Retrov* 14(1):25-30.

117. Hill CM, *et al.* (1998) The Amino Terminus of Human CCR5 Is Required for Its Function as a Receptor for Diverse Human and Simian Immunodeficiency Virus Envelope Glycoproteins. *Virology* 248(2):357-371.

118. Hoffman TL & Doms RW (1999) HIV-1 envelope determinants for cell tropism and chemokine receptor use. *Mol Membr Biol* 16(1):57-65.

119. Korber BT, *et al.* (1994) Genetic differences between blood- and brain-derived viral sequences from human immunodeficiency virus type 1-infected patients: evidence of conserved elements in the V3 region of the envelope protein of brain-derived sequences. *J Virol* 68(11):7467-7481.

120. Martín-García J, Cao W, Varela-Rohena A, Plassmeyer ML, & González-Scarano F (2006) HIV-1 tropism for the central nervous system: Brain-derived envelope glycoproteins with lower CD4 dependence and reduced sensitivity to a fusion inhibitor. *Virology* 346(1):169-179.

121. Ogert RA, *et al.* (2009) Structure-function analysis of human immunodeficiency virus type 1 gp120 amino acid mutations associated with resistance to the CCR5 coreceptor antagonist vicriviroc. *J Virol* 83(23):12151-12163.

122. Peters P, Maria J. Dueñas-Decamp, W. Matthew Sullivan and Paul R. Clapham (2007) Variation of Macrophage Tropism among HIV-1 R5 Envelopes in Brain and Other Tissues. *J NeuroImmune Pharm* 2(1):32-41.

123. Pugach P, *et al.* (2009) Inefficient entry of vicriviroc-resistant HIV-1 via the inhibitor-CCR5 complex at low cell surface CCR5 densities. *Virology* 387(2):296-302.

124. Roche M*, et al.* (2011) HIV-1 Escape from the CCR5 Antagonist Maraviroc Associated with an Altered and Less-Efficient Mechanism of gp120-CCR5 Engagement That Attenuates Macrophage Tropism. *J Virol* 85(9):4330-4342.

125. Salazar-Gonzalez JF*, et al.* (2009) Genetic identity, biological phenotype, and evolutionary pathways of transmitted/founder viruses in acute and early HIV-1 infection. *J Exp Med* 206(6):1273-1289.

126. Arrildt KT, Joseph SB, & Swanstrom R (2012) The HIV-1 env protein: a coat of many colors. *Curr HIV/AIDS Rep* 9(1):52-63.

127. Pfaff JM*, et al.* (2010) HIV-1 Resistance to CCR5 Antagonists Associated with Highly Efficient Use of CCR5 and Altered Tropism on Primary CD4+ T Cells. *J Virol* 84(13):6505-6514.

128. Agrawal-Gamse C*, et al.* (2009) Adaptive Mutations in a Human Immunodeficiency Virus Type 1 Envelope Protein with a Truncated V3 Loop Restore Function by Improving Interactions with CD4. *J Virol* 83(21):11005-11015.

129. Salimi H. RM, Webb N., Gray L., Chikere K., Sterjovski J., Ellett A., Wesselingh S., Ramsland P., Lee B., Churchill M., Gorry PR., (2012) Macrophage‐tropic HIV-1 variants from brain demonstrate alterations in the way gp120 engages both CD4 and CCR5. *J Leukocyte Biol*.

130. Wu Y, Beddall MH, & Marsh JW (2007) Rev-dependent lentiviral expression vector. *Retrovirology* 4(1):12.

131. Boyd MT, Simpson GR, Cann AJ, Johnson MA, & Weiss RA (1993) A single amino acid substitution in the V1 loop of human immunodeficiency virus type 1 gp120 alters cellular tropism. *J Virol* 67(6):3649-3652.

132. Reeves JD (2002) Sensitivity of HIV-1 to entry inhibitors correlates with envelope/coreceptor affinity, receptor density, and fusion kinetics. *Proc Natl Acad Sci USA* 99(25):16249-16254.

133. Rizzuto CD (1998) A Conserved HIV gp120 Glycoprotein Structure Involved in Chemokine Receptor Binding. *Science* 280(5371):1949-1953.

134. Oswald-Richter K*, et al.* (2007) Identification of a CCR5-expressing T cell subset that is resistant to R5-tropic HIV infection. *PLoS Pathog* 3(4):e58.

135. Virgin HW & Walker BD (2010) Immunology and the elusive AIDS vaccine. *Nature* 464(7286):224-231.

136. Haase AT (2010) Targeting early infection to prevent HIV-1 mucosal transmission. *Nature* 464(7286):217-223.

137. Grivel J-C, Shattock RJ, & Margolis LB (2010) Selective transmission of R5 HIV-1 variants: where is the gatekeeper? *J Transl Med* 9(Suppl 1):S6.

138. Keele BF*, et al.* (2008) Identification and characterization of transmitted and early founder virus envelopes in primary HIV-1 infection. *Proc Natl Acad Sci USA* 105(21):7552-7557.

139. Walker LM*, et al.* (2009) Broad and potent neutralizing antibodies from an African donor reveal a new HIV-1 vaccine target. *Science*, United States), Vol 326, pp 285-289.

140. Zhou T, *et al.* (2010) Structural Basis for Broad and Potent Neutralization of HIV-1 by Antibody VRC01. *Science* 329(5993):811-817.

141. Li Y, *et al.* (2011) Mechanism of neutralization by the broadly neutralizing HIV-1 monoclonal antibody VRC01. *J Virol*, United States), Vol 85, pp 8954-8967.

142. Trkola A, *et al.* (2009) Elite Suppressor–Derived HIV-1 Envelope Glycoproteins Exhibit Reduced Entry Efficiency and Kinetics. *PLoS Pathog* 5(4):e1000377.

143. Jiang C, *et al.* (2011) Primary Infection by a Human Immunodeficiency Virus with Atypical Coreceptor Tropism. *J Virol* 85(20):10669-10681.

144. Bleul CC, Wu L, Hoxie JA, Springer TA, & Mackay CR (1997) The HIV coreceptors CXCR4 and CCR5 are differentially expressed and regulated on human T lymphocytes. *Proc Natl Acad Sci USA* 94(5):1925-1930.

145. Mo H, *et al.* (1998) Expression patterns of the HIV type 1 coreceptors CCR5 and CXCR4 on CD4+ T cells and monocytes from cord and adult blood. *AIDS Res Hum Retrov* 14(7):607-617.

146. Benito JM, *et al.* (1997) Quantitative alterations of the functionally distinct subsets of CD4 and CD8 T lymphocytes in asymptomatic HIV infection: changes in the expression of CD45RO, CD45RA, CD11b, CD38, HLA-DR, and CD25 antigens. *J Acquir Immune Defic Syndr Hum Retrovirol* 14(2):128-135.

147. Helbert MR, Walter J, L'Age J, & Beverley PC (1997) HIV infection of CD45RA+ and CD45RO+ CD4+ T cells. *Clin Exp Immunol* 107(2):300-305.

148. Spina CA, Prince HE, & Richman DD (1997) Preferential replication of HIV-1 in the CD45RO memory cell subset of primary CD4 lymphocytes in vitro. *J Clin Invest* 99(7):1774-1785.

149. Silvestri G, *et al.* (2012) Lymphoid Tissue Damage in HIV-1 Infection Depletes Naïve T Cells and Limits T Cell Reconstitution after Antiretroviral Therapy. *PLoS Pathog* 8(1):e1002437.

150. Schacker TW, *et al.* (2006) Lymphatic Tissue Fibrosis Is Associated with Reduced Numbers of Naive CD4+ T Cells in Human Immunodeficiency Virus Type 1 Infection. *Clin and Vaccine Immunol* 13(5):556-560.

151. Duncan CJA & Sattentau QJ (2011) Viral Determinants of HIV-1 Macrophage Tropism. *Viruses* 3(11):2255-2279.

152. Cullen BR, *et al.* (2011) HIV-1 Replication in the Central Nervous System Occurs in Two Distinct Cell Types. *PLoS Pathog* 7(10):e1002286.

153. Salazar-Gonzalez JF, *et al.* (2008) Deciphering Human Immunodeficiency Virus Type 1 Transmission and Early Envelope Diversification by Single-Genome Amplification and Sequencing. *J Virol* 82(8):3952-3970.

154. Kearney M, *et al.* (2008) Human Immunodeficiency Virus Type 1 Population Genetics and Adaptation in Newly Infected Individuals. *J Virol* 83(6):2715-2727.

155. Trkola A, *et al.* (2009) Inflammatory Genital Infections Mitigate a Severe Genetic Bottleneck in Heterosexual Transmission of Subtype A and C HIV-1. *PLoS Pathog* 5(1):e1000274.

156. Masharsky Alexey E*, et al.* (2010) A Substantial Transmission Bottleneck among Newly and Recently HIV‐1–Infected Injection Drug Users in St Petersburg, Russia. *J Infect Dis* 201(11):1697-1702.

157. Young JAT*, et al.* (2011) Recurrent Signature Patterns in HIV-1 B Clade Envelope Glycoproteins Associated with either Early or Chronic Infections. *PLoS Pathog* 7(9):e1002209.

158. Isaacman-Beck J*, et al.* (2009) Heterosexual Transmission of Human Immunodeficiency Virus Type 1 Subtype C: Macrophage Tropism, Alternative Coreceptor Use, and the Molecular Anatomy of CCR5 Utilization. *J Virol* 83(16):8208-8220.

159. Alexander M*, et al.* (2010) Donor and recipient envs from heterosexual human immunodeficiency virus subtype C transmission pairs require high receptor levels for entry. *J Virol* 84(8):4100-4104.

160. Wilen CB*, et al.* (2011) Phenotypic and immunologic comparison of clade B transmitted/founder and chronic HIV-1 envelope glycoproteins. *J Virol* 85(17):8514-8527.

161. Ochsenbauer C*, et al.* (2011) Generation of Transmitted/Founder HIV-1 Infectious Molecular Clones and Characterization of Their Replication Capacity in CD4 T Lymphocytes and Monocyte-Derived Macrophages. *J Virol* 86(5):2715-2728.

162. Trkola A, *et al.* (2012) Transmitted/Founder and Chronic Subtype C HIV-1 Use CD4 and CCR5 Receptors with Equal Efficiency and Are Not Inhibited by Blocking the Integrin α4β7. *PLoS Pathog* 8(5):e1002686.

163. Hope TJ, *et al.* (2009) Soluble CD4 and CD4-Mimetic Compounds Inhibit HIV-1 Infection by Induction of a Short-Lived Activated State. *PLoS Pathog* 5(4):e1000360.

164. Sterjovski J, *et al.* (2012) Structural elements of primary CCR5-using HIV-1 gp120 proteins influencing sensitivity and resistance to the broadly neutralizing monoclonal antibody b12. *Virology* 432(2):394-404.

165. Ping L-H, et al. (2012 Submitted) Comparison of the Viral Env Protein From Acute and Chronic Infections of Subtype C HIV-1 Suggests A New Strategy For Immunogen Design. *PLoS Pathog*.Submitted.

166. Parker Z, et al. (2012) Transmitted/Founder and Chronic HIV-1 Envelope Proteins Differentially Utilize CCR5. *J Virol*.Submitted.

167. Nedellec R, *et al.* (2009) Virus entry via the alternative coreceptors CCR3 and FPRL1 differs by human immunodeficiency virus type 1 subtype. *J Virol* 83(17):8353-8363.

168. Renjifo B, *et al.* (2004) Preferential in-utero transmission of HIV-1 subtype C as compared to HIV-1 subtype A or D. *AIDS* 18(12):1629-1636.

169. Ball SC, *et al.* (2003) Comparing the ex vivo fitness of CCR5-tropic human immunodeficiency virus type 1 isolates of subtypes B and C. *J Virol* 77(2):1021-1038.

170. Mo H, *et al.* (1997) Human immunodeficiency virus type 1 mutants that escape neutralization by human monoclonal antibody IgG1b12. off. *J Virol* 71(9):6869-6874.

171. Bunnik EM, *et al.* (2010) Emergence of monoclonal antibody b12-resistant human immunodeficiency virus type 1 variants during natural infection in the absence of humoral or cellular immune pressure. *J Gen Virol* 91(5):1354-1364.

172. Pfaff JM, *et al.* (2012) HIV-1 Resistance to CCR5 Antagonists Associated with Highly Efficient Use of CCR5 and Altered Tropism on Primary CD4+ T Cells. *J Virol* 84(13):6505-6514.

173. Keele BF, *et al.* (2012) Identification and characterization of transmitted and early founder virus envelopes in primary HIV-1 infection. *Proceedings of the National Academy of Sciences* 105(21):7552-7557.

174. Salazar-Gonzalez JF, *et al.* (2012) Genetic identity, biological phenotype, and evolutionary pathways of transmitted/founder viruses in acute and early HIV-1 infection. *The Journal of Experimental Medicine* 206(6):1273-1289.

175. Sundaravaradan V, *et al.* (2007) Role of HIV-1 subtype C envelope V3 to V5 regions in viral entry, coreceptor utilization and replication efficiency in primary T-lymphocytes and monocyte-derived macrophages. *Virology Journal* 4(1):126.

176. Pilcher CD, *et al.* (2004) Brief but efficient: acute HIV infection and the sexual transmission of HIV. *J Infect Dis* 189(10):1785-1792.

177. Wawer MJ, *et al.* (2005) Rates of HIV-1 transmission per coital act, by stage of HIV-1 infection, in Rakai, Uganda. *J Infect Dis* 191(9):1403-1409.

178. Zhou T, *et al.* (2010) Structural Basis for Broad and Potent Neutralization of HIV-1 by Antibody VRC01. *Science* 329(5993):811-817.

Appendix A

Generation of GGR Affinofile Cell Line

Generation of GGR Vector and GGR Affinofile cell line.

We engineered the *Gaussia* luciferase gene upstream of the GFP reporter (linked via an IRES sequence) in the tat/rev dependent vector previously generated by *Marsh et al*(1). The original vector contained a tat-responsive LTR, several splice donor and acceptor sites from the HIV genome, and the Rev-responsive element (RRE) placed downstream of the GFP reporter gene such that the intact Gaussia luciferse and GFP reading frame is only exported in the presence of HIV Rev. Thus this vector expresses increased levels of *Gaussia* luciferase and GFP only in the presence of HIV.

We then generated VSVG pseudotyped virus using the GGR vector. Concentrated VSVG pseudotyped GGR virus was used to transduce low passage parental Affinofile cell. Transduced Affinofile cells were passaged continually until basal *Gaussia* luciferase levels stabilized. To discover/ the cell clone with the best signal to noise ratio, we created a 96 well replicate of individual grown cells, with one plate being induced and infected with JRCSF virus. Supernatant was collected 24 hours post infection. Initially, 12 individual cell clones were selected based on signal to noise ratio above 10. Those clones were allowed to grow (Figure A-1). Final cell clone was selected for low basal expression of CD4 and CCR5, best induction and signal to noise properties (Figure A-2, A-3). Final clone selected was dubbed the GGR Affinofile cell line.

Comparison Between firefly luciferase expression and *Gaussia* luciferase expression in infected GGR Affinofile cells.

To get a better understanding of how our novel GGR Affinofiles compared to conventional infectivity assays; we induced GGR Affinofile at medium and high induction 24 hours later infected with pseudotyped virus that expresses firefly luciferase in cells infected. 48 hour post infection cell supernatant (1/15 of total) was taken and assayed for *Gaussia* lucifease activity, in conjunction, cell lysate (1/2 of total) was measured for firefly luciferase activity. Compared to firefly luciferase readings, our novel GGR cell line demonstrated a comparable response to changes in infection due to the different levels of induction. One important thing to note is that firefly luciferase gave larger error bars compared to *Gaussia* luciferase, which is likely due to cumbersome nature of lysing cells.

GGR Vector integration number determination in GGR Affinofile cell line.

Alu-gag pcr was done in according to previously published protocol (2). GGR Affinofile cell DNA was subjected to an initial round of pcr to amplify GGR vector integrated DNA using *Alu* and gag primers. Subsequently, a nested pcr was done on the previous pcr product using primers unique to the long terminal repeat region. Results from both assays confirmed the presence of two integration events.

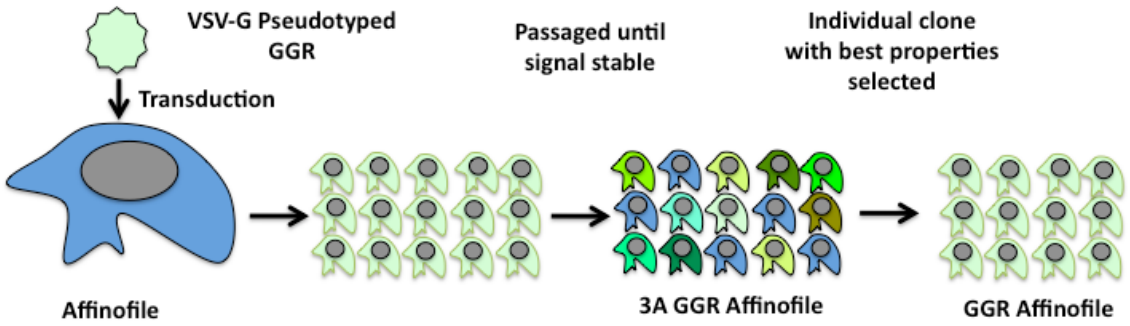

Figure A-1: Schematic diagram of GGR Affinofile cell line

The GGR vector was packaged into a VSV-G pseudotyped lentivirus. This virus was subsequently used to transduce parental Affinofile cells. Transduced Affinofile cells were passaged continually until basal *Gaussia* luciferase levels stabilized.

Signal/Noise

	2	3	4	5	6	7	8	9	10	11
B	1	1	2	**17**	1	**17**	7	1	6	9
C	1	0	11	0	6	1	3	0	10	8
D	4	1	9	12	1	7	**14**	1	13	**17**
E	6	3	11	13	1	10	11	1	**28**	1
F	7	**15**	1	1	1	1	1	1	1	1
G	2	12	1	**15**	1	**28**	3	10	1	**14**

Figure A-2: Signal to noise ratio of GGR clones

Select clones were expanded and infected with a R5-tropic HIV upon full-induction of CD4 and CCR5. Clones with the highest signal to noise ratio upon infection are indicated in **red**. Clones with best signal to noise ratio were expanded. Sample plate 1 of 2.

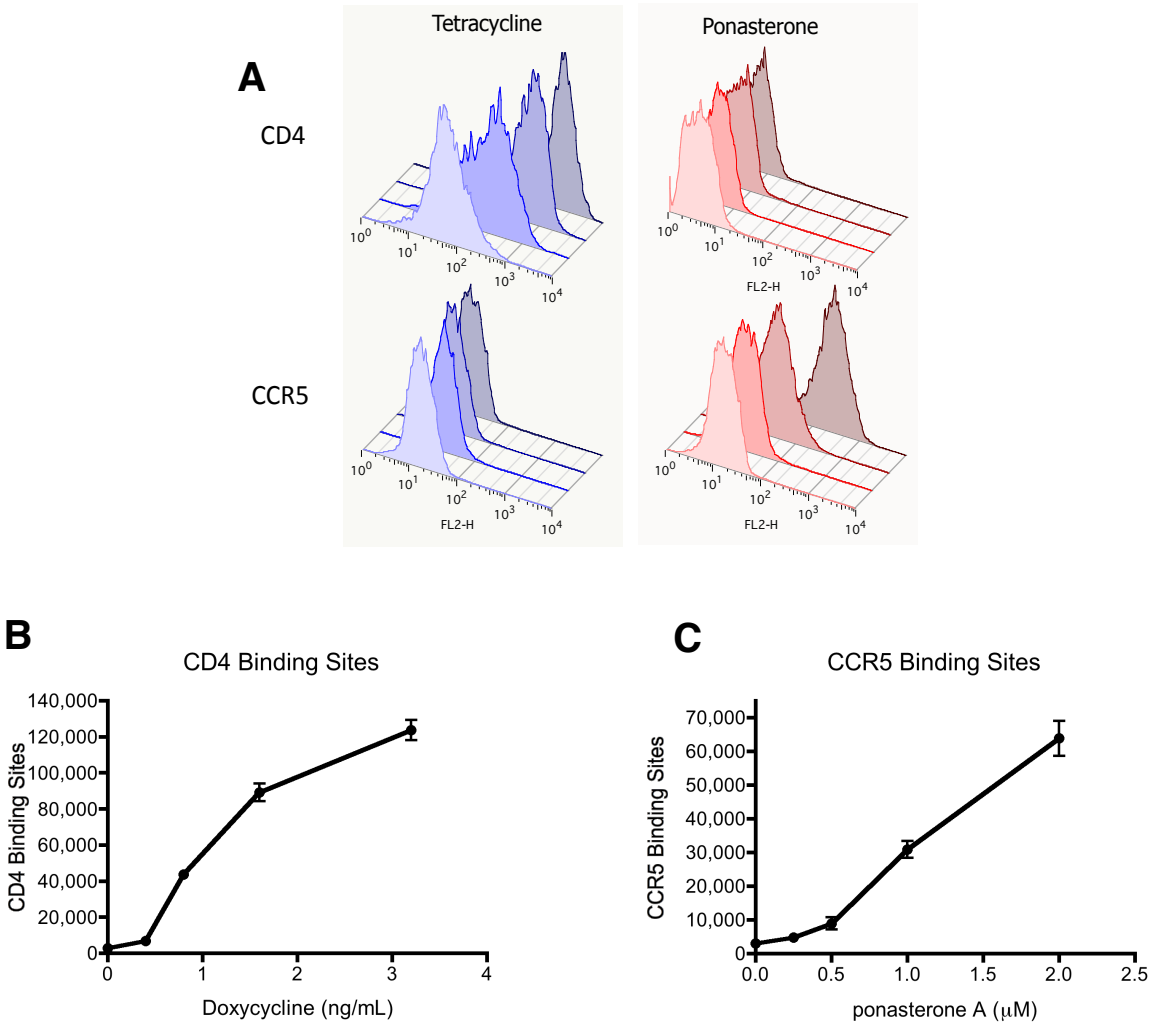

Figure A-3: GGR Affinofile cells demonstrate independent and simultaneous expression of CD4 and CCR5

Ponasterone and doxycycline induced CD4 and CCR5 expression without affecting one another. Raw histogram data from a representative experiment are presented (A). Quantification of CD4 and CCR5 expression is shown (B and C). Data shown is from seven independent experiments.

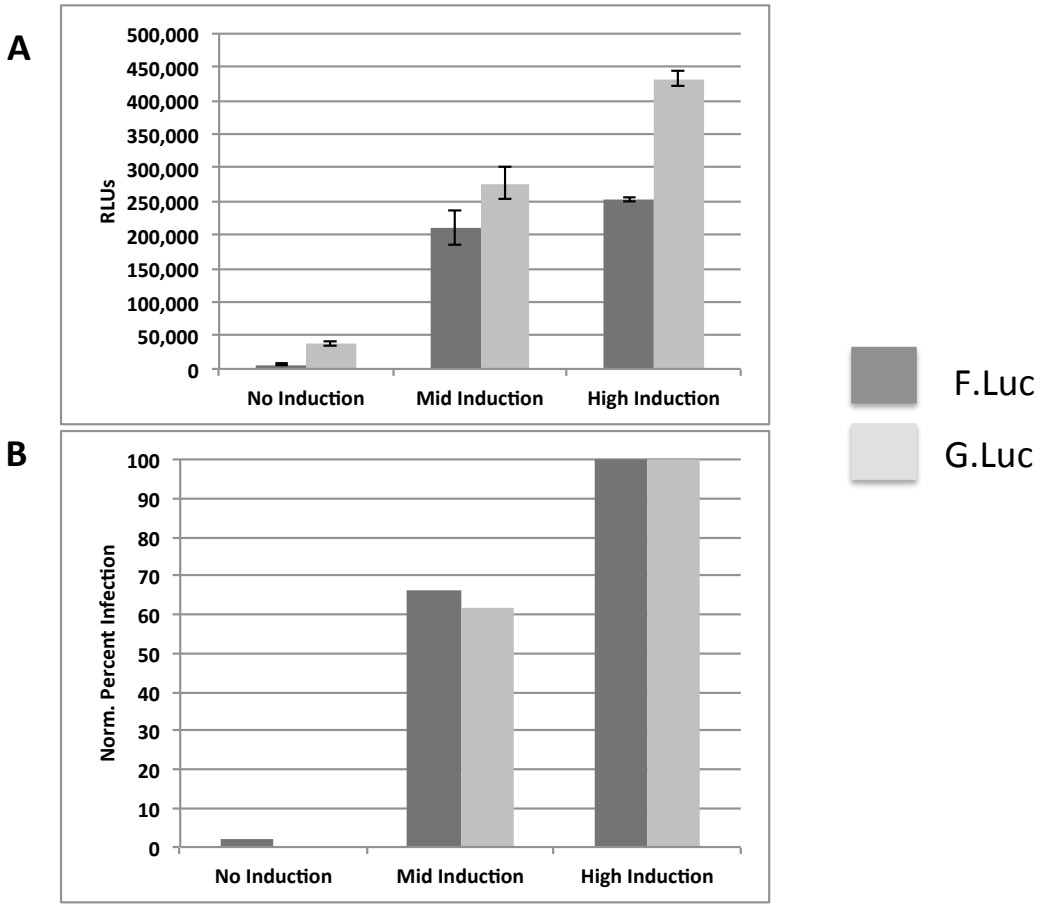

Figure A-4: Comparison between Firefly luciferase expression and Gaussia luciferase expression in infected GGR Affinofile cells

GGR Affinofile cells were infected with firefly pseudotyped virus. 72 hours later cell supernatant was analyzed for Gaussia Luciferase activity. In conjunction, cells were lysed and assayed for firefly luciferase activity. Raw luciferase values (A) and Normalized data are shown (B). Data is representative of four repeats

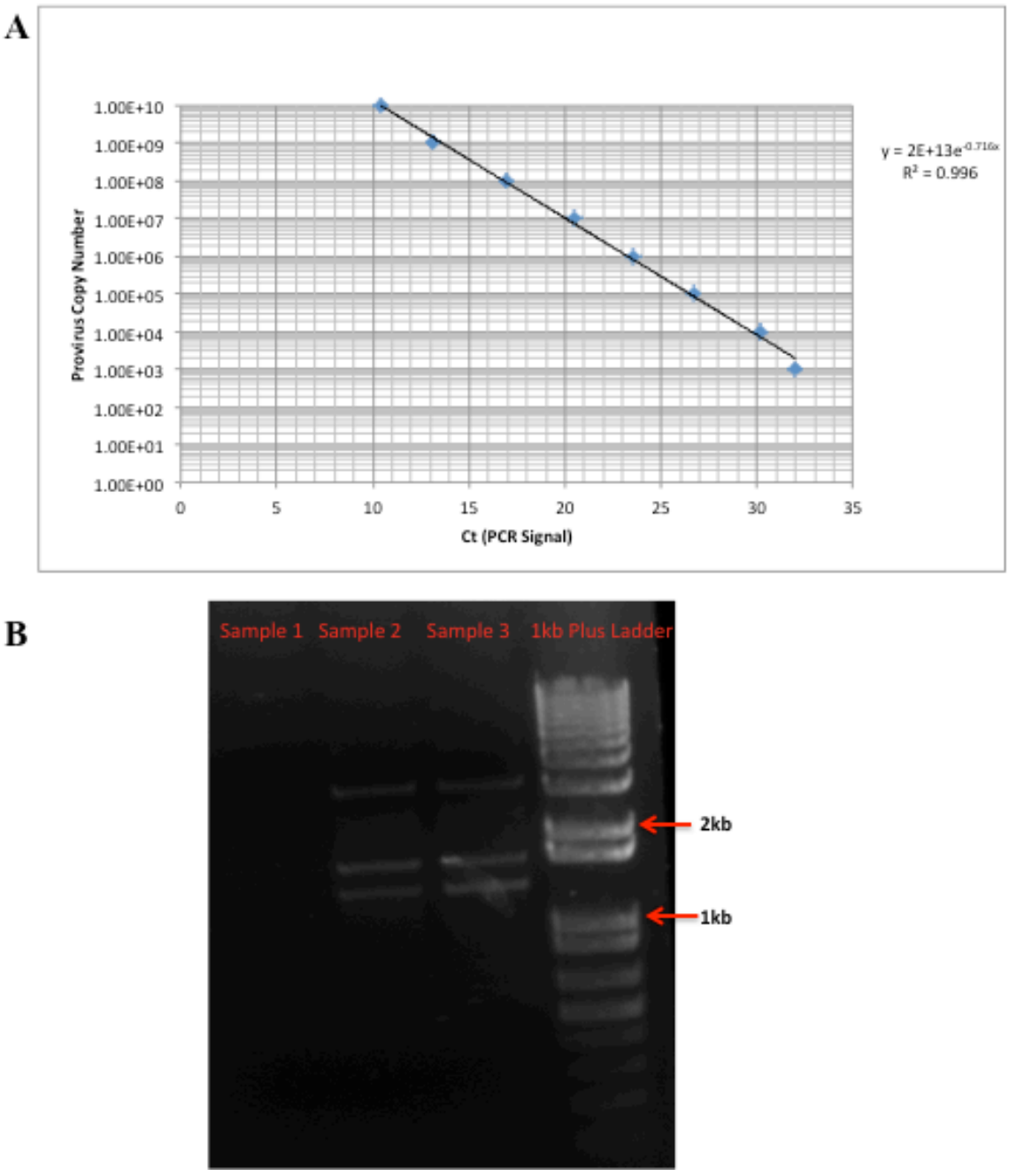

Figure A-5: Quantifying integrated vector copies in GGR Affinofile cells using *Alu*-gag qPCR

GGR cells were subject to *Alu*-gag pcr. (A) GGR Affinofile cells were determined to have two integrated copies of the GGR vector. (B) The primary nested pcr product was ran on 1 % aagarose gel to confirm the presence of two distinct integrated vectors. Sample 1 pcr was done on 1st generation Affinofile genomic DNA. Sample 2 and 3 pcr was done on GGR Affinofiles genomic DNA. The last lane is the 1kb plus ladder

References

1. Wu Y, Beddall MH, & Marsh JW (2007) Rev-dependent lentiviral expression vector. *Retrovirology* 4(1):12.
2. Liszewski MK, Yu JJ, & O'Doherty U (2009) Detecting HIV-1 integration by repetitive-sampling Alu-gag PCR. *Methods* 47(4):254-260.

Appendix B

Interferon-Inducible Cholesterol-25-Hydroxylase Broadly Inhibits Viral Entry by Production of 25-Hydroxycholesterol

SUMMARY

Interferons (IFN) are essential antiviral cytokines that establish the cellular antiviral state through upregulation of hundreds of interferon-stimulated genes (ISGs), most of which have uncharacterized functions and mechanisms. We identified cholesterol-25-hydroxylase (*CH25H*) as a broadly antiviral ISG. CH25H converts cholesterol to a soluble antiviral factor, 25-hydroxycholesterol (25HC). 25HC treatment in cultured cells broadly inhibited growth of enveloped viruses including VSV, HSV, HIV, and MHV68 and acutely pathogenic EBOV, RVFV, RSSEV, and Nipah viruses under BSL4 conditions. It suppressed viral growth by blocking membrane fusion between virus and cell. In animal models, *Ch25h*-deficient mice were more susceptible to MHV68 lytic infection. Moreover, administration of 25HC in humanized mice suppressed HIV replication and rescued T-cell depletion. Thus, our studies demonstrate a unique mechanism by which IFN achieves its antiviral state through the production of a natural oxysterol to inhibit viral entry and implicate membrane-modifying oxysterols as potential antiviral therapeutics.

INTRODUCTION

Viruses are obligate intracellular pathogens that—despite having unique structures and functions--undergo lifecycle stages of entry, replication, protein synthesis, assembly, and egress. Upon binding to cell surface molecules, non-enveloped virus can enter the cell directly while enveloped viruses undergo a fusion process that requires specific interactions between viral and cellular receptors and membranes. In the cellular cytoplasm or the nucleus, incipient viral proteins may be sufficient to initiate early lifecycle processes, but full replication, transcription and translation require utilization of cellular factors. The newly synthesized viral proteins and genome are coordinately assembled into virions, which then exit the cell by lysis or budding.

While viruses exploit host factors to successfully replicate, the innate immune system inhibits viral growth by production of interferons (IFN), which are essential antiviral cytokines that induce wide array of antiviral effectors. Many IFN-stimulated genes (ISGs) work by inhibiting particular viral lifecycle stages. IFITM proteins block viral entry and ISG20, a 3'-5' exonuclease, degrades single stranded viral RNA; PKR inhibits viral translation through suppression of eIF2a elongation factors and tetherin prevents release of virions from the cell (Degols *et al*., June; García *et al*., 2006; Neil *et*

al., 2008; Van Damme *et al*., 2008; Brass *et al*., 2009). These ISGs exemplify only a few of the hundreds of confirmed ISGs; most of them are uncharacterized.

Cholesterol-25-hydroxylase (*Ch25h*) is a conserved ISG that encodes an endoplasmic-reticulum-associated enzyme that catalyzes oxidation of cholesterol to 25-hydroxycholesterol (25HC)(Holmes *et al*., 2011). 25HC belongs to a diverse class of endogenous oxysterols, the oxidation products of cholesterol. It is widely understood to be a soluble factor that controls sterol biosynthesis through regulation of sterol-responsive element binding proteins (SREBP) and nuclear receptors (Kandutsch *et al*., 1978; Janowski *et al*., 1999). While oxysterols have unique roles in metabolism, studies have implicated their importance in immunity. Macrophages and dendritic cells express CH25H in response to various toll-like receptor (TLR) ligands and IFN (Bauman *et al*., 2009; Park and Scott, 2010). *Ch25h* is a suppressor of IgA production in B-Cells and may promote intracellular bacterial growth (Bauman *et al*., 2009; Zou *et al*., 2011). Dysregulation of 25HC is associated with atherosclerosis, which is partly attributed to its induction of the inflammatory cytokine, IL-8 (Andrew J and Jessup, 1999; Wang *et al*., 2012). Although these studies support a conserved immunological role of *Ch25h* and 25HC, their functions in the antiviral immune response remain elusive.

We have found that *Ch25h* is important for the host immune response against viral infection. This study explores the antiviral function of *Ch25h*, the mechanism of its viral inhibition, as well as its physiological significance during viral infections.

RESULTS

Ch25h is an IFN-dependent Gene with Antiviral Activity

In a microarray analysis of IFNα and IFNγ stimulated murine bone marrow-derived macrophages (BMMs), we found both types of IFNs induced expression of *Ch25h* within 3hrs (Fig. B-1A; accession no. GSE35825). Gene expression analysis by qRT-PCR showed that *Ch25h* is induced by polyI:C (TLR3 agonist) in bone marrow derived macrophage (BMM) or dendritic cells (BMDC). BMMs had higher induction in response to IFN (Fig. B-1B). In mice infected with $5x10^6$ pfu of VSV i.p., *Ch25h* was induced after 18 and 36h in lung, liver, and kidney, with highest induction in liver and kidneys (Fig. B-1C). An RNAseq analysis showed toll-like receptor 4 (TLR4) induction of *Ch25h* was dependent on IFN receptor (*IFNAR1*) but independent of IL-27, a cytokine that mediates IFN secondary gene expression, such as IL-10 (Fig. B-1D). This result was confirmed by qRT-PCR showing that *Ch25h* expression was induced by TLR2, 3, 4, and 9 agonists, with highest expression induced by polyI:C (TLR3) and lipid (TLR4). IFN receptor deficient ($Ifnar1^{-/-}$) BMMs had abrogated *Ch25h* expression when treated with these agonists showing that *Ch25h* expression is IFN-dependent (Fig. B-1E).

In a previous study, we performed a blinded, unbiased screen for antiviral ISGs against vesicular stomatitis virus co-expressing GFP (VSV-GFP) (Liu *et al*., 2012). We co-transfected individual plasmids encoding an ISG with a plasmid encoding a red fluorescent protein, DsRed. Transfection proceeded for 36h before infection with VSV-GFP. At 9hpi, we quantified VSV-GFP with FACs by gating on DsRed-positive population, which are cells that highly express the ISG (Fig1. F). Expression of human *CH25H* inhibited VSV-GFP replication by ~89% at 9hpi (Fig1. G). IFN activators like *TBK1*, *IFIH1*, and *IRF1* strongly inhibited VSV as well as the RNA exonuclease, *ISG20*. To validate the antiviral effect of *CH25H*, we generated a doxycycline-inducible *CH25H*-flag construct co-expressing a red-red mCherry (*CH25H*-mCherry). Doxycycline addition to HEK293T expressing this construct increased *CH25H*-mCherry expression (Fig. B-2A top) and—after infection--- inhibited VSV-GFP expression compared to vector control in a dose-dependent manner (Fig 2A, bottom). Taken together, *CH25H* overexpression is sufficient to inhibit VSV.

Loss of function of *Ch25h* leads to Susceptibility to Viral Infections *in vitro*

We sought to determine whether *Ch25h* might be a required antiviral factor. We generated *Ch25h* stable knockdown cell lines from murine macrophage cell line,

RAW264.7, with two distinct shRNA sequences against *Ch25h* and confirmed the knockdown by qRT-PCR (Fig. B-2B). Both knockdown cell lines demonstrated increased VSV replication compared to scramble control (Fig. B-2C). To further validate these results, macrophage and B-cell lines were derived from *Ch25h*-deficient ($Ch25h^{-/-}$) and matching wild-type ($Ch25h^{+/+}$) mice. In our conditions, we could not establish VSV infection in primary cell lines; hence we immortalized BMMs and B-cells with J2 and BCR-ABL oncogenic retroviruses, respectively. $Ch25h^{-/-}$ J2 BMMs displayed 5-fold increased susceptibility to VSV infection compared to $Ch25h^{+/+}$ J2 BMMs at 14hpi. In B-cells transformed with BCR-ABL, we observed about 100 fold increase in VSV-GFP replication in 3 different $Ch25h^{-/-}$ B-Cell clones at 48hpi compared to 2 $ch25h^{+/+}$ B-cell clones (Fig. B-2E). These results show that *Ch25h* may be required for host antiviral immunity.

***Ch25h* produces a soluble antiviral factor that is not IFN**

In overexpression studies described in Fig. B-1, HEK293T were transfected with ISG plasmids and DsRed in 3:1 ratio such that DsRed-positive cells (DsRed+) should represent cells that highly expressed the ISG, whereas DsRed-negative (DsRed-) cells should represent low ISG expressers (Fig. B-3A). IFN activators, *TBK1*, *IFIH1*, and

IRF1, inhibited VSV-GFP expression in both populations showing DsRed+ cells confer viral resistance to DsRed- through a soluble factor, which is IFN (Fig. B-3B). In contrast, the cytoplasmic viral RNA exonuclease, *ISG20*, only inhibited VSV growth in DsRed+ population, but not DsRed- population. Overexpression of *CH25H* also inhibited virus in both DsRed+ and DsRed- populations suggesting that CH25H produced a soluble factor that acts *in trans* to confer antiviral activity onto other cells.

To determine if CH25H produced a soluble antiviral factor, we tested whether conditioned medium from cells overexpressing *CH25H* had antiviral activity. HEK293T cells were transfected with vector, interferon activators (*TBK1*, *IFIH1*, and *IRF1*), *CH25H*, or *ISG20*, and the conditioned media was transferred onto freshly plated HEK293T cells for 8h before infection with VSV-GFP (0.01MOI). As expected, conditioned media from IFN activators inhibited VSV growth, but not *ISG20*-conditioned media (Fig. B-3 C). Conditioned medium from *CH25H* generated ~60% VSV-GFP inhibition. We have also observed similar effect in several human and murine cell lines including HeLa, 3T3, BHK, Veros, MDCK, and Huh751 (Fig. B-S1 A). These results demonstrate that *CH25H* produces a soluble antiviral factor.

IFN induces many ISGs that positively feedback and amplify its production, leading to the hypothesis that the *CH25H*-induced soluble factor is IFN. *CH25H*

conditioned medium, however, had no detectable IFNβ by ELISA and did not induce an IFN-stimulated responsive element (ISRE) luciferase reporter (Fig. B-S1 B and C). More importantly, *CH25H*-conditioned medium inhibited VSV replication in both *Ifnar1*$^{-/-}$ fibroblasts and J2 BMMs. As positive control, conditioned media from IFN activators, IRF1, IFIH1, and RIG-I, were unable to confer antiviral activity to *Ifnar1*$^{-/-}$ cell lines (Fig. B-3 E and F). Taken together, CH25H produces a soluble factor that is not IFN and can confer antiviral activity independent of IFNAR.

25-hydroxycholesterol (25HC), the product of CH25H, has antiviral activity

Ch25h catalyzes oxidation of cholesterol to 25-hydroxycholesterol (25HC), a soluble oxysterol that acts as an autocrine and paracrine mediator (Fig. B-4 A, top). We hypothesized that the soluble antiviral factor generated by CH25H is 25HC. Treatment of HEK293T cells with 25HC for 8h inhibited VSV-GFP expression in a dose-dependent manner with IC_{50} of ~1μM (Fig. B-4 A, bottom). Two other oxysterols, 22-(R)-hydroxycholesterol (22R-HC) and 22-(S)-hydroxycholesterol (22S-HC), had no effect on VSV. 22R-HC is also an agonist for the nuclear hormone receptor LXR and 22S-HC is an inactive ligand. Since 25HC has been implicated as a LXR agonist, these results also

suggest that the antiviral effect was LXR-independent. In addition, 25HC treatment of *Ch25h*$^{+/+}$ and *Ch25h*$^{-/-}$ J2 BMMs reduced VSV replication (Fig. B-4B).

The effect of 25HC on cell viability and toxicity was also assessed. 25HC treatment at 10 times IC_{50} (10μM) did not increase LDH in supernatants of cells after 16h of treatment; LDH level increased only after 30-40h treatment at 40μM of 25HC (Fig. B-S2 A and B). Similarly, *CH25H*-conditioned medium did not alter cell viability as measured by ATP levels (Fig. B-S2 C). Therefore, CH25H carries out its antiviral effect through its enzymatic product, 25HC, which has a specific antiviral effect.

CH25H and 25HC are broadly antiviral

To determine the breadth of antiviral activity of *Ch25h*, we tested the effect of *CH25H*-conditioned medium and 25HC on various viruses. For HIV, primary peripheral blood mononuclear cells (PBMCs) were treated with conditioned medium or oxysterol and subsequently infected with HIV NL4-3. At 3dpi, *CH25H*- and *IRF1*- conditioned media caused ~75% reduction of HIV NL4-3 p24 expression (Fig. B-4C). Similarly, 25HC (1μM) inhibited p24 expression by ~80% at 3dpi compared to vehicle treatment, whereas 22S-HC had no effect (Fig. B-4D). *CH25H*-conditioned medium also inhibited herpes simplex virus 1 (HSV-1) by plaque assay (Fig. B-4E) and expression of *Ch25h* in

HEK293T also reduced murine gammaherpes virus (MHV68) infection by plaque assay (Fig. B-4F).

HIV, HSV-1, and MHV68 are viruses that achieve chronically persistent infections. To determine whether 25HC can inhibit acutely pathogenic viruses, we tested the effect of 25HC on live Ebola virus (EBOV, strain Zaire), Nipah virus (NiV, strain Bangladesh), Russian Spring-Summer Encephalitis Virus (RSSEV, strain Sofjin), and Rift Valley fever virus (RVFV, wild-type strain ZH501 and vaccine strain MP12) under BSL4 conditions. Figures 4 G, H, I, and J show that 1μM of 25HC inhibited replication of these live viruses. 25HC also inhibited replication of NiV and RVFV (MP12) in a dose-dependent manner (Fig. B-S2 D and E). In contrast, 25HC did not affect the growth of a GFP-expressing adenovirus, which is a non-enveloped virus, as measured by FACs (Fig. B-4K). Taken together, *Ch25h*-induced 25HC has antiviral activity against several types of enveloped DNA and RNA viruses, while it does not affect a non-enveloped virus.

25HC inhibits VSV entry

We took advantage of tools available for VSV and HIV to study the mechanism of *CH25H* inhibition on the viral lifecycle. First, we utilized the pseudotyped VSVΔG-

Luc reporter virus system that has the receptor-binding G gene (VSV-G) replaced with a luciferase reporter gene that is capable of single-round infection (Negrete *et al*., 2006). Quantification of luciferase activity is indicative of viral lifecycle processes from entry to protein synthesis. *CH25H*- and *IRF1*-conditioned media inhibited VSVΔG-Luc expression suggesting inhibition of viral replication at an early stage (Fig. B-5A). In a time-of-addition experiment, longer pre-treatment times correlated with greater inhibition of VSVΔG-Luc expression, compared to vehicle treated controls (Fig. B-5B). These results suggest that 25HC does not inhibit VSV during infection or after infection has taken place. Rather, it is likely that 25HC establishes an antiviral state prior to infection.

Since these data implicate early viral lifecycle steps may be affected, we carried out experiments to determine whether 25HC affects attachment (Weidner *et al*., 2010). HEK293Ts were treated for 8h with ethanol (EtOH), 25HC (1μM), CPZ (10μg/mL), an endocytosis inhibitor that would have no effect on binding. To measure binding, VSV (1MOI) was incubated with HEK293T at 4°C for 1h to allow for binding but not cell entry. After washing 3 times with cold PBS, quantification of VSV genomic RNA (gRNA) showed that 25HC did not inhibit viral binding significantly ($P>0.05$) (Fig. B-5C).

To determine if 25HC affects efficiency of fusion, we established a VSV-G β-lactamase (βla) entry assay based on the ability of VSV-G to be pseudotyped onto viral-like particles made from the βla-Nipah virus matrix fusion protein, herein called VSV-G-βlaM (Wolf *et al*., 2009). VSV-G mediated fusion will result in cytoplasmic delivery of βla-M; by addition of lipophilic fluorescent CCF2-AM substrate, the βla activity can be measured by the green (525nm) to blue (485nm) fluorescence shift as a result of CCF2-AM cleavage (Zlokarnik *et al*., 1998). Hence, efficiency of virus-cell fusion can be measured by the increase in the ratio of blue to green (blue:green) fluorescence, which is reflective of the βla activity associated with βlaM that was been released into the cytoplasm after VSV-G mediated fusion (Cavrois *et al*., 2002; Wolf *et al*., 2009). Unlike the VSVΔG-Luc pseudotyped virus, this VSV-G-βlaM entry assay does not require transcription and translation of viral proteins for reporter gene expression. Fusion is proportional to βlaM concentration, which is estimated by the rate constant (*k*) derived from the slope of the reaction during the linear phase of the reaction within the first hour.

We first demonstrated that IFN treatment of HEK293Ts could cause a dose-dependent inhibition of viral entry by VSV-G-βlaM assay (Fig. B-5D), suggesting there exist ISGs that block viral entry. To test whether CH25H may partly mediate this effect,

HEK293Ts were transfected with several ISGs for 48 hours and infected with VSV-G-βlaM. Figure B-5E showed that *CH25H* expression reduced efficiency of VSV fusion. Compared to vector control, βlaM activity from *CH25H*-transfected cells proceeded at 48% of vector-transfected cell (compare rate constants in inset table) and reached a plateau level. The previously described entry inhibitor, *IFITM3*, also reduced VSV-G-βlaM fusion (Brass *et al*., 2009). Expression of *ISG20*, a viral RNA exonuclease, had no effect on viral entry. *IRF1*-transfected cells also inhibited fusion, presumably by up-regulation of IFN. *CH25H*-conditioned medium similarly inhibited VSV-G-βlaM entry, with a more pronounced effect than *IRF1*-conditioned medium (Fig. B-5F). Furthermore, treatment of 25HC at 1, 2.5, and 5μM inhibited VSV-G-βlaM activity, by 44%, 56%, and 70%, respectively (Fig. B-5G). These results demonstrate that CH25H, and its cognate product, 25HC, inhibits efficiency of virus-cell fusion.

To delineate whether 25HC affects viral or cellular membrane, we tested how infectivity of the virions was affected when they were produced from 25HC treated cells. HEK293T cells were treated with and without 25HC (2.5μM) for 8h and infected with live VSV at 0.01 MOI for 1h. Viral supernatants were purified and cleared of residual 25HC by ultracentrifugation through a 20% sucrose cushion. As expected, there was >60% reduction in the amount of VSV from 25HC treated samples versus control, as

measured by qRT-PCR for the number of viral genome copies (gRNA) (Fig. B-S3 A). To assess infectivity, we normalized viral titer from 25HC- or vehicle-treated cells based on gRNA. After normalization, VSV titer from 25HC-treated cells was equivalent to the titer from vehicle-treated cells by plaque assay (Fig. B-S3 B). These results show that 25HC does not affect viral infectivity but rather, affects the cellular membrane property.

25HC is a suppressor of SREBP2, a factor that controls sterol biosynthesis. We tested the hypothesis that suppression of SREBP2 by 25HC can inhibit viral growth by testing whether active (cleaved) forms of SREBPs in HEK293T would overcome 25HC's anti-viral effect. Overexpression of active forms of *Srebp1a*, *Srebp1-c*, and *Srebp2* in HEK293Ts, however, did not reverse 25HC's antiviral effect (Supp Fig. B-S3 C). 25HC also suppresses many sterol biosynthetic enzymes including HMG-CoA reductase, which produces the key intermediate mevalonate (Pezacki *et al*., 2009) (Fig. B-S3 D). We hypothesized that mevalonate may reverse the antiviral effect of 25HC. Addition of exogenous mevalonate (300μM) to HEK293T before and during 25HC treatment, however, did not reverse the antiviral effect of 25HC (Fig. B-S3 E).

25HC also may inhibit production of another intermediate isopentenyl-pyrophosphate (Isopentyl-PP), which is substrate for prenylation of proteins mediated by farnesyltransferase (FTase) and geranylgeranyltransferase (GTase). We tested the

hypothesis that inhibition of prenylation can inhibit VSV growth. HEK293T were treated with FTase and GTase inhibitors, FTI-276 and GGTI-298 (5-20μM), and infected with VSV-GFP. FTI-276 treatment had no effect on VSV, whereas GGTI-298 reduced viral growth at 10-20μM (Fig. B-S3 F). GGTI-298, however, caused >10% reduction in cell viability by ATP content, whereas 25HC and FTI had no effect (Fig. B-S3 G). Furthermore, FTI-276 and GGTI-298 did not reduce VSV fusion by VSV-G-βlaM assay (Fig. B-S3 H and I). Taken together, although prenylation inhibition may have some antiviral effect, it also inhibits cell viability and has no effect on viral entry as seen with 25HC.

***Ch25h* and 25HC inhibits HIV entry**

We sought to validate CH25H and 25HC antiviral mechanism on HIV, a virus that undergoes pH-independent entry. In CEM cells, 25HC inhibited >50% luciferase expression from single round infection of pseudotyped HIV-IIIB coexpressing luciferase (Fig. B-6A). AZT, an inhibitor of reverse transcription that served as positive control, inhibited the expression by ~70%. Hence, 25HC inhibits HIV lifecycle prior to or at translation.

HIV initiates reverse transcription of its genomic RNA to DNA immediately after entry. We examined the effect of 25HC on the production of full-length, reverse-transcribed DNA (lateRT). CEM cells were infected with pseudotyped HIV-IIIB and lateRT was measured by qRT-PCR. 25HC inhibited lateRT expression ~70% at 6hpi (Fig. B-6B). AMD3100, a HIV entry inhibitor, served as positive control and Elvitegravir, an inhibitor of DNA integration, was used as a negative control. Hence, 25HC inhibits HIV life cycle before reverse transcription.

We next tested whether *CH25H* inhibits HIV growth at the level of entry. We coexpressed pNL4-3 with βla-VPR fusion gene to produce virions containing βla-VPR (NL4-3-βla). CEM cells treated with *CH25H*-conditioned medium exhibited ~65% reduction in viral entry compared to vector- and *ISG20*-conditioned medium. AMD3100 abrogated NL4-3-βla entry (Fig. B-6C). We further confirmed our findings by FACs analysis and observed ~50% decrease in the number of cells expressing cleaved CCF2-AM substrate (blue population) in CEM treated with *Ch25h* conditioned medium compared to control (supp. Fig. B-S4 A). Treatment of CEM cells with 25HC (5μM) for 24h caused ~60% decrease in NL4-3-βla blue-green ratio at endpoint (Fig. B-6D) and >85% reduction in cells expressing cleaved CCF2-AM by FACs analysis (Fig. B-6E).

Since 25HC may have diverse cellular effects, we asked whether 25HC might affect other HIV life cycle processes. To assess its effect on HIV transcription, HEK293Ts were transfected with pNL4-3 co-expressing GFP (NL4-3-GFP) and treated with 25HC 4h post transfection. NL4-3-GFP expression after 24h was not suppressed by FACs, suggesting that 25HC did not affect HIV transcription and translation (Fig. B-S4 B). Concurrently, treatment with 25HC did not reduce budding of HIV virions from NL4-3-GFP transfected cells as measured by p24 in the supernatants, while Nelfinavir, an HIV protease inhibitor that reduces subsequent budding, inhibited p24 expression by >50% at 24 and 48h post transfection (Fig. B-S4 C). Taken together, *CH25H* and 25HC inhibits efficiency of HIV membrane fusion and did not affect HIV transcription, translation, and budding processes.

25HC inhibits virus-cell membrane fusion

While the βlaM entry assays demonstrated 25HC inhibits viral entry processes up to fusion, we sought to test whether 25HC actually inhibits the viral-mediated membrane fusion. Since 25HC inhibited live Nipah replication (Fig. B-4H), we took advantage of the robust system of NiV fusion (F) and attachment (G) proteins to induce pH-independent cell-cell membrane fusion to form syncytias. Vero cells were transfected

with recombinant NiV F and G at equal ratios for 5h and refreshed with media containing 25HC or vehicle control. At 21h post transfection, cells were fixed and stained by Giemsa. Grossly, 25HC treatment led to less syncytia formation and fewer nuclei per syncytia compared to control (Fig. B-6F). In a blinded count of numbers of nuclei per syncytia, a standard measure of fusion, 2μM of 25HC reduced fusion by ~50% and 10μM by ~60% relative to control (Fig. B-6G). These data demonstrate that 25HC modifies the cellular membrane to inhibit viral membrane fusion.

25HC Directly Modifies Cell Membrane to Impede Viral Infection

We further explored whether 25HC can directly change membrane property to inhibit fusion. We hypothesized artificial liposomes with 7:3 phosphatidylcholine:cholesterol ratio, which has similar in composition to cell membranes, would compete with the ability for 25HC to incorporate into cell membrane. While liposome treatment alone had no effect on viral infection in HEK293T, they caused a dose-dependent reversal of VSV growth inhibition by 25HC (Fig. B-6H). As a positive control, we demonstrated that liposome could compete with a known viral membrane fusion inhibitor, LJ001, as described previously (Wolf *et al*., 2010). These results show that 25HC directly modifies cellular membrane to inhibit viral fusion.

25HC reduces HIV infection *in vivo*

We used HIV infection in a humanized mouse model to determine the antiviral effect of 25HC *in vivo*. Humanized NOD-Rag1^{null}Il2rg^{null} mice (NRG-hu) were administered 25HC (50mg/kg) 12h prior to infection with HIV NL4-R3A by intraperitoneal (i.p) injection. 25HC or the vehicle, 2-hydroxypropyl-β-cyclodextrin (HβCD), was administered daily and the serum was collected 7dpi. Quantification of HIV RNA in the serum from 2 combined experiments showed >80% reduction of HIV RNA (copies/mL) in 25HC-treated mice compared to vehicle-treated mice ($P<0.0001$) (Fig. B-7 A). At termination of the experiment on 14dpi, HIV p24 was significantly lower in CD4 T-cells from spleens of 25HC treated mice than control (Fig. B-7 B). Moreover, at 10dpi, 25HC prevented HIV-mediated CD4+ T-cell depletion compared to vehicle control in CD3+(live T-cell) population in peripheral blood leukocytes ($P<0.05$); this effect was less significant in the spleen ($P=0.06$) (Fig. B-7C). These data show that administration of 25HC has antiviral effect against HIV *in vivo*.

***Ch25h*-deficient mice are more susceptible to viral infections**

To determine whether *Ch25h* has a physiological role in host defense against viral infection, we tested whether *Ch25h*$^{-/-}$ mice had increased susceptibility to infection when compared to matching wild-type mice (*Ch25h*$^{+/+}$). Since *Ch25h* expression inhibited MHV68 *in vitro*, we used MHV68 coexpressing luciferase (MHV68-Luc) to infect mice so that viral lytic growth kinetics could be measured in real time by bioluminescence. Eight-week old female *Ch25h*$^{+/+}$ and *Ch25h*$^{-/-}$ mice (N=4 in each group) were infected with 500pfu of MHV68-Luc i.p. and imaged every day after 3dpi. Average and maximal luminescence intensities from ventral, right, left, and dorsal side of every mouse were measured. We observed significantly higher MHV68-Luc activity in *Ch25h*$^{-/-}$ mice over *Ch25h*$^{+/+}$ mice starting 5 dpi and maximal differences between day 7 and 8 (Fig. B-7 D and E). MHV68-Luc activity began to wane in both groups by 9dpi with higher activity in *Ch25h*$^{-/-}$ mice. To validate the imaging results, *Ch25h*$^{-/-}$ spleens had approximately ~3.5 fold higher MHV68 genomic DNA than spleens of *Ch25h*$^{+/+}$ mice at 10dpi (Fig. B-7 F and G). These results show that *Ch25h* is a physiologically important antiviral factor.

DISCUSSION

We have identified the antiviral activity of an IFN-inducible gene, *CH25H*, through a systematic, functional screen. Distinct from known IFN-mediated antiviral

mechanisms, CH25H inhibits growth of a wide range of enveloped viruses by production of a soluble oxysterol, 25-hydroxycholesterol. It also exemplifies the only soluble antiviral ISG that is not IFN itself. Independent of its known regulatory effect on metabolism, 25HC impairs viral entry at the virus-cell fusion step by inducing cellular membrane changes. In animal models, administration of 25HC reduces HIV infection in humanized mice. Moreover, the immune response against viral infections requires *Ch25h in vivo*. These findings illustrate an essential function of *Ch25h* in immunity.

This study shows an unappreciated relationship between the host IFN response and an oxysterol. While antiviral effects of some oxysterols have been documented (Moog *et al*., 1998; Pezacki *et al*., 2009), we have found 25HC broadly inhibits viral membrane fusion, which is not specific to particular structural classes of fusion proteins. For example, HIV and Ebola have class-I fusion peptides, RVFV and RSSEV use class-II peptides, whereas VSV and HSV belong to class III (Kielian and Rey, 2006; Vaney and Rey, 2011). 25HC is also antiviral against viruses that undergo either pH-dependent or pH-independent fusion as exemplified by VSV and HIV, respectively. These findings suggest that 25HC affects a more basic fusion process involving the viral and cellular membrane.

Since 25HC can permeate through membranes, it likely modifies cellular membranes to exert its antiviral effect. Our study showed that artificial liposomes similar to cell membranes in composition reduce antiviral activity of 25HC, suggesting they take up 25HC. In support of this finding, prior literature showed that 25HC increased cellular cholesterol accessibility by directly mobilizing cholesterol from membranes and prevented cholesterol's condensing effects on membrane (Lange *et al*., 1995; Olsen *et al*., 2011). In artificial membranes, 25HC altered solvent exposure of phospholipid head groups (Gale *et al*., 2009). One model suggested that while membrane cholesterol orients in parallel to adjacent acyl chains, 25HC adopts a tilted position in the membrane because of its hydroxyl group and may lead to membrane expansion. We also hypothesize that the hydrophilic interactions of the hydroxyl groups of 25HC lead to aggregation in the membrane. These perturbations could affect viral-cellular fusion, which is fundamentally dependent on membrane properties such as spacing of lipid head groups, receptor accessibility, membrane curvature, and fluidity (Pécheur *et al*., 1998; Teissier and Pécheur, 2007). Studies on viral entry have predominantly focused on viral fusion components and their interactions with specific cellular receptors. How membrane properties modulate viral fusion remains the subject of further research.

Our data suggest viral entry is a point of viral growth inhibition by CH25H and 25HC under the conditions described, which are generally 8-16h pre-treatment with 1-10μM of 25HC in standard growth medium. Given the expanding role of oxysterol functions, other antiviral mechanisms may exist and manifest with different conditions or viruses. Of note, overexpression of *CH25H* caused more pronounced inhibition of live VSV-GFP replication than VSV-G-βlaM fusion, about ~85% and ~51% respectively. However, in *CH25H*-conditioned-medium- or 25HC- treated cells, the reduction was comparable, ranging about 55-70%. One interpretation is that the CH25H protein may have addition antiviral mechanisms to 25HC, perhaps through its association with the endoplasmic reticulum. These results encourage further study into other antiviral mechanisms of *CH25H* and 25HC.

This study provides further understanding to the intricate connection of IFN and metabolism. Although 25HC has been associated with pathological conditions like atherosclerosis and Alzheimer's disease, our study show it plays a beneficial role in host immunity against viral infections. These results encourage the exploration of antiviral oxysterols or cellular membrane modifiers as viral entry inhibitors against acute infections.

ACKNOWLEDGEMENTS

We thank D. Russell (UT Southwestern) for providing *Ch25h*$^{-/-}$ bone marrow cells, and E. Tarling, P. Edwards, and S. Bensinger at UCLA for *Srebp* plasmids. We thank G. Boxx and S.Iyer for access to experimental samples and RNAseq data and R. Modlin for his editorial advice. This project was funded NIH Grants R01 AI078389, AI069120, AI080432, AI095097, AI077454, AI070010, AI028697 (the UCLA CFAR), Tumor Immunology Training Grant, and the Warsaw Fellowship.

MATERIALS AND METHODS

Cell and Reagents are detailed in Supplemental Methods

VSV, HSV, MHV68, HIV Viral Infection

HEK293T and RAW264.7 were infected with VSV-GFP at 0.01 MOI for 1h and the media was changed with fresh media. For J2 BMMs and BCR-ABL B-cells, 1MOI VSV-GFP was used. Approximately 150μL of supernatants were collected at various times between 8-16hpi for plaque assay. For HSV and MHV68, 0.25MOI was used for infection and supernatants were collected at 24hpi. Titers were measured by standard plaque assays. Detail conditions and HIV infection in hPBMCs are described in Supplemental Methods.

Ebola, RSSEV, Nipah and RVFV Infections

HeLa cells were pre-treated with 25HC (1μM) or EtOH containing medium for indicated times prior to infection with 0.1MOI of Ebola-Zaire-GFP (EBOV) or RVFV (wild type strain ZH501 or vaccine strain MP12), Nipah virus (Bangladesh), or RSSEV (Sofjin). Cell culture supernatant pooled from biological triplicates at indicated time

points, prior virus titration by plaque assay. Titers were measured by standard plaque assays (Supp. Methods).

VSV-G-βlaM Infection

VSV-G-βlaM was produced as previously described and detailed in Supp. Methods (Wolf *et al*., 2009). HEK293Ts were treated with 25HC and EtOH as before and infected with VSV-G-βlaM at the empirically determined concentration for 1h. Cells were washed and CCF2-AM was added according to manufacture's protocol (Invitrogen).

NL4-3 VPR-βlaM Infection of CEM cells

CEMs cells were treated with 25HC or EtOH for a minimum of six hours and AMD3100 (20μM) for 15 minutes before infection with concentrated NL4-3 βlaM or bald virus. Infections were spin inoculated for 60 minutes at 2,000RPM, and incubated for 2 hours at 37C. After washing, CCF2-AM (Invitrogen) was added according to manufacture's protocol. Kinetic readings were taken for 4 hours. After the kinetic reading, the cells were washed with FACs Buffer, fixed with 2 % paraformaldehyde, and examined by FACs. Data was analyzed using FlowJo (Tree Star Inc.).

Nipah Fusion Assay and Liposome Competition Assay

Vero cells were plated in 6-well dish at $5x10^5$ per well overnight and transfected with 0.5μg of expression plasmids encoding Nipah F and G in OptiMEM (Invitrogen). At 5h post transfection, media was changed to DMEM (10%FBS) with or without 25HC. The cells were fixed by methanol 21h after transfection for 10min, Giemsa stained for 2h, and decolorized with 95% ethanol. Nuclei inside syncytia were counted under light microscopy. Syncytia were defined as four or more nuclei within a common cell membrane. Relative fusion was defined by normalizing the number of nuclei per syncytia formed under the experimental conditions to that formed by in vehicle (ethanol) treated cells, which was set at 100%. Liposome competition assay are described in detail in Supplemental Methods.

HIV infection in NRG-hu mice

NOD-Rag1^{null}Il2rg^{null} (NRG-hu) mice with stable human leukocyte reconstitution were administered 25HC (50mg/kg) or the vehicle control (HBCD) by *i.p.* injection for 12h before infection with HIV NL4-R3A (5ng of p24/mouse) or mock supernatant by intravenously injection (i.v.). Mice were administered equal amount of 25HC or HBCD

every day. HIV replication (genome copy/ml in the plasma) was measured by qRT-PCR or by p24 intracellular staining (Supp. Methods). All animals were housed and treated in accordance with protocols approved by the institutional care and use committee for animal research at the University of North Carolina.

Mouse Infections and Bioluminescence Imaging

C57BL/6 and *Ch25h*$^{-/-}$ mice were purchased from Jackson Labs. MHV68 (500 pfu) in 200μL of PBS was administered by i.p. After 3dpi, mice were imaged every day (IVIS, Xenogen) (Supp. Methods). At 9dpi, mice were euthanized the spleens were extracted and homogenized in DMEM. Total DNA was extracted using DNeasy Blood & Tissue Kit (Qiagen) and MHV68 DNA was quantified by qRT-PCR. All animals were housed and treated in accordance with protocols approved by the institutional care and Animal Research Committed at UCLA.

Statistics

For comparison of different experimental conditions at one time point, student's t-test with unpaired, 2-tailed hypothesis was used. For kinetic assays, two-way ANOVA with repeated measures was used.

REFERENCES

Andrew J, and Jessup, W. (1999). Oxysterols and atherosclerosis. Atherosclerosis *142*, 1–28.

Bauman, D.R., Bitmansour, A.D., McDonald, J.G., Thompson, B.M., Liang, G., and Russell, D.W. (2009). 25-Hydroxycholesterol secreted by macrophages in response to Toll-like receptor activation suppresses immunoglobulin A production. Proceedings of the National Academy of Sciences *106*, 16764 –16769.

Brass, A.L., Huang, I.-C., Benita, Y., John, S.P., Krishnan, M.N., Feeley, E.M., Ryan, B.J., Weyer, J.L., Van der Weyden, L., Fikrig, E., *et al*. (2009). The IFITM Proteins Mediate Cellular Resistance to Influenza A H1N1 Virus, West Nile Virus, and Dengue Virus. Cell *139*, 1243–1254.

Cavrois, M., De Noronha, C., and Greene, W.C. (2002). A sensitive and specific enzyme-based assay detecting HIV-1 virion fusion in primary T lymphocytes. Nat Biotech *20*, 1151–1154.

Van Damme, N., Goff, D., Katsura, C., Jorgenson, R.L., Mitchell, R., Johnson, M.C., Stephens, E.B., and Guatelli, J. (2008). The Interferon-Induced Protein BST-2 Restricts HIV-1 Release and Is Downregulated from the Cell Surface by the Viral Vpu Protein. Cell Host Microbe *3*, 245–252.

Degols, G., Eldin, P., and Mechti, N. (June). ISG20, an actor of the innate immune response. Biochimie *89*, 831–835.

Gale, S.E., Westover, E.J., Dudley, N., Krishnan, K., Merlin, S., Scherrer, D.E., Han, X., Zhai, X., Brockman, H.L., Brown, R.E., *et al*. (2009). Side Chain Oxygenated Cholesterol Regulates Cellular Cholesterol Homeostasis through Direct Sterol-Membrane Interactions. Journal of Biological Chemistry *284*, 1755 –1764.

García, M.A., Gil, J., Ventoso, I., Guerra, S., Domingo, E., Rivas, C., and Esteban, M. (2006). Impact of Protein Kinase PKR in Cell Biology: from Antiviral to Antiproliferative Action. Microbiology and Molecular Biology Reviews *70*, 1032 –1060.

Holmes, R., VandeBerg, J., and Cox, L. (2011). Genomics and proteomics of vertebrate cholesterol ester lipase (*LIPA*) and cholesterol 25-hydroxylase (*CH25H*). 3 Biotech *1*, 99–109.

Janowski, B.A., Grogan, M.J., Jones, S.A., Wisely, G.B., Kliewer, S.A., Corey, E.J., and Mangelsdorf, D.J. (1999). Structural requirements of ligands for the oxysterol liver X receptors LXRα and LXRβ. Proceedings of the National Academy of Sciences *96*, 266 – 271.

Kandutsch, A., Chen, H., and Heiniger, H. (1978). Biological activity of some oxygenated sterols. Science *201*, 498 –501.

Kielian, M., and Rey, F.A. (2006). Virus membrane-fusion proteins: more than one way to make a hairpin. Nat Rev Micro *4*, 67–76.

Lange, Y., Ye, J., and Strebel, F. (1995). Movement of 25-hydroxycholesterol from the plasma membrane to the rough endoplasmic reticulum in cultured hepatoma cells. Journal of Lipid Research *36*, 1092 –1097.

Liu, S.-Y., Sanchez, D.J., Aliyari, R., Lu, S., and Cheng, G. (2012). Systematic identification of type I and type II interferon-induced antiviral factors. Proceedings of the National Academy of Sciences *109*, 4239 –4244.

Moog, C., Aubertin, A., Kim, A., and Luu, B. (1998). Oxysterols, but not cholesterol, inhibit human immunodeficiency virus replication *in vitro*. Antiviral Chemistry & Chemotherapy *9*, 491–496.

Negrete, O.A., Wolf, M.C., Aguilar, H.C., Enterlein, S., Wang, W., Mühlberger, E., Su, S.V., Bertolotti-Ciarlet, A., Flick, R., and Lee, B. (2006). Two Key Residues in EphrinB3 Are Critical for Its Use as an Alternative Receptor for Nipah Virus. PLoS Pathog *2*, e7.

Neil, S.J.D., Zang, T., and Bieniasz, P.D. (2008). Tetherin inhibits retrovirus release and is antagonized by HIV-1 Vpu. Nature *451*, 425–430.

Olsen, B.N., Schlesinger, P.H., Ory, D.S., and Baker, N.A. (2011). 25-Hydroxycholesterol Increases the Availability of Cholesterol in Phospholipid Membranes. Biophysical Journal *100*, 948–956.

Park, K., and Scott, A.L. (2010). Cholesterol 25-hydroxylase production by dendritic cells and macrophages is regulated by type I interferons. Journal of Leukocyte Biology *88*, 1081 –1087.

Pécheur, E.-I., Sainte-Marie, J., Bienvenüe, A., and Hoekstra, D. (1998). Lipid Headgroup Spacing and Peptide Penetration, but Not Peptide Oligomerization, Modulate Peptide-Induced Fusion†. Biochemistry *38*, 364–373.

Pezacki, J., Sagan, S., Tonary, A., Rouleau, Y., Belanger, S., Supekova, L., and Su, A. (2009). Transcriptional profiling of the effects of 25-hydroxycholesterol on human hepatocyte metabolism and the antiviral state it conveys against the hepatitis C virus. BMC Chemical Biology *9*, 2.

Teissier, É., and Pécheur, E.-I. (2007). Lipids as modulators of membrane fusion mediated by viral fusion proteins. European Biophysics Journal *36*, 887–899.

Vaney, M.-C., and Rey, F.A. (2011). Class II enveloped viruses. Cellular Microbiology *13*, 1451–1459.

Wang, F., Xia, W., Liu, F., Li, J., Wang, G., and Gu, J. (2012). Interferon regulator factor 1/retinoic inducible gene I (IRF1/RIG-I) axis mediates 25-hydroxycholesterol-induced interleukin-8 production in atherosclerosis. Cardiovascular Research *93*, 190 –199.

Weidner, J.M., Jiang, D., Pan, X.-B., Chang, J., Block, T.M., and Guo, J.-T. (2010). Interferon-Induced Cell Membrane Proteins, IFITM3 and Tetherin, Inhibit Vesicular Stomatitis Virus Infection via Distinct Mechanisms. Journal of Virology *84*, 12646 – 12657.

Wolf, M., Wang, Y., Freiberg, A., Aguilar, H., Holbrook, M., and Lee, B. (2009). A catalytically and genetically optimized beta-lactamase-matrix based assay for sensitive, specific, and higher throughput analysis of native henipavirus entry characteristics. Virology Journal *6*, 119.

Wolf, M.C., Freiberg, A.N., Zhang, T., Akyol-Ataman, Z., Grock, A., Hong, P.W., Li, J., Watson, N.F., Fang, A.Q., Aguilar, H.C., *et al*. (2010). A broad-spectrum antiviral targeting entry of enveloped viruses. Proceedings of the National Academy of Sciences *107*, 3157 –3162.

Zlokarnik, G., Negulescu, P.A., Knapp, T.E., Mere, L., Burres, N., Feng, L., Whitney, M., Roemer, K., and Tsien, R.Y. (1998). Quantitation of Transcription and Clonal Selection of Single Living Cells with β-Lactamase as Reporter. Science *279*, 84 –88.

Zou, T., Garifulin, O., Berland, R., and Boyartchuk, V.L. (2011). Listeria monocytogenes Infection Induces Prosurvival Metabolic Signaling in Macrophages. Infection and Immunity *79*, 1526 –1535.

FIGURES

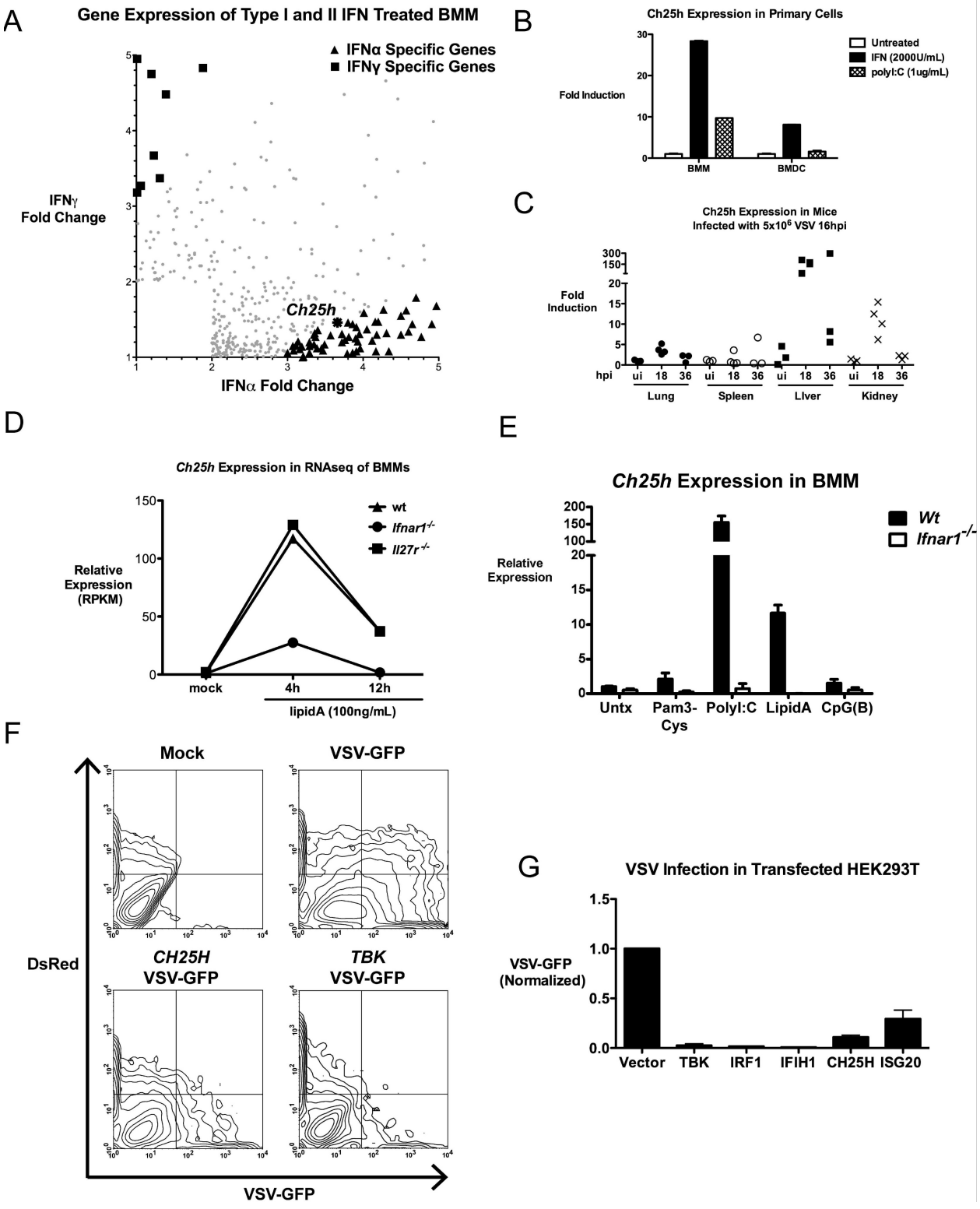
A
Gene Expression of Type I and II IFN Treated BMM
IFNα Specific Genes
IFNγ Specific Genes
IFNγ Fold Change
IFNα Fold Change
Ch25h
B
Ch25h Expression in Primary Cells
Untreated
IFN (2000U/mL)
polyI:C (1ug/mL)
Fold Induction
BMM
BMDC
C
Ch25h Expression in Mice Infected with 5x10^6 VSV 16hpi
Fold Induction
hpi
ui 18 36 ui 18 36 ui 18 36 ui 18 36
Lung
Spleen
Liver
Kidney
D
Ch25h Expression in RNAseq of BMMs
wt
Ifnar1-/-
Il27r-/-
Relative Expression (RPKM)
mock
4h
12h
lipidA (100ng/mL)
E
Ch25h Expression in BMM
Wt
Ifnar1-/-
Relative Expression
Untx
Pam3-Cys
PolyI:C
LipidA
CpG(B)
F
Mock
VSV-GFP
CH25H VSV-GFP
TBK VSV-GFP
DsRed
VSV-GFP
G
VSV Infection in Transfected HEK293T
VSV-GFP (Normalized)
Vector
TBK
IRF1
IFIH1
CH25H
ISG20

Figure B-1. *Ch25h* is an IFN-dependent Antiviral ISG

A) Gene expression profile of BMMs treated for 2.5 h with IFNα and IFNγ at 62 U/mL and 1 U/mL, respectively. IFNα-stimulated genes that were 3-fold higher than induction of IFNγ stimulated genes were categorized as IFNα-specific (green triangles) and vice versa for IFNγ-specific genes (blue squares).

B) *Ch25h* expression was measured by qRT-PCR in BMMs and BMDCs after IFN (2000U/mL) or polyI:C (1ug/mL) treatment for 4h.

C) *Ch25h* expression quantified by qRT-PCR from tissues of uninfected (ui) and VSV-infected C57B/6 mice collected at indicated times.

D) Wildtype, *Ifnar1*$^{-/-}$, and *Il-27r*$^{-/-}$ BMMs were treated with lipid A (100ng/mL) or saline control for 4h and 12h. *Ch25h* expression values are presented as RKPM values.

E) *Ch25h* gene expression measured by qRT-PCR of *Ifnar1*$^{+/+}$ and *Ifnar1*$^{-/-}$ BMMs stimulated with TLR agonists, Pam-3-Cys (100ng/mL), polyI:C(25ug/mL), lipid(10ng/mL), CpG-B(100μM) for 4 hours. Mean±SD

F) HEK293T was co-transfected with fluorescent red marker (DsRed) and with individual plasmids encoding human *TBK1*, *CH25H*, or vector for 36h and infected with VSV-GFP (0.01MOI) for 9h. Representative contour plots are shown.

G) As described in Part E, VSV-GFP was quantified in the DsRed-positive population normalized to vector control. VSV-GFP was defined as the product of %GFP-positive and geometric mean of the fluorescence index (MFI). Mean±SEM; *P<0.001

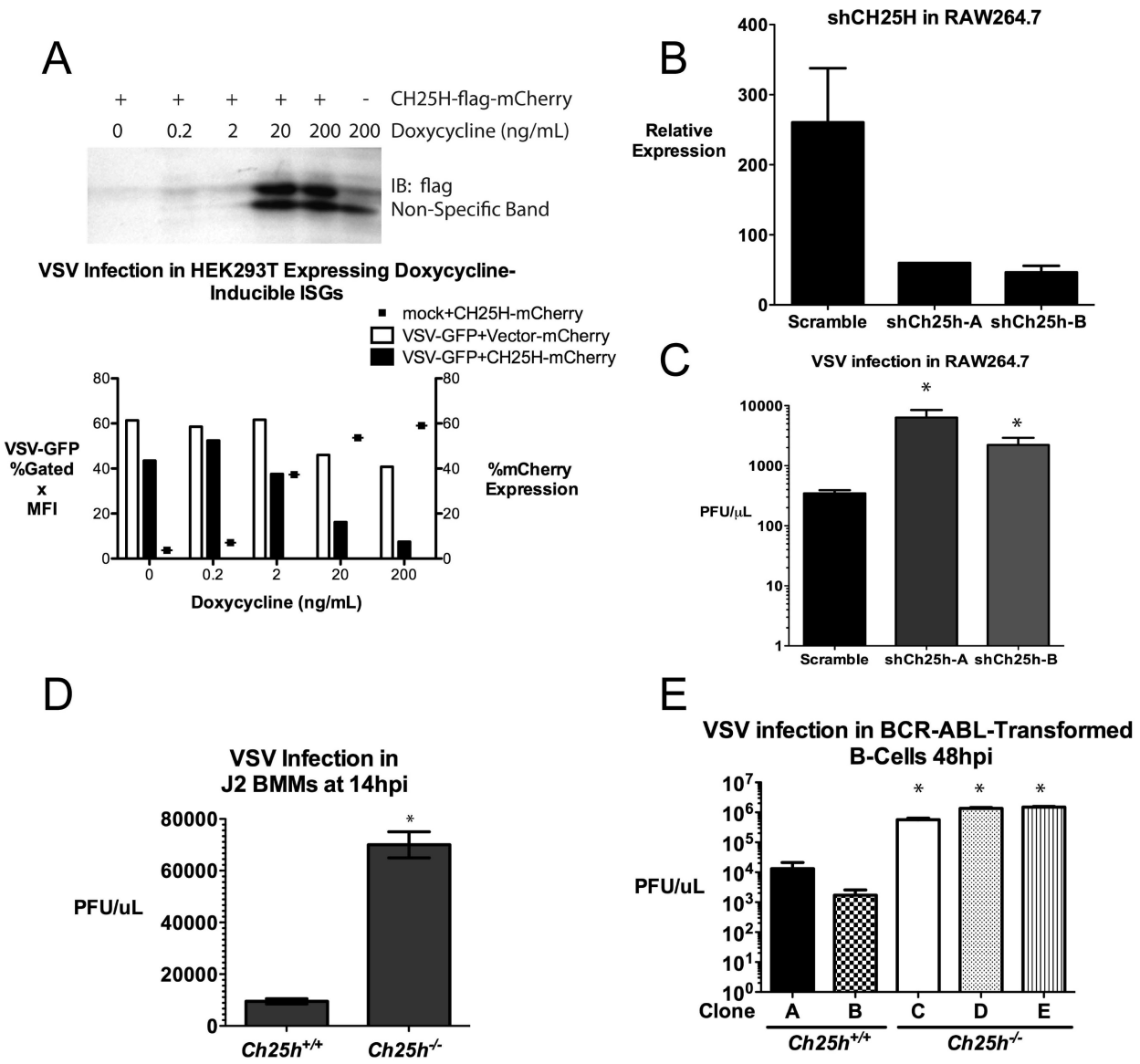

Figure B-2. *Ch25h*-deficiency increases susceptibility to viral infection *in vitro*

A) HEK293T was transfected with doxycycline-inducible vector or *CH25H*-flag constructs that co-express red fluorescent mCherry for 24h and doxycycline was added for 12h at indicated concentrations. Expression of *CH25H*-flag was

confirmed by western blot (upper panel). After treatment, cells were infected with VSV-GFP (0.01MOI) for 9hrs and VSV-GFP was quantified by (%GFP+ X GeoMean MFI). Dots represent percent positive mCherry (lower panel).

B) RAW264.7 stably knocked down with shRNA against *Ch25h* were generated by retro-viral infection. Two shRNA constructs were made (shCh25h-A and shCh25h-B) along with scramble control. Knockdown was confirmed by qRT-PCR. Mean±SD, *P<0.01

C) shCh25h-A, shCh25hB, and scrambled stable RAW264.7 were infected with VSV-GFP (0.1 MOI) and the VSV-GFP was measured by plaque assay 14hpi. Mean±SEM, *P<0.01.

D) J2 BMM were derived from $Ch25h^{+/+}$ and $Ch25h^{-/-}$ mice and passed for 2 weeks. The cells were infected VSV-GFP (0.1MOI) and viral titers 14hpi in the supernatants was quantified by plaque assay. Mean±SD *P<0.01

E) Individual clonal populations of BCR-ABL transformed B-cells from $Ch25h^{+/+}$ and $Ch25h^{-/-}$ mice were infected with VSV-GFP (0.1MOI) in biological triplicates and the viral titers were measured by plaque assay at indicated times. Mean±SD *P<0.01

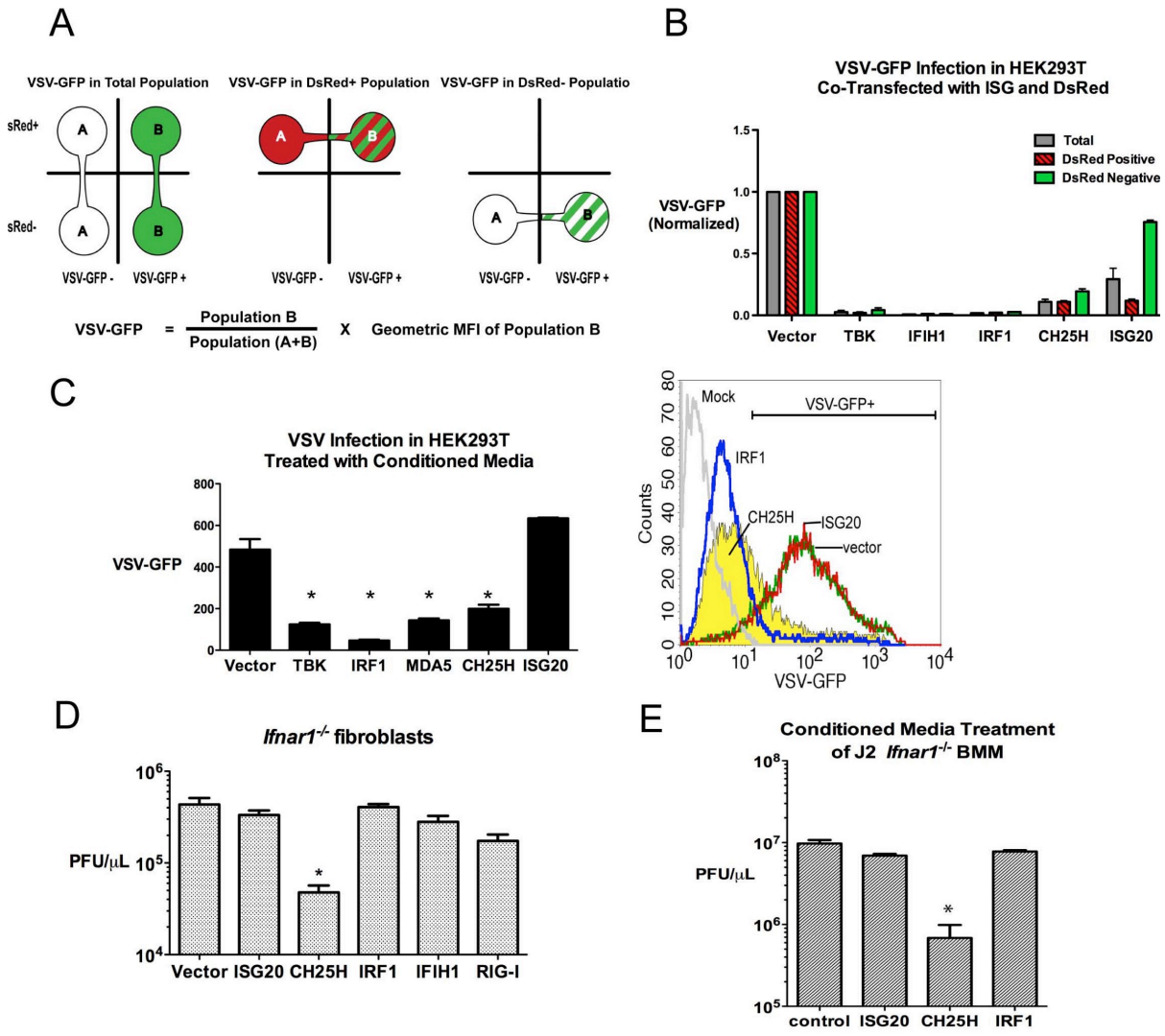

Figure B-3. *CH25H* produces a soluble antiviral factor that is not IFN (see also Fig. B-S1)

A) HEK293Ts were co-transfected with ISGs and DsRed as Fig. B-1D. Schematic of FACs analyses of VSV-GFP in total, DsRed+, and DsRed- populations. VSV-GFP was defined as %GFP+ X geometric MFI.

B) HEK293T transfected with DsRed and indicated expression plasmids were infected with VSV-GFP and measured as described in Fig. B-3A. Mean±SEM.

C) Media collected from HEK293T after 48h transfection with indicated expression vector was treated on to freshly plated HEK293T for 8h and infected with VSV-GFP (0.01MOI) for 9h. VSV-GFP was quantified as described in Fig 3A. Representative histogram of FACs data (right). Mean±SEM, *P<0.01

D) *Ifnar1*$^{-/-}$ tail-derived fibroblasts were treated for 12h with conditioned-medium of HEK293T cells transfected with indicated expression vector. The fibroblasts were infected with VSV-GFP (0.1 MOI) and the viral titer in the supernatant was measured by plaque assay. Mean±SEM, *P<0.05

E) *Ifnar1*$^{-/-}$ derived J2 BMMs were treated for 12h with conditioned-medium of HEK293T cells transfected with indicated expression vector. J2 BMMs were

infected with VSV-GFP (0.1 MOI) and the viral titer in the supernatant at 14hpi was quantified by plaque assay. Mean±SEM, *P<0.05

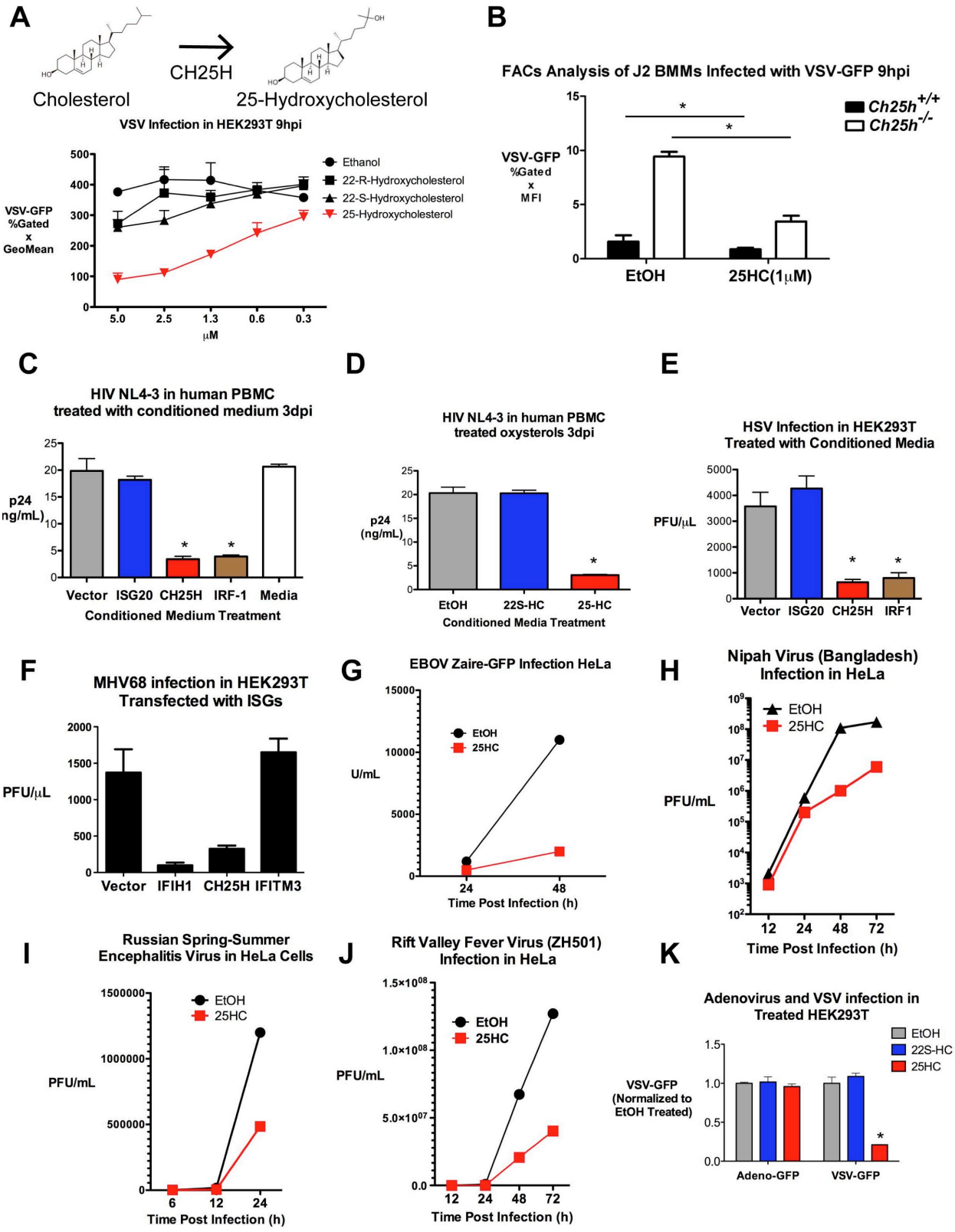
A
Cholesterol
CH25H
25-Hydroxycholesterol
VSV Infection in HEK293T 9hpi
VSV-GFP %Gated x GeoMean
Ethanol
22-R-Hydroxycholesterol
22-S-Hydroxycholesterol
25-Hydroxycholesterol
μM
B
FACs Analysis of J2 BMMs Infected with VSV-GFP 9hpi
Ch25h+/+
Ch25h-/-
VSV-GFP %Gated x MFI
EtOH
25HC(1μM)
C
HIV NL4-3 in human PBMC treated with conditioned medium 3dpi
p24 ng/mL)
Vector ISG20 CH25H IRF-1 Media
Conditioned Medium Treatment
D
HIV NL4-3 in human PBMC treated oxysterols 3dpi
p24 (ng/mL)
EtOH 22S-HC 25-HC
Conditioned Media Treatment
E
HSV Infection in HEK293T Treated with Conditioned Media
PFU/μL
Vector ISG20 CH25H IRF1
F
MHV68 infection in HEK293T Transfected with ISGs
PFU/μL
Vector IFIH1 CH25H IFITM3
G
EBOV Zaire-GFP Infection HeLa
EtOH
25HC
U/mL
Time Post Infection (h)
H
Nipah Virus (Bangladesh) Infection in HeLa
EtOH
25HC
PFU/mL
Time Post Infection (h)
I
Russian Spring-Summer Encephalitis Virus in HeLa Cells
EtOH
25HC
PFU/mL
Time Post Infection (h)
J
Rift Valley Fever Virus (ZH501) Infection in HeLa
EtOH
25HC
PFU/mL
Time Post Infection (h)
K
Adenovirus and VSV infection in Treated HEK293T
EtOH
22S-HC
25HC
VSV-GFP (Normalized to EtOH Treated)
Adeno-GFP
VSV-GFP

Figure B-4. *CH25H* produces 25-hydroxycholesterol, a broadly antiviral oxysterol. (see also Fig. B-S2)

A) CH25H converts cholesterol to 25-hydroxycholesterol (25HC, top). HEK293T was treated with 22(S)-, 22(R)-, or 25- hydroxycholesterol and the vehicle, ethanol (EtOH) for 8h with indicated concentrations and infected with VSV-GFP. VSV-GFP was quantified at 8hpi as described in Fig. B-3A. Mean±SEM.

B) *Ch25h*$^{+/+}$ and *Ch25h*$^{-/-}$ J2 BMMs were treated with 25HC(1μM) or EtOH and infected with VSV-GFP (0.01MOI). VSV-GFP was quantified by FACs at 12hpi. Mean±SD; *P<0.02

C) Costimulated PBMC were pre-incubated for 24h in conditioned media before infection with HIV NL4-3. At 3dpi, p24 in triplicate samples were quantified by ELISA. Mean±SEM; *P<0.001

D) Costimulated PBMC ($1x10^6$) were pre-incubated for 24h in 22(S)-HC (1μM), 25HC(1μM), and vehicle (EtOH) containing media before infection with HIV NL4-3 in triplicates (30ng of HIV strain NL4-3). At 3dpi, p24 was quantified by ELISA. Mean±SEM; *P<0.001

E) HEK293T was treated with indicated conditioned media for 12h and infected with HSV (0.25MOI) for 24h. HSV titer in the supernatant was quantified by plaque assay. Mean±SEM; *P<0.001

F) HEK293Ts were transfected with indicated expression plasmids and infected with MHV68 (0.2MOI) for 24h. MHV68 titer in the supernatant was quantified by plaque assay. Mean±SEM; *P<0.001

G) HeLa cells were pretreated with 25HC (1μM) or EtOH containing media for 5h and infected with Ebola Zaire-GFP (EBOV) at 0.1MOI. At indicated time points, supernatants from biological triplicates were combined and measured by plaque assay.

H) HeLa cells were pretreated with media containing indicated concentrations of 25HC or EtOH for 18h and infected with Nipah virus at 0.1MOI. At indicated time points, supernatants from biological triplicates were combined and measured by plaque assay.

I) HeLa cells were pretreated as in Fig. B-4H and infected with RSSEV at 0.1MOI. At indicated time points, supernatants from biological triplicates were combined and measured by plaque assay.

J) HeLa cells were pretreated with media containing indicated concentrations of 25HC or EtOH for 5h and infected with wildtype Rift Valley Fever Virus ZH501 (RVFV) at 0.1MOI. Viral titer at indicated time points was measured by plaque assay. Values represent means of samples from triplicates.

K) HEK293T were treated with EtOH, 22S-HC, and 25HC for 12h and infected with adenovirus-GFP and VSV-GFP and quantified by FACs (%GFP+ X Geometric MFI). Mean±SEM; *P<0.001

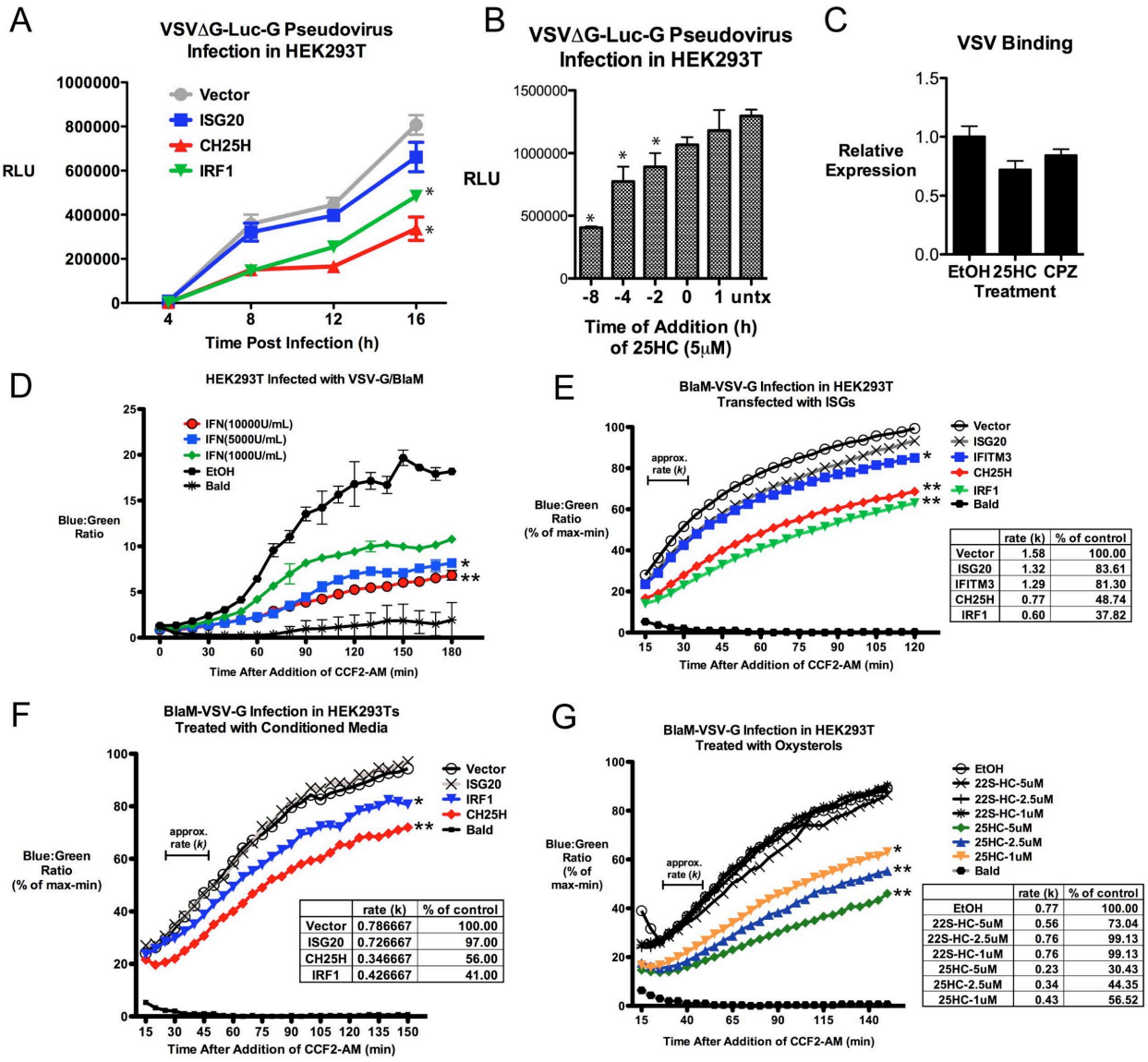

Figure B-5. 25HC inhibits VSV Entry. (see also Fig. B-S3)

A) HEK293Ts were treated with conditioned media for 12h and infected with VSV-G pseudovirus encoding VSVΔG luciferase (VSVΔG-Luc-G). The cell lysates were collected at indicated times and measured for luciferase activity. Mean±SEM, *P<0.001.

B) HEK293T were treated with 25HC (5μM) at different times relative to the VSVΔG-Luc-G infection. For time 0, VSVΔG-Luc-G and 25HC were added together to the cells for 1h. Negative numbers indicate addition of 25HC before infection; positive number indicates addition after infection. Relative Light Units (RLU) is represented as Mean±SD *P<0.01

C) HEK293T were treated with respective agonists for 8h in triplicates. VSV was bound to cells at 4ºC, washed 3 times with PBS, and let sit for 30min before total RNA collection. VSV genomic RNA was quantified by qRT-PCR Mean±SEM; *P<0.05

D) HEK293T were treated with pan-IFN for 12hours at indicated concentrations and infected with VSV-G-βlaM in triplicates. βlaM activity was measured by CCF2-AM cleavage. Mean±SEM, *P<0.05, **P<0.01.

E) HEK293T was transfected with indicated expression plasmids for 24h and infected with pseudovirus with encoding NipahM-β-lactamase inside VSV-G (VSV-G-βlaM) for 1.5h. βla activity was measured by blue:green ratio of the cleaved CCF2-AM. The rate constant (k) (table, inset) estimated from the

slope of the reactions in the bracketed time interval measures relative fusion. *P<0.05, **P<0.01.

F) HEK293T was treated with indicated conditioned media for 12h and infected with VSV-G-βlaM. Analysis was same as part D. *P<0.05, **P<0.01.

G) HEK293T was treated with indicated concentration of 22(S)-HC, 25HC, and equivalent volume of vehicle (EtOH) for 12h and infected with VSV-G-βlaM. Analysis was same as part D. *P<0.05, **P<0.01.

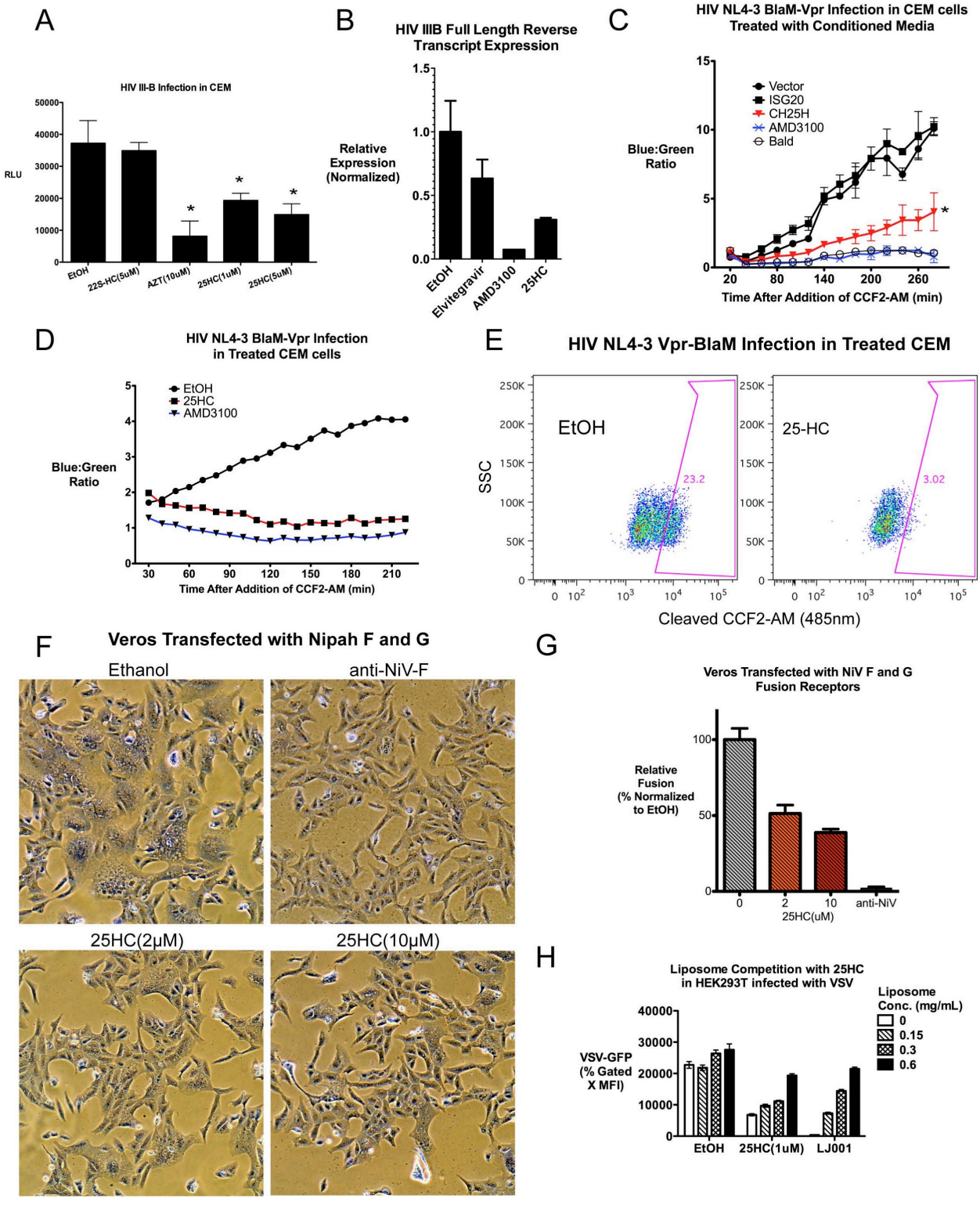
A
HIV III-B Infection in CEM
RLU
50000
40000
30000
20000
10000
0
EtOH
22S-HC(5uM)
AZT(10uM)
25HC(1uM)
25HC(5uM)
B
HIV IIIB Full Length Reverse Transcript Expression
Relative Expression (Normalized)
1.5
1.0
0.5
0.0
EtOH
Elvitegravir
AMD3100
25HC
C
HIV NL4-3 BlaM-Vpr Infection in CEM cells Treated with Conditioned Media
Blue:Green Ratio
15
10
5
0
Vector
ISG20
CH25H
AMD3100
Bald
20
80
140
200
260
Time After Addition of CCF2-AM (min)
D
HIV NL4-3 BlaM-Vpr Infection in Treated CEM cells
Blue:Green Ratio
5
4
3
2
1
0
EtOH
25HC
AMD3100
30
60
90
120
150
180
210
Time After Addition of CCF2-AM (min)
E
HIV NL4-3 Vpr-BlaM Infection in Treated CEM
SSC
250K
200K
150K
100K
50K
0
EtOH
23.2
25-HC
3.02
0
10^2
10^3
10^4
10^5
Cleaved CCF2-AM (485nm)
F
Veros Transfected with Nipah F and G
Ethanol
anti-NiV-F
25HC(2μM)
25HC(10μM)
G
Veros Transfected with NiV F and G Fusion Receptors
Relative Fusion (% Normalized to EtOH)
100
50
0
0
2
10
anti-NiV
25HC(uM)
H
Liposome Competition with 25HC in HEK293T infected with VSV
Liposome Conc. (mg/mL)
0
0.15
0.3
0.6
VSV-GFP (% Gated X MFI)
40000
30000
20000
10000
0
EtOH
25HC(1uM)
LJ001

Figure B-6. 25HC inhibits HIV Entry and Viral-Cellular Membrane Fusion (see also Fig. B-S4)

A) CEM cells were treated as indicated for 12h and underwent single-round infection with HIV-IIIB coexpressing luciferase. Cell lysates were collected after 24h and measured for luciferase activity. Relative Light Units (RLU) is represented as Mean±SD. *P<0.05

B) CEM cells were treated with elvitegravir (10μM), AMD3100(10μM), 25HC (1μM), and vehicle (EtOH) for 12h and infected with HIV III-B pseudovirus. At 6 hpi, HIV full-length late reverse transcript (LateRT) was quantified by qRT-PCR with Taqman probe and normalized to mitochondrial DNA. Mean±SD, P≤0.05.

C) CEM cells were treated with indicated conditioned media or AMD3100 for 8h and infected with HIV NL4-3 encoding Vpr-βlaM (NL4-3/βlaM) in duplicates. βla activity was measured by cleavage of CCF2-AM by fluorescence plate reader. Mean±SD, *P≤0.01.

D) Similar to Part C. CEM cells were treated with indicated 25HC(5μM) and vehicle (EtOH) for 12h and infected with HIV NL4-3/βlaM.

E) After kinetic assay in Fig. B-6D, % cleaved CCF2-AM (blue) population (485nm) was confirmed by FACs.

F) Vero cells were transfected with Nipah F and G receptors. 5h after transfection, the cells were treated with indicated conditions. The cells were fixed 21h after transfection and Giemsa stained.

G) Syncytias were defined by the presence of 4 or more nuclei in a common cell membrane. Relative fusion was determined by normalizing the number of nuclei per syncytia under the experimental conditions to the vehicle (ethanol) treated group, set to 100%. Mean±SEM, $P<0.0001$

H) HEK293T was incubated with 25HC (1μM) for 12h and varying concentrations of PC:cholesterol (7:3) liposomes for 30min before infection with VSV-GFP. As positive control, VSV-GFP was treated with LJ001, a known entry inhibitor, for 10 min prior to infection (Wolf *et al*., 2009) (See Supp. methods). VSV-GFP was quantified by FACs as described in Fig. B-3A, Mean±SEM.

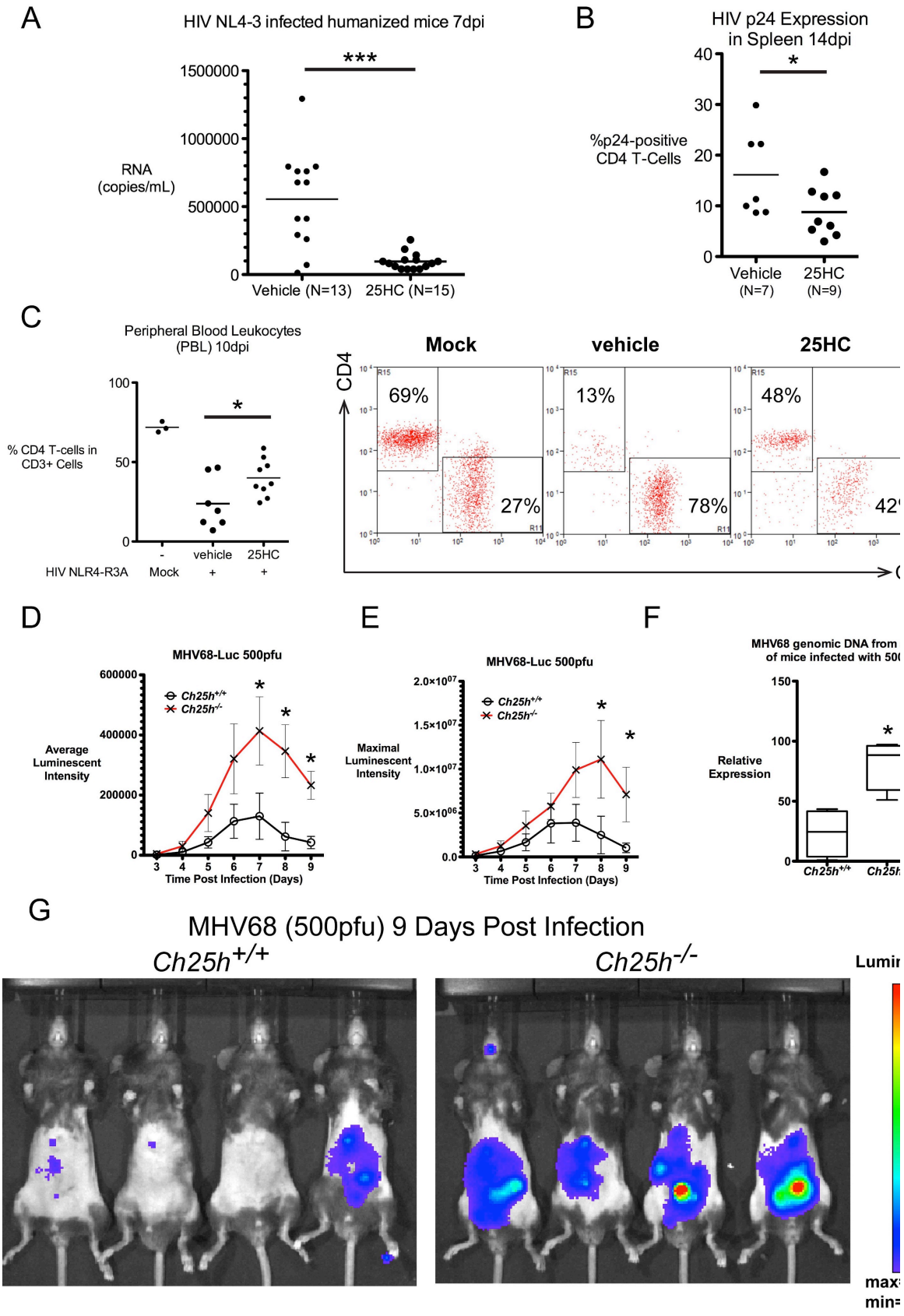
A
HIV NL4-3 infected humanized mice 7dpi
***
1500000
1000000
500000
0
RNA (copies/mL)
Vehicle (N=13)
25HC (N=15)
B
HIV p24 Expression in Spleen 14dpi
*
40
30
20
10
0
%p24-positive CD4 T-Cells
Vehicle (N=7)
25HC (N=9)
C
Peripheral Blood Leukocytes (PBL) 10dpi
100
50
0
% CD4 T-cells in CD3+ Cells
-
vehicle
25HC
HIV NLR4-R3A
Mock
+
+
Mock
vehicle
25HC
CD4
69%
27%
13%
78%
48%
D
MHV68-Luc 500pfu
600000
400000
200000
0
Average Luminescent Intensity
Ch25h+/+
Ch25h-/-
3 4 5 6 7 8 9
Time Post Infection (Days)
E
MHV68-Luc 500pfu
2.0×10^07
1.5×10^07
1.0×10^07
5.0×10^06
0.0
Maximal Luminescent Intensity
Ch25h+/+
Ch25h-/-
3 4 5 6 7 8 9
Time Post Infection (Days)
F
MHV68 genomic DNA from
of mice infected with 50
150
100
50
0
Relative Expression
Ch25h+/+
Ch25h
G
MHV68 (500pfu) 9 Days Post Infection
Ch25h+/+
Ch25h-/-
Lumin
max
min

Figure B-7. 25HC inhibits HIV replication and *Ch25h* is required for antiviral immunity *in vivo*

A) 25HC (50mg/kg) or vehicle (HβCD) was administered 12h before HIV NL4-3 infection in humanized mice (NRG-hu). Treatment was administered daily after infection. Viral titer in serum was measured by qRT-PCR 7dpi. Results are combined from 2 experiments. ***P<0.001.

B) Spleens from NRG-hu mice were harvested 14dpi and quantified by FACs after HIV p24 intracellular staining. *P<0.05

C) Percent CD4+ T-cells was compared by FACs in 25HC and EtOH treated group. Representative FACs plots are shown (right). *P<0.05

D) *Ch25h*$^{+/+}$ and *Ch25h*$^{-/-}$ mice were infected with MHV68-Luc (500pfu) and the amount of infection was quantified everyday by bioluminescence imaging. Average intensities (photons/sec/cm^2/steradian) from ventral, right, left, and dorsal sides were measured for all mice. Mean±SEM, *P<0.05 by student's t-test at indicated time point.

E) Similar to Fig. B-7D, maximum intensities (photons/sec/cm^2/steradian) were averaged. Mean±SEM, *P<0.05 by student's t-test at indicated times.

F) MHV68 genomic DNA from *Ch25h*$^{+/+}$ and *Ch25h*$^{-/-}$ infected mice 9dpi was quantified by qRT-PCR and normalized to a genomic promoter of *Ccl2* gene. *P<0.01

G) Bioluminescent images of *Ch25h*$^{+/+}$ and *Ch25h*$^{-/-}$ mice 9dpi.

SUPPLEMENTAL DATA

A

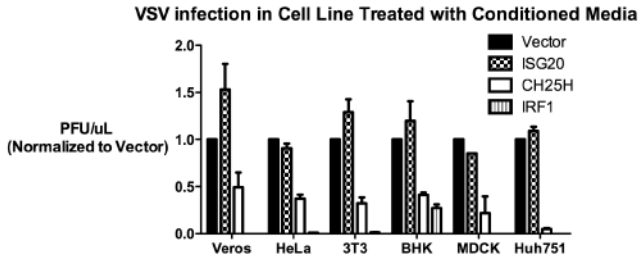

B

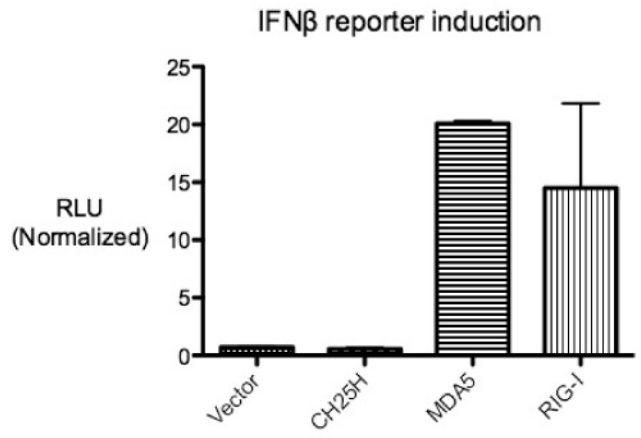

C

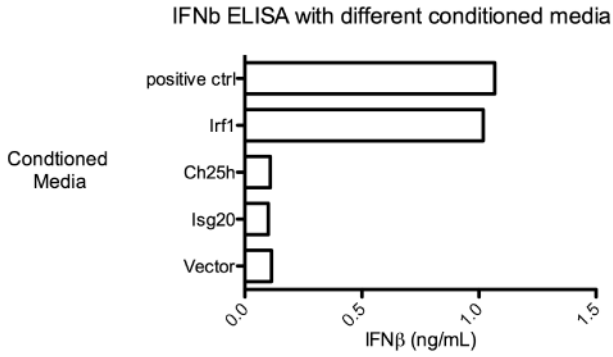

Figure B-S1 (related to Figure B-3)

A. Indicated cell lines were treated for 8-12h with conditioned media from HEK293T transfected with indicated expression vectors. They were infected with VSV at 0.01MOI for 9-14h, depending on the cell line. VSV-GFP was quantified by FACs (%GFP+ X Geometric MFI) and normalized to VSV-GFP in cell treated with vector-conditioned media. Mean±SEM.

B. HEK293T was transfected with indicated expression vector and IFNβ-luciferase reporter. Luciferase activity was measured after 16h. RLU-relative light units. Mean±SEM

C. IFNβ ELISA of conditioned media from HEK293T transfected with indicated expression vectors after 24h.

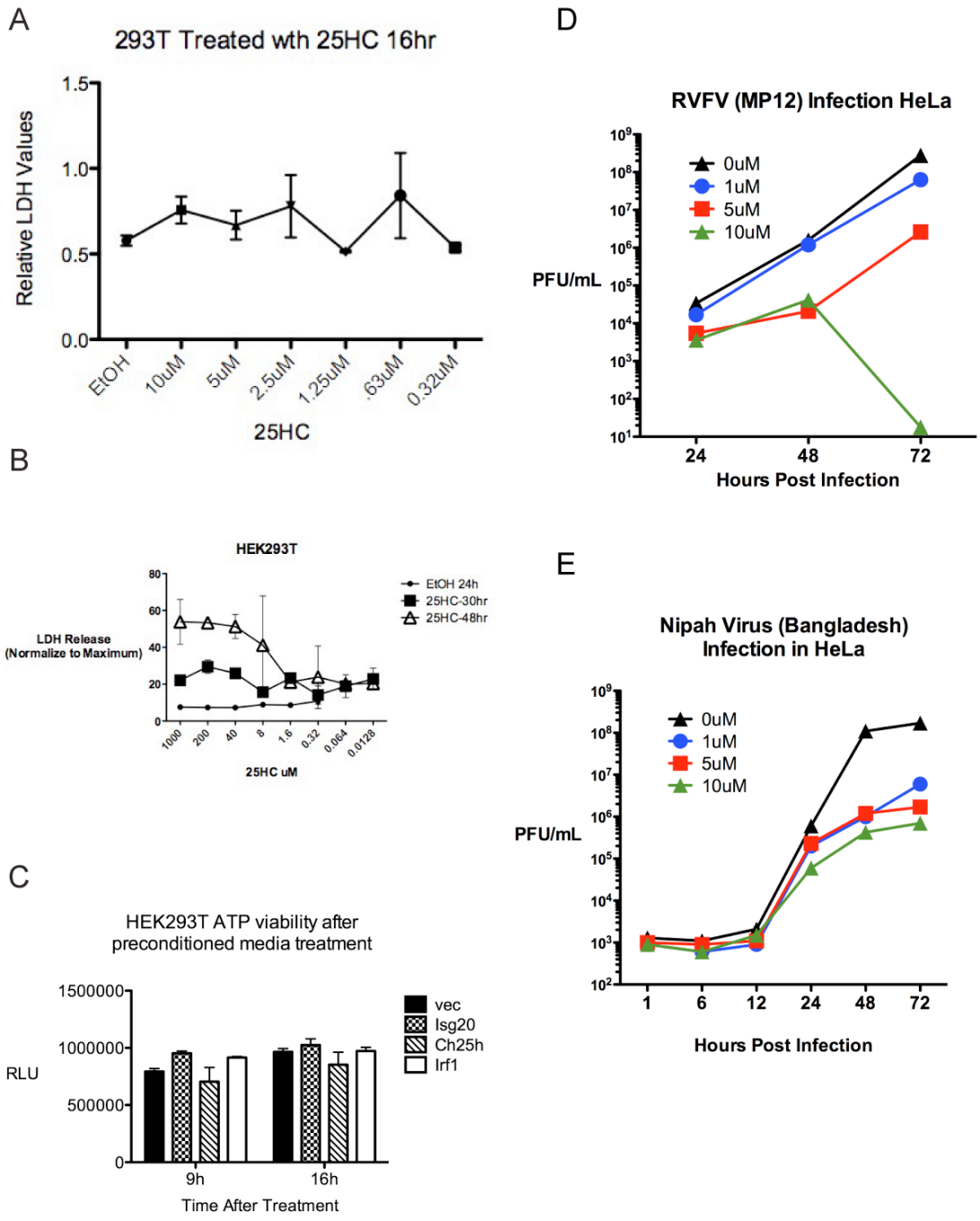

Figure. B-S2 (related to Figure B-4)

A. HEK293T were treated with increasing amount of 25HC and LDH values was measured after 16h. Mean±SD.

B. HEK293T were treated with increasing amount of 25HC and LDH was measured after 30 and 48h. Mean±SD

C. HEK293T was treated with indicated condition media for 16h. Cell viability was measured by quantitation of ATP present in the cell by luminescent substrate. Mean±SD

D. HeLa cells were pretreated with media containing indicated concentrations of 25HC or EtOH for 18h and infected with RVFV (MP12 vaccine strain) at 0.1MOI. Viral titer at indicated time points was measured by plaque assay. Values represent means of samples from triplicates.

E. HeLa cells were pretreated with media containing indicated concentrations of 25HC or EtOH for 18h and infected with Nipah virus (Bangladesh strain) at 0.1MOI. Viral titer at indicated time points was measured by plaque assay. Values represent means of samples from triplicates.

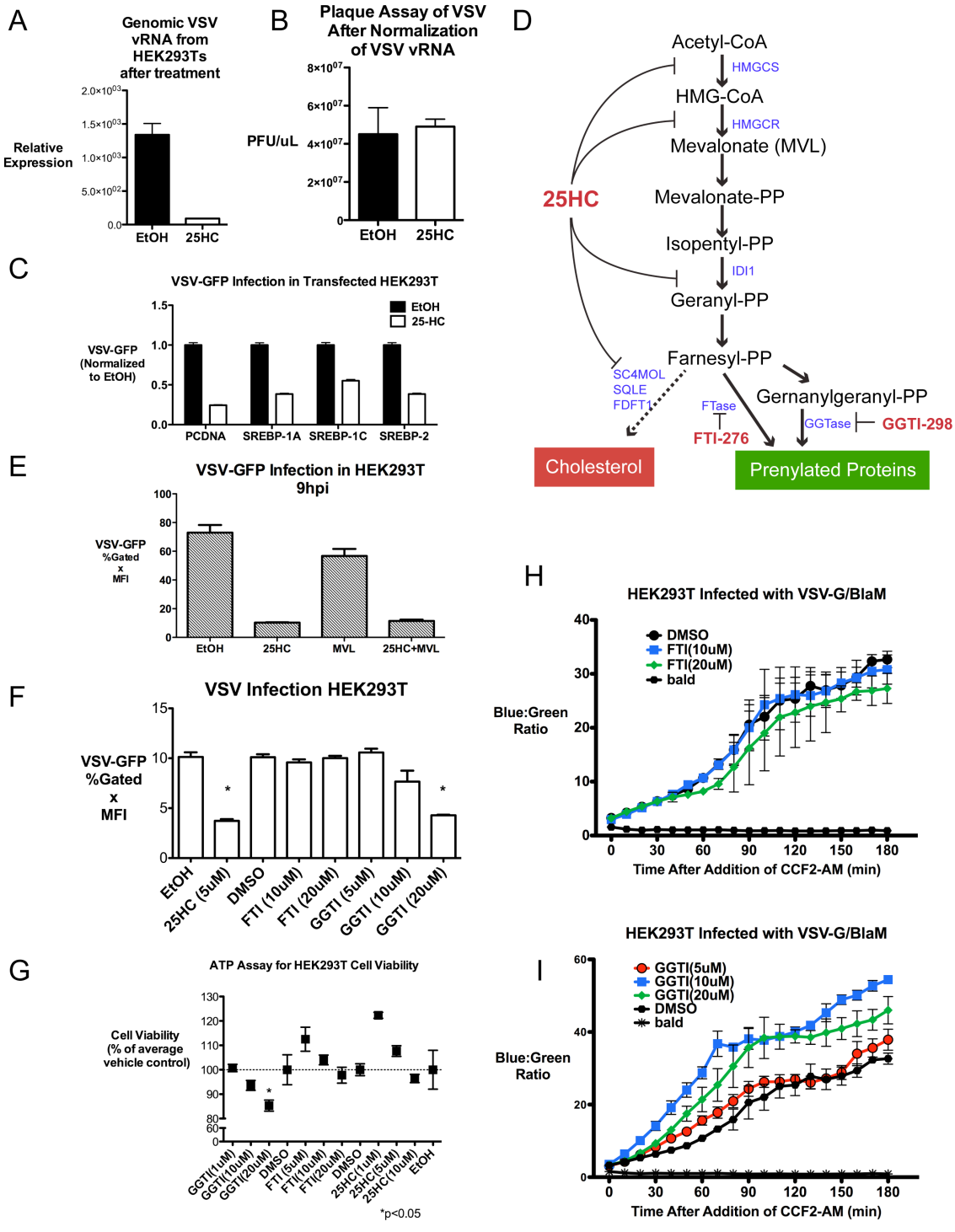
A
Genomic VSV vRNA from HEK293Ts after treatment
Relative Expression
EtOH
25HC
B
Plaque Assay of VSV After Normalization of VSV vRNA
PFU/uL
EtOH
25HC
C
VSV-GFP Infection in Transfected HEK293T
EtOH
25-HC
VSV-GFP (Normalized to EtOH)
PCDNA
SREBP-1A
SREBP-1C
SREBP-2
D
Acetyl-CoA
HMGCS
HMG-CoA
HMGCR
Mevalonate (MVL)
25HC
Mevalonate-PP
Isopentyl-PP
IDI1
Geranyl-PP
Farnesyl-PP
SC4MOL
SQLE
FDFT1
FTase
FTI-276
Gernanylgeranyl-PP
GGTase
GGTI-298
Cholesterol
Prenylated Proteins
E
VSV-GFP Infection in HEK293T 9hpi
VSV-GFP %Gated x MFI
EtOH
25HC
MVL
25HC+MVL
F
VSV Infection HEK293T
VSV-GFP %Gated x MFI
EtOH
25HC (5uM)
DMSO
FTI (10uM)
FTI (20uM)
GGTI (5uM)
GGTI (10uM)
GGTI (20uM)
G
ATP Assay for HEK293T Cell Viability
Cell Viability (% of average vehicle control)
GGTI(1uM)
GGTI(10uM)
GGTI(20uM)
DMSO
FTI (5uM)
FTI(10uM)
FTI(20uM)
DMSO
25HC(1uM)
25HC(5uM)
25HC(10uM)
EtOH
*p<0.05
H
HEK293T Infected with VSV-G/BlaM
DMSO
FTI(10uM)
FTI(20uM)
bald
Blue:Green Ratio
Time After Addition of CCF2-AM (min)
I
HEK293T Infected with VSV-G/BlaM
GGTI(5uM)
GGTI(10uM)
GGTI(20uM)
DMSO
bald
Blue:Green Ratio
Time After Addition of CCF2-AM (min)

Figure. B-S3 (related to Figure B-5)

A. HEK293T were treated with 25HC (2.5μM) and vehicle (EtOH) for 8h and infected with VSV-GFP at 0.01 MOI. The cells were treated against with 25HC after infection. Supernatants were collected 24hpi and virus was concentrated by centrifugation. For a part of the concentrated virus, VSV genomic RNA (gRNA) was quantified by qRT-PCR. Mean±SEM.

B. Concentrated virus from part A was normalized based on VSV gRNA and standard plaque assay was performed. Mean±SEM

C. HEK293T were transfected with mature form of SREBP1a, SREBP1c, and SREBP2 for 24 and treated with 25HC for 12h. The cells were infected with VSV-GFP(0.01MOI) and quantified by FACs. Mean±SEM

D. Schematic of sterol synthesis and isopentyl-PP pathway. 25HC inhibit several enzymes within the pathway (purple): HMG-CoA Reductase (HMGCR1), 3-hydroxy-3-methylglutaryl-CoA synthase (HMGCS1), sterol-C4-methyl oxidase (SC4MOL), squalene epoxidase (SQLE), acetyl-CoA acetyltransferase (ACAT), farnesyl-diphosphate farnesyltransferase (FDFT), isopentenyl-diphosphate

isomerase (IDI1). Two inhibitors of prenylation FTI-276 and GGTI-298 used are also shown.

E. HEK293Ts were treated 25HC, mevalonic acid (300uM), or both for 12h and infected with VSV-GFP (0.01MOI). VSV-GFP was quantified by FACs at 9hpi. Mean±SEM

F. HEK293T was treated as indicated for 12h and infected with VSV-GFP (0.01MOI). VSV-GFP was quantified by FACs at 9hpi.

G. Cytotoxicity of treatments in part. C were measured by ATP content and normalized to respective control (DMSO for GGTI-298 and FTI-276, EtOH for 25HC). Mean±SEM, *P<0.05

H. HEK293T were treated with FTI-276 at indicated concentration and respective concentrations for 12h and infected with VSV-G-βlaM . β-lactamase activity was measured by blue:green ratio of the cleaved CCF2-AM. Mean±SEM.

I. HEK293T were treated with GGTI-298 at indicated concentration and respective concentrations for 12h and infected with VSV-G-βlaM . β-lactamase activity was measured by blue:green ratio of the cleaved CCF2-AM. Mean±SEM.

A

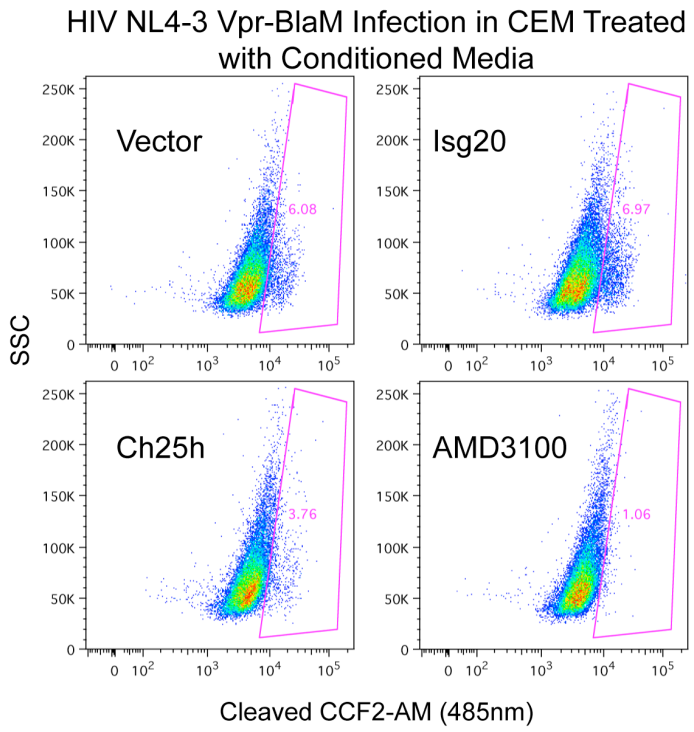
HIV NL4-3 Vpr-BlaM Infection in CEM Treated with Conditioned Media
Vector
Isg20
Ch25h
AMD3100
6.08
6.97
3.76
1.06
SSC
Cleaved CCF2-AM (485nm)

B

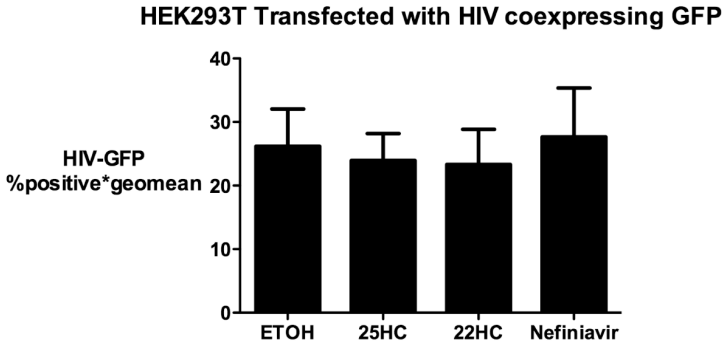
HEK293T Transfected with HIV coexpressing GFP
HIV-GFP %positive*geomean
ETOH
25HC
22HC
Nefiniavir

C

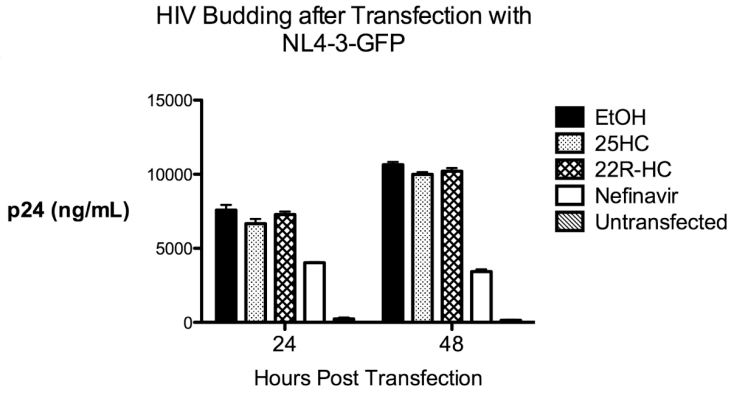
HIV Budding after Transfection with NL4-3-GFP
p24 (ng/mL)
EtOH
25HC
22R-HC
Nefinavir
Untransfected
Hours Post Transfection

Figure. B-S4 (related to Figure B-6)

A. CEM cells were treated with indicated conditioned media for 8h and spin-infected with HIV NL4-3 encoding Vpr-BlaM (NL4-3/BlaM) in duplicates for 2h. CCF2-AM substrate was added and βla activity was measured for 4h at room temperature as shown in Fig 6.C. After the kinetic read, CCF2-AM cleavage was confirmed by FACs with gating on percentage cells expressing cleaved form of CCF2AM (blue, 485nm).

B. HEK293T were transfected with proviral plasmid of HIV coexpressing GFP and treated with indicated agonists 6h after transfection. HIV-GFP was quantified by FACs after 48h. Mean±SEM.

C. Viral supernatants from part A were collected after 48h and p24 was quantified by ELISA. Mean±SD.

SUPPLEMENTAL EXPERIMENTAL PROCEDURES

Cells and Reagents

RAW264.7 (ATCC), Veros, HeLa, 3T3, BHK, MDCK, Huh751, and HEK293T cells were grown in standard DMEM with 10% FBS, 1% Penicillin/Streptomycin (GIBCO). CEM cells were cultured in RPMI media supplemented with 10% fetal calf serum (Hyclone) and 1 % Pen/Strep (Invitrogen). Dr. Glen Barber (University of Miami, Florida) provided VSV-GFP. MHV68-Luc was provided by Dr. Ren Sun in MIMG in UCLA. Luciferase activity was measured using firefly luciferase substrate kit (Promega). LDH Assay and ATP cell viability (Promega) were done on cells treated with Ch25h-conditioned media and 25HC according to manufacturer's instructions. FTI276 and GGTI-298 (Sigma) were used at 5-20μM, consistent with published doses of prenylation inhibition(Wilson *et al*., 1998; Liu *et al*., 2012; Miller *et al*., 2012).

Expression plasmids were obtained from Genecopoeia, Inc. Doxycycline inducible expression system was purchased from Clonetec. SREBP2 expression plasmids were gifts from Dr. Elizabeth Tarling and Dr. Peter Edwards (UCLA). SREBP1 expression plasmids were gifts from Dr. Steven Bensinger (UCLA).

Primary cells and cell lines

Bone marrow was harvested from 6-8 week C57B/L6 mice (Jackson Labs) and differentiated in DMEM+10%FBS for 7 days with 10ng/mL of M-CSF or GM-CSF for macrophage (BMM) or dendritic cells (BMDC), respectively. On day 6 the media was replaced and on day 7 the cells were stimulated with IFNα or IFNγ (PBL Interferon Source). The cells were treated for 2.5 hours and harvested in Trizol (Invitrogen). The RNA was isolated by isopropanol precipitation for microarray analyses. For J2 immortalized macrophages, bone marrow was infected with J2 retrovirus. A retrovirus expressing v-raf and c-myc expressing cell line was established (called GG2EE) and grown in RPMI (10mM Hepes ph7.8, 10%FBS, 1% Pen/strep). Virus containing supernatant was harvested and filtered through 0.45μM filter(Palleroni *et al*., 1991). For BCR-ABL transformed B-cells were derived by infecting bone marrow with BCR-ABL retrovirus as described previously(Scherle *et al*., 1990). Stable knockdown in RAW264.7 were generated using pSiren shRNA knockdown system (Clonetec) according to the published protocol. Knockdown primers sequences are available by request. Tail-derived fibroblasts were derived by skinning the tails of mice and incubating them

directly in culture dishes in DMEM 10%FBS. Cells were scraped and re-plated after 7 days.

Human peripheral blood mononuclear cells (PBMC) were obtained from the UCLA Virology Core. These cells were cultured in RPMI Medium 1640 (Invitrogen) containing 10% FBS, 100 units/ml of Penicillin + 100 μg/ml of Streptomycin (Pen/Strep, Invitrogen), and 20 units/ml of interleukin-2 (Roche). PBMC were costimulated for 3 days with plate-bound anti-CD3 and soluble anti-CD28 antibodies as previously described(Korin and Zack, 1999).

VSV Screening and Flow-cytometry:

HEK293T cells were plated 12 wells on collagen coated plates 0.5mg/mL rat-tail collagen I (BD Biosciences) in PBS. Individual ISGs expression plasmid was transfected with DsRed construct (Clontech) at 3:1 ratio Fugene 6 (Roche) transfection reagents. After 36 hours, the cells were infected as described above. At 9hpi, cells were collected in 2% paraformaldehyde solution in PBS. FACs was done with standard compensation (FACSCaliber, BDBiosciences) and the data was analyzed using CellQuest (BDBiosciences).

VSV, HSV, and MHV68 Viral Plaque Assay

HEK293T and RAW264.7 were infected with VSV-GFP at 0.01 MOI for 1h and the media was changed with fresh media. For J2 BMMs and BCR-ABL B-cells, 1MOI VSV-GFP was used. Approximately 150uL of supernatants were collected at various timepoints between 8-16hpi for plaque assay. For HSV and MHV68, 0.25MOI was used for infection and supernatants were collected at 24hpi. Plaque Assays were done on Vero cells in 12-well plates at $2x10^5$ and $2x10^4$ cells per well for VSV and MHV68 plaque assay, respectively. Supernatants from infected cells were serially diluted and infected on Veros for 1hr. The cells were then covered with growth medium containing 0.6% low-melting point agarose. Plaques stained with crystal violet 0.5% (m/v) in 20% ethanol (v/v) and were counted after 16hrs or 6 days for VSV and MHV68, respectively.

Ebola, Nipah, RVFV, RSSEV Plaque Assay

Plaque Assays were performed on Vero cells (for EBOV, Nipah, and RVFV) in 12-well plates or BHK-SA cells (for RSSEV) in 6 well plates. Cells were infected for 1hr at 37ºC with serial 10-fold dilutions of supernatant aliquots from infected cells. The cells were then overlain with growth medium containing 0.6% methyl cellulose (for EBOV,

Nipah, and RVFV) or 0.5% tragacanth gum (for RSSEV). After 3 days (RVFV, Nipah), 4 days (RSSEV) and 10 days (EBOV), cells were fixed with 10% buffered formalin, stained with crystal violet and plaques counted. All work involving EBOV, Nipah, RSSEV and wild-type RVFV, were performed at the Robert E. Shope BSL-4 laboratory at UTMB.

HIV Infections in hPBMCs

Costimulated PBMC were pre-incubated for 24h at a density of $3x10^6$ cells/ml in conditioned media before infection with HIV. Infections were set-up in 200 μl volumes of conditioned media containing 10^6 cells, 30 ng of HIV strain NL4-3 (as determined by p24 antigen ELISA [Beckman Coulter]), and 10 μg/ml of polybrene. The mixture was incubated for 2h at 37°C on a rocking platform. Following infection, cells were washed twice with media and then split into triplicate 2ml cultures in conditioned media, each containing $3.3x10^5$ cells. At various post-infection timepoints, 100 μl of cell-free supernatant was removed and added to 2% Triton-x-100 in PBS for storage at 4°C before quantitation of p24 concentration by ELISA.

VSV Screening and Flow-cytometry:

HEK293T cells were plated 12 wells on collagen coated plates 0.5mg/mL rat-tail collagen I (BD Biosciences) in PBS. Individual ISGs expression plasmid was transfected with DsRed construct (Clontech) at 3:1 ratio Fugene 6 (Roche) transfection reagents. After 36 hours, the cells were infected as described above. At 9hpi, cells were collected in 2% paraformaldehyde solution in PBS. FACs was done with standard compensation (FACSCaliber, BDBiosciences) and the data was analyzed using CellQuest (BDBiosciences).

VSV-G pseudotyped VSV-G Luciferase pseudovirus production

VSV-G pseudotyped VSV-G luciferase pseudovirus (VSVΔG-Luc/G) was generated by methods previously described(Takada *et al*., 1997) and concentrated by ultracentifugation on 20% sucrose cushion. The VLPs were resuspended in NTE buffer (100 mM NaCl; 10 mM Tris–HCl, pH 7.5; 1 mM EDTA) and stored in -80C. The concentrations used to generate linear range of luciferase signal were determined empirically.

VSV-G/BlaM Production

A previously described construct encoding Nipah-M1 fusion with β-lactamase (BlaM) was used to package inside VSV-G(Wolf *et al*., 2009). HEK293Ts were transfected with constructs encoding BlaM and VSV-G or BlaM alone (bald) at 3:1 ratio in 10cm dishes by PEI transfection reagent. The viral supernatants were collected, clarified, and concentrated by ultracentrifugation at >75,000g on 20% sucrose cushion,

HIV IIIB pseudotyped virus production

HIV-IIIB pseudovirus were made of HIV-IIIB envelope on a NL4-3 backbone coexpressing luciferase (pNL4-3.Luc.-R-E). Plasmids were obtained through the NIH AIDS and Research and Reference Reagent Program. Pseudovirus were generated by cotransfection of 293T cells with envelope deleted LucRE- vector and envelope expressing vector at a 3:1 μg ratio with Bioline Bio T transfection reagent. 72 hours post transfection viral supernatant was collected, clarified by low speed centrifugation and stored at -80c. The number of infectious virus particles was determined by serial dilution assay on Ghost HI-X4 cells, cells that express GFP controlled by a HIV LTR promoter. Briefly, 4 X 10^4 Ghost HI-X4 cells were seeded into a 48 well dish. 24 hour later, cells are infected with 2 fold serially diluted pseudovirions. 48 hours later, cells were collected and the percentage of positive cells were determined using FACs.

CEM Infection with pseudotyped IIIB Virus

CEMs cells were treated with 25HC, 22HC or EtOH for a minimum of six hours. Prior to infection previously untreated cells were incubated with AMD3100, AZT, Elvitegravir or Nelfinavir at a concentration of 10uM to 20uM for a minimum of 15 minutes. IIIB pseudovirus was used to infect treated and untreated CEM cells at 0.1MOI. Infections were spin inoculated for 60 minutes at 2,000RPM, at 37C. After spin inoculation, cells were transferred into a 37C incubator. 48 hours post infection cells were lysed with 1% triton-X 100 and assayed for luciferase activity. P24 Assay was done in with PerkinElmer's HIV-1 P24 Elisa kit (NEK050B). Accompanied protocol was followed.

Generation of VPR-BlaM Fusion Gene

VPR-BlaM was generated by overlapping pcr and cloned into PCDNA3.1. VPR was amplified from SG3Δ. Catalytically optimized beta lactamase described previously in (cite) was amplified with primers (3,4). The two pcr products were used in the overlapping pcr using primers (1,4) to generate VPR-BlaM . VPR-BlaM pcr product was cloned into pcdna3.1 expression vector previously cut with BamHI and XhoI using the Infusion system (CloneTech).

NL4-3 VPR-BlaM Virus Production

NL4-3 VPR-BlaM was produced in according to the methods outlined previously(Cavrois *et al*., 2002). Briefly, 2 µg of VPR BlaM , 1µg of padvantage (Promega) and 8 µg of NL4-3 were cotransfected into 293Ts in 10cm plate with PEI reagent. 48 hours post transfection viral supernatant was collected, clarified by low speed centrifugation, and concentrated on 20% sucrose cushion. VLPs were resuspended in small volume of NTE and stored at -80c.

Liposome Competition Experiment with 25HC and LJ001

Recombinant unilamillar liposomes with a composition of 7:3 phosphatidylcholine:cholesterol (Encapsula Inc.) was added to HEK293T with or without 25HC (1uM) for 8h. Cells were washed with PBS and infected with VSV-GFP for 1h and quantified by FACs at 9hpi. LJ001 treatment was described previously (Wolf *et al*., 2010). Briefly, LJ001 was mixed with liposomes and VSV-GFP for 10min prior to infection because it intercalates into viral membrane to inhibit fusion.

PCR

Cells were collected in trizol and RNA was isolated by standard isopropanol precipitation. RNA was quantitated and 1 μg of RNA was reversed transcribed using IScript (BioRad) according to the manufacturer's instructions with either random hexamer as primers. Q-PCR analysis was done using the iCycler thermocycler (Bio-Rad). Q-PCR was conducted in a final volume of 20 μL containing: Native Taq polymerase (Invitrogen), 1× Taq buffer (Stratagene), 125 μM dNTP, SYBR Green I (Molecular Probes), and Fluoroscein (Bio-Rad), and 1% cDNA. Amplification conditions were: 95°C (3 min), 40 cycles of 95°C (20 s), 55°C (30 s), 72°C (20 s). Expression values were normalized to L32 control and fold induction was normalized to untreated control.qRT-PCR of Ch25h was done with primers: Ch25h fwd: 5'-TGCTACAACGGTTCGGAGC-3'. Ch25h rev: 5'-AGAAGCCCACGTAAGTGATGAT-3'. L32 fwd: 5'-AAGCGAAACTGGCGGAAAC-3'; L32 rev: 5'-TAACCGATGTTGGGCATCAG-3'.

For detection of VSV genomic RNA, cells infected with VSV was collected in Trizol and RNA was isolated and reverse transcribed with VSV specific primer N1-5' GATAGTACCGGAGGATTGACGACTA using Superscript II (Invitrogen) according to manufacturer's protocol. Real time PCR with Taqman probe with conditions described above. VSV fwd: 5′-GATAGTACCGGAGGATTGACGACTA-3′; VSV rev: 5′-

TCAAACCATCCGAGCCATTC-3; VSV Probe: 5' (FAM)-TGCACCGCCACAAGGCAGAGA-(TAMRA)-3'.

CEM cells were infected with HIV IIIB expressing GFP and or Luciferase. After spinoculation, the cells were collected at indicated time and total DNA was extracted with DNAeasy Blood &Tissue Kit (Qiagen). Full length LateRT was measured by Taqman qRT-PCR as described previously (Butler *et al*., 2001) and normalized to mitochondrial DNA. Primers used: late RT forward: 5'-TGTGTGCCCGTCTGTTGTGT-3'; late RT reverse: 5'-GAGTCCTGCGTCGAGAGAGC-3';

late RT probe, 5'-(FAM)-CAGTGGCGCCCGAACAGGGA-(TAMRA)-3'; Mitochondrial forward primer, 5'-ACCCACTCCCTCTTAGCCAATATT-3'; mitochondrial reverse primer, 5'-GTAGGGCTAGGCCCACCG-3'

RNA isolation and RNAseq of Bone Marrow Derived Macrophage Stimulation

$5x10^5$ BMMs from wildtype (C57BL/6), IFNAR-deficient and IL-27R (TCCR/WSX-1) deficient mice were stimulated with Lipid A (100ng/mL) or saline control for 4hr and 12hr, respectively. Cells were harvested in Trizol (Invitrogen) and RNA was isolated via chloroform extraction.

Prior to cDNA library construction for RNA-Seq analyses, RNA was quantified and assessed for quality (RNA Integrity Value) using an Agilent 2100 Bioanalyzer (Santa Clara, CA). 1ug of RNA per condition was used for library construction using TruSeq SBS Kit v3 (FC-401-3001) according to the manufacturers guidelines (Illumina, San Diego, CA). Multiplex Sequence Analysis was performed using a Illumina HiSeq2000 Single End 100bp read parameters according to the manufacturers guidelines (www.illumina.com). Sequencing was performed by the Southern California Genotyping Consortium (SCGC) in the Epigenetics and Genetics Core at UCLA. Sequence reads from each cDNA library (100 bp, single-read) were trimmed to 80 bp long and mapped onto the mouse genome build NCBI37/mm9 using Bowtie (bowtie-0.12.1, http://bowtie-bio.sourceforge.net/index.shtml) with setting '-v 2 -k 11 -m 10 -t–best–strata'. The mappable data were then processed by the ERANGE v. 3.3 RNA-seq analysis program(Mortazavi *et al*., 2008). Assuming total transcriptional activity is comparable between different cell types, the obtained data (data units in RPKM, reads per kilobase exon model per million mapped reads) were first $\log_2$ transformed and linearly normalized between individual samples, then averaged among biological replicates or triplicates. At the same time, in order to find genes that were changed in expression between two populations to a statistically significant degree, ERANGE processed data

were analyzed by the Bioconductor DEGseq program (Wang *et al*., 2010) (http://www.bioconductor.org/packages/2.6/bioc/html/DEGseq.html) (data units in RPM, reads per million mapped reads, method = "MARS," $p < 0.001$). Data is presented using RPKM values.

HIV infection in NRG-hu mice

We used an HIV molecular clone with a highly pathogenic dual tropic envelope, R3A in NL4-3 Backbone for infection. HIV-1 viral stocks were produced in 293T cells, and titered on Hela-CD4-LTR-gal cells (NIH AIDS Research and Reference Reagent Program, Division of AIDS, NIAID). NRG-hu mice with stable human leukocyte reconstitution were administered 50mg/kg of 25HC or the vehicle control (2-hydroxypropyl)-β-cyclodextrin (HBCD) intraperitonial (i.p.) injection for 12h before infection with HIV NL4-R3A at 5ng of p24/mouse by intravenously injection (i.v.). Mice were administered 50mg/kg of 25HC or HBCD control every day. NRG-hu mice infected with mock supernatant were included as control groups. RNA was extracted by Qiagen RNA extraction mini plus kit(Cat#52904) and HIV replication (genome copy/ml in the plasma) was measured using TaqMan One step RT PCR Master Mix Reagents Kit

from Roche (Cat # 4309169). Intracellular staining and FACs analysis were done as previously described (Zhang *et al*., 2011).

Mouse Infections and Bioluminescence Imaging

C57BL/6 and *ch25h-/-* mice were purchased from Jackson. Mice were first anaesthetized by intraperitoneal (*i.p.*) injection with 200 mg/kg ketamine, 4 mg/kg xylazine in PBS. MHV68 (500 pfu) in 200uL of PBS was administered by i.p. and shaved. On days 3 following infection, mice were imaged using the *in vivo* imaging system (IVIS, Xenogen). Briefly, mice were anesthetized with isoflurane and administered 3mg D-luciferin/mouse by intraperitoneal injection prior to imaging. Grayscale photographs and color images of imaged mice were superimposed with LivingImage (Xenogen) and Igor (Wavemetrics) programs, similar to that previously described. The mice were imaged on dorsal, ventral, right, and left side until the maximal luminescence has passed. The peak intensity of average and maximum photon flux value was measured for each mouse at every angle and expressed as photons/sec/cm^2/steradian. These values were averaged for each group of mice.

SUPPLEMENTAL REFERENCES

Butler, S.L., Hansen, M.S.T., and Bushman, F.D. (2001). A quantitative assay for HIV DNA integration *in vivo*. Nat Med *7*, 631–634.

Cavrois, M., de Noronha, C., and Greene, W.C. (2002). A sensitive and specific enzyme-based assay detecting HIV-1 virion fusion in primary T lymphocytes. Nat Biotech *20*, 1151–1154.

Korin, Y.D., and Zack, J.A. (1999). Nonproductive Human Immunodeficiency Virus Type 1 Infection in Nucleoside-Treated G0 Lymphocytes. Journal of Virology *73*, 6526 – 6532.

Liu, X.V., Ho, S.S.W., Tan, J.J., Kamran, N., and Gasser, S. (2012). Ras Activation Induces Expression of Raet1 Family NK Receptor Ligands. The Journal of Immunology *189*, 1826 –1834.

Miller, B.T., Ueta, C.B., Lau, V., Jacomino, K.G., Wasserman, L.M., and Kim, B.W. (2012). Statins and Downstream Inhibitors of the Isoprenylation Pathway Increase Type 2 Iodothyronine Deiodinase Activity. Endocrinology *153*, 4039 –4048.

Mortazavi, A., Williams, B.A., McCue, K., Schaeffer, L., and Wold, B. (2008). Mapping and quantifying mammalian transcriptomes by RNA-Seq. Nat Meth *5*, 621–628.

Palleroni, A.V., Varesio, L., Wright, R.B., and Brunda, M.J. (1991). Tumoricidal alveolar macrophage and tumor infiltrating macrophage cell lines. Int. J. Cancer *49*, 296–302.

Scherle, P.A., Dorshkind, K., and Witte, O.N. (1990). Clonal lymphoid progenitor cell lines expressing the BCR/ABL oncogene retain full differentiative function. Proceedings of the National Academy of Sciences *87*, 1908 –1912.

Takada, A., Robison, C., Goto, H., Sanchez, A., Murti, K.G., Whitt, M.A., and Kawaoka, Y. (1997). A system for functional analysis of Ebola virus glycoprotein. Proceedings of the National Academy of Sciences *94*, 14764 –14769.

Wang, L., Feng, Z., Wang, X., Wang, X., and Zhang, X. (2010). DEGseq: an R package for identifying differentially expressed genes from RNA-seq data. Bioinformatics *26*, 136 –138.

Wilson, A.L., Erdman, R.A., Castellano, F., and Maltese, W.A. (1998). Prenylation of Rab8 GTPase by type I and type II geranylgeranyl transferases. Biochem. J. *333*, 497–504.

Wolf, M., Wang, Y., Freiberg, A., Aguilar, H., Holbrook, M., and Lee, B. (2009). A catalytically and genetically optimized beta-lactamase-matrix based assay for sensitive,

specific, and higher throughput analysis of native henipavirus entry characteristics. Virology Journal *6*, 119.

Wolf, M.C., Freiberg, A.N., Zhang, T., Akyol-Ataman, Z., Grock, A., Hong, P.W., Li, J., Watson, N.F., Fang, A.Q., Aguilar, H.C., *et al*. (2010). A broad-spectrum antiviral targeting entry of enveloped viruses. Proceedings of the National Academy of Sciences *107*, 3157 –3162.

Zhang, L., Jiang, Q., Li, G., Jeffrey, J., Kovalev, G.I., and Su, L. (2011). Efficient infection and impairment of pDC in the bone marrow and peripheral lymphoid organs during early HIV-1 infection in humanized rag2-/-γC-/- mice *in vivo*. Blood.

Appendix C

Macrophage-tropic HIV-1 variants from brain demonstrate alterations in the way gp120 engages both CD4 and CCR5

JLB

Article

Macrophage-tropic HIV-1 variants from brain demonstrate alterations in the way gp120 engages both CD4 and CCR5

Hamid Salimi,[,†] Michael Roche,[*] Nicholas Webb,[‡] Lachlan R. Gray,*[,§] Kelechi Chikere,[‡] Jasminka Sterjovski,[*] Anne Ellett,[*] Steve L. Wesselingh,[‖] Paul A. Ramsland,[¶,**,††] Benhur Lee,[‡] Melissa J. Churchill,*[,†,‡‡] and Paul R. Gorry*[,‡‡,§§,1]*

Centers for [*]Virology and [¶]Immunology, Burnet Institute, Melbourne, Victoria, Australia; Departments of [†]Microbiology, [‡‡]Medicine, [§]Biochemistry, and Molecular Biology, and [**]Immunology, Monash University, Melbourne, Victoria, Australia; [‡]Department of Microbiology, Immunology, and Molecular Genetics, David Geffen School of Medicine, University of California Los Angeles, Los Angeles, California, USA; [‖]South Australian Health and Medical Research Institute, Adelaide, Australia; and Departments of [††]Surgery, Austin Health, and [§§]Microbiology and Immunology, University of Melbourne, Melbourne, Victoria, Australia

RECEIVED JUNE 25, 2012; REVISED SEPTEMBER 25, 2012; ACCEPTED OCTOBER 4, 2012. DOI: 10.1189/jlb.0612308

ABSTRACT

BR-derived HIV-1 strains have an exceptional ability to enter macrophages via mechanisms involving their gp120 Env that remain incompletely understood. Here, we used cell-based affinity-profiling methods and mathematical modeling to generate quantitative VERSA metrics that simultaneously measure Env-CD4 and Env-CCR5 interactions. These metrics were analyzed to distinguish the phenotypes of M-tropic and non-M-tropic CCR5-using HIV-1 variants derived from autopsy BRs and LNs, respectively. We show that highly M-tropic Env variants derived from brain can be defined by two distinct and simultaneously occurring phenotypes. First, BR-derived Envs demonstrated an enhanced ability to interact with CD4 compared with LN-derived Envs, permitting entry into cells expressing scant levels of CD4. Second, BR-derived Envs displayed an altered mechanism of engagement between CD4-bound gp120 and CCR5 occurring in tandem. With the use of epitope mapping, mutagenesis, and structural studies, we show that this altered mechanism is characterized by increased exposure of CD4-induced epitopes in gp120 and by a more critical interaction between BR-derived Envs and the CCR5 N-terminus, which was associated with the predicted presence of additional atomic contacts formed at the gp120-CCR5 N-terminus interface. Our results suggest that BR-derived HIV-1 variants with highly efficient macrophage entry adopt conformations in gp120 that simultaneously alter the way in which the Env interacts with CD4 and CCR5. *J. Leukoc. Biol.* 93: 000–000; 2013.

Abbreviations: 3D=three-dimensional, BR=brain, CD4bs=CD4-binding site, ECL=extracellular loop, Env=HIV-1 envelope glycoprotein, M-tropic=macrophage tropic, MVC=maraviroc, NHMRC=Australian National Health and Medical Research Council, NIAID=National Institute of Allergy and Infectious Diseases, PNGS=potential N-linked glycosylation site, ponA=ponasterone A, sCD4=soluble CD4, $TCID_{50}$=50% tissue culture-infective dose, VERSA=viral entry receptor sensitivity analysis

The online version of this paper, found at www.jleukbio.org, includes supplemental information.

Introduction

HIV-1 establishes infection in the CNS, causes HIV-1-associated neurological disorders in infected subjects, and presents a barrier to effectively treating HIV-1 infection [1, 2]. Microglia and perivascular macrophages are target cells for HIV-1 replication in the brain [1, 3]. They are less susceptible to the cytopathic effects of HIV-1 than activated $CD4^+$ T cells [4, 5], so they may continue to shed virus for the duration of their normal lifespan. As most antiretroviral therapies have poor CNS penetration [6], the brain is a significant reservoir for viral persistence within macrophage-lineage cells.

The genetic evolution of HIV-1 within the CNS is distinct from that in lymphoid tissues and other organs [7–20]. Specific sequences within the viral Env, particularly the gp120 V3 region, have been associated with CNS infection [12, 13, 19, 21–26], although no conserved genetic signature sequence has been identified. The genetic compartmentalization of viral variants in the CNS, which has been shown recently to occur very early in HIV-1 infection [16], suggests that adaptive changes may occur in response to unique constraints of the CNS microenvironment, such as different target cell populations and immune-selection pressures.

The HIV-1 Env is organized into trimers on virions and consists of the gp120 surface and gp41 transmembrane subunits. HIV-1 entry into cells is initiated by a high-affinity interaction between gp120 and CD4 [27], which induces a conformational change in gp120 that exposes the binding site for a chemokine coreceptor, either CCR5 or CXCR4 [28, 29]. Current

1. Correspondence: Burnet Institute, GPO Box 2284, Melbourne, Victoria, Australia, 3001. E-mail: gorry@burnet.edu.au

models of gp120 binding to coreceptor suggest that the gp120 V3-loop tip interacts principally with the coreceptor ECL2 region, whereas the V3-loop stem and the gp120 bridging sheet, which is formed among the C1, C2, and C4 domains of gp120 after CD4 binding, interact with the coreceptor N-terminus [30–33]. The V3-loop of gp120 is the primary determinant of coreceptor specificity [34, 35]. Whereas the coreceptor N-terminus and ECL2 region appear to be important for gp120-coreceptor binding, the ECL1 and ECL3 regions may also influence coreceptor function of CCR5 and CXCR4 [36–38]. The interaction of CD4-bound gp120 with coreceptor induces additional conformational changes in gp120, which leads to a structural rearrangement in gp41 that enables fusion and virus entry.

The tropism of HIV-1 for particular target cell populations in different tissue compartments is influenced by the coreceptor used by HIV-1 Env for virus entry [3, 39, 40]. Macrophage-tropic HIV-1 primarily uses CCR5 (R5) as a coreceptor [41–43], whereas T cell line tropic viruses use CXCR4 (X4) [44]. Dual-tropic viruses can use both coreceptors (R5X4) [45, 46]. Thus, the coreceptor specificity of primary HIV-1 isolates is frequently, but incorrectly, used to define cellular tropism. For example, R5 viruses are often collectively grouped as M-tropic viral strains [40]. However, several studies have demonstrated the presence of non-M-tropic R5 viruses, which were replication-competent in primary $CD4^+$ T cells but could not productively infect MDMs [10, 47–51]. Thus, there is a notable distinction between HIV-1 tropism and coreceptor use [40, 52, 53]; whereas most M-tropic viruses use CCR5 for HIV-1 entry, not all R5 viruses are M-tropic [40, 53, 54].

In fact, recent studies have shown that M-tropism is relatively rare among R5 HIV-1 variants isolated from blood and lymphoid tissues but that most R5 viruses isolated from the CNS are highly M-tropic [10, 15, 49–51, 55–58]. However, M-tropic R5 variants can be detected in blood of some subjects with advanced infection [47, 48, 59]. The CNS, therefore, selects for viral variants that have characteristics favorable for efficient entry into macrophage-lineage cells or facilitates their evolution via a unique microenvironment that may involve reduced immune surveillance and low anti-HIV-1-neutralizing antibody concentrations.

The mechanisms underlying the efficient macrophage entry of BR-derived HIV-1 variants are incompletely understood. Several studies have shown that the gp120 Env glycoproteins of CNS-derived viruses have conformational alterations within the CD4-binding domain that increase the efficiency of the interaction between gp120 and CD4, thus permitting these variants to scavenge relatively low levels of CD4 expressed on the surface of macrophages and microglia [15, 49, 50, 55–58, 60–64]. Other studies have shown that certain BR-derived variants have Env glycoproteins that exhibit increased affinity for CCR5 [11]. Moreover, our recent studies have shown that efficient CCR5-mediated HIV-1 entry of certain blood-derived variants into macrophages involves an altered mechanism of Env-CCR5 engagement, characterized by reduced dependence of Env on the CCR5 N-terminus and increased dependence on the CCR5 ECL2 region [65, 66].

In the present study, we used an innovative and highly quantitative HIV-1 receptor affinity-profiling system and mathematical modeling combined with epitope mapping studies, mutagenesis, and structural modeling to more completely understand the virus–cell interactions underlying efficient macrophage entry by BR-derived HIV-1 Env variants. We show that highly M-tropic HIV-1 variants derived from the brain have alterations in the way their Env glycoproteins engage CD4 and CCR5, characterized by a highly efficient interaction between gp120 and CD4 occurring in tandem with a modified mechanism of engagement between CD4-bound gp120 and CCR5. Our findings more completely define the macrophage-tropic phenotype of HIV-1 variants derived from the brain.

MATERIALS AND METHODS

Cells

293T cells, JC53 cells [67], and NP2-CD4 cells [68] were cultured in DMEM supplemented with 10% (vol/vol) FCS and 100 μg penicillin and streptomycin/ml. The dually inducible 293-Affinofile cell line [69], in which expression of CD4 and CCR5 can be induced and regulated by the addition of minocycline or ponA, respectively, was maintained in DMEM supplemented with 10% (vol/vol) FCS, 100 μg penicillin and streptomycin/ml, 50 μg blasticidin/ml, and 200 μg G418/ml. PBMCs were purified from blood of healthy HIV-1-negative donors by density gradient centrifugation, stimulated with 10 μg PHA (Sigma, St. Louis, MO, USA)/ml for 3 days, and cultured in RPMI-1640 medium, supplemented with 10% (vol/vol) FCS, 100 μg penicillin and streptomycin/ml, and 20 U IL-2 (Roche, Basel, Switzerland)/ml. Monocytes were purified from PBMC by plastic adherence and allowed to differentiate into MDM by culturing for 5 days in IMEM, supplemented with 10% (vol/vol) pooled AB+ human sera, 100 μg penicillin and streptomycin/ml, and 12.5 ng M-CSF/ml.

HIV-1 Env plasmids

This study characterized six Envs cloned from HIV-1 viruses isolated from autopsy brain of three subjects who died from AIDS (subjects Macs2, Macs3, and UK1), as well as six Envs cloned from HIV-1 viruses isolated from autopsy LN of two of the same subjects (subjects Macs2 and Macs3; LN-derived Envs from UK1 were not available). The subjects, including their clinical and neuropathological details, have been described previously [10, 11]. The Env clones used were Macs2-BR-2, Macs2-BR-8, Macs3-BR-1, Macs3-BR-8, UK1-BR-2, UK1-BR-10, Macs2-LN-2, Macs2-LN-3, Macs2-LN-5, Macs2-LN-6, Macs3-LN-8, and Macs3-LN-9. JR-CSF and YU2 Envs were included as controls. All of the Envs are cloned into the pSVIII-Env mammalian expression vector [70] and have been described previously [25, 26].

Production and quantitation of Env-pseudotyped luciferase reporter viruses

Env-pseudotyped, luciferase reporter viruses were produced by transfection of 293T cells with pCMVΔP1ΔenvpA, pHIV-1Luc, and pSVIII-Env plasmids using Lipofectamine 2000 (Invitrogen, Life Technologies, Grand Island, NY, USA) at a ratio of 1:3:1, as described previously [71–73]. Supernatants were harvested 48 h later, filtered through 0.45 μm filters, and stored at −80°C. The $TCID_{50}$ of virus stocks was determined by titration in JC53 cells [67], as described previously [25, 74, 75].

Single-round HIV-1 entry assays

For single-round entry assays using JC53 cells, 293-Affinofile cell populations, or NP2-CD4 cells expressing WT or mutant CCR5 coreceptors, 2×10^4 cells cultured in 96-well plates, were inoculated with 200 $TCID_{50}$ of Env-pseudotyped luciferase reporter virus (equating to a MOI of 0.01) in a volume of 100 μl for 12 h at 37°C. The cells were washed twice with culture medium to remove residual inoculum and incubated for a further 60 h at 37°C. For single-round entry assays using MDM, cell monolayers,

which were ~90% confluent in 48-well tissue-culture plates, were inoculated with 1500 $TCID_{50}$ of Env-pseudotyped luciferase reporter virus in a volume of 300 μl for 12 h at 37°C. The MDMs were then washed twice with culture medium to remove residual inoculum and incubated for a further 96 h at 37°C. For single-round entry assays in PBMC, 2×10^5 cells were inoculated with 2000 $TCID_{50}$ of Env-pseudotyped luciferase reporter virus in a volume of 200 μl for 12 h at 37°C. The cells were then washed twice with culture medium to remove residual inoculum and incubated a further 72 h at 37°C. In all cell types, the level of HIV-1 entry was measured by luciferase activity in cell lysates (Promega, Madison, WI, USA), according to the manufacturer's protocol. Luminescence was measured using a FLUOStar Optima microplate reader (BMG Labtech GmbH, Germany). Negative controls included mock-infected cells that were incubated with culture medium instead of virus, and cells inoculated with luciferase reporter virus pseudotyped with the nonfunctional ΔKS Env [76].

Affinofile cell assays and quantitative vector analysis

Infection of 293-Affinofile cells with Env-pseudotyped luciferase reporter viruses was performed as described previously [69]. Briefly, 48 populations of cells expressing different combinations of CD4 and CCR5 levels were generated by inducing the cells with twofold serial dilutions of minocycline (0.156–5.0 ng/ml, resulting in six induction levels of CD4 increasing linearly from 750 to 95,000 CD4 molecules/cell) and ponA (0.0156–2.0 μM, resulting in eight induction levels of CCR5 increasing linearly from 3500 to 110,000 CCR5 molecules/cell). CD4 and CCR5 concentrations were determined by quantitative flow cytometry (quantitative FACS), as described previously [69, 77]. The induced cell populations were then inoculated with equivalent amounts of Env-pseudotyped reporter virus and analyzed for levels of HIV-1 entry as described above. The relative level of virus entry achieved by each Env tested was expressed as a percentage of that achieved in 293-Affinofile cells expressing the highest concentrations of CD4 and CCR5. The robustness of the 293-Affinofile assay for measuring alterations in CD4 and CCR5 dependence was validated using a CD4-independent virus (SIV 316), which was highly sensitivity to alterations in the expression levels of CCR5 but not CD4, and with a CXCR4 using virus (IIIB), which was highly sensitivity to alterations in the expression levels of CD4 but not CCR5 (data not shown). After normalization of the virus entry data, the relative dependence of Env-pseudotyped reporter viruses on CD4 and CCR5 expression levels was mathematically modeled using the VERSA computational platform (http://versa.biomath.ucla.edu), as described previously [69, 78]. With the use of this model, viral infectivity is quantified using a single vector. The vector magnitude and mean induction reflect the efficiency of virus entry, and the vector angle represents the relative dependence on CD4 or CCR5. The mathematical derivation of these metrics has been described in detail previously [69] and is summarized in Supplemental Fig. 1. In theoretical extremes, viruses that have the greatest possible sensitivity to alterations in CD4 expression but are unaffected by alterations in CCR5 expression have a vector angle of 0°, and conversely, viruses that have the greatest possible sensitivity to alterations in CCR5 expression but are unaffected by alterations in CD4 expression have a vector angle of 90°.

gp120-binding assays

293T cells were transfected with Env expression plasmids using Lipofectamine 2000 (Invitrogen, Life Technologies), according to the manufacturer's protocol, and stained for surface gp120 expression using pooled polyclonal HIV+ sera BB10, as described previously [66, 72]. Approximately 2×10^5 293T cells transfected with each Env expression plasmid were used in binding reactions. In binding reactions with the Env mAb 17b [79–82], cells were preincubated in FACS buffer [PBS containing 10% (vol/vol) FCS and 0.05% (wt/vol) sodium azide], with or without 20 μg sCD4/ml (Progenics Pharmaceuticals, Tarrytown, NY, USA) for 1 h at room temperature. Cells were then washed twice with 200 μl FACS buffer and resuspended in 50 μl FACS buffer containing 10 μg 17b [79–84]/ml. This concentration was empirically determined to be within the linear range of binding [66]. Following incubation for 1 h at room temperature, cells were washed twice with 200 μl FACS buffer and resuspended in 50 μl FACS buffer containing a 1:200 dilution of FITC-conjugated anti-human IgG $F(Ab)_2$ fragment (Millipore, Billerica, MA, USA). Cells were incubated for 1 h at room temperature, prior to being washed twice with 200 μl FACS buffer and resuspended in 150 μl PBS containing 4% (wt/vol) PFA and analyzed by flow cytometry as described previously [85].

HIV-1 neutralization/inhibition assays

The ability of the Env mAb b12 or sCD4 to neutralize/inhibit the infectivity of Env-pseudotyped luciferase reporter viruses was assayed using JC53 cells. Two hundred $TCID_{50}$ of each Env-pseudotyped luciferase reporter virus (equating to a MOI of 0.01) were incubated with tenfold-increasing concentrations of b12 (0.0005–50 μg/ml) or sCD4 (Progenics Pharmaceuticals; 0.001–100 μg/ml) for 45 min at 37°C. The virus-inhibitor mixtures were then used to inoculate JC53 cells for 12 h at 37°C. Cells were rinsed twice with culture medium to remove residual virus inoculum and incubated a further 60 h at 37°C. Virus infectivity was then measured by assaying luciferase activity in cell lysates (Promega), according to the manufacturer's protocol. Negative controls included mock-infected cells that were incubated with culture medium instead of virus. After subtracting background luciferase activity, the amount of luciferase activity in the presence of antibody or inhibitor was expressed as a percentage of the amount produced in control cultures containing no antibody or inhibitor. The percent inhibition was calculated by subtracting this number from 100. Data were fitted with a nonlinear function, and IC_{50} values were calculated by least squares regression analysis of inhibition curves, as described previously [11, 48, 72, 86].

gp120 structural modeling

3D protein structures of BR- and LN-derived gp120 sequences were prepared using the Discovery Studio suite, version 3.0 (Accelrys, San Diego, CA, USA), as we have described previously [65, 66, 75, 87]. The crystal structure of YU2 gp120 bound to CD4, and mAb 17b [88] was used as a template to generate homology models of Macs2-LN-2 and Macs2-BR-2 gp120 sequences. The interface between gp120 and CD4 or 17b was mapped to atoms predicted to be within 4 Å of the ligand. PNGS were identified by the amino acid sequon "NXS or T", where X does not equal a proline residue. The crystal structure of CD4-bound YU2 gp120 containing the V3-variable loop and docked with the NMR structure of an N-terminal peptide of CCR5 (residues 2–15; kindly provided by Peter D. Kwong [89]) was used as a template to generate homology models of BR-derived (Macs2-BR-2, UK1-BR-10) and LN-derived (Macs2-LN-2) gp120 sequences. Harmonic restraints were applied prior to optimization using the steepest descent protocol, which incorporates iterative cycles of conjugate-gradient energy minimization against a probability density function that includes spatial restraints derived from the template and residue-specific properties [90].

In silico glycosylation was performed using the GlyProt web-based server (http://www.glycosciences.de/modeling/glyprot/php/main.php) [91]. Homology models of Macs2-LN-2 and Macs2-BR-2 gp120 proteins generated using the 17b-bound gp120 crystal structure template were submitted for analysis. Briefly, potential glycosylation sites were identified in the amino acid sequence of the 3D structures, and spatially accessible sites were identified. The core regions of basic glycoforms were then added to the predicted glycosylation sites in orientations using the preferred values for the χ_1, χ_2, Φn, and Ψn dihedral angles observed in 3000 experimentally determined 3D structures of N-glycan chains from glycoproteins.

RESULTS

Highly M-tropic Env variants derived from the CNS

In this study, we characterized the HIV-1 entry mechanisms of CCR5-using (R5) Env variants derived from BR and LN. These Envs and the HIV-1 isolates and subjects from whom they were

derived have been described in detail previously [10, 11, 25, 26]. We first determined the ability of the Envs to enter MDMs when pseudotyped onto luciferase HIV-1 reporter viruses (**Fig. 1**). As controls, we used luciferase reporter viruses pseudotyped with JR-CSF or YU2 Envs, which have poorly M-tropic and highly M-tropic phenotypes, respectively [66], and virus pseudotyped with the nonfunctional ΔKS Env [76] to determine background levels of luciferase activity. Our results show that all of the BR-derived Envs tested are highly M-tropic, exhibiting entry levels in MDM similar to those achieved by YU2, and that all of the LN-derived Envs tested are poorly M-tropic with entry levels in MDM lower than that achieved by JR-CSF (Fig. 1A). In contrast, the BR- and LN-derived Envs showed similar levels of HIV-1 entry into PBMC (Fig. 1B) and the JC53 cell line that expresses high levels of CD4 and CCR5 (Fig. 1C).

Highly M-tropic Envs can efficiently scavenge low levels of cell-surface CD4

To better understand the virus–cell interactions underlying efficient MDM entry, we next used the 293-Affinofile affinity-profiling system [69] to quantify the CD4- and CCR5-usage efficiencies of the BR- and LN-derived Envs. In this system, CD4 and CCR5 expression is controlled by separate inducible promoters, permitting independent variation of CD4 and CCR5 expression over a physiological concentration range [69]. When 48 differentially induced cell populations are subjected to single-round entry assays with Env-pseudotyped luciferase reporter viruses, and data sets are analyzed quantitatively by mathematical modeling using the VERSA computational platform [69], three vector metrics are generated that capture the essential phenotypic characteristics of the Env. This is graphically illustrated in Supplemental Fig. 1. The vector angles measure the degree of CD4 and CCR5 dependence, and the vector magnitude measures the efficiency of virus entry characterized by the overall responsiveness to changes in CD4 and CCR5 levels; in other words, it measures the overall steepness or gradient of the surface plot. Lastly, the vector mean induction measures the efficiency of virus entry characterized by the level of infection averaged across the entire matrix of distinct CD4 and CCR5 expression levels.

These quantitative metrics can be used to dissect simultaneously occurring gp120-CD4/CCR5 interactions. For example, a concordant increase in vector angle and mean induction signifies that the increased infection response to CCR5 levels is a result of a comparative increase in the efficiency of CCR5 usage, whereas a "discordant" increase in vector angle accompanied by a decrease in the mean induction indicates that the increase in CCR5 dependence is a result of a decrease in CCR5 usage efficiency, as would occur when an Env exhibits efficient infection only at higher levels of CCR5 [69]. Thus, the combined analysis of vector angle with the vector magnitude or mean induction permits the VERSA metrics to determine how efficiently a particular Env can interact with CD4 and CCR5. The following analysis of our BR- and LN-derived Envs will exemplify the physiological meaning of these vector metrics.

Figure 2A shows the inducible levels of CD4 and CCR5 expression achieved by minocycline or ponA, respectively. The

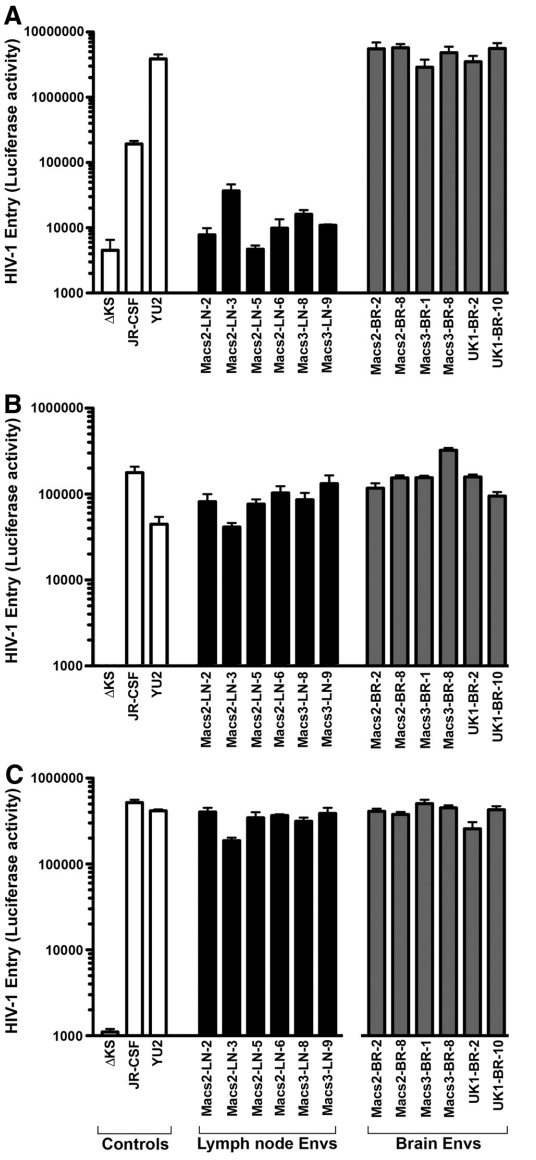

Figure 1. BR-derived Envs are highly M-tropic. Luciferase reporter viruses pseudotyped with BR- or LN-derived Envs were produced and titrated as described in Materials and Methods, and equivalent infectious units were used to infect cultures of MDM (A), PBMC (B), or JC53 cells (C). Controls included luciferase reporter viruses pseudotyped with JR-CSF or YU2 Envs or with the nonfunctional ΔKS Env [76]. The results shown are means of triplicate wells and are representative of four independent experiments. For experiments in MDM and PBMC, the independent experiments were conducted in cells obtained from different donors. Error bars represent SD.

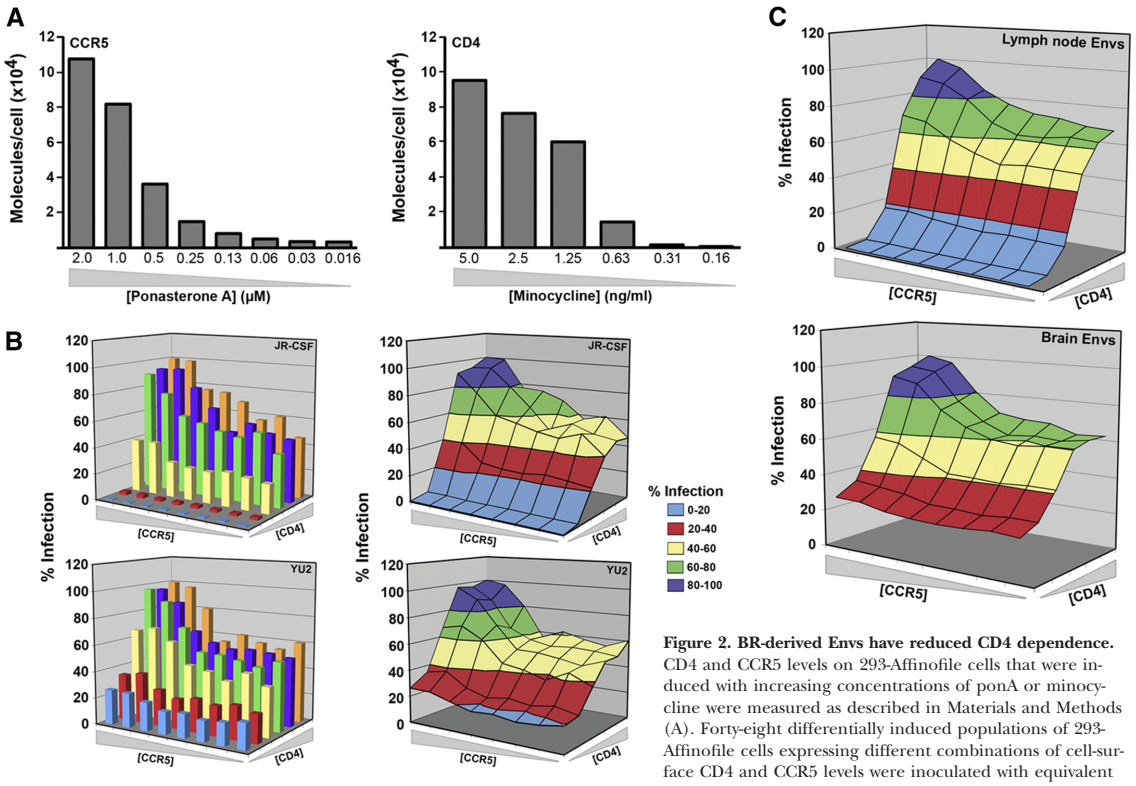

Figure 2. BR-derived Envs have reduced CD4 dependence. CD4 and CCR5 levels on 293-Affinofile cells that were induced with increasing concentrations of ponA or minocycline were measured as described in Materials and Methods (A). Forty-eight differentially induced populations of 293-Affinofile cells expressing different combinations of cell-surface CD4 and CCR5 levels were inoculated with equivalent infectious units of luciferase reporter virus pseudotyped with JR-CSF or YU2 Envs (B) or with each of the BR- and LN-derived Envs. The data are expressed as a percentage of the entry levels attained in cells expressing the highest levels of CD4 and CCR5. The individual 293-Affinofile plots are shown in Supplemental Figs. 2 and 3, and a compilation of those data is presented (C). The data presented are means of duplicates and are representative of three independent experiments.

293-Affinofile profiles of control JR-CSF and YU2 Envs show that the highly M-tropic YU2 Env can enter cells expressing scant levels of CD4, where it achieves 20–25% of maximal entry when low or high levels of CCR5 are present, whereas the poorly M-tropic JR-CSF Env is dependent on much higher levels of CD4 to enter cells (Fig. 2B). The individual 293-Affinofile plots of the BR- and LN-derived Envs are shown in Supplemental Fig. 2, and the corresponding surface plots are shown in Supplemental Fig. 3. These data are compiled together in Fig. 2C. Together, these results show that all of the BR-derived Envs efficiently use very low levels of CD4 to enter cells, similar to YU2, whereas all the LN-derived Envs are dependent on higher levels of CD4 to enter cells, similar to JR-CSF. The entry of the BR-derived Envs and YU2 Env into 293-Affinofile cells could be inhibited completely by the CCR5 antagonist MVC (Supplemental Fig. 4), confirming the specificity of the entry levels by these Envs at low CD4 concentrations.

These results are reflected quantitatively by the VERSA metrics (**Fig. 3**). For example, the BR-derived Envs had significantly higher vector angles and lower vector magnitudes compared with the LN-derived Envs ($P<0.001$; Fig. 3A and B). These data indicate that the BR-derived Envs are less dependent on CD4 (angle; ~24° vs. ~10° for BR- and LN-derived Envs, respectively), and as a consequence of their higher baseline infection at low CD4 levels (see Fig. 2C), their overall responsiveness to increasing CD4/CCR5 levels is also comparatively muted (magnitude; ~55 vs. ~80 for BR- and LN-derived Envs, respectively). The BR-derived Envs also had significantly higher vector mean inductions than the LN-derived Envs ($P<0.001$; Fig. 3C), also principally a result of their increased ability to enter 293-Affinofile cells expressing lower levels of CD4 (see Fig. 2C). Interestingly, when the alternative VERSA metrics were plotted on a 3D axis, the primary Envs studied formed two distinct tissue-specific clusters (Supplemental Fig. 5). For these particular Envs, this occurred in the absence of intersubject genetic compartmentalization [26], suggesting that VERSA metrics could be applied in future studies to reveal novel Env phenotypic signatures. The altered responsiveness to increasing CD4 levels by the BR- and LN-derived Envs in the presence of low or high levels of CCR5 is illustrated further when the 293-Affinofile data are analyzed with five-parameter logistics (Fig. 3D and E). In this case, it is apparent that

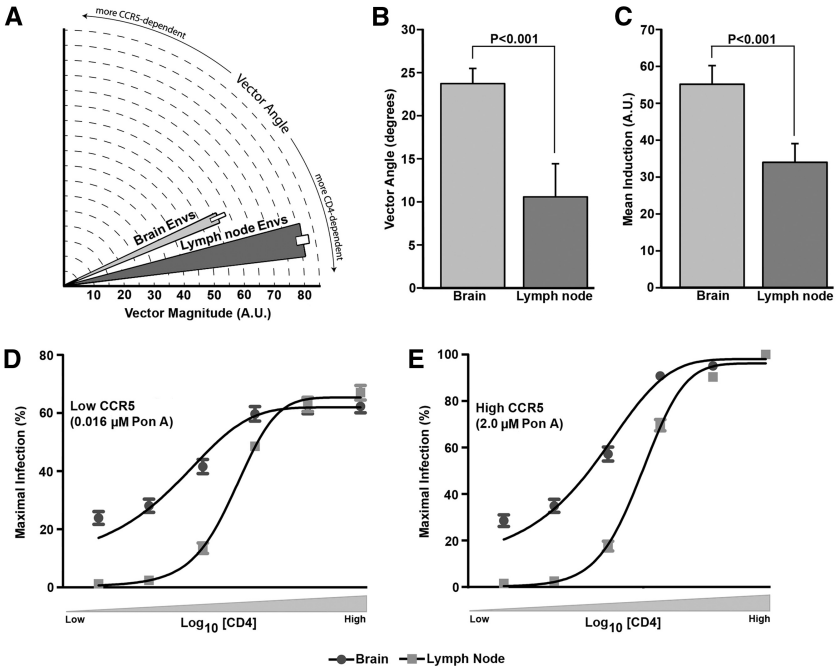

Figure 3. VERSA metrics distinguish BR- and LN-derived Envs. The VERSA metrics were calculated from the 293-Affinofile data as described in Materials and Methods. A graphical representation of the VERSA metrics comparing vector angles and vector magnitudes is shown in A. The shaded wedges represent the SEM of the vector angles, and the boxes represent the SEM of the vector magnitudes. Statistical analysis was conducted using an unpaired *t*-test to compare the differences in vector angle (B) and vector mean induction (C) between the BR- and LN-derived Envs. P values < 0.05 were considered statistically significant. The response of the BR- and LN-derived Envs to increasing CD4 levels when CCR5 levels were low (D) or high (E) was determined by five-parameter logistical analysis of the 293-Affinofile data, using Prism, version 5.0 (GraphPad Software, San Diego, CA, USA).

the increased vector magnitude is a reflection of the steeper slopes exhibited by the LN-derived Envs. Together, the 293-Affinofile data and quantitative VERSA metrics confirm that highly M-tropic Envs have the ability to scavenge low levels of CD4 on the cell surface to mediate HIV-1 entry, whereas non-M-tropic Envs do not.

Highly M-tropic Envs have greater exposure of the CD4bs

To further understand the Env determinants contributing to highly efficient MDM entry, we next conducted virus inhibition studies in JC53 cells with sCD4 and the Env mAb b12 [92–94] whose epitope in gp120 overlaps the CD4bs.

The individual inhibition curves of Env-pseudotyped luciferase reporter viruses by sCD4 are shown in **Fig. 4A** and **B**, and the IC_{50} for the BR- and LN-derived Envs are plotted in Fig. 4C. These results show that the BR-derived Envs are significantly more sensitive to inhibition by sCD4 than the LN-derived Envs. The results also show that the BR-derived Envs exhibit a largely homogeneous response to inhibition by sCD4, whereas the LN-derived Envs show a high degree of heterogeneity in their sensitivity to inhibition by sCD4. We also observed a direct relationship between the sensitivity of virus inhibition by sCD4 and the ability of the Env to enter 293-Affinofile cells, expressing low levels of CD4 together with low (Fig. 4D), medium (Fig. 4E), or high levels of CCR5 (Fig. 4F).

The individual neutralization curves of Env-pseudotyped luciferase reporter viruses by b12 are shown in Supplemental Fig. 6A and B, and the IC_{50} values are shown in Supplemental Fig. 6C. Interestingly, the BR- and LN-derived Envs from subject Macs3 were resistant to neutralization by b12 (Supplemental Fig. 6A–C), which is consistent with the results of previous studies of other Envs cloned from this subject [61]. When these Envs were excluded from analysis, the remaining BR-derived Envs showed significantly greater sensitivity to neutralization by b12 compared with the remaining LN-derived Envs (Supplemental Fig. 6D). Together, the results of the sCD4 and b12 inhibition studies suggest that the ability of highly M-tropic Envs to scavenge low levels of cell-surface CD4 is principally due to the Envs existing in a conformation that has increased exposure of the CD4bs in gp120.

Evidence that highly M-tropic Envs have altered presentation of the CD4-induced CCR5-binding domain in gp120

The preceding studies illustrate the use of the 293-Affinofile affinity-profiling system and VERSA metrics for demonstrating enhanced Env-CD4 interactions by highly M-tropic Envs derived from brain, thus unifying the results of recent studies [15, 49, 50, 55–58, 60–64] in a highly quantitative fashion. However, our recent studies also show that certain blood-derived M-tropic Envs have increased exposure of CD4-induced epitopes in gp120 that is associated with an altered interaction with CCR5 [65, 66] and may not be immediately evident from the 293-Affinofile data. We therefore next compared the ability of the BR- and LN-derived Envs to bind to the 17b mAb, whose epitope overlaps the CD4-induced CCR5-binding site in gp120. After incubation with sCD4, collectively, the BR-derived Envs showed significantly greater

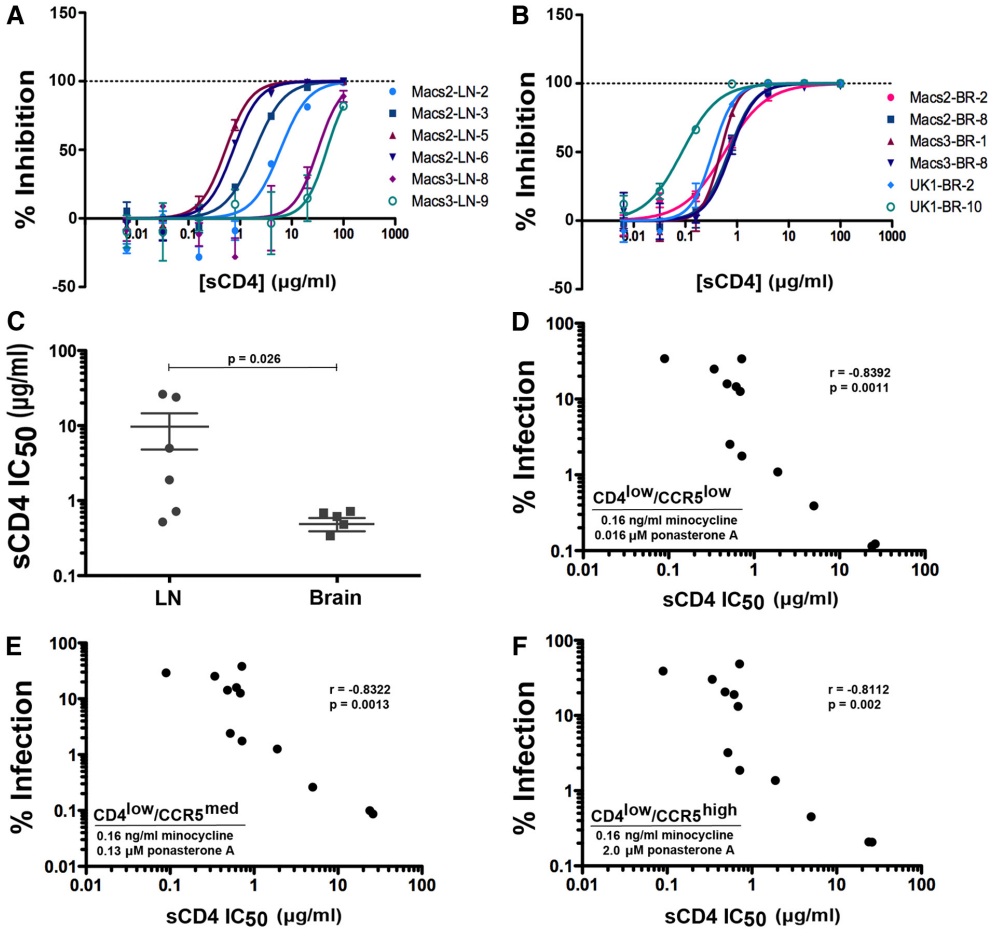

Figure 4. BR-derived Envs have greater sensitivity to inhibition by sCD4. Virus inhibition assays were conducted in JC53 cells, as described in Materials and Methods (A and B), and the sCD4 IC_{50} values for viruses pseudotyped with BR- or LN-derived Envs were calculated from the virus inhibition curves using Prism, version 5.0 (GraphPad Software; C). Statistical comparisons were made with a nonparametric Mann-Whitney *U*-test. The ability of the Envs to enter 293-Affinofiles expressing low levels of CD4 and low (D), medium (E), or high (F) levels of CCR5 was plotted against the sCD4 IC_{50} values using Prism, version 5.0 (GraphPad Software). The data shown are means of triplicates and are representative of two independent experiments. The Spearman correlation coefficients (r) and *P* values are shown. *P* values < 0.05 were considered statistically significant.

binding to 17b compared with the LN-derived Envs (**Fig. 5A**), although at the individual level, it is clear that two of the BR-derived Envs (Macs3-BR-1 and -8) have 17b-binding profiles that are similar to those of the LN-derived Envs. In the absence of sCD4, there was equivalent, low-level binding to 17b by the BR- and LN-derived Envs (data not shown). Similar levels of gp120 were expressed on the surface of the cells used in the binding assays, as shown by equivalent levels of staining with polyclonal HIV+ sera (Fig. 5B). These data indicate that the highly M-tropic BR-derived Envs from subjects Macs2 and UK1, but not those from Macs3, have increased exposure of the CD4-induced 17b epitope.

To investigate the potential mechanisms by which these BR-derived Envs have greater presentation of the 17b epitope, we first compared the gp120 sequences of representative BR (Macs2-BR-2 and UK1-BR-10)- and LN (Macs2-LN-2)-derived Envs that had differences in 17b-binding profiles. Sequence analysis identified a conserved shift in the pattern of PNGS within the gp120 V4-loop region that segregated the BR- from LN-derived Envs (Fig. 5C). The Macs2-LN Env clones have a PNGS at Asn386, whereas the Macs2-BR and UK1-BR Env clones have Asp at this position, eliminating the PNGS, but contain a small insertion of 3–4 aa in V4 that reintroduces the PNGS at Asn397. To determine whether this shift in N-linked

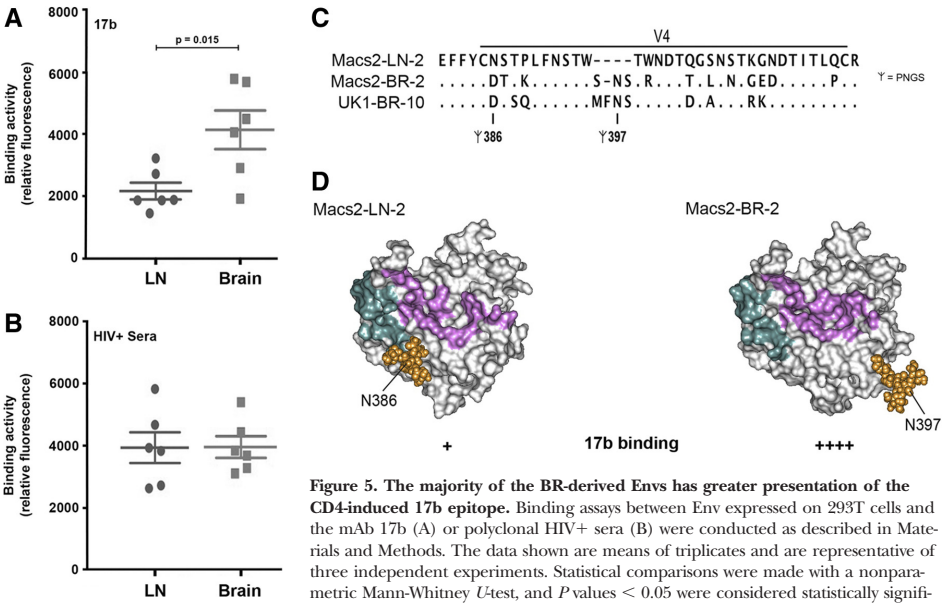

Figure 5. The majority of the BR-derived Envs has greater presentation of the CD4-induced 17b epitope. Binding assays between Env expressed on 293T cells and the mAb 17b (A) or polyclonal HIV+ sera (B) were conducted as described in Materials and Methods. The data shown are means of triplicates and are representative of three independent experiments. Statistical comparisons were made with a nonparametric Mann-Whitney *U*-test, and *P* values < 0.05 were considered statistically significant. The gp120 V4 amino acid sequence of Macs2-LN-2, Macs2-BR-2, and UK1-BR-10 Envs and location of PNGS are shown in C. Homology models of Macs2-LN-2 and Macs2-BR-2 gp120 proteins were generated using the 17b-bound gp120 crystal structure template, as described in Materials and Methods (D). The molecular surface of gp120 is shown in gray, and the CD4bs and the 17b epitope are shown in pink and aqua, respectively. The N-glycan core of PNGS at positions N386 (Macs2-LN-2) and N397 (Macs2-BR-2) is shown as orange space-filling sphere representations.

glycosylation may potentially influence 17b binding, we next produced 3D homology models of Macs2-LN-2 and Macs2-BR-2 gp120 proteins in their 17b-bound conformations using the 17b-bound gp120 crystal structure as template [88] and modeled the glycosylation at positions Asn386 or Asn397 (Fig. 5D). For Macs2-LN-2, the glycan is located proximal to the 17b epitope and therefore, has the potential to obscure part of the CCR5-binding domain. In contrast, for Macs2-BR-2, repositioning the glycan to aa 397 places it distal to the 17b epitope, thus facilitating greater exposure of the CCR5-binding domain. Supplemental Fig. 7 shows that glycosylation at Asn386 can also potentially occlude the 17b-binding site on gp120 and modulate 17b binding in the context of other glycosylated residues. Similar results were obtained from models of 17b-bound gp120 of UK1-BR-10 (data not shown). Although further mutagenesis studies are required to determine the role of V4-loop glycan alterations in exposing or occluding the 17b epitope, these analyses provide evidence that the majority of the highly M-tropic Envs exists in a conformation that has greater presentation of CD4-induced epitopes, which may alter the interaction between CD4-bound gp120 and CCR5.

Highly M-tropic Envs derived from brain display an altered mechanism of engagement with CCR5

To determine whether the BR-derived Envs have an altered interaction with CCR5, we next elucidated the mechanism of gp120-CCR5 engagement by the BR- and LN-derived Envs. Single-round entry assays were conducted in NP2-CD4 cells expressing WT CCR5 or CCR5 containing various mutations in the N-terminal domain or ECL regions, using luciferase reporter viruses pseudotyped with each of the BR- and LN-derived Envs (**Fig. 6**). The levels of virus entry in cells expressing CCR5 mutants were expressed as percentages of that attained in cells expressing equivalent levels of WT CCR5, which was verified by flow cytometry. The results show that the BR-derived Envs have significantly increased dependence on Tyr10, Asp11, Tyr14, Tyr15, Gly18, and Lys22 within the CCR5 N-terminus compared with the LN-derived Envs. In particular, most of the BR-derived Envs are critically dependent on the sulfated Tyr10, Tyr14, and Tyr15 residues in the CCR5 N-terminus, whereas most of the LN-derived Envs are not. The results also show that the BR-derived Envs have increased dependence on His88 and His181 in the CCR5 ECL1 and ECL2 regions, respectively. No differences in dependence on Val5 in the CCR5 N-terminus, Tyr89 in the CCR5 ECL1 region, or Tyr184 and Gln188 in the CCR5 ECL2 region were observed between the BR- and LN-derived Envs (data not shown). Together, these results illustrate an increased reliance of the BR-derived Envs on the CCR5 N-terminus and novel interactions with charged elements of the CCR5 ECL1 and ECL2 regions.

Potential structural basis for the altered engagement between BR-derived Envs and the CCR5 N-terminus

Sequence analysis identified 7 aa polymorphisms in gp120, located within or immediately adjacent to coreceptor-binding

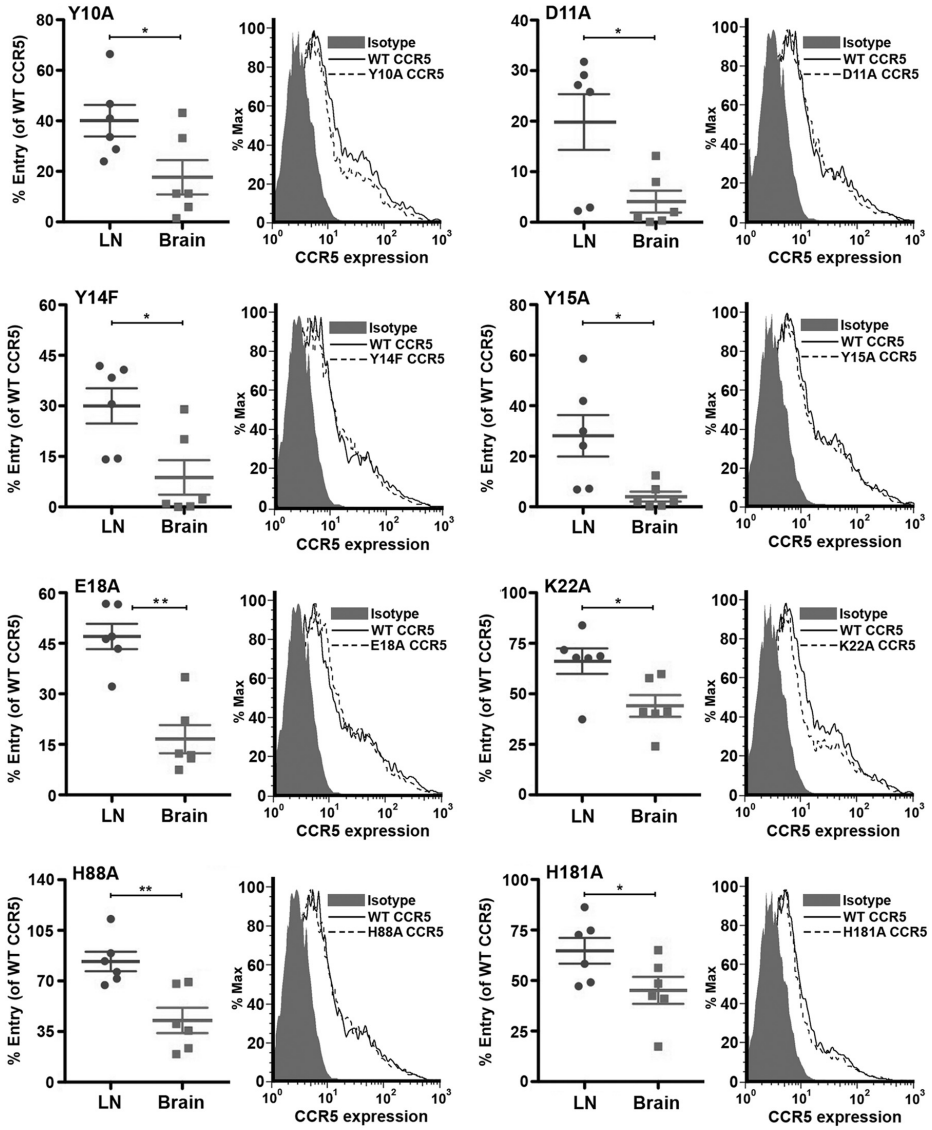

Figure 6. BR-derived Envs have reduced dependence on the CCR5 N-terminus and on charged elements of CCR5. Luciferase reporter viruses were used to infect NP2-CD4 cells expressing equivalent levels of WT CCR5 or CCR5 with alternative mutations in the CCR5 N-terminus (Y10A, D11A, Y14F, Y15A, E18A, K22A), ECL1 (H88A), or ECL2 regions (H181A), as described in Materials and Methods. Entry levels were expressed as a percentage of those attained in cells expressing WT CCR5. The results shown are means of triplicates and are representative of three independent experiments. Statistical comparisons were made with a nonparametric Mann-Whitney *U*-test. $*P < 0.05$; $**P < 0.01$. *P* values < 0.05 were considered statistically significant.

sites that segregated Macs2-LN from Macs2-BR and UK1-BR Envs. These polymorphisms include Arg/Gln328 and Gly/Arg335 within or near the gp120 V3-loop; Asn/Asp386 within the gp120 V4-loop; and Arg/Lys121, Arg/Lys432, Leu/Gln442, and Val/Ile443 within or near the gp120 bridging sheet (**Fig. 7A**). To identify the potential molecular interactions associated with the increased reliance of the BR-derived Envs on the CCR5 N-terminus and the potential influence of these amino acid polymor-

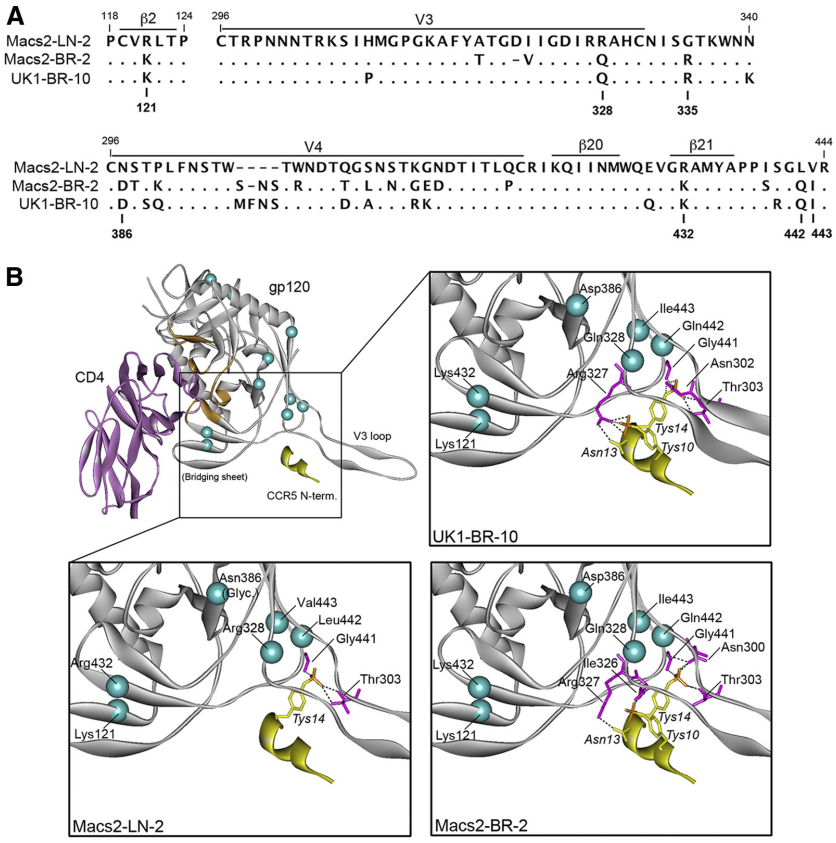

Figure 7. BR-derived Envs have structural alterations at the gp120-CCR5 N-terminus interface. Amino acid polymorphisms associated with BR-derived Envs were identified within or near CCR5-binding sites in gp120, as indicated in the multiple sequence alignment (A). The locations of common alterations occurring in Macs2-BR-2 and UK1-BR-10 Envs are highlighted. 3D homology models of gp120 of UK1-BR-10, Macs2-BR-2, and Macs2-LN-2 Envs, in their CD4-bound conformation and docked to a $CCR5_{2–15}$ N-terminal peptide, were produced as described in Materials and Methods (B). The α-carbon atoms of amino acids, occurring at positions 121, 328, 335, 386, 432, 442, and 443, are shown as blue space-filled models. gp120 is shown as gray ribbon, CD4 as purple ribbon, and the CCR5 N-terminal peptide (aa 7–15) as yellow ribbon. The CD4bs, as defined by gp120 amino acids within 4 Å of the CD4 molecule [66, 87], is colored orange. In the enlarged boxes, the amino acids in gp120 making hydrogen-bond contacts with the CCR5 N-terminus peptide are shown as magenta stick models. The CCR5 N-terminus hydrogen-bond partners are shown as yellow stick models, with sulfate groups on Tyr10 and Tyr14 (Tys10 and Tys14, respectively) colored orange. Hydrogen bonds are shown as black dotted lines. Residues are numbered according to the HXB2 gp120 sequence.

phisms on such interactions, we next produced full-length 3D homology models of UK1-BR-10, Macs2-BR-2, and Macs2-LN-2 gp120 proteins based on the crystal structure of CD4-bound YU2 gp120 [89]. This structure is particularly useful, as it is docked to a sulfated CCR5 N-terminal peptide ($CCR5_{2–15}$) and thus, permits the investigation of the molecular interactions at the gp120-CCR5 N-terminus interface. Analysis of the potential atomic contacts at the gp120-CCR5 N-terminus interface shows that Gly441 and Thr303 of all three gp120 structures are predicted to interact directly with sulfated Tyr14 of the CCR5 N-terminus (Fig. 7B). However, Macs2-BR-2 and UK1-BR-10 gp120 structures can potentially form several additional contacts with the CCR5 N-terminus. Specifically, Macs2-BR-2 has additional predicted atomic contacts between Ile326 and sulfated Tyr10, Arg327, and Asn13 and Asn300 and sulfated Tys14 of gp120 and the CCR5 N-terminus, respectively. UK1-BR-10 has additional predicted atomic contacts between Arg327 and sulfated Tyr10, Arg327, and Asn13 and Asn302 and sulfated Tyr14 of gp120 and the CCR5 N-terminus, respectively. These results suggest that the BR-derived Envs may rely on more atomic contacts with the CCR5 N-terminus than the LN-derived Envs to enter cells. Further mutagenesis studies are required to determine precisely whether this is the case. However, our modeling studies provide a potential structural basis for why the entry of BR-derived Envs into cells is more readily abrogated by CCR5 N-terminus mutations.

DISCUSSION

Although it is well-established that M-tropic HIV-1 variants are more likely to persist in the CNS than in peripheral tissues and that several studies have illustrated an enhanced interaction between gp120 of M-tropic viruses and CD4 (reviewed in ref. [54]), we still do not have a firm understanding of the broader virus–cell interactions that contribute to M-tropism of BR-derived HIV-1 variants. Here, we took advantage of the 293-Affinofile affinity-profiling system [69] to model, in a quantitative fashion, the tandem interactions between BR-derived Envs and both CD4 and CCR5, which are associated with efficient macrophage entry. In addition to demonstrating a dramatically reduced dependence of BR-derived Envs on CD4 levels, our results identify an alteration in the way BR-derived Envs interact with CCR5. In the majority of

cases, this alteration was characterized by increased exposure of the CD4-induced CCR5-binding domain in gp120, which was associated with repositioning of the glycan shield within the V4 region, and by increased dependence on the CCR5 N-terminus and on charged elements within the CCR5 ECLs, which was associated with the predicted formation of additional atomic contacts at the gp120-CCR5 N-terminus interface. When viewed in context with the 293-Affinofile profiles and VERSA metrics, these results suggest that the highly M-tropic BR-derived Envs have an altered but not necessarily more efficient interaction with CCR5 that occurs in tandem with an enhanced interaction with CD4.

In addition to providing a more detailed understanding of how M-tropic Envs interact with cellular receptors, our results further illustrate the distinction between coreceptor use of HIV-1 and cellular tropism. An important conclusion that we draw is that CCR5 use of HIV-1 per se is insufficient to confer M-tropism. This interpretation is consistent with our original classification made more than 10 years ago—that a significant proportion of CCR5-using HIV-1 strains can be termed non-M-tropic R5 viruses based on their ability to enter and replicate in PBMC but not in MDM and primary cultures of human fetal microglia [10]. In fact, there is now evidence to suggest that most of the circulating R5 HIV-1 strains and those residing in lymphoid tissues are T cell-tropic rather than M-tropic [10, 15, 49–51, 55]. In addition, a subset of highly M-tropic HIV-1 strains has been shown to enter macrophages efficiently via CXCR4 [10, 25, 65]. These results underscore that the determinants of M-tropism by HIV-1 strains are significantly more complex than the coreceptor specificity of their Env glycoproteins (reviewed in ref. [40]).

Whereas there is convincing evidence that reduced CD4 dependence permits the ability of BR-derived Envs to scavenge low levels of CD4 expressed on the surface of macrophages and microglia [15, 49, 50, 55–58, 60–64], it is presently unclear how an altered interaction between gp120 and the CCR5 N-terminus may also contribute to the entry of BR-derived Envs into these cells. It is possible that BR-derived Envs have undergone adaptations to reflect the differences in CCR5 conformation [28, 95] and/or post-translational modifications, such as sulfation [32] or O-linked glycosylation [32, 96, 97], which exist among macrophages, resting T cells, and activated T cells.

The pattern of increased reliance on the CCR5 N-terminus and on charged elements within the CCR5 ECLs exhibited by the BR-derived Envs is remarkably similar to the pattern of altered CCR5 engagement that we and others have shown to be the major mechanism by which HIV-1 can develop allosteric resistance to CCR5 antagonists, including MVC [75, 78, 98–101]. This raised the possibility that the BR-derived Envs may exhibit baseline resistance to MVC. However, we showed that all of the BR- and LN-derived Envs are completely inhibited by MVC (Supplemental Fig. 8). As resistance to CCR5 antagonists is characterized by plateaus of virus inhibition below 100% rather than by shifts in IC_{50} values [102], none of the Envs tested exhibited resistance to MVC. In fact, the majority of the BR-derived Envs could be inhibited completely by ~20-fold lower concentrations of MVC than the majority of the LN-derived Envs (Supplemental Fig. 8). From these results, we can conclude that the BR-derived Envs remain highly sensitive to inhibition by MVC, despite having a mechanism of CCR5 engagement that could be considered predictive of CCR5 antagonist resistance. These findings underscore the strain-dependent nature of Env phenotypes and suggest that CCR5 antagonists could effectively treat CNS infection, should they be developed with suitable pharmacological properties that allow sufficient CNS penetrance and bioavailability.

The increased dependence of the highly M-tropic BR-derived Envs on the CCR5 N-terminus was an intriguing, unexpected result. We recently characterized the association between the efficiency of macrophage entry by certain blood-derived Envs and the ability of the Envs to tolerate mutations in the CCR5 N-terminus and showed that efficient CCR5-mediated macrophage entry was associated with reduced, rather than increased, dependence on elements within the CCR5 N-terminus, which included Asp11, Tyr14, Tyr15, and Glu18 [65, 66]. In these studies, we also saw correlations between the efficiency of macrophage entry and the ability of the Env to enter 293-Affinofile cells expressing low levels of CCR5 and also with the MVC IC_{50}, suggesting that unlike the BR-derived Envs, the M-tropic blood-derived Envs studied had a more efficient interaction with CCR5. Thus, there appears to be dichotomous mechanisms of altered Env-CCR5 engagement by M-tropic Envs, depending on whether they were derived from brain or from blood—the former involving increased dependence on the CCR5 N-terminus that does not increase the efficiency of the Env-CCR5 interaction and the latter involving reduced dependence on the CCR5 N-terminus that increases the efficiency of the Env-CCR5 interaction. Thus, the R5 M-tropic phenotype or "color", as termed recently by Swanstrom and colleagues [53], may indeed be comprised of at least two distinct M-tropic subphenotypes.

Although all the BR-derived Envs studied had reduced CD4 dependence that was associated with increased sensitivity to inhibition by sCD4, two of the BR-derived Envs—Macs3-BR-1 and Macs3-BR-8—were resistant to neutralization by b12, as were the Envs derived from LNs of the same subject (see Supplemental Fig. 6). The determinants of b12 resistance by these Envs are unclear, but it is noteworthy that other Envs, which were amplified and cloned directly from tissues of this subject, were also shown to be resistant to b12 [61]. The BR-derived Envs from Macs3 also showed reduced exposure of the CD4-induced 17b epitope than the other BR-derived Envs, and they also had less pronounced dependence on the CCR5 N-terminus than the other BR-derived Envs. These results indicate that some highly M-tropic BR-derived Envs can efficiently engage CD4 through a mechanism that does not involve greater exposure of the b12 epitope. The results also suggest that a subset of BR-derived Envs may not necessarily exist in conformations that have greater presentation of the 17b epitope nor exhibit an altered interaction with CCR5. Further studies are required to determine how frequently this occurs among highly M-tropic BR-derived Envs.

In summary, the results of our study provide new mechanistic insights into the virus–cell interactions involved in macrophage tropism of HIV-1 variants derived from brain, using quantitative affinity-profiling techniques and mathematical modeling of biological data that account for the simultaneous alterations in the way the Env glycoproteins of M-tropic viruses interact with both CD4 and CCR5.

AUTHORSHIP

H.S., M.R., L.R.G., J.S., and A.E. performed experiments. N.W., K.C., S.L.W., P.A.R., B.L., M.J.C., and P.R.G. analyzed data. P.A.R., B.L., M.J.C., and P.R.G. designed experiments. P.R.G. and B.L. wrote the manuscript. All authors edited the manuscript.

ACKNOWLEDGMENTS

This study was supported, in part, by grants from the NHMRC to P.R.G., M.J.C., and S.L.W. (#603708 and #1006534) and by a grant from U.S. National Institutes of Health/NIAID to B.L. (R21 AI092218). H.S. is supported by a postgraduate research scholarship from the Iranian Ministry of Health and Medical Education. P.A.R. is the Sir Zelman Cowen Senior Research Fellow (Sir Zelman Cowen Fellowship Fund, Burnet Institute). P.R.G. is the recipient of an Australian NHMRC Level 2 Biomedical Career Development Award. L.R.G. is the recipient of an Australian NHMRC Early Career Research Fellowship. The authors gratefully acknowledge the contribution to this work of the Victorian Operational Infrastructure Support Program received by the Burnet Institute. We thank J. Sodroski for providing JR-CSF, YU2, ΔKS Env, pCMVΔP1ΔenvpA, and pHIV-1Luc plasmids. We thank D. Kabat for providing JC53 cells, H. Hoshino for permission to use NP2-CD4 cells, and D. Mosier and R. Nedellec for supplying the NP2-CD4 cells. We also thank J. Sodroski and R. Doms for providing CCR5 mutants, D. Gabuzda for providing primary HIV-1 isolates, and D. Burton for providing the b12 mAb. The following reagent was obtained through the U.S. National Institutes of Health AIDS Research and Reference Reagent Program, Division of AIDS, NIAID: HIV-1 gp120 mAb (17b) from Dr. James E. Robinson.

DISCLOSURES

The funders had no role in study design, data collection and analysis, decision to publish, or preparation of the manuscript.

REFERENCES

1. Gonzalez-Scarano, F., Martin-Garcia, J. (2005) The neuropathogenesis of AIDS. *Nat. Rev. Immunol.* **5,** 69–81.
2. Trono, D., Van Lint, C., Rouzioux, C., Verdin, E., Barre-Sinoussi, F., Chun, T. W., Chomont, N. (2010) HIV persistence and the prospect of long-term drug-free remissions for HIV-infected individuals. *Science* **329,** 174–180.
3. Dunfee, R., Thomas, E., Gorry, P. R., Wang, J., Ancuta, P., Gabuzda, D. (2006) Mechanisms of HIV-1 neurotropism. *Curr. HIV Res.* **4,** 267–278.
4. Gartner, S., Markovits, P., Markovitz, D. M., Betts, R. F., Popovic, M. (1986) Virus isolation from and identification of HTLV-III/LAV-producing cells in brain tissue from a patient with AIDS. *JAMA* **256,** 2365–2371.
5. Gartner, S., Markovits, P., Markovitz, D. M., Kaplan, M. H., Gallo, R. C., Popovic, M. (1986) The role of mononuclear phagocytes in HTLV-III/LAV infection. *Science* **233,** 215–219.
6. Letendre, S., Marquie-Beck, J., Capparelli, E., Best, B., Clifford, D., Collier, A. C., Gelman, B. B., McArthur, J. C., McCutchan, J. A., Morgello, S., Simpson, D., Grant, I., Ellis, R. J. (2008) Validation of the CNS penetration-effectiveness rank for quantifying antiretroviral penetration into the central nervous system. *Arch. Neurol.* **65,** 65–70.
7. Chang, J., Jozwiak, R., Wang, B., Ng, T., Ge, Y. C., Bolton, W., Dwyer, D. E., Randle, C., Osborn, R., Cunningham, A. L., Saksena, N. K. (1998) Unique HIV type 1 V3 region sequences derived from six different regions of brain: region-specific evolution within host-determined quasispecies. *AIDS Res. Hum. Retroviruses* **14,** 25–30.
8. Donaldson, Y. K., Bell, J. E., Holmes, E. C., Hughes, E. S., Brown, H. K., Simmonds, P. (1994) In vivo distribution and cytopathology of variants of human immunodeficiency virus type 1 showing restricted sequence variability in the V3 loop. *J. Virol.* **68,** 5991–6005.
9. Gartner, S., McDonald, R. A., Hunter, E. A., Bouwman, F., Liu, Y., Popovic, M. (1997) gp120 sequence variation in brain and in T-lymphocyte human immunodeficiency virus type 1 primary isolates. *J. Hum. Virol.* **1,** 3–18.
10. Gorry, P. R., Bristol, G., Zack, J. A., Ritola, K., Swanstrom, R., Birch, C. J., Bell, J. E., Bannert, N., Crawford, K., Wang, H., Schols, D., De Clercq, E., Kunstman, K., Wolinsky, S. M., Gabuzda, D. (2001) Macrophage tropism of human immunodeficiency virus type 1 isolates from brain and lymphoid tissues predicts neurotropism independent of coreceptor specificity. *J. Virol.* **75,** 10073–10089.
11. Gorry, P. R., Taylor, J., Holm, G. H., Mehle, A., Morgan, T., Cayabyab, M., Farzan, M., Wang, H., Bell, J. E., Kunstman, K., Moore, J. P., Wolinsky, S. M., Gabuzda, D. (2002) Increased CCR5 affinity and reduced CCR5/CD4 dependence of a neurovirulent primary human immunodeficiency virus type 1 isolate. *J. Virol.* **76,** 6277–6292.
12. Hughes, E. S., Bell, J. E., Simmonds, P. (1997) Investigation of the dynamics of the spread of human immunodeficiency virus to brain and other tissues by evolutionary analysis of sequences from the p17gag and env genes. *J. Virol.* **71,** 1272–1280.
13. Korber, B. T., Kunstman, K. J., Patterson, B. K., Furtado, M., McEvilly, M. M., Levy, R., Wolinsky, S. M. (1994) Genetic differences between blood- and brain-derived viral sequences from human immunodeficiency virus type 1-infected patients: evidence of conserved elements in the V3 region of the envelope protein of brain-derived sequences. *J. Virol.* **68,** 7467–7481.
14. Ritola, K., Robertson, K., Fiscus, S. A., Hall, C., Swanstrom, R. (2005) Increased human immunodeficiency virus type 1 (HIV-1) env compartmentalization in the presence of HIV-1-associated dementia. *J. Virol.* **79,** 10830–10834.
15. Schnell, G., Joseph, S., Spudich, S., Price, R. W., Swanstrom, R. (2011) HIV-1 replication in the central nervous system occurs in two distinct cell types. *PLoS Pathog.* **7,** e1002286.
16. Schnell, G., Price, R. W., Swanstrom, R., Spudich, S. (2010) Compartmentalization and clonal amplification of HIV-1 variants in the cerebrospinal fluid during primary infection. *J. Virol.* **84,** 2395–2407.
17. Schnell, G., Spudich, S., Harrington, P., Price, R. W., Swanstrom, R. (2009) Compartmentalized human immunodeficiency virus type 1 originates from long-lived cells in some subjects with HIV-1-associated dementia. *PLoS Pathog.* **5,** e1000395.
18. Shapshak, P., Segal, D. M., Crandall, K. A., Fujimura, R. K., Zhang, B. T., Xin, K. Q., Okuda, K., Petito, C. K., Eisdorfer, C., Goodkin, K. (1999) Independent evolution of HIV type 1 in different brain regions. *AIDS Res. Hum. Retroviruses* **15,** 811–820.
19. Van 't Wout, A. B., Blaak, H., Ran, L. J., Brouwer, M., Kuiken, C., Schuitemaker, H. (1998) Evolution of syncytium-inducing and non-syncytium-inducing biological virus clones in relation to replication kinetics during the course of human immunodeficiency virus type 1 infection. *J. Virol.* **72,** 5099–5107.
20. Wong, J. K., Ignacio, C. C., Torriani, F., Havlir, D., Fitch, N. J., Richman, D. D. (1997) In vivo compartmentalization of human immunodeficiency virus: evidence from the examination of pol sequences from autopsy tissues. *J. Virol.* **71,** 2059–2071.
21. Ohagen, A., Devitt, A., Kunstman, K. J., Gorry, P. R., Rose, P. P., Korber, B., Taylor, J., Levy, R., Murphy, R. L., Wolinsky, S. M., Gabuzda, D. (2003) Genetic and functional analysis of full-length human immunodeficiency virus type 1 env genes derived from brain and blood of patients with AIDS. *J. Virol.* **77,** 12336–12345.
22. Power, C., McArthur, J. C., Johnson, R. T., Griffin, D. E., Glass, J. D., Perryman, S., Chesebro, B. (1994) Demented and nondemented patients with AIDS differ in brain-derived human immunodeficiency virus type 1 envelope sequences. *J. Virol.* **68,** 4643–4649.
23. Power, C., McArthur, J. C., Nath, A., Wehrly, K., Mayne, M., Nishio, J., Langelier, T., Johnson, R. T., Chesebro, B. (1998) Neuronal death induced by brain-derived human immunodeficiency virus type 1 envelope genes differs between demented and nondemented AIDS patients. *J. Virol.* **72,** 9045–9053.
24. Wang, T. H., Donaldson, Y. K., Brettle, R. P., Bell, J. E., Simmonds, P. (2001) Identification of shared populations of human immunodeficiency virus type 1 infecting microglia and tissue macrophages outside the central nervous system. *J. Virol.* **75,** 11686–11699.
25. Gray, L., Roche, M., Churchill, M. J., Sterjovski, J., Ellett, A., Poumbourios, P., Sheffiel, S., Wang, B., Saksena, N., Purcell, D. F., Wesselingh, S., Cunningham, A. L., Brew, B. J., Gabuzda, D., Gorry, P. R. (2009) Tissue-specific sequence alterations in the human immunodeficiency virus type 1 envelope favoring CCR5 usage contribute to persistence of dual-tropic virus in the brain. *J. Virol.* **83,** 5430–5441.
26. Gray, L., Sterjovski, J., Ramsland, P. A., Churchill, M. J., Gorry, P. R. (2011) Conformational alterations in the CD4 binding cavity of HIV-1 gp120 influencing gp120-CD4 interactions and fusogenicity of HIV-1 envelopes derived from brain and other tissues. *Retrovirology* **8,** 42.

27. Dalgleish, A. G., Beverley, P. C., Clapham, P. R., Crawford, D. H., Greaves, M. F., Weiss, R. A. (1984) The CD4 (T4) antigen is an essential component of the receptor for the AIDS retrovirus. *Nature* **312,** 763–767.
28. Doms, R. W. (2000) Beyond receptor expression: the influence of receptor conformation, density, and affinity in HIV-1 infection. *Virology* **276,** 229–237.
29. Doms, R. W., Trono, D. (2000) The plasma membrane as a combat zone in the HIV battlefield. *Genes Dev.* **14,** 2677–2688.
30. Cormier, E. G., Dragic, T. (2002) The crown and stem of the V3 loop play distinct roles in human immunodeficiency virus type 1 envelope glycoprotein interactions with the CCR5 coreceptor. *J. Virol.* **76,** 8953–8957.
31. Huang, C. C., Tang, M., Zhang, M. Y., Majeed, S., Montabana, E., Stanfield, R. L., Dimitrov, D. S., Korber, B., Sodroski, J., Wilson, I. A., Wyatt, R., Kwong, P. D. (2005) Structure of a V3-containing HIV-1 gp120 core. *Science* **310,** 1025–1028.
32. Farzan, M., Mirzabekov, T., Kolchinsky, P., Wyatt, R., Cayabyab, M., Gerard, N. P., Gerard, C., Sodroski, J., Choe, H. (1999) Tyrosine sulfation of the amino terminus of CCR5 facilitates HIV-1 entry. *Cell* **96,** 667–676.
33. Brelot, A., Heveker, N., Adema, K., Hosie, M. J., Willett, B., Alizon, M. (1999) Effect of mutations in the second extracellular loop of CXCR4 on its utilization by human and feline immunodeficiency viruses. *J. Virol.* **73,** 2576–2586.
34. Hoffman, T. L., Doms, R. W. (1999) HIV-1 envelope determinants for cell tropism and chemokine receptor use. *Mol. Membr. Biol.* **16,** 57–65.
35. Cardozo, T., Kimura, T., Philpott, S., Weiser, B., Burger, H., Zolla-Pazner, S. (2007) Structural basis for coreceptor selectivity by the HIV type 1 V3 loop. *AIDS Res. Hum. Retroviruses* **23,** 415–426.
36. Doranz, B. J., Lu, Z. H., Rucker, J., Zhang, T. Y., Sharron, M., Cen, Y. H., Wang, Z. X., Guo, H. H., Du, J. G., Accavitti, M. A., Doms, R. W., Peiper, S. C. (1997) Two distinct CCR5 domains can mediate coreceptor usage by human immunodeficiency virus type 1. *J. Virol.* **71,** 6305–6314.
37. Doranz, B. J., Orsini, M. J., Turner, J. D., Hoffman, T. L., Berson, J. F., Hoxie, J. A., Peiper, S. C., Brass, L. F., Doms, R. W. (1999) Identification of CXCR4 domains that support coreceptor and chemokine receptor functions. *J. Virol.* **73,** 2752–2761.
38. Farzan, M., Choe, H., Vaca, L., Martin, K., Sun, Y., Desjardins, E., Ruffing, N., Wu, L., Wyatt, R., Gerard, N., Gerard, C., Sodroski, J. (1998) A tyrosine-rich region in the N terminus of CCR5 is important for human immunodeficiency virus type 1 entry and mediates an association between gp120 and CCR5. *J. Virol.* **72,** 1160–1164.
39. Gorry, P., Sterjovski, J., Churchill, M., Witlox, K., Gray, L., Cunningham, A., Wesselingh, S. (2004) The role of viral coreceptors and macrophage tropism in human immunodeficiency virus type 1 disease progression. *Sex Health* **1,** 23–35.
40. Gorry, P. R., Ancuta, P. (2011) Coreceptors and HIV-1 pathogenesis. *Curr. HIV/AIDS Reports* **8,** 45–53.
41. Alkhatib, G., Combadiere, C., Broder, C. C., Feng, Y., Kennedy, P. E., Murphy, P. M., Berger, E. A. (1996) CC CKR5: a RANTES, MIP-1α, MIP-1β receptor as a fusion cofactor for macrophage-tropic HIV-1. *Science* **272,** 1955–1958.
42. Choe, H., Farzan, M., Sun, Y., Sullivan, N., Rollins, B., Ponath, P. D., Wu, L., Mackay, C. R., LaRosa, G., Newman, W., Gerard, N., Gerard, C., Sodroski, J. (1996) The β-chemokine receptors CCR3 and CCR5 facilitate infection by primary HIV-1 isolates. *Cell* **85,** 1135–1148.
43. Dragic, T., Litwin, V., Allaway, G. P., Martin, S. R., Huang, Y., Nagashima, K. A., Cayanan, C., Maddon, P. J., Koup, R. A., Moore, J. P., Paxton, W. A. (1996) HIV-1 entry into CD4+ cells is mediated by the chemokine receptor CC-CKR-5. *Nature* **381,** 667–673.
44. Feng, Y., Broder, C. C., Kennedy, P. E., Berger, E. A. (1996) HIV-1 entry cofactor: functional cDNA cloning of a seven-transmembrane, G protein-coupled receptor. *Science* **272,** 872–877.
45. Collman, R., Balliet, J. W., Gregory, S. A., Friedman, H., Kolson, D. L., Nathanson, N., Srinivasan, A. (1992) An infectious molecular clone of an unusual macrophage-tropic and highly cytopathic strain of human immunodeficiency virus type 1. *J. Virol.* **66,** 7517–7521.
46. Yi, Y., Isaacs, S. N., Williams, D. A., Frank, I., Schols, D., De Clercq, E., Kolson, D. L., Collman, R. G. (1999) Role of CXCR4 in cell-cell fusion and infection of monocyte-derived macrophages by primary human immunodeficiency virus type 1 (HIV-1) strains: two distinct mechanisms of HIV-1 dual tropism. *J. Virol.* **73,** 7117–7125.
47. Li, S., Juarez, J., Alali, M., Dwyer, D., Collman, R., Cunningham, A., Naif, H. M. (1999) Persistent CCR5 utilization and enhanced macrophage tropism by primary blood human immunodeficiency virus type 1 isolates from advanced stages of disease and comparison to tissue-derived isolates. *J. Virol.* **73,** 9741–9755.
48. Gray, L., Sterjovski, J., Churchill, M., Ellery, P., Nasr, N., Lewin, S. R., Crowe, S. M., Wesselingh, S. L., Cunningham, A. L., Gorry, P. R. (2005) Uncoupling coreceptor usage of human immunodeficiency virus type 1 (HIV-1) from macrophage tropism reveals biological properties of CCR5-restricted HIV-1 isolates from patients with acquired immunodeficiency syndrome. *Virology* **337,** 384–398.
49. Peters, P. J., Bhattacharya, J., Hibbitts, S., Dittmar, M. T., Simmons, G., Bell, J., Simmonds, P., Clapham, P. R. (2004) Biological analysis of human immunodeficiency virus type 1 R5 envelopes amplified from brain and lymph node tissues of AIDS patients with neuropathology reveals two distinct tropism phenotypes and identifies envelopes in the brain that confer an enhanced tropism and fusigenicity for macrophages. *J. Virol.* **78,** 6915–6926.
50. Peters, P. J., Duenas-Decamp, M. J., Sullivan, W. M., Brown, R., Ankghuambom, C., Luzuriaga, K., Robinson, J., Burton, D. R., Bell, J., Simmonds, P., Ball, J., Clapham, P. R. (2008) Variation in HIV-1 R5 macrophage-tropism correlates with sensitivity to reagents that block envelope: CD4 interactions but not with sensitivity to other entry inhibitors. *Retrovirology* **5,** 5.
51. Peters, P. J., Sullivan, W. M., Duenas-Decamp, M. J., Bhattacharya, J., Ankghuambom, C., Brown, R., Luzuriaga, K., Bell, J., Simmonds, P., Ball, J., Clapham, P. R. (2006) Non-macrophage-tropic human immunodeficiency virus type 1 R5 envelopes predominate in blood, lymph nodes, and semen: implications for transmission and pathogenesis. *J. Virol.* **80,** 6324–6332.
52. Goodenow, M. M., Collman, R. G. (2006) HIV-1 coreceptor preference is distinct from target cell tropism: a dual-parameter nomenclature to define viral phenotypes. *J. Leukoc. Biol.* **80,** 965–972.
53. Arrildt, K. T., Joseph, S. B., Swanstrom, R. (2012) The HIV-1 env protein: a coat of many colors. *Curr. HIV/AIDS Reports* **9,** 52–63.
54. Peters, P. J., Duenas-Decamp, M. J., Sullivan, W. M., Clapham, P. R. (2007) Variation of macrophage tropism among HIV-1 R5 envelopes in brain and other tissues. *J. Neuroimmune Pharmacol.* **2,** 32–41.
55. Gonzalez-Perez, M. P., O'Connell, O. J., Lin, R., Sullivan, W. M., Bell, J., Simmonds, P., Clapham, P. R. (2012) Independent evolution of macrophage-tropism and increased charge between HIV-1 R5 envelopes present in brain and immune tissue. *Retrovirology* **9,** 20.
56. Dunfee, R. L., Thomas, E. R., Gorry, P. R., Wang, J., Taylor, J., Kunstman, K., Wolinsky, S. M., Gabuzda, D. (2006) The HIV Env variant N283 enhances macrophage tropism and is associated with brain infection and dementia. *Proc. Natl. Acad. Sci. USA* **103,** 15160–15165.
57. Dunfee, R. L., Thomas, E. R., Wang, J., Kunstman, K., Wolinsky, S. M., Gabuzda, D. (2007) Loss of the N-linked glycosylation site at position 386 in the HIV envelope V4 region enhances macrophage tropism and is associated with dementia. *Virology* **367,** 222–234.
58. Thomas, E. R., Dunfee, R. L., Stanton, J., Bogdan, D., Taylor, J., Kunstman, K., Bell, J. E., Wolinsky, S. M., Gabuzda, D. (2007) Macrophage entry mediated by HIV Envs from brain and lymphoid tissues is determined by the capacity to use low CD4 levels and overall efficiency of fusion. *Virology* **360,** 105–119.
59. Tuttle, D. L., Anders, C. B., Aquino-De Jesus, M. J., Poole, P. P., Lamers, S. L., Briggs, D. R., Pomeroy, S. M., Alexander, L., Peden, K. W., Andiman, W. A., Sleasman, J. W., Goodenow, M. M. (2002) Increased replication of non-syncytium-inducing HIV type 1 isolates in monocyte-derived macrophages is linked to advanced disease in infected children. *AIDS Res. Hum. Retroviruses* **18,** 353–362.
60. Duenas-Decamp, M. J., Peters, P. J., Burton, D., Clapham, P. R. (2009) Determinants flanking the CD4 binding loop modulate macrophage tropism of human immunodeficiency virus type 1 R5 envelopes. *J. Virol.* **83,** 2575–2583.
61. Dunfee, R. L., Thomas, E. R., Gabuzda, D. (2009) Enhanced macrophage tropism of HIV in brain and lymphoid tissues is associated with sensitivity to the broadly neutralizing CD4 binding site antibody b12. *Retrovirology* **6,** 69.
62. Martin, J., LaBranche, C. C., Gonzalez-Scarano, F. (2001) Differential CD4/CCR5 utilization, gp120 conformation, and neutralization sensitivity between envelopes from a microglia-adapted human immunodeficiency virus type 1 and its parental isolate. *J. Virol.* **75,** 3568–3580.
63. Martin-Garcia, J., Cao, W., Varela-Rohena, A., Plassmeyer, M. L., Gonzalez-Scarano, F. (2006) HIV-1 tropism for the central nervous system: brain-derived envelope glycoproteins with lower CD4 dependence and reduced sensitivity to a fusion inhibitor. *Virology* **346,** 169–179.
64. Musich, T., Peters, P. J., Duenas-Decamp, M. J., Gonzalez-Perez, M. P., Robinson, J., Zolla-Pazner, S., Ball, J. K., Luzuriaga, K., Clapham, P. R. (2011) A conserved determinant in the V1 loop of HIV-1 modulates the V3 loop to prime low CD4 use and macrophage infection. *J. Virol.* **85,** 2397–2405.
65. Cashin, K., Roche, M., Sterjovski, J., Ellett, A., Gray, L. R., Cunningham, A. L., Ramsland, P. A., Churchill, M. J., Gorry, P. R. (2011) Alternative coreceptor requirements for efficient CCR5- and CXCR4-mediated HIV-1 entry into macrophages. *J. Virol.* **85,** 10699–10709.
66. Sterjovski, J., Roche, M., Churchill, M. J., Ellett, A., Farrugia, W., Gray, L. R., Cowley, D., Poumbourios, P., Lee, B., Wesselingh, S., Cunningham, A. L., Ramsland, P. A., Gorry, P. R. (2010) An altered and more efficient mechanism of CCR5 engagement contributes to macrophage tropism of CCR5-using HIV-1 envelopes. *Virology* **404,** 269–278.
67. Platt, E. J., Wehrly, K., Kuhmann, S. E., Chesebro, B., Kabat, D. (1998) Effects of CCR5 and CD4 cell surface concentrations on infections by macrophagetropic isolates of human immunodeficiency virus type 1. *J. Virol.* **72,** 2855–2864.

68. Shimizu, N., Tanaka, A., Oue, A., Mori, T., Ohtsuki, T., Apichartpiyakul, C., Uchiumi, H., Nojima, Y., Hoshino, H. (2009) Broad usage spectrum of G protein-coupled receptors as coreceptors by primary isolates of HIV. *AIDS* **23,** 761–769.
69. Johnston, S. H., Lobriz, M. A., Nguyen, S., Lassen, K., Delair, S., Posta, F., Bryson, Y. J., Arts, E. J., Chou, T., Lee, B. (2009) A quantitative affinity-profiling system that reveals distinct CD4/CCR5 usage patterns among human immunodeficiency virus type 1 and simian immunodeficiency virus strains. *J. Virol.* **83,** 11016–11026.
70. Gao, F., Morrison, S. G., Robertson, D. L., Thornton, C. L., Craig, S., Karlsson, G., Sodroski, J., Morgado, M., Galvao-Castro, B., von Briesen, H., Beddows, S., Weber, J., Sharp, P. M., Shaw, G. M., Hahn, B. H. (1996) Molecular cloning and analysis of functional envelope genes from human immunodeficiency virus type 1 sequence subtypes A through G. The WHO and NIAID networks for HIV isolation and characterization. *J. Virol.* **70,** 1651–1667.
71. Gray, L., Churchill, M. J., Keane, N., Sterjovski, J., Ellett, A. M., Purcell, D. F., Poumbourios, P., Kol, C., Wang, B., Saksena, N. K., Wesselingh, S. L., Price, P., French, M., Gabuzda, D., Gorry, P. R. (2006) Genetic and functional analysis of R5X4 human immunodeficiency virus type 1 envelope glycoproteins derived from two individuals homozygous for the CCR5Δ32 allele. *J. Virol.* **80,** 3684–3691.
72. Sterjovski, J., Churchill, M. J., Ellett, A., Gray, L. R., Roche, M. J., Dunfee, R. L., Purcell, D. F., Saksena, N., Wang, B., Sonza, S., Wesselingh, S. L., Karlsson, I., Fenyo, E. M., Gabuzda, D., Cunningham, A. L., Gorry, P. R. (2007) Asn 362 in gp120 contributes to enhanced fusogenicity by CCR5-restricted HIV-1 envelope glycoprotein variants from patients with AIDS. *Retrovirology* **4,** 89.
73. Yang, X., Wyatt, R., Sodroski, J. (2001) Improved elicitation of neutralizing antibodies against primary human immunodeficiency viruses by soluble stabilized envelope glycoprotein trimers. *J. Virol.* **75,** 1165–1171.
74. Roche, M., Jakobsen, M. R., Ellett, A., Salimiseyedabad, H., Jubb, B., Westby, M., Lee, B., Lewin, S. R., Churchill, M. J., Gorry, P. R. (2011) HIV-1 predisposed to acquiring resistance to maraviroc (MVC) and other CCR5 antagonists in vitro has an inherent, low-level ability to utilize MVC-bound CCR5 for entry. *Retrovirology* **8,** 89.
75. Roche, M., Jakobsen, M. R., Sterjovski, J., Ellett, A., Posta, F., Lee, B., Jubb, B., Westby, M., Lewin, S. R., Ramsland, P. A., Churchill, M. J., Gorry, P. R. (2011) HIV-1 escape from the CCR5 antagonist maraviroc associated with an altered and less efficient mechanism of gp120-CCR5 engagement that attenuates macrophage-tropism. *J. Virol.* **85,** 4330–4342.
76. Etemad-Moghadam, B., Sun, Y., Nicholson, E. K., Fernandes, M., Liou, K., Gomila, R., Lee, J., Sodroski, J. (2000) Envelope glycoprotein determinants of increased fusogenicity in a pathogenic simian-human immunodeficiency virus (SHIV-KB9) passaged in vivo. *J. Virol.* **74,** 4433–4440.
77. Lee, B., Sharron, M., Montaner, L. J., Weissman, D., Doms, R. W. (1999) Quantification of CD4, CCR5, and CXCR4 levels on lymphocyte subsets, dendritic cells, and differentially conditioned monocyte-derived macrophages. *Proc. Natl. Acad. Sci. USA* **96,** 5215–5220.
78. Pfaff, J. M., Wilen, C. B., Harrison, J. E., Demarest, J. F., Lee, B., Doms, R. W., Tilton, J. C. (2010) HIV-1 resistance to CCR5 antagonists associated with highly efficient use of CCR5 and altered tropism on primary CD4+ T cells. *J. Virol.* **84,** 6505–6514.
79. Kwong, P. D., Wyatt, R., Robinson, J., Sweet, R. W., Sodroski, J., Hendrickson, W. A. (1998) Structure of an HIV gp120 envelope glycoprotein in complex with the CD4 receptor and a neutralizing human antibody. *Nature* **393,** 648–659.
80. Sullivan, N., Sun, Y., Sattentau, Q., Thali, M., Wu, D., Denisova, G., Gershoni, J., Robinson, J., Moore, J., Sodroski, J. (1998) CD4-induced conformational changes in the human immunodeficiency virus type 1 gp120 glycoprotein: consequences for virus entry and neutralization. *J. Virol.* **72,** 4694–4703.
81. Thali, M., Moore, J. P., Furman, C., Charles, M., Ho, D. D., Robinson, J., Sodroski, J. (1993) Characterization of conserved human immunodeficiency virus type 1 gp120 neutralization epitopes exposed upon gp120-CD4 binding. *J. Virol.* **67,** 3978–3988.
82. Wyatt, R., Kwong, P. D., Desjardins, E., Sweet, R. W., Robinson, J., Hendrickson, W. A., Sodroski, J. G. (1998) The antigenic structure of the HIV gp120 envelope glycoprotein. *Nature* **393,** 705–711.
83. Trkola, A., Dragic, T., Arthos, J., Binley, J. M., Olson, W. C., Allaway, G. P., Cheng-Mayer, C., Robinson, J., Maddon, P. J., Moore, J. P. (1996) CD4-dependent, antibody-sensitive interactions between HIV-1 and its co-receptor CCR-5. *Nature* **384,** 184–187.
84. Wyatt, R., Moore, J., Accola, M., Desjardin, E., Robinson, J., Sodroski, J. (1995) Involvement of the V1/V2 variable loop structure in the exposure of human immunodeficiency virus type 1 gp120 epitopes induced by receptor binding. *J. Virol.* **69,** 5723–5733.
85. Gorry, P. R., Howard, J. L., Churchill, M. J., Anderson, J. L., Cunningham, A., Adrian, D., McPhee, D. A., Purcell, D. F. (1999) Diminished production of human immunodeficiency virus type 1 in astrocytes results from inefficient translation of gag, env, and nef mRNAs despite efficient expression of Tat and Rev. *J. Virol.* **73,** 352–361.
86. Gorry, P. R., Dunfee, R. L., Mefford, M. E., Kunstman, K., Morgan, T., Moore, J. P., Mascola, J. R., Agopian, K., Holm, G. H., Mehle, A., Taylor, J., Farzan, M., Wang, H., Ellery, P., Willey, S. J., Clapham, P. R., Wolinsky, S. M., Crowe, S. M., Gabuzda, D. (2007) Changes in the V3 region of gp120 contribute to unusually broad coreceptor usage of an HIV-1 isolate from a CCR5 Δ32 heterozygote. *Virology* **362,** 163–178.
87. Sterjovski, J., Churchill, M. J., Roche, M., Ellett, A., Farrugia, W., Wesselingh, S. L., Cunningham, A. L., Ramsland, P. A., Gorry, P. R. (2011) CD4-binding site alterations in CCR5-using HIV-1 envelopes influencing gp120-CD4 interactions and fusogenicity. *Virology* **410,** 418–428.
88. Huang, C. C., Venturi, M., Majeed, S., Moore, M. J., Phogat, S., Zhang, M. Y., Dimitrov, D. S., Hendrickson, W. A., Robinson, J., Sodroski, J., Wyatt, R., Choe, H., Farzan, M., Kwong, P. D. (2004) Structural basis of tyrosine sulfation and VH-gene usage in antibodies that recognize the HIV type 1 coreceptor-binding site on gp120. *Proc. Natl. Acad. Sci. USA* **101,** 2706–2711.
89. Huang, C. C., Lam, S. N., Acharya, P., Tang, M., Xiang, S. H., Hussan, S. S., Stanfield, R. L., Robinson, J., Sodroski, J., Wilson, I. A., Wyatt, R., Bewley, C. A., Kwong, P. D. (2007) Structures of the CCR5 N terminus and of a tyrosine-sulfated antibody with HIV-1 gp120 and CD4. *Science* **317,** 1930–1934.
90. Sali, A., Blundell, T. L. (1993) Comparative protein modelling by satisfaction of spatial restraints. *J. Mol. Biol.* **234,** 779–815.
91. Bohne-Lang, A., von der Lieth, C. W. (2005) GlyProt: in silico glycosylation of proteins. *Nucleic Acids Res.* **33,** W214–W219.
92. Burton, D. R., Barbas III, C. F., Persson, M. A., Koenig, S., Chanock, R. M., Lerner, R. A. (1991) A large array of human monoclonal antibodies to type 1 human immunodeficiency virus from combinatorial libraries of asymptomatic seropositive individuals. *Proc. Natl. Acad. Sci. USA* **88,** 10134–10137.
93. Burton, D. R., Pyati, J., Koduri, R., Sharp, S. J., Thornton, G. B., Parren, P. W., Sawyer, L. S., Hendry, R. M., Dunlop, N., Nara, P. L.. (1994) Efficient neutralization of primary isolates of HIV-1 by a recombinant human monoclonal antibody. *Science* **266,** 1024–1027.
94. Roben, P., Moore, J. P., Thali, M., Sodroski, J., Barbas III, C. F., Burton, D. R. (1994) Recognition properties of a panel of human recombinant Fab fragments to the CD4 binding site of gp120 that show differing abilities to neutralize human immunodeficiency virus type 1. *J. Virol.* **68,** 4821–4828.
95. Hill, C. M., Kwon, D., Jones, M., Davis, C. B., Marmon, S., Daugherty, B. L., DeMartino, J. A., Springer, M. S., Unutmaz, D., Littman, D. R. (1998) The amino terminus of human CCR5 is required for its function as a receptor for diverse human and simian immunodeficiency virus envelope glycoproteins. *Virology* **248,** 357–371.
96. Carlsson, S. R., Sasaki, H., Fukuda, M. (1986) Structural variations of O-linked oligosaccharides present in leukosialin isolated from erythroid, myeloid, and T-lymphoid cell lines. *J. Biol. Chem.* **261,** 12787–12795.
97. Fukuda, M., Carlsson, S. R., Klock, J. C., Dell, A. (1986) Structures of O-linked oligosaccharides isolated from normal granulocytes, chronic myelogenous leukemia cells, and acute myelogenous leukemia cells. *J. Biol. Chem.* **261,** 12796–12806.
98. Berro, R., Sanders, R. W., Lu, M., Klasse, P. J., Moore, J. P. (2009) Two HIV-1 variants resistant to small molecule CCR5 inhibitors differ in how they use CCR5 for entry. *PLoS Pathog.* **5,** e1000548.
99. Ogert, R. A., Ba, L., Hou, Y., Buontempo, C., Qiu, P., Duca, J., Murgolo, N., Buontempo, P., Ralston, R., Howe, J. A. (2009) Structure-function analysis of human immunodeficiency virus type 1 gp120 amino acid mutations associated with resistance to the CCR5 coreceptor antagonist vicriviroc. *J. Virol.* **83,** 12151–12163.
100. Ogert, R. A., Hou, Y., Ba, L., Wojcik, L., Qiu, P., Murgolo, N., Duca, J., Dunkle, L. M., Ralston, R., Howe, J. A. (2010) Clinical resistance to vicriviroc through adaptive V3 loop mutations in HIV-1 subtype D gp120 that alter interactions with the N-terminus and ECL2 of CCR5. *Virology* **400,** 145–155.
101. Tilton, J. C., Wilen, C. B., Didigu, C. A., Sinha, R., Harrison, J. E., Agrawal-Gamse, C., Henning, E. A., Bushman, F. D., Martin, J. N., Deeks, S. G., Doms, R. W. (2010) A maraviroc-resistant HIV-1 with narrow cross-resistance to other CCR5 antagonists depends on both N-terminal and extracellular loop domains of drug-bound CCR5. *J. Virol.* **84,** 10863–10876.
102. Westby, M., Smith-Burchnell, C., Mori, J., Lewis, M., Mosley, M., Stockdale, M., Dorr, P., Ciaramella, G., Perros, M. (2007) Reduced maximal inhibition in phenotypic susceptibility assays indicates that viral strains resistant to the CCR5 antagonist maraviroc utilize inhibitor-bound receptor for entry. *J. Virol.* **81,** 2359–2371.

KEY WORDS:
Env · Affinofile · CNS · signature · phenotype

Appendix D

Nipah virus envelope pseudotyped lentiviruses efficiently target ephrinB2+ stem cell populations *in vitro* and bypass the liver sink when administered *in vivo*

Introduction

Lentiviruses are common vectors used in gene therapy because they can transduce non-dividing cells and offer stable integration into a target cell's genome. The host range can be altered by pseudotyping with glycoproteins derived from other enveloped viruses. The most commonly used is the glycoprotein (G) of vesicular stomatitis virus (VSV), which has great stability in the vector particle allowing concentration to high titers, and also has a ubiquitous host cell receptor allowing transduction of most cell types (1, 2). VSV-G pseudotyped particles (VSV-Gpp) have become the standard for evaluating the efficiency of transduction by other viral envelope pseudotypes. However, VSV-Gpp cannot be targeted to specific populations of cells, which is necessary for *in vivo* gene transfer applications.

More specific cell targeting can be achieved by pseudotyping with envelopes modified in various ways that allow for re-retargeting via some ligand specific domain (3, 4). Measles virus (MeV) glycoproteins (Edmonston strain) can also be efficiently pseudotyped onto a lentiviral vector, but only when the cytoplasmic tails of both envelope glycoproteins, the hemagglutinin (H) and fusion (F) proteins, were truncated. MeV_{Edm} uses CD46 and/or SLAM as entry receptors. In humans, CD46 is expressed on all nucleated cells (5), thus its natural tropism does not offer MeVpp any specific targeting advantage *in vivo*. However, *ex vivo*, MeVpp can transduce unstimulated primary human B and T cells that are relatively resistant to even VSV-Gpp transduction, suggesting that MeVpp are at least useful as an experimental tool (6, 7).

More recently, the unique features of MeV entry have allowed for some innovations that have attracted considerable interest (8-10). Measles virus is a member of the morbillivirus genus in the *Paramyxovirinae* subfamily of paramyxoviruses. Paramyxovirus entry requires the coordinated action of both the fusion (F) and attachment glycoproteins (designated HN, H, or G depending on its receptor binding properties); receptor binding to the viral attachment glycoprotein induces an allosteric change that triggers F to undergo a conformational cascade that results in virus-cell membrane fusion and entry (11-13). Morbillivirus is one of only two genera of paramyxoviruses that use protein-based receptors, the others use ubiquitous glycan-based receptors such as sialic acids. The aforementioned innovation takes advantage of the wealth of structure-function information that have not only mapped the receptor binding sites on MeV-H, but have also characterized key features of the ensuing receptor-binding triggerred fusion cascade (12, 14). Thus, by mutating the native receptor-binding sites on MeV-H, and appending to the C-terminus of the mutated MeV-H (a type II transmembrane protein), the single-chain variable fragment (scFv) from a monoclonal antibody recognizing specific cell-surface antigens, MeVpp can be successfully re-targeted, at least *in vitro*, to neurons, endothelial cells, and hematopoietic progenitors (15). Nevertheless, the development as MeVpp as *in vivo* targeted human gene therapy vectors is limited by the wide-spread presence of pre-existing neutralizing antibodies in the vast majority of the human population that have received MeV vaccination.

Nipah (NiV) and Hendra (HeV) viruses belong to the only other genera (*Henipavirus*) of paramyxoviruses that use protein-based receptors. A recent study

showed that the full-length Nipah virus envelope glycoproteins could be pseudotyped onto a lentiviral vector and mediate entry into various cell lines, although infectious titers were not determined (16). For NiV, the attachment glycoprotein, NiV-G, functions in recognition of the receptor. As for MeV, binding of the receptor to NiV-G triggers a series of conformational changes that eventually lead to NiV-F triggering and virus-cell membrane fusion (reviewed in (13)). Henipaviruses use ephrinB2 as the primary receptor, and, somewhat less efficiently, ephrinB3 as an alternate receptor (17-19). The remarkably high affinity of NiV-G for ephrinB2 (K_d = 0.06 nM) (19) suggests that NiV pseudotyped particles (NiVpp) can be efficiently and specifically targeted to ephrinB2+ cells. Thus, instead of re-targeting strategies, we sought to exploit the natural tropism of NiV for specific targeting of primary ephrinB2-expressing cell types that are of significant biological and clinical interest to the gene targeting community.

Eph-ephrin receptor-ligand pairs are membrane-associated receptor tyrosine kinases (RTKs) with well-established roles in many developmental processes; they regulate cell boundaries during tissue and bone formation, as well as provide guidance cues during neurogenesis and angiogenesis (20). EphrinB2-ephB4 interactions have been strongly implicated in tumor angiogenesis, migration, and invasion (21). In addition, ephrinB2 has been proposed as a molecular marker of stemness, being expressed on murine embryonic stem cells, hematopoietic stem cells and neural stem cells (22). Thus, the ability to target lentiviral vectors specifically to ephrinB2+ cells may be of utility for studying specific stem cell populations, or be of use for disrupting tumorigenesis where the ephrinB2-ephB4 axis plays a critical role (20).

Here, we systematically investigated what modifications to the cytoplasmic tails of the NiV glycoproteins could best enhance the efficiency of pseudotyping onto lentiviral particles. We found that efficient functional pseudotyping with NiV envelope requires only truncation of the F protein cytoplasmic tail, while full-length NiV-G can be used. Unlike MeVpp, full-length and truncated F were equally incorporated into NiVpp, indicating that the requirements for functional lentiviral pseudotyping differ between MeV and NiV. NiVpp can specifically target ephrinB2+ cells in a 1000-fold excess of ephrinB2-negative cells, and NiVpp transduced *human* embryonic, hematopoietic and neural stem cell populations in an ephrinB2-specific manner. Intravenous administration of the luciferase reporter NiVpp resulted in signals detected in the spleen and lung, but not the liver. Biodistribution studies quantifying genome integrated vector copy numbers in various tissues confirm these observations. Bypassing the liver sink is a critical barrier for targeted gene therapy (23, 24), suggesting that the extraordinary specificity of NiV-G for ephrinB2 may allow for targeting of specific ephrinB2+ populations *in vivo*, or *in vitro* without the need for prior cell purification.

Materials and Methods

Plasmid construction. The codon-optimized NiV-F and NiV-G genes were tagged at their C termini with an AU1 (DTYRYI) or HA (YPYDVPDYA) tag, respectively, as previously described (25). The β-lactamase (β-la) gene was fused to NiV-M as previously described (26). NiV-G cytoplasmic truncation mutants were generated using the QuikChange site-directed mutagenesis kit (Stratagene, Cedar Creek, TX) with primers designed corresponding to the deletions. NiV T234F and T5FΔN3 mutants were previously made (27, 28). FUhLucW and FG12 were constructed from FUGW, as previously described (29, 30). pNL4-3.Luc.R^-.E^- was obtained through the NIH AIDS Research and Reference Reagent Program. VSV-ΔG-Luc has the G protein envelope replaced with *Renilla* Luc, as previously described (19).

Cells and culture conditions. 293T cells were cultured in IMDM with 10% FBS, 1% NEAA, 1% Glutamax, and antibiotics. CHO-pgsA745 is a mutant cell line derived from Chinese hamster ovary (CHO) cells that lack the endogenous expression of heparin sulfate proteoglycans (31), and was maintained in DMEM-F12 medium supplemented with 10% FBS. CHO cells expressing either ephrin-B2 (CHO-B2) or ephrin-B3 (CHO-B3) were made as previously described (19), and maintained in DMEM-F12 medium supplemented with 10% FBS and 1 mg/ml of G418 to drive plasmid expression through neomycin resistance. Vero (African green monkey kidney fibroblast) cells were maintained in α-MEM with 10% FBS. U87 cells were maintained in DMEM with 10%

FBS. Human embryonic stem cells (hESCs) (H1, H9, and UCLA1 lines) were cultured on gelatin-coated plates on a feeder layer of mitotically-inactivated murine embryonic fibroblasts (MEFs). hESC medium is composed of DMEM/F:12 supplemented with 20% KnockOut Serum Replacement (KOSR, Life Technologies), 0.1 mM NEAA (Life Technologies), 1 mM L-Glutamine (Life Technologies), 0.1 mM 2-mercaptoethanol (Sigma-Aldrich), and 4 ng/ml basic fibroblast growth factor (bFGF, R&D Systems – obtained via National Cancer Institute Biological Resources Branch). hESCs were passaged in small clumps every 5-7 days using collagenase (Life Technologies). For viral transductions, hESCs were transferred to feeder-free conditions. hESCs were dissociated to single cells using trypsin (Life Technologies) for counting and then plated on Matrigel- (BD Biosciences) coated plates in hESC medium that was conditioned overnight on MEFs and supplemented with 10 μM HA-1077 (ROCK inhibitor, Sigma-Aldrich) to promote hESC survival (32). CD34+ cells were isolated from human fetal liver as previously described (33). For viral transductions, the cells were seeded onto Retronectin (Takara)-coated plates with 2% bovine serum albumin in Yssel's medium (Gemini). As previously described (34), neuralization of undifferentiated HSF1 hESC colonies was induced *in situ* by switching to rosette media containing DMEM:F12, N-2 supplement (Gibco), B27 supplement (Gibco), 1uM retinoic acid (Sigma), 1uM Smoothened Agonist (Calbiochem), and 20 ng/mL FGF2. After 10-14 days, rosettes were mechanically isolated and passaged onto poly-ornithine- (Sigma) and laminin- (Sigma) coated plates. Once picked, rosettes were placed into neural progenitor cell (NPC) media containing DMEM:F12, N-2, B27, 50 ng/mL EGF (Peprotech), and 20 ng/mL FGF2

allowing for expansion and maintenance. 100,000 NPCs (passage #2) were plated onto 24-well plates using TrypLE (Gibco) for viral infection.

Virus production. Lentiviral vectors were produced by calcium phosphate-mediated transient transfection of 293T cells. 24 hours prior to transfection, 1.6 x 10^7 293T cells were seeded into a T175 flask. On the day of transfection, the medium was replaced with 25ml fresh medium containing 10mM chloroquine. 7 μg of NiV-F variant, 7 μg of NiV-G variant, 12.5 μg of the packaging plasmid pCMVΔR8.9, and 12.5 μg of the lentiviral transfer vector plasmid (FG12 or FUhLucW) were mixed with 133 μl of 2M $CaCl_2$ and brought up to a final volume of 980 μl with ddH_20. Next, 1,110 μl of 2X HEPES buffer saline buffer was added dropwise. Following a 20-minute incubation on ice, the precipitate was added to the cells. After 8 hours, the medium was replaced with 30 ml of AIM-V serum-free medium. 48 hours post-transfection, the cell supernatant containing the pseudotyped lentiviral vector particles was layered over a 20% sucrose cushion and concentrated by centrifugation at 28,000 rpm at 4°C for 2 hours (Beckman SW-32 rotor). The viral pellet was resuspended in 300 μl of PBS and filtered (0.45μm filter). To determine viral titer, serial dilutions of unconcentrated and concentrated stocks were added to 2 x 10^5 293T cells and incubated for 2 hours at 37°C. The medium was replaced with fresh medium. 72 hours post-infection, the cells were collected and analyzed by flow cytometry for eGFP expression. The titers are expressed as infectious units per ml (IU/ml). Typical unconcentrated titers for NiVpp are 10^6 IU/ml, and can be concentrated to 10^8-10^9 IU/ml upon ultracentrifugation.

Western blot analysis. Concentrated viral stocks were normalized to HIV p24 (50 ng of p24 per lane). The samples were boiled in 6X sodium dodecyl sulfate (SDS) loading buffer containing 2-mercaptoethanol for 10 minutes, subjected to electrophoresis through a 10% SDS polyacrylamide gel, and transferred onto a PVDF (Millipore) membrane. Mouse anti-HA-tag (Covance), mouse anti-AU1-tag (Covance), and mouse anti-p24 (NIH AIDS Research and Reference Reagent Program) monoclonal antibodies were used to detect NiV-G, NiV-F, and p24 proteins, respectively. A goat anti-mouse IRDye 800CW (LI-COR Biosciences) was used as a secondary antibody. Signals were detected using the Odyssey infrared imaging system (LI-COR Biosciences).

β-lactamase-matrix entry assay. NiV and VSV-G β-lactamase-matrix virus-like particles (β-la-M VLPs) were produced as previously described (26). 293T cells were seeded in a 24-well dish at 7.5 x 10^4 per well. 24 hours after seeding, concentrated NiV wt F/wt G, NiV T5F/wt G or VSV-G pseudotyped βla-M VLPs were added to the cells and spin-inoculated for 1 hour at 2,000 rpm at 4°C. After spin-inoculation, cells were gently washed and CCF2-AM (Invitrogen) was added according to manufacturer recommendations. Cells were then transferred to a pre-warmed 37°C micro-plate fluorometer (TECAN Infinite® M1000). Green (uncleaved CCF2-AM) and blue (cleaved CCF2-AM) fluorescence was monitored at 530 nm and 460 nm, respectively. Kinetic readings were taken every 10 min for up to 5 hours.

***In vitro* infection of cells.** Increasing amounts of virus (based on MOI or p24) were added to 1 x 10^5 cells of each cell type and centrifuged at 2,000 rpm at 37°C for 2 hours. As a specificity control, 10 nM of soluble ephrinB2 (R&D Systems) was added to the infection medium. To exclude pseudotransduction, 5μM of nevirapine was added. For stem cell transductions, 4 ng/ml of polybrene (Sigma) was added. Following an overnight incubation with virus, the infection medium was removed and replaced with fresh medium. 72 hours post-infection, the cells were harvested and analyzed by flow cytometry for eGFP expression. For transduction of a mixed population of cells, ephrinB2+ human U87 cells were mixed with ephrinB2- non-human Chinese hamster ovary (CHO) cells at different ratios (U87:CHO ratios = 1:1, 1:10, 1:100, and 1:1000), and seeded at a density of 50,000 cells per well in 24-well plates. The next day, cells were infected with 1 or 10 ng of NiV T5F/wt G, T5FΔN3/wt G, and VSV-G pseudotypes. 72h post-infection, the cells were harvested, stained with the mouse W6/32 anti-human HLA-ABC monoclonal antibody (eBioscience), followed by Alexa 647-conjugated goat anti-mouse secondary antibodies. Samples were fixed and then analyzed by dual-color flow cytometry for human HLA and eGFP expression.

FACS-sorting of CD34+ fetal liver cells. CD34+ cells were isolated from human fetal liver as previously described (33). The cell suspensions were stained with DAPI, CD34-APC, CD38-PE-Cy7, and CD90-FITC (BD-Biosciences) antibodies for 20 minutes on ice in the dark. Following washing, the cells were sorted on a BD FACS Aria into 4 populations: CD90+CD34+CD38-, CD90-CD34+CD38-, CD90-CD34+CD38+, and

CD90-CD34-CD38+. Immediately following sorting, RNA was extracted from each population using a RNeasy Micro kit (Qiagen) and used for preparation of cDNA using a QuantiTect Reverse Transcription kit (Qiagen). Specific primers for ephrinB2 (Forward- TCCCGATTGAGCCTTACGACACTT, Reverse- TTCACCTTGACACAGAGCACC) and GAPDH (Forward- ATCAAGAAGGTGGTGAAGCAGG, Reverse- TCAAAGGTGGAGGAGTGGGTGT) were used for real-time PCR analysis of gene expression.

Immunostaining. Coverslips were fixed in 4% PFA at room temperature for 15 minutes, permeabilized in 0.5% Triton-X-100 at room temperature for 10 minutes, and blocked in 5% bovine serum, 1% BSA, and 0.2% Triton-X-100 at room temperature for 30 minutes. They were then incubated overnight at 4°C with a mouse anti-Nestin antibody (Neuromics). Next, the coverslips were incubated with goat anti-mouse 594 (Molecular Probes) at room temperature for 1 hour and mounted in Prolong Gold with DAPI (Invitrogen). Imaging was performed using the Zeiss Axio Imager A1.

***In vivo* analysis of infection.** 5-week-old female C57/BL6 (The Jackson Laboratory) were maintained in the animal facilities at UCLA in accordance with the University of California Animal Research Committee guidelines. The FUhLucW vector was pseudotyped with VSV-G, T5F/wt G, or T5F ΔN3/wt G envelopes. 5 or 10 μg of p24 of each virus stock was injected into the tail vein. 5 days post-injection, the mice were anesthetized and injected intraperitoneally with 3 mg of D-luciferin (Xenogen). A cooled

IVIS CCD camera (Xenogen) was used to obtain whole-body images. Organs (brain, lung, heart, spleen, liver) were excised from sacrificed mice for imaging. For biodistribution studies, which required the quantitation of integrated vector copy number in various tissues, the FG12 vector was pseudotyped with VSV-G or NiV envelopes. 5 μg of p24 of each virus stock was administered as above. 4 days post-injection, the mice were sacrificed and organs (liver, spleen, lung, brain, heart, kidney, bone marrow) were harvested. Organs were minced and cells dissociated as previously described (35). We modified the protocol to extend the digestion time to one hour. Genomic DNA was harvested using an Allprep kit (Qiagen). Quantitation of the vector copy number and cell number in the DNA isolate was performed with LightCycler 480 SYBR Green I Master (Roche) using the LightCycler 480 real-time PCR system (Roche). The FG12 plasmid was used as the standard for quantitation of vector copy number. The primers for the analysis of vector copy number were GFP-For (5' GCAGAAGAACGGCATCAAGGTG3') and GFP-Rev (5' TGGGTGCTCAGGTAGTGGT3'). The primers for the analysis of cell number were HPRT-For (5' GCAGCGTTTCTGAGCCATT3') and HPRT-Rev (5' AAAGCGGTCTGAGGAGGA3').

Gene Expression Analysis. The gene expression profiles of various pluripotent stem cell (PSC)-derived and primary (fetal and adult) tissues were determined by the human U133plus2.0 array (Affymetrix) at the UCLA Clinical Microarray Core. Multiple independent arrays (>3) were performed on each cell type shown in Table D-I.

Results

Efficient pseudotyping of a lentiviral vector with the Nipah virus envelope glycoproteins only requires truncations in the cytoplasmic tail of the F protein. Previous studies have shown that pseudotyping of lentiviral vectors with unmodified paramyxoviral glycoproteins is highly inefficient (36). However, recent studies with the measles virus envelope showed that when the cytoplasmic tails of both the fusion (F) and attachment (H) glycoproteins are truncated, infectious particles are produced (6, 7). The highest titers were obtained when only 3 residues were left in the F protein cytoplasmic tail and 15 residues in the H protein cytoplasmic tail. In contrast, a study with the Nipah virus (NiV) envelope showed that the full-length glycoproteins (F and G) could be used to pseudotype a lentiviral luciferase reporter vector, although a truncated F mutant with only 4 residues left in its cytoplasmic tail did result in a ten-fold increase in luciferase expression compared to wild-type F (16). However, no data regarding the infectious titers produced were given, and neither the transduction efficiency of their NiVpp on relevant primary cells, nor the potential of NiVpp for targeted transduction *in vivo* was examined.

To confirm and extend these findings, we took advantage of a previously characterized truncated variant of NiV-F, T5F (27), with 5 residues left in the cytoplasmic tail (Fig. D-1A, top panel), but which was otherwise expressed and processed at wild-type levels (27). When used in combination with wild-type (wt) NiV-G to pseudotype the FG12 lentiviral vector containing a GFP reporter gene, T5F/wtG NiVpp gave a titer of ~10^6 I.U./ml on 293T cells, a 100-fold increase in titer compared to

wtF/wtG pseudotypes (Fig. D-1B). Pseudotyping of NiV T5F/wtG onto the pNL4-3-Luc-E^-R^+ vector that was used in the above mentioned study (16) also resulted in a 100-fold increase in luciferase expression compared to wtF/wtG NiVpp across a three-log dilution of the virus stock (Fig. D-1C). However, pNL4-3-Luc-E^-R^+ is obviously not suitable as a gene therapy vector as it expresses the entire set of HIV genes except for Env, and lacks the cardinal safety features of lentiviral-based gene therapy vectors. Thus, in our subsequent studies, we will focus on using the FG12 vector, a HIV derived self-inactivating lentiviral vector designed for gene therapy purposes (30, 33).

In an effort to further increase viral titers, we generated variants with stepwise truncations in the NiV-G cytoplasmic tail (Fig. D-1A, bottom panel) and screened them in combination with T5F. Although the T5F/Δ10G and T5F/Δ25G variants demonstrated similar titers to T5F/wtG, none of the NiV-G variants produced greater titers than wtG (Fig. D-1B). Moreover, all combinations of wt F with the different NiV-G truncation variants produced extremely low titers (data not shown). Collectively, these results indicate that only truncations in NiV-F are critical for producing high titer functional pseudotypes when combined with wt NiV-G. Thus, all subsequent experiments were performed with the T5F/wtG variant as a starting point. As for VSV-Gpp, NiVpp could be concentrated by ultracentrifugation without lost of infectivity to produce titers of ~10^8-10^9 IU/ml compared to 10^{10} for VSV-G (data not shown).

To determine whether the difference in titer between the T5F/wtG and wtF/wtG pseudotypes was due to the efficiency of envelope incorporation onto the lentiviral particle, we purified NiVpp by ultracentrifugation and determined the amount of F and G

on an equivalent amount of virions (normalized by the amount of HIV capsid p24) by western blot. Unlike that for MeVpp, where full-length wtF/wtH were not detectably incorporated into pseudotyped particles, there was no difference in levels of NiV F and G incorporated between wtF/wtG and T5F/wtG pseudotypes (Fig. D-1D). In addition, both wtF and T5F were equivalently processed (F_0/F_1). Thus, truncation of the NiV-F cytoplasmic tail did not necessarily enhance incorporation onto virus particles, as was demonstrated by studies with the measles virus envelope (6, 7, 37). This suggests that there may be some incompatibility of the cytoplasmic tail of wild-type NiV-F with the matrix (gag) protein of HIV that compromises the fusogenicity of NiV-F, and hence the infectivity of NiVpp.

We hypothesized that if the incompatibility is specific to the HIV gag protein, then wtF/wtG "pseudotyped" onto NiV matrix (NiV-M), to make infectious virus-like particles (VLPs), should not show a significant difference in infectivity compared to VLPs produced with T5F/wtG. To test this, we used an established β-lactamase-NiV matrix (βla-M) based assay to compare entry of wild-type NiV-F and T5F VLPs (26). Entry of VLPs is detected by cytosolic delivery of βla-M to target 293T cells preloaded with the fluorescent CCF2-AM substrate. βla-mediated cleavage of CCF2-AM results in a shift of green to blue fluorescence. Thus, the blue to green fluorescence ratio can be monitored in real-time to compare the relative differences in entry efficiency due to virus-cell fusion. Fig. D-1E shows that the rate and extent of virus-cell fusion between wt F and T5F VLPs were very similar, plateauing at 2.38 and 2.65, respectively. To further confirm this finding, we pseudotyped wild-type NiV-G with either NiV-F or T5F

onto a VSVΔG-rLuc core, and infected 293T cells with 10-fold dilutions of each virus stock. T5F pseudotypes demonstrated only up to a 2-fold difference in R.L.U. compared to wt F pseudotypes (Fig. D-1F). Thus, the 100-fold difference in titers of wt F and T5F lentiviral pseudotypes is most likely due to a specific incompatibility of the long cytoplasmic tail of NiV-F with HIV gag that compromises the fusogenic activity of NiV-F but not its ability to be incorporated into lentiviral particles.

A hypoglycosylated hyperfusogenic NiV-F mutant demonstrates increased infectivity *in vitro*. EphrinB2 is likely the primary entry receptor for NiV (17, 18), while ephrinB3 may serve an alternate receptor on some cell types (19, 38). Chinese hamster ovary (CHO) cells do not express endogenous ephrinB2 and B3, and are therefore refractory to NiV envelope-mediated infection. However, stable CHO cell lines expressing ephrinB2 (CHO-B2) or ephrinB3 (CHO-B3) can readily support NiV infection (19). To compare the relative entry efficiency of NiVpp via the ephrinB2 and ephrinB3 receptors, we first infected CHO-B2 or CHO-B3 cells with 0.01, 0.1, and 1 ng p24 equivalents of NiVpp bearing T5F/wtG (Fig. D-2, A-C, grey bars), and normalized the infectivity observed with that obtained with 1 ng of VSV-Gpp (Fig. D-2D). Since VSV-Gpp infection should *not* depend on the presence of ephrinB2 or B3, this normalization allows for comparison across multiple independent experiments. Fig. D-2, A-C shows that T5F/wtG pseudotypes infected a similar percentage of CHO-B2 and CHO-B3 cells in a dose-dependent manner such that at the maximal viral input (1 ng

p24), 38% of CHO-B2 and 39% of CHO-B3 cells were infected relative to an equivalent amount of VSV-Gpp (compare Fig. D-2C and 2-2D, grey bars at 1 ng).

Since we found that only modifications to NiV-F were critical for pseudotyping (Fig. D-1), we sought to further improve transduction efficiency by pseudotyping lentiviral particles with a hyperfusogenic NiV-F variant in which an N-linked glycosylation site has been removed (T5FΔN3) (28). The titer of T5FΔN3/wtG pseudotypes on highly permissive 293T cells was similar to that of T5F/wtG pseudotypes (data not shown). However, on CHO-B2 cells, the hyperfusogenic T5FΔN3/wtG pseudotypes consistently exhibited a two-fold increase in infectivity relative to the T5F/wtG pseudotypes (Fig. D-2, A-C). This held true across a 100-fold difference in the amount of viral inoculum used. Although receptor specificity is determined by the attachment protein, there are examples of hyperfusogenic mutations in paramyxoviral F proteins that enable fusion triggering in the absence of their homotypic attachment proteins (39-42). This does not appear to be true for the hyperfusogenic NiV-F as the increased infectivity of T5FΔN3/wtG pseudotypes was abrogated by soluble ephrinB2. Similar results were observed on CHO-B3 cells at moderate (0.1 ng) and high (1 ng) viral input levels (Fig. D-2, B-C, compare black and grey bars); however, no specific infectivity was detected at the lowest viral inoculum level on CHO-B3 cells (Fig. D-2A). At the highest viral inoculum used, T5FΔN3/wtG NiVpp infection approached the transduction efficiency of VSV-Gpp, infecting 80% and 97% of CHO-B2 and CHO-B3 cells, respectively (Fig. D-2D).

Lastly, since ephrinB2 is endogenously expressed at high levels on endothelial cells and cells of the central nervous system, we compared the transduction efficiencies of T5F/wtG and T5FΔN3/wtG pseudotypes on human microvascular endothelial cells (HMVECs) and the U87 glioblastoma cell line (Fig. D-2, E-F). The two-fold increase in infection efficiency of T5FΔN3/wtG over T5F/wtG pseudotypes was observed for U87 (59.8% versus 32.3% at 1 ng) cells, but not for HMVECs (96.6% versus 87.6%), which were already highly permissive to NiVpp infection. In summary, although both pseudotypes had similar infectivity on highly permissive cells such as 293Ts and HMVECs, the hyperfusogenic T5FΔN3/wt G pseudotypes nevertheless exhibited increased infectivity on some cell lines.

NiV pseudotypes specifically target ephrinB2-positive cells in a vast excess of receptor-negative cells. Entry of T5F/wtG and T5FΔN3/wtG pseudotypes into multiple cell types was inhibited by soluble ephrinB2 (Fig. D-2), confirming the specificity of receptor-mediated entry. Next, we investigated whether the NiV pseudotypes could specifically target ephrinB2-positive cells in a mixture of ephrinB2-positive and -negative cells. U87 (ephrinB2-positive) cells were mixed with CHO (ephrinB2-negative) cells in 1:1, 1:10, 1:100, and 1:1000 ratios, and transduced with 1 or 10 ng p24 equivalents of NiV or VSV-G pseudotypes (Fig. D-3). To distinguish infection of the human U87 cells from non-human CHO cells, the infected cells were stained with an anti-HLA (anti-MHC class I) monoclonal antibody specific for human HLAs. At a 1:1 ratio and 1 ng of virus, the GFP+ cells transduced by both the T5F/wtG and T5FΔN3/wtG pseudotypes remained

entirely within the HLA+ population (Fig. D-3A, top panel). Increasing the amount of virus inoculum by 10-fold (10 ng) did not affect the specificity, since the NiVpp transduced GFP+ cells remained within the HLA+ population (Fig. D-3A, bottom panel). Furthermore, across all cell ratios, the NiV pseudotypes selectively transduced the ephrinB2+ U87 cells even after accounting for the differential permissivity of CHO cells versus U87 cells for HIV-1 based lentiviral transduction (Fig. D-3, B-C). VSV-G pseudotypes, on the other hand, transduced both HLA+ and HLA- cells, indicating its relative lack of specificity. In sum, our data suggest that NiV pseudotypes can selectively target ephrinB2-positive U87 cells even in a 1000-fold excess of ephrinB2-negative CHO cells (Fig. D-3C). Our data also demonstrates that increasing the fusogenicity of NiVpp did not necessarily compromise its specificity.

NiV pseudotypes mediate entry into human embryonic, neural and hematopoietic stem cells. On the basis of microarray and bioinformatics analysis, ephrinB2 has been identified as a molecular stem cell signature common to mouse embryonic (ESCs), hematopoietic (HSCs) stem cells, and neural (NSCs) (22). To determine if ephrinB2 also marks for their human stem cell counterparts, we determined if our NiVpp could mediate gene transfer into human ESCs, HSCs, and NSCs (Fig. D-4). Indeed, adding increasing amounts of T5F/wtG pseudotypes to H9 hESCs resulted in a dose-dependent increase (14-36%) in the amount of cells positive for GFP and SSEA-4, a cell-surface human pluripotency marker (Fig. D-4A). This infection was specific since it was blocked by soluble ephrinB2 (Fig. D-4B). To ensure that this ephrinB2-mediated transduction was

not specific to the H9 hESC line, we infected two other hESC lines (H1 and UCLA1) and obtained similar results (Fig. D-4B). Since stem cells are more difficult to transduce than standard cell lines, we expected that the hyperfusogenic T5FΔN3/wt G variant would mediate entry more efficiently than T5F/wtG NiVpp. However, we did not see an increase in infection using the T5FΔN3/wt G pseudotypes (Fig. D-4C).

Next, we infected purified CD34+ cells isolated from human fetal liver with NiV pseudotypes. CD34 is expressed on human hematopoietic stem and progenitor cells (HSPCs), although only a small fraction of CD34+ cells are true hematopoietic stem cells (HSCs) that have extensive self-renewal capacity *in vitro* and can engraft immunodeficient mice (30, 43). At a multiplicity of infection (MOI) of 1000, both T5F/wtG and T5FΔN3/wt G pseudotypes reproducibly transduced 3.6% and 3.5% of CD34+ cells, respectively. The specificity of this low-level infection was confirmed by blocking with soluble ephrinB2 (Fig. D-4D). True human HSCs have two cardinal properties: multipotency, defined as the ability to differentiate into all blood cell lineages, and long-term self-renewal, defined by the inexhaustible ability to produce progeny functionally identical to the parent upon cell division (43). Human HSCs with these properties are enriched in the Lin-CD90+CD34+CD38- fraction of cord blood (44). To determine whether ephrinB2 is expressed in this fraction, we FACS-sorted 4 populations from CD34+ cells isolated from human fetal liver: CD90+CD34+CD38-, CD90-CD34+CD38-, CD90-CD34+CD38+, and CD90-CD34-CD38+ (Fig. D-4E). RNA was extracted from each sorted population and ephrinB2 expression quantified using real-time PCR analysis. Our results indicate that ephrinB2 is expressed the highest in the

CD90+CD34+CD38- fraction (Fig. D-4F). Thus, the NiV pseudotypes may be targeting the cognate population of CD34+ cells enriched for true HSC activity.

Lastly, we assessed the transduction efficiencies of the NiV pseudotypes on nestin+ NSCs derived from hESCs (Fig. D-4G). Unlike hESCs and CD34+ HSPCs, increasing the MOI resulted in a dose-dependent increase in the percent of NSCs transduced such that the percent of GFP+ cells approached 100% at a MOI of 100 (Fig. D-4H). However, similar to the hESC and hHSC transductions, the T5FΔN3/wt G pseudotypes did not demonstrate increased infectivity compared to the T5F/wtG pseudotypes. Nevertheless, we confirmed that ephrinB2 is functionally expressed on human ESCs, HSCs, and NSCs, at least at levels that can mediate NiVpp infection.

NiV pseudotypes bypass the liver sink *in vivo*. EphrinB2 is expressed on endothelial cells, smooth muscle cells, and neurons (45, 46). In contrast, ephrinB3 is not expressed in the endothelium, and demonstrates overlapping but also distinct expression patterns in the central nervous system (47). This is consistent with our own microarray expression studies in a variety of human- and fetal tissue-derived as well as pluripotent stem cell (PSC) derived cell types (Table D-1). The ephrinB2/ephrinB3 expression patterns are in concordance with NiV infection *in vivo*, since histopathological studies on human patients detected the highest levels of viral antigens in neurons and endothelial cells of small blood vessels in the brain, but some was also observed in the vasculature of the lung and spleen. (48, 49). Importantly, no viral antigens were detected in the liver (49),

also consistent with our data in Table D-1, which shows the lack of ephrinB2 and B3 expression in adult tissue derived hepatocytes.

The inability to detect viral antigens in liver autopsy tissues from NiV infected patients, and the lack of viral receptor expression in the liver prompted us to examine whether intravenous administration of NiVpp might bypass the liver sink and target accessible ephrinB2+ cell types *in vivo*. We pseudotyped the FvcFlw lentiviral vector containing a firefly luciferase reporter gene with the NiV and VSV-G envelopes, and administered the viruses intravenously through the tail vein of C57/BL6 mice (Fig. D-5). A CCD camera was used to quantify the level of luciferase expression in the mice after injection of the D-luciferin substrate. Consistent with previous studies, VSV-Gpp-mediated transgene expression was detected primarily in the liver and spleen (Fig. D-5B, top panel). For the T5F/wtG pseudotypes, a slight signal was detected in the spleen in one case (Fig. D-5B, middle panel). Strikingly, the T5FΔN3/wt G pseudotypes showed a substantially enhanced signal in the spleen in all cases and lung in one case (Fig. D-5B, bottom panel). Thus, the T5FΔN3/wt G hyperfusogenic mutant demonstrates increased infectivity *in vitro* and *in vivo*. Significantly, neither the T5F/wtG or T5FΔN3/wtG pseudotypes exhibited any signal in the liver in all cases.

To complement and confirm these results, we also examined genomic vector integration in various tissues in an independent set of mice. The FG12 vector was pseudotyped with VSV-G and NiV envelopes, and viruses were administered as above. Four days post-injection, whole organs (liver, spleen, and lung) were harvested and cells dissociated. Genomic DNA was extracted and quantitation of vector integration was

performed using real-time PCR analysis. This PCR based assay was more sensitive (limit of sensitivity ~0.01 vector integrants/10,000 cells) and confirmed key aspects of our luciferase imaging results: while VSV-Gpp and NiVpp transduced the spleen with high efficiencies, only the VSV-Gpp transduced the liver, confirming that the NiVpp clearly bypassed the liver sink (Fig. D-5C). Interestingly, using the FG12 vector, VSV-G also transduced the lung as well as the NiVpp, although it is unclear whether the same cell types were transduced. The significance of these findings will be discussed.

Discussion

Measles virus and Nipah virus belong to the only two paramyxovirus genera that use protein-based receptors for entry. Studies with the measles virus envelope have shown that complex modifications to its attachment protein, including disruption of its binding site to its natural receptors and appending scFv or other targeting domains, result in specific re-targeting to desired cell populations *in vitro* and *in vivo* (9, 50). Some of these modifications have been successfully adapted to make scFV-directed targeting lentiviral MeVpp (7, 51). However, pre-existing neutralizing antibodies due to wide-spread MeV vaccination may compromise the transduction efficiency of MeVpp when administered *in vivo*, although deletion of immunodominant epitopes on MeV-H and other modifications have reduced the sensitivity of MeVpp to serum neutralization *in vitro* (52). In contrast, NiV is an emerging and lethal pathogen thus far confined to Southeast Asia (53). Thus, it is unlikely that pre-existing antibodies will pose a barrier to the development of NiVpp as a vehicle for targeted gene therapy. However, in the case of NiV, we sought to take advantage of the physiologically restricted and pathologically relevant expression patterns of ephrinB2, the primary high affinity receptor for NiV. Thus, instead of mimicking the re-targeting strategies used for MeV, we investigated the prospects of generating high-titer NiV pseudotypes that allow for specific targeting of biologically significant ephrinB2+ populations *in vitro* and *in vivo.*

The picomolar affinity of NiV-G for ephrinB2 is amongst the strongest viral envelope-receptor interactions known (13). This likely accounts for the extraordinary

specificity of NiVpp for ephrinB2-expressing cells. We examined whether further increasing the *efficiency* of transduction on a per virion basis without compromising the specificity of NiV-G-mediated infection may facilitate the development of NiVpp for targeted gene therapy to ephrinB2 expressing cells. To that end, we generated NiVpp with a hyperfusogenic F and wt G. Our hyper-fusogenic T5FΔN3/wt G NiVpp appeared to infect some cell types (CHO-B2, CHO-B3, and U87 cells) twice as well as T5F/wt G pseudotypes, but not in other highly permissive cells such as 293T cells and HMVECs, where transduction efficiencies of the normo-fusogenic T5F/wt G NiVpp already approached that of VSV-Gpp.

Unexpectedly, in hard-to-transduce stem cell populations such as human ESCs and HSCs, the hyper-fusogenic T5FΔN3/wt G pseudotypes also did not show an increase in transduction efficiency over T5F/wt G NiVpp. In addition, both demonstrated similar dose-dependent transduction efficiencies that plateaued at a relatively low percentage of the putative stem cell population. Thus, even at a saturating MOI of 1,000, both T5F- and T5FΔN3-based NiVpp transduced only ~36% and ~3.5% of SSEA4+ hESCs and CD34+ hHSCs, respectively. The limited transduction efficiency seen in human ESCs and CD34+ HSCs may be due to ephrinB2 expression only on a subset of these stem cell populations.

In hESCs, which are optimally passaged as colonies of cells, each colony contains heterogeneous subpopulations of cells that interact as an "ecosystem" to maintain the cardinal properties of hESCs: self-renewal and pluripotency (54, 55). For example, Stella and Nanog expressing subpopulations are biased towards self-renewal, whereas GATA-6

expressing subpopulations are more poised towards differentiation, and in between is a continuum of cells that contributes to the unique phenotypic properties of each hESC line (56). The ephrinB2+ subpopulation, or rather the fraction of ephrinB2+ cells that is maintained in hESC colonies, may be regulated to provide the optimal milieu for maintaining the cardinal properties of "stemness". This speculation is consistent with the known properties of ephrin-eph ligand-receptor interactions (both are receptor tyrosine kinases) for maintaining or enforcing tissue and cell type boundaries (57, 58). Thus, the ability to mark a subpopulation of hESCs with NiVpp-mediated transduction provides an experimentally tractable tool to examine the role of these ephrinB2+ subsets in hESC fate: survival, self-renew and pluripotency.

On the other hand, only a small subpopulation of CD34+ cells harbors true multipotent HSCs capable of long-term (LT) self-renewal, operationally defined by multi-lineage reconstitution in immunodeficient NOD-SCID mice. These LT-SCID repopulating cells can be found at least within the CD34+/CD38-/CD90+ subset (44, 59, 60). Intriguingly, we found that ephrinB2 is expressed highest in this subset (Fig. D-4F). This is also consistent with the finding that ephrinB2 is found in the functional murine equivalent of LT-HSC (22). Moreover, data from Fig. D-4, E-F indicate that the CD38-/CD90+ subset comprises less than 8% of total CD34+ cells from human fetal liver, which is close to but more than the ~3.5% of CD34+ cells infected by NiVpp at maximal MOI. Since LT-SCID repopulating cells are highly enriched in, but do not comprise the totality of CD34+/CD38-/CD90+ cells, this raises the possibility that NiVpp may indeed be targeting the elusive "true" HSC population within the CD34+/CD38-/CD90+ subset.

Functional confirmation will require limiting dilution in LT-SCID repopulating assays, which is a focus for future studies.

We are cognizant that cell-type dependent post-entry restriction factors may limit the efficiency of NiVpp transduction no matter how fusogenic we make the F protein to be. However, the extraordinary specificity of NiVpp exhibited by its ability to selectively target ephrinB2+ cells even in a 1000-fold excess of ephrinB2-negative cells (Fig. D-3), prompted us to examine the transduction efficiency of NiVpp *in vivo*, especially when the NiV pseudotypes are administered intravenously, and therefore subjected not only to dilution into the blood and tissue volume, but also to the problem of hepatic clearance, a critical barrier for *in vivo* virus-based gene therapy (23, 24, 61). Interestingly, when VSVpp and NiVpp carrying a luciferase reporter gene were injected into mice intravenously, and subsequently subjected to whole animal and organ imaging for D-luciferin-induced bioluminescent signals, T5FΔN3/wt G pseudotypes demonstrated an enhanced signal in the spleen and lungs compared to T5F/wt G (Fig. D-5B). Significantly, we did *not* detect a signal in the liver with either NiVpp as was observed with the VSV-G pseudotypes, suggesting that NiVpp could bypass the liver sink. However, *in vivo* bioluminescent imaging has limited sensitivity as signals are generally detected only when high local concentrations of cells are transduced (typically $>10^3$ to 10^4) (62, 63). Thus, we performed a sensitive PCR based biodistribution study to quantify the copy number of genomic vector integrants in these tissues (Fig. D-5C). This PCR assay confirmed that NiVpp did not transduce the liver to any significant level above background, while VSV-Gpp clearly could.

Rapid clearance and degradation of intravenously administered viral vectors by the liver has long been noted as an important obstacle in virus-based gene therapy (23, 24, 61). Our data suggests that the NiVpp can effectively bypass the liver sink and target ephrinB2+ cells in selected organs *in vivo* without the need for modifying the intrinsic specificity of the receptor binding attachment protein (NiV-G). Interestingly, our PCR based biodistribution studies (Fig. D-5C) showed that both normo- (T5F/wt G) and hyper- fusogenic (T5FD3)/wt G) NiVpp could transduce the spleen and lung with equivalent efficiencies, which is in contrast to the bioluminescent results (Fig. D-5B). Additionally, our biodistribution assay also showed that VSV-Gpp (FG12 vector based) could transduce the lung at the same levels as NiVpp, but bioluminescent signals was clearly lacking in the lung of VSV-Gpp (FvcF1w vector based) transduced animals. VSV-Gpp can transduce a wide array of tissues, and thus the lack of detec bioluminescent signals in the lung is likely a reflection of the limits of the detection methodology as discussed above. However, identification of the specific cell populations infected in the spleen and lungs is necessary for future optimization of the NiVpp platform for targeted gene therapy. EphrinB2 is expressed *highly* on endothelial cells, smooth muscle cells surrounding some arterioles, and neurons (45, 46). Unlike ephrinB2, ephrinB3 is mostly expressed in the CNS (47). Our own expression studies on multiple cell types and tissues confirm and extend these findings (Table D-1). As mentioned, these expression patterns are in concordance with the tissues that are targeted in the context of a natural human Nipah virus infection (64). Importantly, Table D-I also shows that endoderm tissues do not express ephrinB2 or B3. Indeed, of the major organs

examined in a large autopsy series, the liver is one of the few organs that exhibited no pathology or presence of any detectable viral antigens (49). The latter observations are consistent with the lack of liver transduction seen with our NiVpp. In spleen, viral antigen staining can be seen in macrophages and multinucleated giant cells. In the lung, viral antigen is most commonly seen in small blood vessels, and less often, in bronchial epithelial cells and alveolar macrophages. Since intravenous administration of NiVpp does not reflect the natural mode of NiV infection, determining the cell types transduced by NiVpp in the spleen and lung will be an important focus of future studies.

Altogether, our data demonstrates that we can generate high-titer, concentrated stocks (10^8-10^9 IU/ml) of NiVpp that can specifically target ephrinB2- and ephrinB3-positive cells *in vitro* and *in vivo*. Although NiV uses ephrinB3 as an alternate receptor, the affinity of NiV-G for ephrinB3 is less than that for ephrinB2 (19). Nevertheless, ephrinB3 is expressed in regions in the CNS where ephrinB2 is lacking, including the corpus callosum and spinal cord (65). Thus, NiV pseudotypes can potentially be used to also target these ephrinB3-positive regions. EphrinB2 has been shown to be upregulated in many types of cancer, including ovarian (66), uterine (67), and colon (68). In the appropriate context, inhibition of ephrinB2-ephB4 interactions has resulted in inhibition of tumor growth and angiogenesis (69). In some cases, breast cancer stromal cells over express ephB4 to attract tumor angiogenic vessels that overexpress ephrinB2 (70). Thus, NiV pseudotypes can be potentially used to either target appropriate tumors where overexpression of ephrinB2 has been linked to poorer prognosis, or antagonize ephrinB2 interactions with ephB4 to inhibit tumor angiogenesis (reviewed in (20, 21)).

Many other viral envelopes have been modified for targeted gene therapy. For many of them, the receptor-binding domain and the fusion domain of the envelope are produced from a single viral *env* gene. Thus, manipulation to enhance receptor-targeting specificity is more likely to adversely affect the fusion domain of the envelope protein, resulting in low viral titers. For paramyxoviruses, the receptor-binding attachment protein and the fusion protein are produced from two independent viral genes. Mechanistic studies as to how receptor binding to the attachment protein leads to allosteric triggering of the fusion protein is an area of intense study by many labs (reviewed in (9, 13, 50, 51, 71, 72)). For the henipaviruses, a large body of work has accumulated regarding the independent determinants of fusogenicity in F and G. Thus, F can be made even more fusogenic by incorporating other mutations that are already well characterized in the literature (4, 27, 28, 73-75). Indeed, even the specificity and fusogenicity of G itself can be optimized based on published structural and functional data (5, 13, 39, 40, 52, 53, 76). Altogether, this confluence of properties makes NiV pseudotypes highly attractive for further development as a targeted gene therapy vector for *in vitro* and *in vivo* applications.

Figure D-1

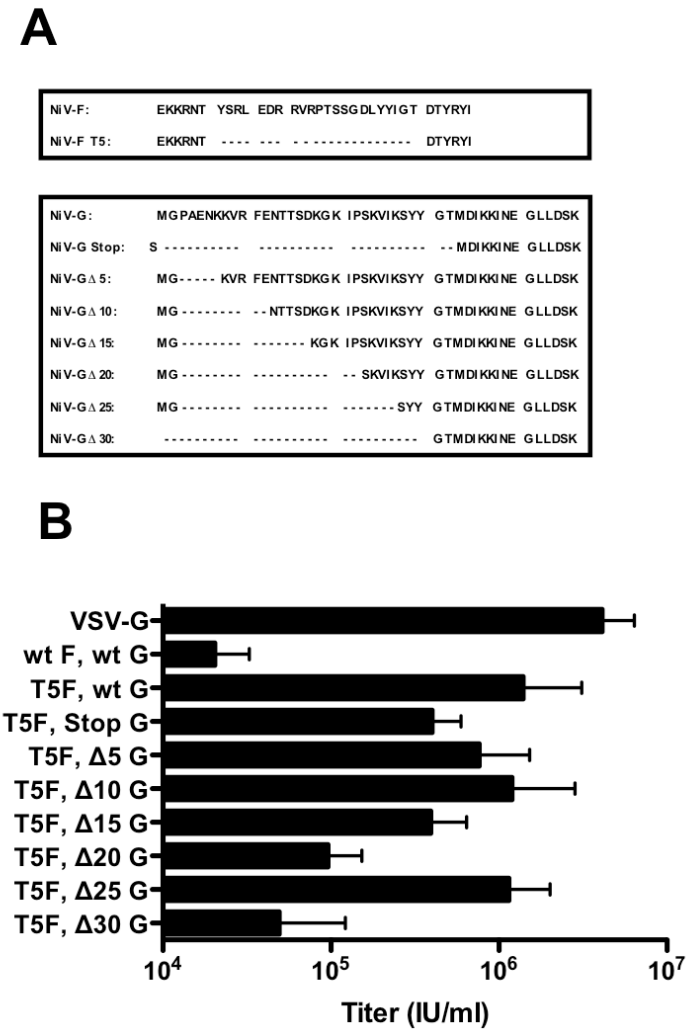

Figure D-1. Characterization of NiV-F and -G protein variants used for pseudotyping of an HIV-1-derived lentiviral vector. (A) A schematic of the amino acid sequences of the cytoplasmic tails of the NiV F (top) and G (bottom) protein variants is shown. T5F is a cytoplasmic tail truncation of NiV-F previously described (27). The 6 amino acids to the right is the AU1 tag at the cytoplasmic C-terminus of the F protein. Stepwise truncations in the cytoplasmic tail of NiV-G were generated and screened in

combination with T5F for the ability to form functional lentivirus pseudotypes. **(B)** Pseudotyped lentiviruses were made with the FG12 vector where the UbiC promoter drives eGFP expression. Codon-optimized NiV-F and NiV-G genes were transfected at a 1:1 ratio and supernatants harvested at 48h after transfection. Serial dilutions of unconcentrated viral supernatants were titered on 293T cells. Cells were examined for GFP expression 72h post-transduction by FACS analysis. Titers are expressed as IU/ml. Data shown are averages ± standard deviations from three independent experiments.

Figure D-1 (continued)

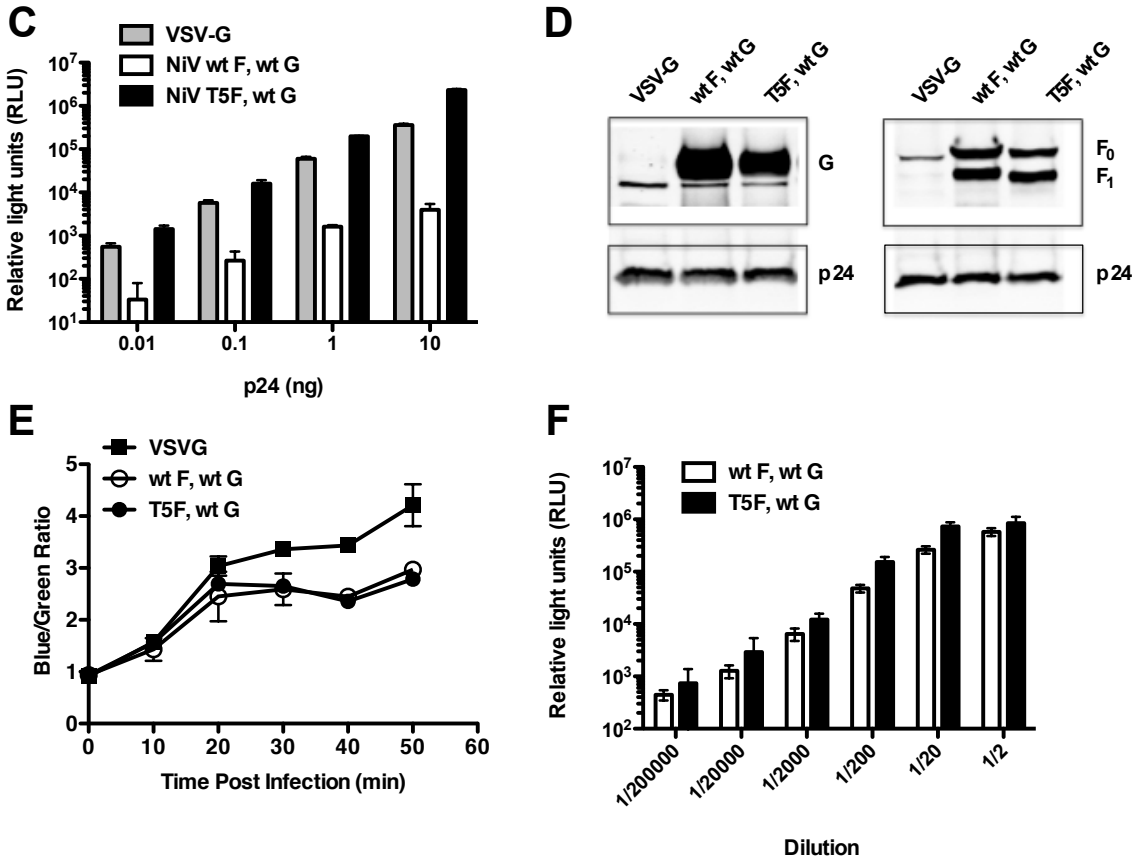

Figure D-1 (cont.) Characterization of NiV-F and -G protein variants used for pseudotyping of an HIV-1-derived lentiviral vector. (C) pNL4-3.Luc.R$^-$.E$^-$ was pseudotyped with VSV-G or NiV envelopes. 293T cells were infected with 0.01 ng, 0.1 ng, 1 ng, and 10 ng (p24 equivalents) of VSV-G or NiV pseudotypes. 72h post-infection, the cells were lysed and analyzed for luciferase activity. Data shown are averages of three replicates ± standard deviations. **(D)** Western blot analysis of HIV-1 pseudotyped

particles, pseudotyped with VSV-G and NiV wild-type or variant proteins. NiV-F was detected using an anti-AU1 antibody and NiV-G with an anti-HA antibody. One out of three representative experiments is shown. **(E)** Virus-like particles (VLPs) were produced with NiV β-lactamase-matrix (β-lac-M) and VSV-G, NiV wt F/wt G or NiV T5F/wt G envelopes. Based on densitometry of βla-M blots, equivalent amounts of concentrated VLPs were added to 293T cells for 1 hour at 4°C and then incubated with CCF2-AM substrate at 37°C. The blue and green fluorescence ratios were monitored as a measure of virus-cell fusion as described in the text and Methods. Data is presented as blue:green ratios every 10 minutes. Kinetic readings up to the 50 minutes time point are shown. Duplicate readings are taken at each time point. Data shown are averages ± standard deviations from three independent experiments. **(F)** A VSV-ΔG-Luc core was pseudotyped with NiV wt F/wt G or NiV T5F/wt G envelopes as previously described (19). Serial dilutions of unconcentrated viral supernatants were titered on Vero cells. 24 hours post-infection, the infected cells were lysed and analyzed for luciferase activity. Data shown are averages of four replicates ± standard deviations.

Figure D-2

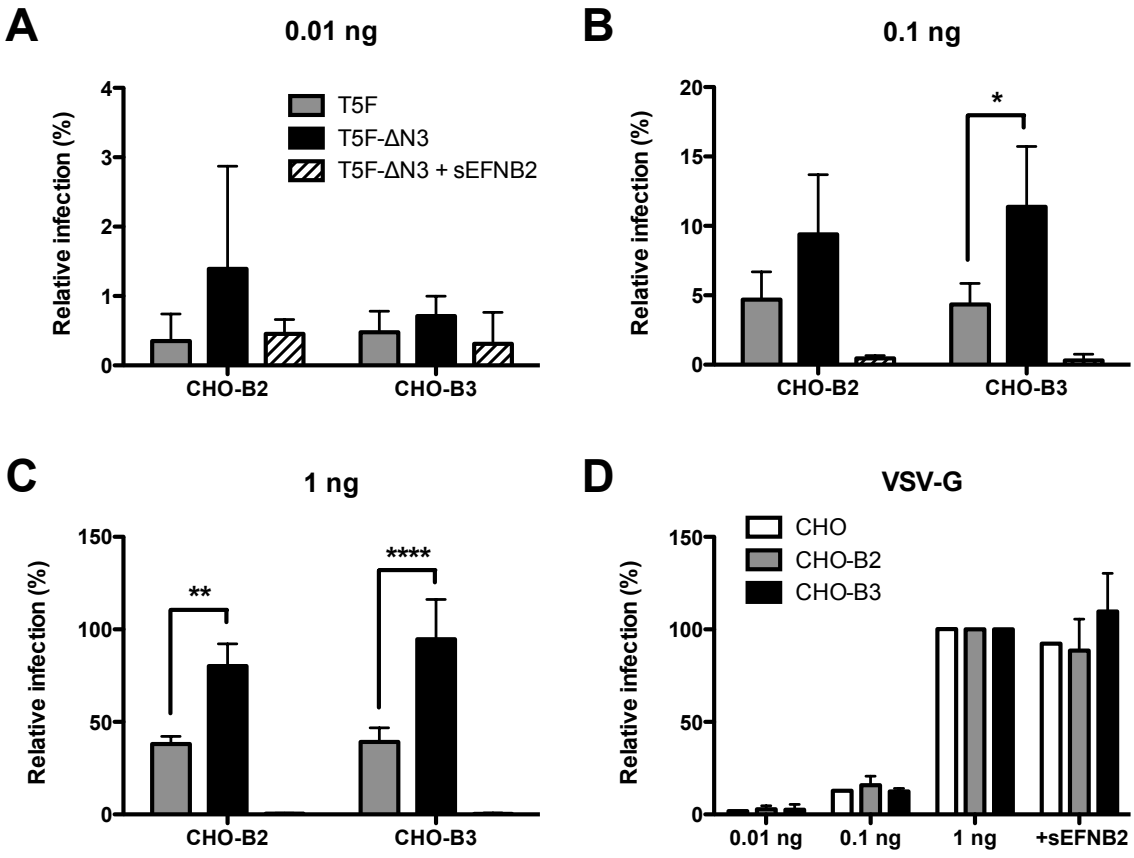

Figure D-2. NiV T5FΔN3/ wt G hyperfusogenic mutant demonstrates increased infectivity *in vitro*. (A-C) CHO, CHO-B2, and CHO-B3 cells were infected with 0.01 ng, 0.1 ng, and 1 ng (p24 equivalents) of NiV envelope or **(D)** VSV-G lentiviral pseudotypes carrying the GFP reporter gene (CHO cells not shown for NiVpp infection). Infectivity was determined by the percent of GFP+ cells at 48h post-infection via FACS analysis. The % GFP+ cells in each of the CHO cell lines infected by VSV-Gpp at maximal viral input (1 ng) was set at 100%, and all other infections in that cell line were normalized to this value. For reference, at 1 ng, VSV-G infected 20.2% of CHO, 22.7%

of CHO-B2, and 21.6% of CHO-B3 cells. For clarity of comparisons, the relative infectivity of T5F/wtG NiVpp versus the hyperfusogenic T5FΔN3/wtG variant on CHO-B2 and CHO-B3 cells using low (0.01 ng), medium (0.1 ng), or high (1 ng) amounts of viral inoculum are shown separately in **(A), (B),** and **(C),** respectively.

Figure D-2 (continued)

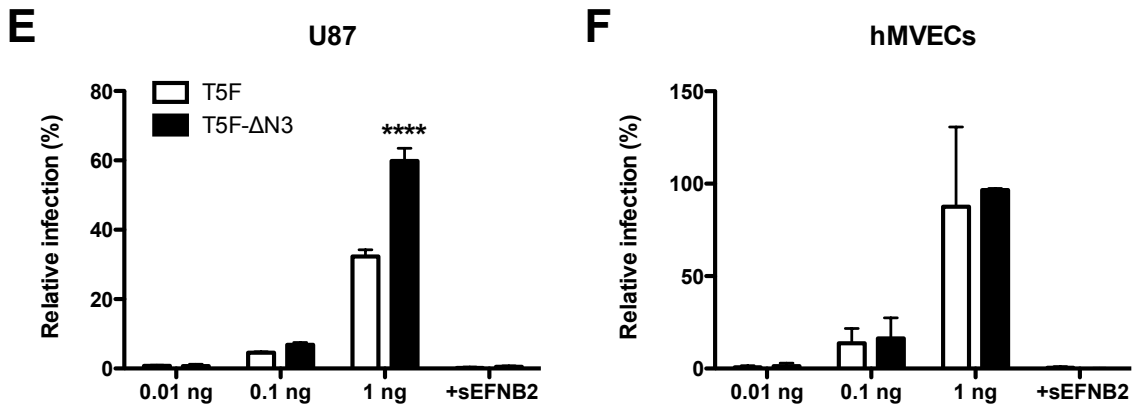

Figure D-2 (cont.) NiV T5FΔN3/ wt G hyperfusogenic mutant demonstrates increased infectivity *in vitro*. (E) U87 cells and **(F)** HMVECs were infected with T5F/wt G and T5FΔN3/wt G pseudotypes as described for (A-C) but normalized to VSV-Gpp infection of the same cell line (U87 or HMVECs) at maximal viral input (1 ng). For reference, at 1 ng, VSV-G infected 36.5% of U87 cells and 14.4% of HMVECs. Inhibition by 10 nM of soluble ephrinB2 (sEFNB2) was used to demonstrate specificity of NiV receptor-mediated entry. All pseudotyped particle infections, regardless of envelope used, were also abrogated by 5 μM niverapine (NVP), a reverse transcriptase inhibitor (data not shown). Data shown in **(A-F)** are averages ± standard deviations for three independent experiments. Statistical analyses were performed using a two-way ANOVA with Bonferroni post-test comparison using GraphPad PRISM™. *: $p < 0.05$, **: $p < 0.01$, ****: $p < 0.0001$.

Figure D-3

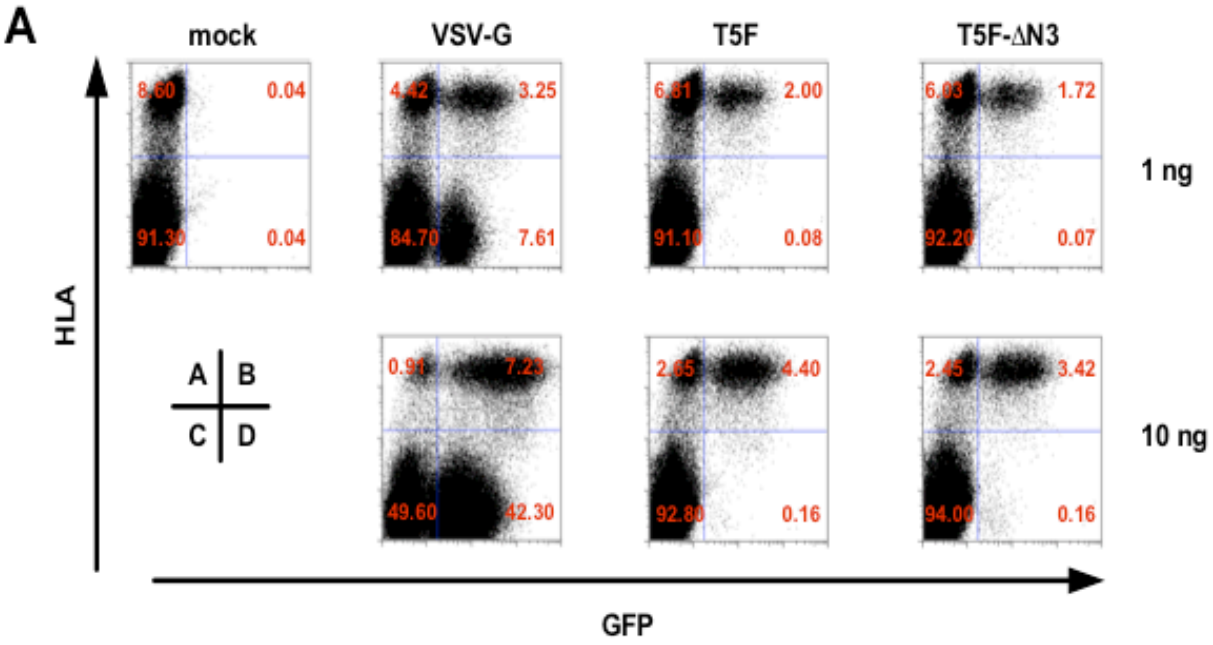

Figure D-3. NiV pseudotypes can specifically target ephrinB2-positive cells in up to a 1000-fold excess of ephrinB2-negative cells. (A) U87 (ephrinB2+) cells were mixed with CHO (ephrinB2-) cells at different ratios (U87:CHO ratios = 1:1, 1:10, 1:100, and 1:1000) and seeded at a density of 50,000 cells per well in 24-well plates. The next day, cells were infected with 1 or 10 ng of NiV T5F/wt G, T5FΔN3/wt G, and VSV-G pseudotypes. 72h post-infection, the cells were harvested and stained with the W6/32 anti-human HLA-ABC monoclonal antibody and the infection rate (GFP-positive cells) was determined by FACS analysis. Representative FACS plots are shown for data acquired on infection of the 1:1 mixture of U87:CHO cells. Although the cells were

seeded and infected at the indicated ratio, the CHO cells divided faster and outgrew the U87 cells by about ten-fold in each sample. Each FACS plot is representative of one of the triplicates at 1 ng and one of the duplicates at 10 ng. Data from 300,000 cells were acquired for every condition used for analysis in part B of this figure.

Figure D-3

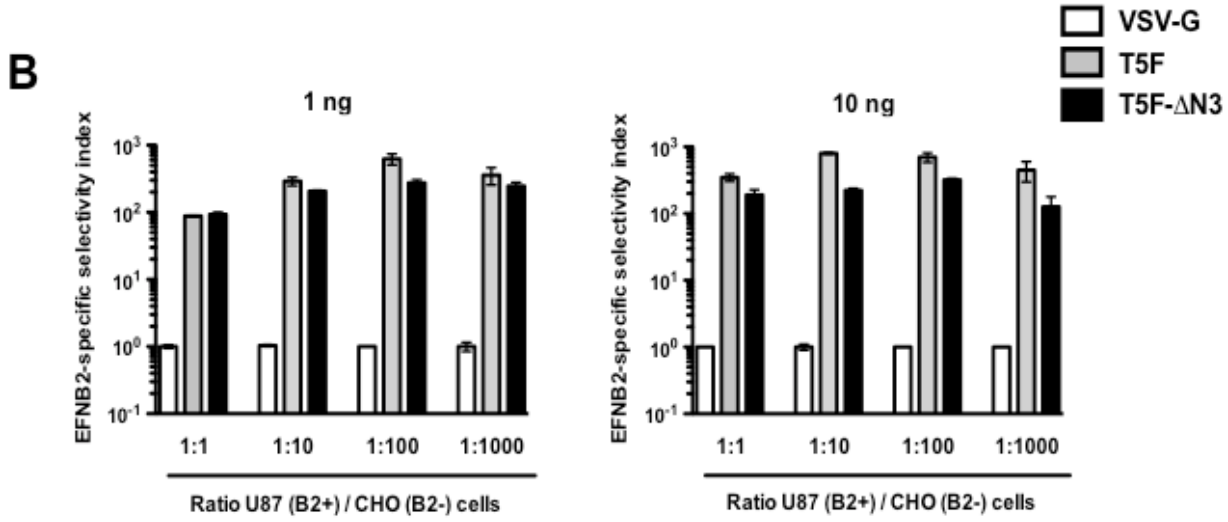

Figure D-3 (cont.) NiV pseudotypes can specifically target ephrinB2-positive cells in up to a 1000-fold excess of ephrinB2-negative cells. (B) To take into account the differential permissivity of U87 and CHO cells to lentiviral transduction, we first calculated the "cell-specific selectivity index" for U87 cells, the U87 SI as {B/(A+B)}/{D/(C+D)} where B and D represents the % of infected (GFP+) U87 and CHO cells, respectively, and A and C represents their uninfected counterparts, such that the total fraction of U87 (A+B) and CHO (C+D) cells in any given mixture upon analysis must equal 100%. A U87 SI of >1 indicates a selective preference for infecting U87 over CHO cells. For VSV-Gpp, the U87 SI at 1 and 10 ng is 5.14 and 1.93, respectively. This likely reflects the receptor-independent preference for U87 over CHO cells due to the HIV-1 based vector backbone alone. The reduction in U87 SI at a higher inoculum of

VSV-Gpp is also consistent with the known ability of VSV-G-delivered gag to saturate non-human post-entry restriction factors such TRIM5a. Since VSV-G is not known to have a cell-type specific receptor, we calculated the "NiV receptor-specific selectivity index", or the "EphrinB2 SI" as the VSV-G or NiV Env specific U87 SI divided by the U87 SI for VSV-G. This normalizes for differences in the intrinsic permissiveness of U87 over CHO cells for lentiviral transduction. This formulation now allows one to evaluate the selectivity of NiVpp for infecting ephrinB2-expressing cells relative to VSV-Gpp under all conditions analyzed. The values of the U87 SI and EphrinB2 SI for the data shown in (A) are indicated here as an example of our analysis. **(C)** The EphrinB2 Selectivity Index for VSV-Gpp, and NiVpp bearing T5F or T5F-DN3 was calculated for all the indicated conditions. Data shown are averages ± standard deviations for triplicates done at 1 ng, and average ± range for duplicates done at 10 ng.

Figure D-4

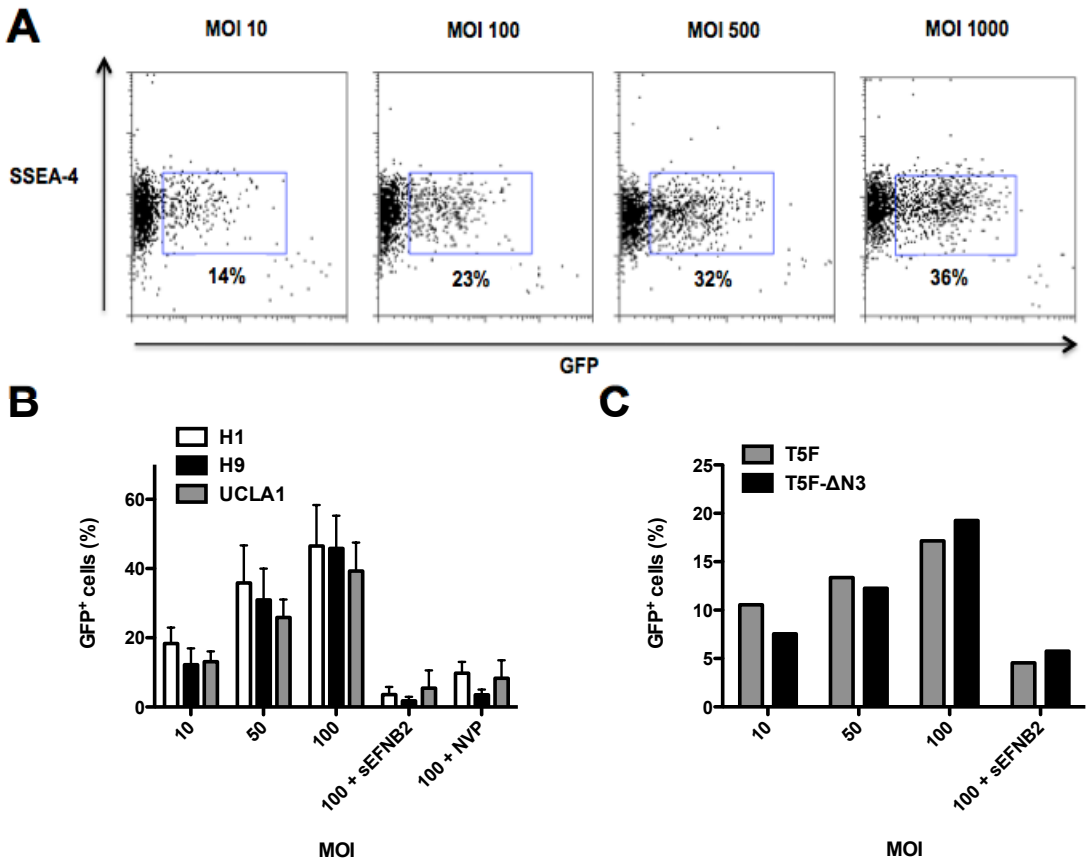

Figure D-4. NiV pseudotyped lentiviruses infect human embryonic, neural and hematopoietic stem cells. (A) Increasing amounts of NiV T5F/wt G pseudotypes were added to H9 hESCs. Cells were stained for the cell-surface pluripotency marker, SSEA-4, and examined for GFP expression 72h post-transduction by FACS analysis. **(B)** H1 and UCLA1 hESC lines were infected with NiV T5F/wt G pseudotypes as in part (A). Infection was blocked with 10 nM soluble ephrinB2 or 5 μM nevirapine. Data shown are

averages ± standard deviations from three independent experiments. **(C)** H9 hESCs were infected with NiV T5F/wt G and T5FΔN3/wt G pseudotypes as in part (A). One out of two representative experiments is shown.

Figure D-4 (continued)

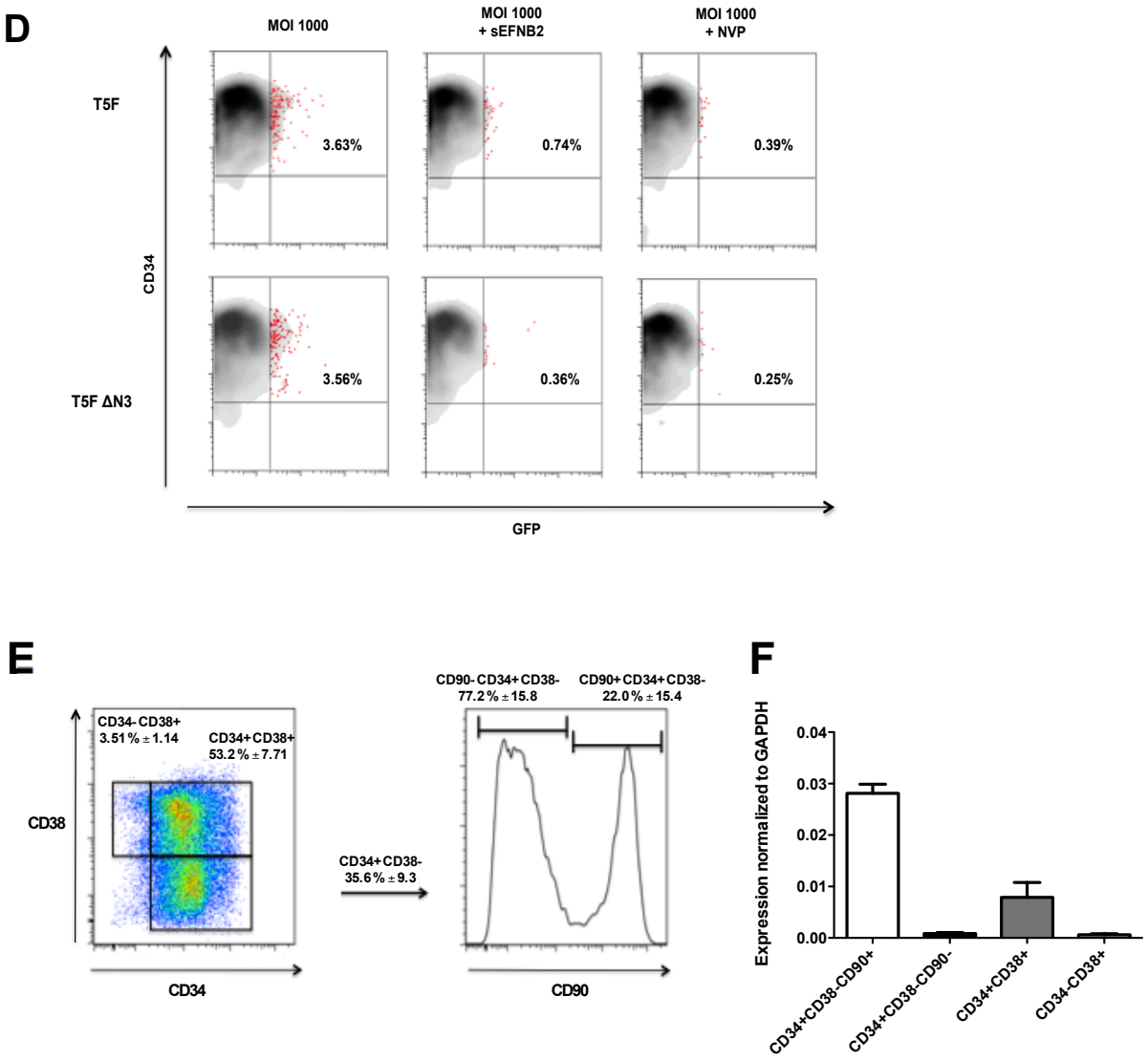

Figure D-4 (cont.) NiV pseudotyped lentiviruses infect human embryonic, neural and hematopoietic stem cells. (D) Purified $CD34^{+}$ cells from human fetal liver were infected with the indicated NiVpp in the presence or absence of 10 nM sEFNB2 and 5

μM NVP. 72h post-transduction, cells were stained for the cell-surface marker, CD34, and analyzed for GFP expression by FACS analysis. One representative donor out of three is shown. **(E)** CD34+ cells isolated from human fetal liver were stained with CD90-FITC, CD34-APC, CD38-PE-Cy7 antibodies and DAPI, and FACS-sorted into the 4 populations as indicated. Data shown are averages ± standard deviations from 3 donors. **(F)** RNA was extracted from each cell population indicated in (**E**) and ephrinB2 expression was examined by real-time PCR analysis and normalized against GAPDH as indicted in methods. Data shown are averages ± standard deviations from 3 donors.

Figure D-4 (continued)

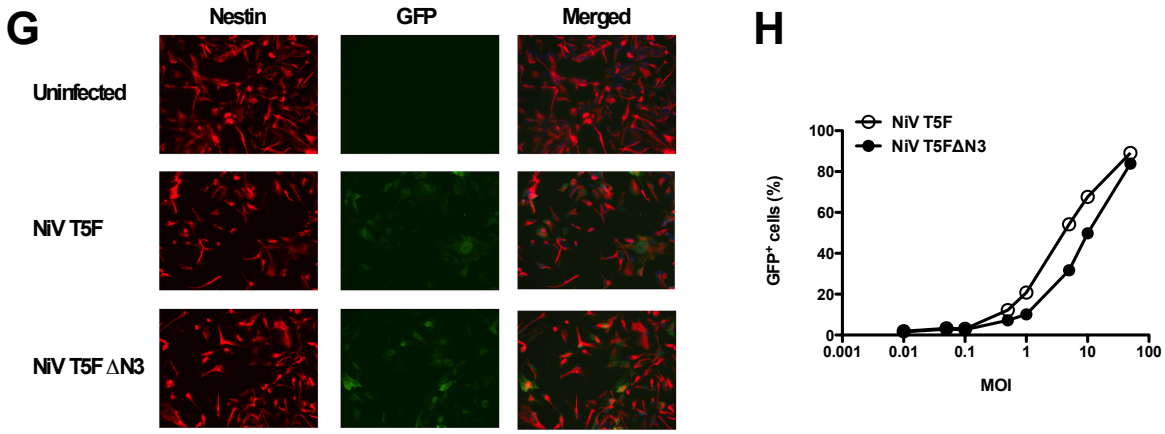

Figure D-4 (cont.) NiV pseudotyped lentiviruses infect human embryonic, neural and hematopoietic stem cells. (G) Neural progenitors were derived from HSF1 hESCs and infected with NiVpp. 72h post-transduction, cells were stained for nestin and examined by microscopy. **(H)** hNSC GFP expression at each M.O.I. (0.01, 0.05, 0.1, 0.5, 1, 5, 10, and 50) was quantified by FACS analysis. Data shown in **(G)** and **(H)** are from one representative experiment out of four.

Figure D-5

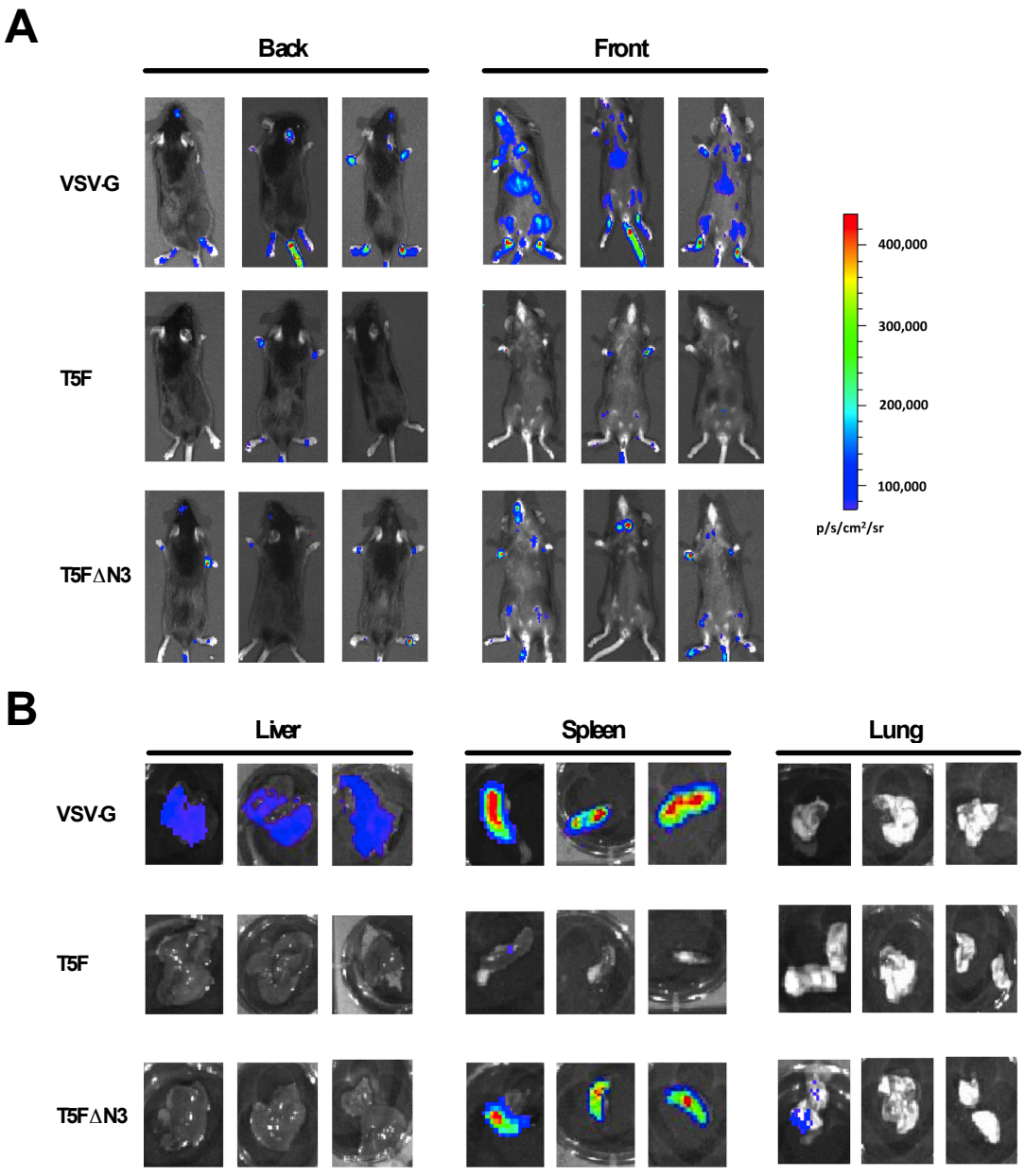
A
Back
Front
VSV-G
T5F
T5FΔN3
400,000
300,000
200,000
100,000
p/s/cm²/sr
B
Liver
Spleen
Lung
VSV-G
T5F
T5FΔN3

Figure D-5. NiV pseudotypes bypass the liver sink *in vivo*. (A) The FvcFlw (firefly luciferase) vector was pseudotyped with VSV-G and the indicated NiV envelopes. 5-10 ng of p24 equivalent of each pseudotyped lentivirus was injected into C57/BL6 mice through the tail vein. 5 days post-injection, luciferase expression was monitored by CCD imaging of the whole animal after injection of the D-luciferin substrate as described in methods. Three mice from three independent experiments are shown per virus. **(B)** Following whole-body imaging, each organ was isolated and luciferase activity was imaged and quantified as in (**A**). Three organs from three different mice are shown per virus.

Figure D-5 (continued)

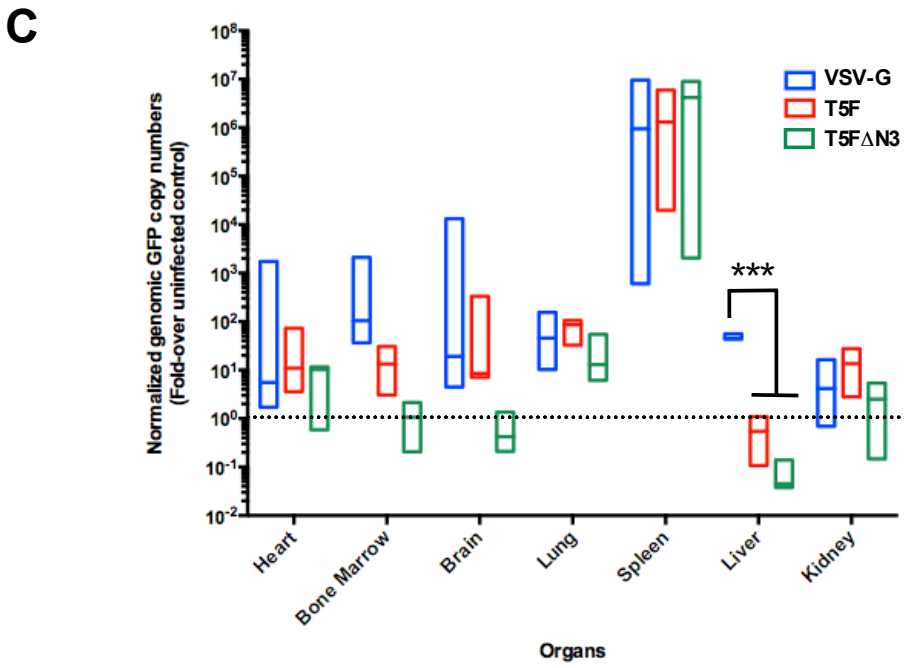

Figure D-5 (cont.) NiV pseudotypes bypass the liver sink *in vivo*. (C) The FG12 (GFP) vector was pseudotyped with VSV-G and the NiV envelopes. 5 μg of p24 equivalent of each pseudotyped lentivirus was administered to mice as above. 4 days post-injection, the mice were sacrificed and the indicated organs harvested. Genomic DNA was extracted and quantitation of the vector copy number was determined using real-time PCR analysis for GFP vector sequences. GFP copy numbers were normalized to HPRT copy numbers. Normalized GFP copy numbers are presented as fold-increase over background numbers obtained from matched organs in an uninfected mouse. 3 mice were used for each indicated pseudotyped vector (VSV-G, NiV-T5F, and NiV-T5FD3).

The median and range are shown as box plots, using the average of quadruplicates for each PCR reaction. Statistical significance was accessed by *t* tests corrected for multiple comparisons by the Holm-Sidak method in GraphPad PRISM^{TM} 6. ***, $p<0.001$.

Table D-1

Gene	Specificity marker	Source: Cell type:	PSC	PSC DE	Adult tissue Hepatocytes	PSC Neural progenitor	PSC Neurons	Fetal tissue Neural progenitor	Adult tissue Keratinocyte	Adult tissue Mesothelial	Adult tissue Kidney epithelial	Adult tissue Blood vessels
EFNB2			1186	716	85	2131	1794	3961	2244	1935	3008	5415
EFNB3			349	525	53	1622	7789	2275	273	190	219	184
GAPDH	Housekeeping genes		19143	17814	13047	17359	17637	17303	19032	22349	21258	19544
ACTB			18106	18917	17098	18191	17065	19266	17449	10505	19893	18052
FABP7	NPCs		281	64	22	4351	4640	15172	31	17	30	25
ALB	Hepatocyte		13	11	22065	11	10	10	10	9	8	10
VWF	Endothelium		65	105	67	63	49	40	37	46	31	12953
KRT14	Keratinocyte		13	11	13	12	12	11	19365	16	11	12
POU5F1	PSCs		8332	13192	229	508	135	123	188	144	369	146
			Pluripotent	Endoderm		Ectoderm				Mesoderm		

Table D-1. Tissue and cell type expression of ephrinB2 and ephrinB3. A human U133plus2.0 array (Affymetrix) was performed on various pluripotent stem cell (PSC)-derived and primary (fetal and adult) tissues to examine whole genome expression. Shown here are the normalized mean expression values from multiple biological repeats ($\geq$ 3). EphrinB2/B3 (yellow for significant positives), housekeeping genes (grey), and cell-specific genes (red) are color coded as indicated.

PSC, Pluripotent Stem Cell

DE, Definitive Endoderm derived from PSC cultured in chemically defined medium (CDM-ABFLY) supplemented with Activin, BMP4, FGF2, and the PI3K inhibitor LY294002. DE gives rise to other endoderm progenitors (pancreatic, endocrine etc.), and can retain expression of the POU5F1 pluripotency marker (also called Oct4) during early stages of PSC→DE differentiation (77).

References

1. Mochizuki H, Schwartz JP, Tanaka K, Brady RO, & Reiser J (1998) High-titer human immunodeficiency virus type 1-based vector systems for gene delivery into nondividing cells. *J Virol* 72(11):8873-8883.
2. Reiser J*, et al.* (1996) Transduction of nondividing cells using pseudotyped defective high-titer HIV type 1 particles. *Proc Natl Acad Sci U S A* 93(26):15266-15271.
3. Morizono K*, et al.* (2005) Lentiviral vector retargeting to P-glycoprotein on metastatic melanoma through intravenous injection. *Nat Med* 11(3):346-352.
4. Morizono K*, et al.* (2010) Redirecting lentiviral vectors pseudotyped with Sindbis virus-derived envelope proteins to DC-SIGN by modification of N-linked glycans of envelope proteins. *J Virol* 84(14):6923-6934.
5. Ni Choileain S & Astier AL (2012) CD46 processing: a means of expression. *Immunobiology* 217(2):169-175.
6. Frecha C*, et al.* (2008) Stable transduction of quiescent T cells without induction of cycle progression by a novel lentiviral vector pseudotyped with measles virus glycoproteins. *Blood* 112(13):4843-4852.
7. Funke S*, et al.* (2008) Targeted cell entry of lentiviral vectors. *Mol Ther* 16(8):1427-1436.

8. Frecha C, Levy C, Cosset FL, & Verhoeyen E (2010) Advances in the field of lentivector-based transduction of T and B lymphocytes for gene therapy. *Mol Ther* 18(10):1748-1757.

9. Buchholz CJ, Muhlebach MD, & Cichutek K (2009) Lentiviral vectors with measles virus glycoproteins - dream team for gene transfer? *Trends Biotechnol* 27(5):259-265.

10. Arce F, Breckpot K, Collins M, & Escors D (2011) Targeting lentiviral vectors for cancer immunotherapy. *Curr Cancer Ther Rev* 7(4):248-260.

11. Chang A & Dutch RE (2012) Paramyxovirus fusion and entry: multiple paths to a common end. *Viruses* 4(4):613-636.

12. Plemper RK, Brindley MA, & Iorio RM (2011) Structural and mechanistic studies of measles virus illuminate paramyxovirus entry. *PLoS Pathog* 7(6):e1002058.

13. Lee B & Ataman ZA (2011) Modes of paramyxovirus fusion: a Henipavirus perspective. *Trends Microbiol* 19(8):389-399.

14. Navaratnarajah CK, Leonard VH, & Cattaneo R (2009) Measles virus glycoprotein complex assembly, receptor attachment, and cell entry. *Curr Top Microbiol Immunol* 329:59-76.

15. Anliker B*, et al.* (2010) Specific gene transfer to neurons, endothelial cells and hematopoietic progenitors with lentiviral vectors. *Nat Methods* 7(11):929-935.

16. Khetawat D & Broder CC (2010) A functional henipavirus envelope glycoprotein pseudotyped lentivirus assay system. *Virol J* 7:312.

17. Negrete OA, *et al.* (2005) EphrinB2 is the entry receptor for Nipah virus, an emergent deadly paramyxovirus. *Nature* 436(7049):401-405.

18. Bonaparte MI, *et al.* (2005) Ephrin-B2 ligand is a functional receptor for Hendra virus and Nipah virus. *Proc Natl Acad Sci U S A* 102(30):10652-10657.

19. Negrete OA, *et al.* (2006) Two key residues in ephrinB3 are critical for its use as an alternative receptor for Nipah virus. *PLoS Pathog* 2(2):e7.

20. Pasquale EB (2008) Eph-ephrin bidirectional signaling in physiology and disease. *Cell* 133(1):38-52.

21. Pasquale EB (2010) Eph receptors and ephrins in cancer: bidirectional signalling and beyond. *Nat Rev Cancer* 10(3):165-180.

22. Ivanova NB, *et al.* (2002) A stem cell molecular signature. *Science* 298(5593):601-604.

23. Elvevold K, Smedsrod B, & Martinez I (2008) The liver sinusoidal endothelial cell: a cell type of controversial and confusing identity. *Am J Physiol Gastrointest Liver Physiol* 294(2):G391-400.

24. Ganesan LP, *et al.* (2011) Rapid and efficient clearance of blood-borne virus by liver sinusoidal endothelium. *PLoS Pathog* 7(9):e1002281.

25. Levroney EL, *et al.* (2005) Novel innate immune functions for galectin-1: galectin-1 inhibits cell fusion by Nipah virus envelope glycoproteins and augments dendritic cell secretion of proinflammatory cytokines. *J Immunol* 175(1):413-420.

26. Wolf MC*, et al.* (2009) A catalytically and genetically optimized beta-lactamase-matrix based assay for sensitive, specific, and higher throughput analysis of native henipavirus entry characteristics. *Virol J* 6:119.

27. Aguilar HC*, et al.* (2007) Polybasic KKR motif in the cytoplasmic tail of Nipah virus fusion protein modulates membrane fusion by inside-out signaling. *J Virol* 81(9):4520-4532.

28. Aguilar HC*, et al.* (2006) N-glycans on Nipah virus fusion protein protect against neutralization but reduce membrane fusion and viral entry. *J Virol* 80(10):4878-4889.

29. Lois C, Hong EJ, Pease S, Brown EJ, & Baltimore D (2002) Germline transmission and tissue-specific expression of transgenes delivered by lentiviral vectors. *Science* 295(5556):868-872.

30. Qin XF, An DS, Chen IS, & Baltimore D (2003) Inhibiting HIV-1 infection in human T cells by lentiviral-mediated delivery of small interfering RNA against CCR5. *Proc Natl Acad Sci U S A* 100(1):183-188.

31. Esko JD, Stewart TE, & Taylor WH (1985) Animal cell mutants defective in glycosaminoglycan biosynthesis. *Proc Natl Acad Sci U S A* 82(10):3197-3201.

32. Damoiseaux R, Sherman SP, Alva JA, Peterson C, & Pyle AD (2009) Integrated chemical genomics reveals modifiers of survival in human embryonic stem cells. *Stem Cells* 27(3):533-542.

33. Shimizu S*, et al.* (2010) A highly efficient short hairpin RNA potently down-regulates CCR5 expression in systemic lymphoid organs in the hu-BLT mouse model. *Blood* 115(8):1534-1544.

34. Karumbayaram S*, et al.* (2009) Directed differentiation of human-induced pluripotent stem cells generates active motor neurons. *Stem Cells* 27(4):806-811.

35. Van Handel B*, et al.* (2012) Scl represses cardiomyogenesis in prospective hemogenic endothelium and endocardium. *Cell* 150(3):590-605.

36. Kobayashi M, Iida A, Ueda Y, & Hasegawa M (2003) Pseudotyped lentivirus vectors derived from simian immunodeficiency virus SIVagm with envelope glycoproteins from paramyxovirus. *J Virol* 77(4):2607-2614.

37. Frecha C*, et al.* (2011) Measles virus glycoprotein-pseudotyped lentiviral vector-mediated gene transfer into quiescent lymphocytes requires binding to both SLAM and CD46 entry receptors. *J Virol* 85(12):5975-5985.

38. Pernet O, Wang YE, & Lee B (2012) Henipavirus receptor usage and tropism. *Curr Top Microbiol Immunol* 359:59-78.

39. Ayllon J, Villar E, & Munoz-Barroso I (2010) Mutations in the ectodomain of newcastle disease virus fusion protein confer a hemagglutinin-neuraminidase-independent phenotype. *J Virol* 84(2):1066-1075.

40. Rawling J, Garcia-Barreno B, & Melero JA (2008) Insertion of the two cleavage sites of the respiratory syncytial virus fusion protein in Sendai virus fusion protein leads to enhanced cell-cell fusion and a decreased dependency on the HN attachment protein for activity. *J Virol* 82(12):5986-5998.

41. Sergel TA, McGinnes LW, & Morrison TG (2000) A single amino acid change in the Newcastle disease virus fusion protein alters the requirement for HN protein in fusion. *J Virol* 74(11):5101-5107.

42. Seth S, Vincent A, & Compans RW (2003) Mutations in the cytoplasmic domain of a paramyxovirus fusion glycoprotein rescue syncytium formation and eliminate the hemagglutinin-neuraminidase protein requirement for membrane fusion. *J Virol* 77(1):167-178.

43. Geisbert TW, Feldmann H, & Broder CC (2012) Animal Challenge Models of Henipavirus Infection and Pathogenesis. *Curr Top Microbiol Immunol*.

44. Majeti R, Park CY, & Weissman IL (2007) Identification of a hierarchy of multipotent hematopoietic progenitors in human cord blood. *Cell Stem Cell* 1(6):635-645.

45. Gale NW*, et al.* (2001) Ephrin-B2 selectively marks arterial vessels and neovascularization sites in the adult, with expression in both endothelial and smooth-muscle cells. *Dev Biol* 230(2):151-160.

46. Shin D*, et al.* (2001) Expression of ephrinB2 identifies a stable genetic difference between arterial and venous vascular smooth muscle as well as endothelial cells, and marks subsets of microvessels at sites of adult neovascularization. *Dev Biol* 230(2):139-150.

47. Flenniken AM, Gale NW, Yancopoulos GD, & Wilkinson DG (1996) Distinct and overlapping expression patterns of ligands for Eph-related receptor tyrosine kinases during mouse embryogenesis. *Dev Biol* 179(2):382-401.

48. Maisner A, Neufeld J, & Weingartl H (2009) Organ- and endotheliotropism of Nipah virus infections *in vivo* and *in vitro*. *Thromb Haemost* 102(6):1014-1023.

49. Wong KT*, et al.* (2002) Nipah virus infection: pathology and pathogenesis of an emerging paramyxoviral zoonosis. *Am J Pathol* 161(6):2153-2167.

50. Galanis E (2010) Therapeutic potential of oncolytic measles virus: promises and challenges. *Clin Pharmacol Ther* 88(5):620-625.

51. Munch RC*, et al.* (2011) DARPins: an efficient targeting domain for lentiviral vectors. *Mol Ther* 19(4):686-693.

52. Levy C*, et al.* (2012) Lentiviral Vectors Displaying Modified Measles Virus gp Overcome Pre-existing Immunity in *In Vivo*-like Transduction of Human T and B Cells. *Mol Ther*.

53. Luby SP & Gurley ES (2012) Epidemiology of Henipavirus Disease in Humans. *Curr Top Microbiol Immunol*.

54. Graf T & Stadtfeld M (2008) Heterogeneity of embryonic and adult stem cells. *Cell Stem Cell* 3(5):480-483.

55. Hough SR, Laslett AL, Grimmond SB, Kolle G, & Pera MF (2009) A continuum of cell states spans pluripotency and lineage commitment in human embryonic stem cells. *PLoS One* 4(11):e7708.

56. Hayashi K, Lopes SM, Tang F, & Surani MA (2008) Dynamic equilibrium and heterogeneity of mouse pluripotent stem cells with distinct functional and epigenetic states. *Cell Stem Cell* 3(4):391-401.

57. Poliakov A, Cotrina M, & Wilkinson DG (2004) Diverse roles of eph receptors and ephrins in the regulation of cell migration and tissue assembly. *Dev Cell* 7(4):465-480.

58. Sela-Donenfeld D & Wilkinson DG (2005) Eph receptors: two ways to sharpen boundaries. *Curr Biol* 15(6):R210-212.

59. Baum CM, Weissman IL, Tsukamoto AS, Buckle AM, & Peault B (1992) Isolation of a candidate human hematopoietic stem-cell population. *Proc Natl Acad Sci U S A* 89(7):2804-2808.

60. Craig W, Kay R, Cutler RL, & Lansdorp PM (1993) Expression of Thy-1 on human hematopoietic progenitor cells. *J Exp Med* 177(5):1331-1342.

61. Zhang L, Dailey PJ, Gettie A, Blanchard J, & Ho DD (2002) The liver is a major organ for clearing simian immunodeficiency virus in rhesus monkeys. *J Virol* 76(10):5271-5273.

62. Contag CH & Ross BD (2002) It's not just about anatomy: *in vivo* bioluminescence imaging as an eyepiece into biology. *J Magn Reson Imaging* 16(4):378-387.

63. Shah K, Jacobs A, Breakefield XO, & Weissleder R (2004) Molecular imaging of gene therapy for cancer. *Gene Ther* 11(15):1175-1187.

64. Wong KT & Tan CT (2012) Clinical and pathological manifestations of human henipavirus infection. *Curr Top Microbiol Immunol* 359:95-104.

65. Liebl DJ, Morris CJ, Henkemeyer M, & Parada LF (2003) mRNA expression of ephrins and Eph receptor tyrosine kinases in the neonatal and adult mouse central nervous system. *J Neurosci Res* 71(1):7-22.

66. Alam SM, Fujimoto J, Jahan I, Sato E, & Tamaya T (2008) Coexpression of EphB4 and ephrinB2 in tumour advancement of ovarian cancers. *Br J Cancer* 98(4):845-851.

67. Alam SM, Fujimoto J, Jahan I, Sato E, & Tamaya T (2007) Overexpression of ephrinB2 and EphB4 in tumor advancement of uterine endometrial cancers. *Ann Oncol* 18(3):485-490.

68. Liu W*, et al.* (2002) Coexpression of ephrin-Bs and their receptors in colon carcinoma. *Cancer* 94(4):934-939.

69. Kertesz N*, et al.* (2006) The soluble extracellular domain of EphB4 (sEphB4) antagonizes EphB4-EphrinB2 interaction, modulates angiogenesis, and inhibits tumor growth. *Blood* 107(6):2330-2338.

70. Noren NK, Lu M, Freeman AL, Koolpe M, & Pasquale EB (2004) Interplay between EphB4 on tumor cells and vascular ephrin-B2 regulates tumor growth. *Proc Natl Acad Sci U S A* 101(15):5583-5588.

71. Russell SJ & Peng KW (2009) Measles virus for cancer therapy. *Curr Top Microbiol Immunol* 330:213-241.

72. Blechacz B & Russell SJ (2008) Measles virus as an oncolytic vector platform. *Curr Gene Ther* 8(3):162-175.

73. Aguilar HC, Aspericueta V, Robinson LR, Aanensen KE, & Lee B (2010) A quantitative and kinetic fusion protein-triggering assay can discern distinct steps in the nipah virus membrane fusion cascade. *J Virol* 84(16):8033-8041.

74. Morizono K*, et al.* (2009) A versatile targeting system with lentiviral vectors bearing the biotin-adaptor peptide. *J Gene Med* 11(8):655-663.

75. Wong LF*, et al.* (2006) Lentivirus-mediated gene transfer to the central nervous system: therapeutic and research applications. *Hum Gene Ther* 17(1):1-9.

76. Xu K*, et al.* (2008) Host cell recognition by the henipaviruses: crystal structures of the Nipah G attachment glycoprotein and its complex with ephrin-B3. *Proc Natl Acad Sci U S A* 105(29):9953-9958.

77. Teo AK*, et al.* (2011) Pluripotency factors regulate definitive endoderm specification through eomesodermin. *Genes Dev* 25(3):238-250.